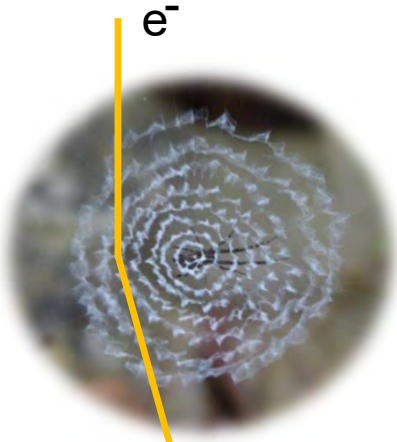

Enhanced Data Generated by Electrons

EDGE2017

8th International Workshop on Electron Energy Loss Spectroscopy and Related Techniques

Final Program and Abstracts

May 14th (Sun) - 19th (Fri) 2017,
Okuma Private Beach & Resort (JAL Private Resort Okuma),
Okuma, Okinawa, Japan

EDGE2017
Okuma, Okinawa, Japan

We are grateful to our conference sponsors,

JEOL Solutions for Innovation

nion

GATAN

FEI™

HREM Research Inc.

Hitachi High-Tech

OXFORD INSTRUMENTS

CEOS Corrected Electron Optical Systems GmbH

ALLIANCE Biosystems

AMETEK®

JPC

KITANO

NEM

STEM

VACUUM DEVICE

endorsements and assents from

The Japanese Society of Microscopy

The Japan Society of Applied Physics

The Ceramic Society of Japan

日本結晶学会

N.K.G.

Table of Contents

Conference Information

Registration

The registration desk is located in the Fountain room (1F) of the Okuma Private Beach & Resort (JAL private resort OKUMA). After you through the main entrance, the Fountain room is on your left (See hotel map in this book). The registration desk will be open from 15:00 on Sunday 14th. The registration desk will be also open from Monday to Thursday, from 8:30 am to 18:00 except for between 11:30 and 12:30.

Meals

The registration fee includes the welcome reception on Sunday 14th, lunches from Monday 15th to Thursday 18th, dinners from Monday 15th to Wednesday 17th, the banquet on Thursday 18th. The charge of the hotel, the Okuma Private Beach & Resort (JAL private resort OKUMA) includes breakfasts. Breakfasts (open at 6:30 am from Monday to Thursday and at 6:00 am on Friday), lunches, dinners are served at “Surfside Café” (See hotel map in this book). The banquet is held on “Beach Side Restaurant” (See hotel map in this book) at 19:00 on Thursday. All meals will be served as buffet style. Main ingredients for meals will be displayed.

Wi-Fi Access

Wi-Fi is available without a password across the Okuma Private Beach & Resort (JAL private resort OKUMA) except for certain areas, OKUMA Eco-Museum (place for posters) and small parts in the areas of Main Cottages and Palm Cottages.

Social Event

Daisekirinzan hiking is scheduled on Wednesday. Shuttle buses for Daisekirinzan will leave from the front of entrance at 14:00. Daisekirinzan (big-rock-forest mountain, in Japanese) is a tropical karst plateau, and is a candidate for a UNESCO World Heritage. We do not recommend flip-flop sandals. In the case of unfavorable weather, Okinawa Churaumi Aquarium would be planed.



Information for Poster Presenters

The Posters Oral Summaries session

Poster presenters can make a very brief talk of one-minute / one-slide in the Posters Oral Summaries sessions.

P001–P060: 18:30–20:00 Monday 15th
P061–P120: 18:00–19:30 Tuesday 16th

If you wish to make it, please prepare a PDF file of your one-page slide. The file name must be "POSTER NUMBER_YOUR LAST NAME.pdf". If you have not submitted your PDF file yet, please give it to the EDGE Registration Desk of the conference site (Fountain, 1F) using a USB memory by 15:30 Monday.

Floor Layout of Poster Presentations, OKUMA Eco-Museum

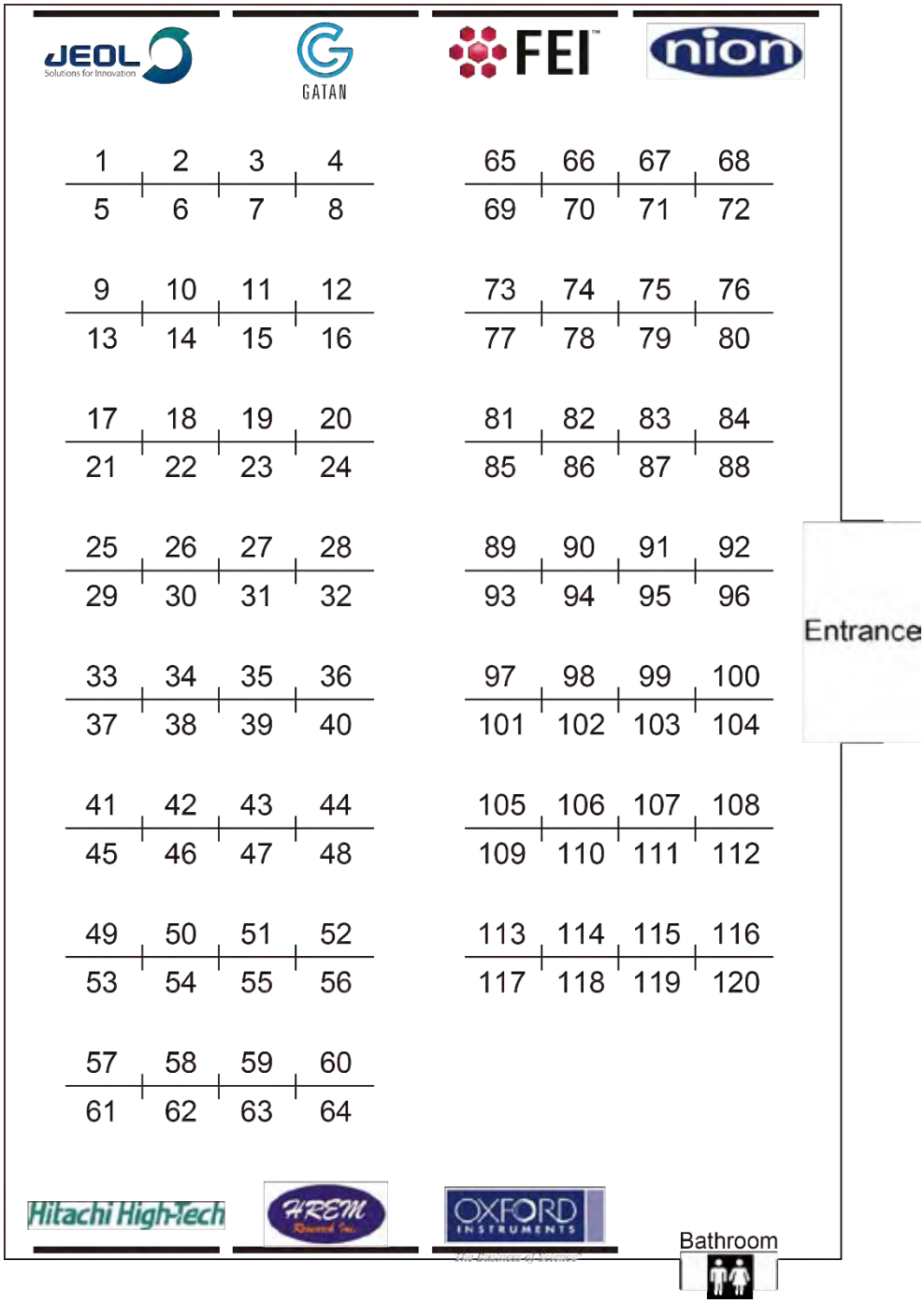

Proceedings

Proceedings (full-length papers) will be published in MICROSCOPY (Oxford Journals) as the "EDGE Special Issue". Participants of EDGE2017 are recommended to prepare each manuscript for the special Issue by the date of the meeting. Color figures will be published in color in online journal, but all figures will appear in black and white in printed journal.
Manuscript submission will be open from May 1st, 2017. The submission deadline for the special Issue will be at the end of May, 2017. See also "Instruction to authors" of MICROSCOPY: https://academic.oup.com/jmicro/pages/general_instructions.

Access to the Naha Airport

Bus Service on Friday (arranged by local organizers)

Free shuttle bus service will be available for EDGE participants from the hotel (Okuma Private Beach & Resort) to Naha Airport on Friday. It would take about 2 hours from the hotel to Naha Airport.

Other Public Transportations

Taxi fare from the hotel to Naha Airport is about 25,000 JPY. We recommend you to reserve a taxi by the day before.
For route buses, please walk for 15 minutes up to the bus stop “OKUMA beach IRIGUCHI” (see map below) and take 67 local bus bound for Nago Bus Terminal. Then, take 111 Expressway bus bound for Naha Airport. Total fare of route buses from the hotel to Naha Airport is about 3,200 JPY.

Way to the nearest route-bus stop “OKUMA Beach IRIGUCHI”

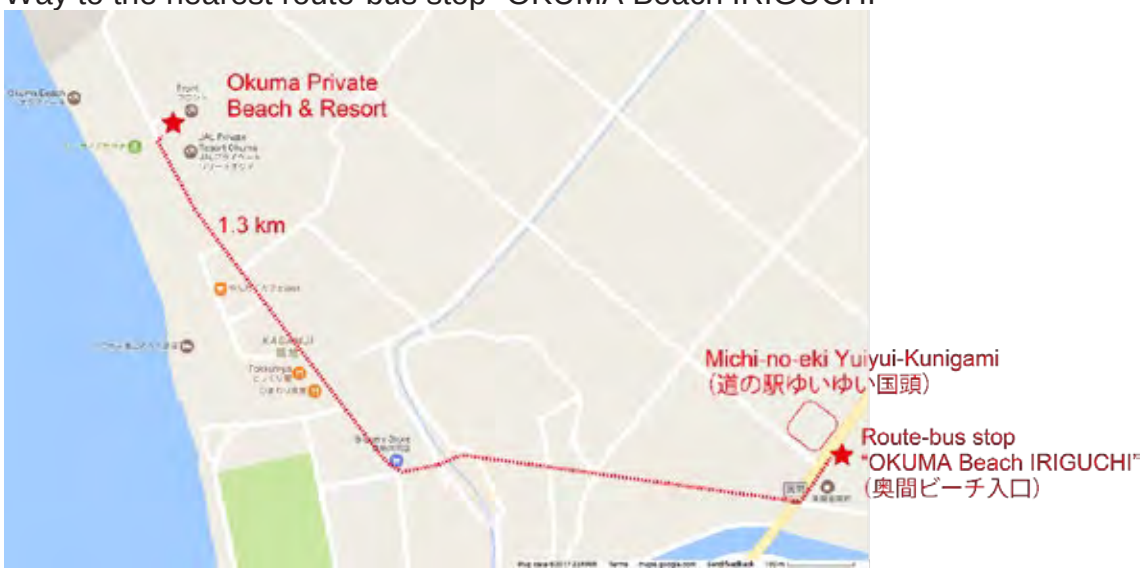

Time table of public route buses

67 local bus (Monday–Friday)	
OKUMA Beach IRIGUCHI	NAGO Bus terminal
6:24	7:16
7:04	7:56
7:29	8:20
8:04	8:56
8:34	9:26
9:09	10:01
10:04	10:56
10:34	11:26
11:19	12:11
12:19	13:11
13:24	14:16
14:24	15:16
15:24	16:16
16:24	17:16
17:19	18:11
17:54	18:46
18:34	19:26
19:14	20:06

http://www.kotsu-okinawa.org/en/time/67_72_73/n1.htm

http://www.kotsu-okinawa.org/en/time/111/n1.htm

111 Expressway (Monday–Sunday)		
NAGO Bus terminal	NAHA KUKO KOKUNAISEN Terminal (Naha Airport, Domestic)	NAHA KUKO KOKUSAISEN Terminal (Naha Airport, International)
5:45	7:26	7:29
6:15	7:56	7:59
6:45	8:26	8:29
7:30	9:11	9:14
8:20	10:01	10:04
8:50	10:31	10:34
9:20	11:01	11:04
9:50	11:31	11:34
10:15	11:56	11:59
10:45	12:26	12:29
11:15	12:56	12:59
11:45	13:26	13:29
12:30	14:11	14:14
13:00	14:41	14:44
13:30	15:11	15:14
14:00	15:41	15:44
14:30	16:11	16:14
15:00	16:41	16:44
15:45	17:26	17:29
16:45	18:26	18:29
17:30	19:11	19:14
18:00	19:41	19:44

Hotel Map


Okuma Private Beach & Resort
(JAL Private Resort Okuma)
Hibiscus – EDGE Meeting Room (Orals)
Fountain (1F) – EDGE Registration Desk
Surfside Café (1F) – Breakfast, Lunch & Dinner
OKUMA Eco-Museum – Posters
Main Cottage
Main Cottage Deluxe
Grand Cottage
Garden Villa
Palm Cottage
Entrance Hall
Parking Area
Beach Café OASIS
Lounge SHIOKAZE
Caution
Look to right, left and right again before crossing the street.
Beach Side Restaurant – Banquet on Thursday
Prohibited to enter this area
N
E
S
W

EDGE2017 Organizing Committee

Program Chairs

Odile Stephan (Université Paris, France)
Peter Crozier (Arizona State University, USA)

Organizing Committee

Michel Bosman (Institute of Materials Research and Engineering, Singapore)
Peter Crozier (Arizona State University, USA)
Joanne Etheridge (Monash University, Australia)
Koji Kimoto (NIMS, Japan)
Gerald Kothleitner (Graz University of Technology)
Lena F. Kourkoutis (Cornell University)
Ondrej Krivanek (NION, Arizona State University, USA)
Quentin Ramasse (SuperSTEM, UK)
Odile Stephan (Université Paris, France)
Peter van Aken (Max Planck Institute for Solid State Research, Germany)
Maria Varela del Arco (ORNL, Complutense University of Madrid, USA/Spain)
Benedicte Warot-Fonrose (CEMES-CNRS, France)

Local Organizing Committee

Koji Kimoto, Jun Kikkawa, Takuro Nagai,
Shogo Koshiya, Shunsuke Yamashita (NIMS, Japan)
Hiroki Kurata, Mitsutaka Haruta (Kyoto University, Japan)
Masami Terauchi, Yohei Sato (Tohoku University, Japan)
Teruyasu Mizoguchi (The University of Tokyo, Japan)

JTB GMT

Nobuyuki Kato

Okuma Private Beach & Resort

Kenji Kamio
Yoshiki Nakamatsu
Takaaki Nakao

Final Program

Sunday 14 May

21:00–21:45		**Plenary Lecture: Sumio Iijima** Structure Characterization of Electron-Beam-Sensitive One-Dimensional Nanomaterials

Monday 15 May

9:00–10:30		**Advances in Instrumentation and Data Processing I – Chairman: David McComb**
9:00– 9:30	T01-invited	Tracy Lovejoy – Invited Pushing the limits: toward 5 meV EELS and 1Å probes at low kV
9:30– 9:45	T02	Huolin Xin 5D Imaging of Multi-Element and Multi-Valence Material Evolution in In-Situ Environmental TEM by On-the-fly and *Quantitative* STEM-EELS Tomography
9:45–10:00	T03	Paolo Longo Advantages of Direct Detection and Electron Counting for Electron Energy Loss Spectroscopy Data Acquisition
10:00–10:15	T04	Renu Sharma Hybrid transmission electron microscope: An integrated platform for in situ imaging and spectroscopies
10:15–10:30	T05	Xiaoyan Zhong Quantitative Experimental Determination of Site-specific Magnetic Structures and Magnetization Curve by Transmitted Electrons
10:30–11:00		**Coffee Break (30min)**
11:00–12:30		**Advances in Instrumentation and Data Processing II – Chairman: Juan Carlos Idrobo**
11:00–11:30	T06-invited	Florent Houdellier – Invited Developments of cold field emission source (CFEG): from higher brightness to ultrafast emission
11:30–11:45	T07	Heiko Müller Correction of the chromatic and spherical aberration in low-voltage TEM enabling EFTEM with large energy windows
11:45–12:15	T08-invited	Damien McGrouther – Invited Opening up new paradigms for imaging in TEM & STEM through hybrid pixel detectors

12:15–12:30	T09	David A. Muller New Science Enabled by Recording Every Electron at STEM speeds with an Electron Microscope Pixel Array Detector (EMPAD)
12:30–13:00		**Discussion** **Leaders: David McComb and Juan Carlos Idrobo**
13:00–14:00		**Lunch (1h)**
13:00–15:45		**Afternoon free for discussion (1h 45min)**
15:45–17:30		**Beyond Traditional Spectroscopy and Imaging I – Chairman: David Muller**
15:45–16:15	T10-invited	Claus Ropers – Invited Free-electron Quantum Optics studied by Ultrafast Transmission Electron Microscopy
16:15–16:30	T11	Masami Terauchi SXES study of electronic structure of sodium borosilicide $Na_8B_{74.5}Si_{17.5}$
16:30–16:45	T12	Giulio Guzzinati Controlling the phase of electron beams for the (symmetry-)selective detection of plasmonic resonances.
16:45–17:00	T13	Makoto Kuwahara Time-resolved TEM-EELS using a pulsed beam extracted from a semiconductor photocathode
17:00–17:30	T14-invited	Luiz. H. G. Tizei – Invited Cathodoluminescence temporal statistics: single photon emitters and lifetime measurements at nanometer scales
17:30–18:00		**Coffee Break (30min)**
18:00–18:30		**Beyond Traditional Spectroscopy and Imaging II – Chairman: David Muller**
18:00–18:30	T15-invited	Johannes Jobst – Invited Nanoscale spectroscopy with low energy electrons
18:30–20:00		**Posters Oral Summaries – Chairman: Peter Crozier** **1 minute/1 slide presentations of posters 1 – 60**
20:00–21:30		**Dinner (1h 30min)**
21:30–23:00		**Poster (1h 30min)**

Tuesday 16 May

9:00–10:15		**Very High Energy Resolution EELS I – Chairman: Ian Maclaren**
9:00– 9:30	T16-invited	Maureen Joel Lagos – Invited Mapping surface and bulk phonon modes in a single nanostructure
9:30– 9:45	T17	Peter Tiemeijer Sub 30meV in the monochromated Themis
9:45–10:00	T18	Quentin Ramasse Triple-axis vibrational spectroscopy in the electron microscope: theory and experiment
10:00–10:15	T19	Christian Dwyer Increasing the spatial resolution of vibrational EELS
10:15–10:30		**Discussion** **Leaders: Ian MacLaren and Ondrej Krivanek**
10:30–11:00		**Coffee Break (30min)**
11:00–12:30		**Materials and Biological Applications I – Chairman: Joanne Etheridge**
11:00–11:30	T20-invited	Lena Kourkoutis – Invited Spectroscopic mapping at cryogenic temperature
11:30–11:45	T21	David W. McComb Optoelectronic properties of organic photovoltaic materials determined via high-resolution monochromated electron energy-loss spectroscopy
11:45–12:00	T22	Catriona M. McGilvery Probing chemical pathways in polyamide reverse osmosis membranes
12:00–12:15	T23	Vesna Srot Investigation of sensitive hybrid organic-inorganic materials by analytical (S)TEM
12:15–12:30	T24	Sean M. Collins Low-dose EELS for ‘thick’ samples: Model-based and machine learning approaches to remove multiple scattering
12:30–13:00		**Discussion** **Leaders: Joanne Etheridge and David Muller**
13:00–14:00		**Lunch (1h)**
13:00–16:00		**Afternoon free for discussion (2h)**

16:00–17:30		**Advances in Theory I – Chairman: Christian Dwyer**
16:00–16:30	T25-invited	Les Allen – Invited Modelling imaging and energy-loss spectra due to phonon excitation
16:30–16:45	T26	Jan Rusz Addressing the accuracy of z-locality approximation in simulations of inelastic electron scattering
16:45–17:00	T27	Ray Egerton Properties of the point-spread function for valence-electron and vibrational-mode inelastic scattering
17:00–17:30	T28-invited	Javier Aizpurua – Invited Probing low-energy hyperbolic polaritons in van der Waals crystals with an electron microscope
17:30–18:00		**Coffee Break (30min)**
18:00–19:30		**Posters Oral Summaries – Chairman: Peter Crozier** **1 minute/1 slide presentations of posters 61 – 120**
19:30–21:00		**Dinner (1h 30min)**
21:00–23:00		**Poster (2h)**

Wednesday 17 May

9:00–10:15		**Advances in Theory II – Chairman: Quentin Ramasse**
9:00– 9:30	T29-invited	Lorenzo Pardini – Invited From orbital mapping to core and valence excitations: a theorist's perspective
9:30– 9:45	T30	Philippe Moreau A hybrid method based on WIEN2k and VASP codes to calculate the complete set of EELS edges in a hundred-atoms system
9:45–10:00	T31	Guillaume Radtke Ab initio vibrational electron energy loss spectroscopy
10:00–10:15	T32	Motofumi Saitoh First principles calculations of electron near edge structures of Li-ion battery materials
10:15–10:30		**Discussion** **Leaders: Christian Dwyer and Quentin Ramasse**
10:30–11:00		**Coffee Break (30min)**

11:00–12:30		**Materials and Biological Applications II – Chairman: Matthieu Bugnet**
11:00–11:30	T33-invited	Gianluigi Botton – Invited Understanding the Properties of Functional Materials with High-Resolution Electron Energy Loss Spectroscopy
11:30–11:45	T34	Demie Kepaptsoglou Oxygen sub-lattice ordering in A-site deficient perovskites through monochromated core-loss EELS mapping
11:45–12:00	T35	Nicolas Gauquelin Applications of Electron microscopy imaging and spectroscopy to understand structure-properties relationships in complex functional materials
12:00–12:15	T36	Ming-Wen Chu Hidden lattice instabilities as origin of the conductive interface between insulating $LaAlO_3$ and $SrTiO_3$
12:15–12:30	T37	Yohei Sato Carrier electron behavior of Cs doped WO_3 in NIR region studied by momentum transfer resolved EELS
12:30–13:00		**Group photo**
13:00–14:00		**Lunch (1h)**
14:00–18:00		**Social event (4h)**
19:00–20:30		**Dinner (1h 30min)**
20:30–21:00		**Very High Energy Resolution EELS II – Chairman: Ondrej Krivanek**
20:30– 21:00	T38-invited	Kazu Suenaga – Invited Is the atomic resolution monochromated EELS really useful?
21:00–23:00		**Poster (2h)**

Thursday 18 May

9:00–10:30		**Spectroscopic Imaging – Chairman: Robert Klie**
9:00– 9:30	T39-invited	Gerald Kothleitner – Invited EELS and X-ray spectroscopic STEM imaging in 2D and 3D

9:30– 9:45	T40	Pascale Bayle-Guillemaud Nanoscale Chemical Evolution of Silicon Negative Electrodes Characterized by Low-Loss STEM-EELS
9:45–10:00	T41	Eric Prestat STEM-EELS study of carbon doping in ferromagnetic Ge_3Mn_5 layers for spin injection
10:00–10:15	T42	Andrew B. Yankovich Surface plasmon measurements using EELS – improving signal to noise ratio and revealing nanostructure coupling phenomena
10:15–10:30	T43	Hikaru Saito Angle-resolved cathodoluminescence spectroscopy for bandgap-based plasmonic structures
10:30–11:00		**Coffee Break (30min)**
11:00–12:30		**Materials and Biological Applications III – Chairman: Peter van Aken**
11:00–11:15	T44	Duncan Alexander Nanofabrication and fast STEM-EELS for systematic studies of plasmon resonances and mode coupling in metallic heterodimers
11:15–11:30	T45	Franz-Philipp Schmidt Hybrid plasmonics: From plasmon-plasmon to plasmon-exciton coupling
11:30–11:45	T46	Junhao Lin Probing the band structure modification in perovskite nanocrystals by low-voltage monochromatic electron energy loss spectroscopy
11:45–12:00	T47	Michael K. Kinyanjui Electronic excitations and molecular orientation in the charge density wave material 1T-TaS_2 intercalated with organic molecules.
12:00–12:30		**Discussion** **Leaders: Peter van Aken and Matthieu Bugnet**
12:30–13:30		**Lunch (1h)**
13:30–16:00		**Afternoon free for discussion (2h 30min)**
16:00–17:00		**Materials and Biological Applications IV – Chairman: Benedicte Warot-Fonrose**
16:00–16:15	T48	Matthieu Bugnet Combining EELS and HRTEM in operando analyses of ceria
16:15–16:30	T49	Robert F. Klie In-Situ Materials Characterization at High Spatial Resolution: 2D Materials Based Liquid-Cell Microscopy

16:30–16:45	T50	Juan Carlos Idrobo Novel Spectroscopy in Aberration-Corrected and Monochromated STEM
16:45–17:00	T51	Rhonda Stroud The Universe is my nano-fab: STEM-EELS-EDX analysis of planetary materials and synthetic analogs
17:00–17:30		**Coffee Break (30 min)**
17:30–18:30		**Phase Contrast Imaging and Diffraction – Chairman: Michel Bosman**
17:30–18:00	T52-invited	Naoya Shibata – Invited Aberration-Corrected Differential Phase Contrast Scanning Transmission Electron Microscopy
18:00–18:15	T53	Eric Van Cappellen New STEM strategies at FEI
18:15–18:30	T54	Joanne Etheridge Mapping the Angular and Spatial Dependence of Phonon Scattering using LACBED
18:30–19:00		**General discussion / prospectives / Conclusion**
19:00–21:00		**Banquet (2h)**

List of Poster Presentations

P001	Influences of geometric aberrations in post-specimen lens system on energy resolution of monochromated EELS Mukai M. Morishita S Sawada H. Maruyama S. Suenaga K.
P002	Valence EELS investigation on $GeSe_xTe_{1-x}$ phase change material Zhang S. Mio A. Cagnoni M. Cojocaru-Mirédin O. Wuttig M. Scheu C.
P003	Monochromated STEM-EELS as a THz electrical probe Bosman M.
P004	Scattering-vector dependent EELS of $LiCoO_2$ Kikkawa J. Mizoguchi T. Nagai T. Kimoto K.
P005	Probing graphitic carbon nitrides via monochromated EELS Haiber D.M. Aoki T. Crozier P.A.
P006	Retrieving the chemical composition of transition metal oxide core/shell nanoparticles Ruiz-Caridad A. Torruella P. López-Conesa L. Gómez-Roca A. Nogués J. Estradé S. Peiró F. Walls M.G.
P007	Nanoscale probing of bandgap states from oxide particles using monochromated STEM EELS Liu Q. Bowman W.J. March K. Crozier P.A.
P008	Particle Shape Effects in Vibrational EELS Kordahl D.D. Dwyer C.
P009	Characterization of individual 1D materials by monochromated STEM Senga R. Pichler T. Suenaga K.
P010	EELS analysis of bonding in quantum computing materials Hudak B. M. Song J. Snijders P. C. Lupini A. R.
P011	High resolution spectroscopy of lithium fluoride March K. Rez P.
P012	Probing Interfacial Effects with Vibrational Electron Energy-Loss Spectroscopy Venkatraman K. Liu Q. March K. Aoki T. Rez P. Crozier P.A.
P013	Understanding guided light modes in oxide nanoparticles with monochromated EELS Liu Q. Quillin S.C. Masiello D.J. Crozier P.A.
P014	Detection of Hydrogen-Oxygen Bonds with Vibrational EELS Crozier P.A. Liu Q. Aoki T.
P015	Characterisation of graphitic carbon nitride single-atom catalysts across the energy loss spectrum, real space and reciprocal space Leary R.K. Collins S.M. Johnstone D.N. Furnival T. Chen Z. Mitchell S. Vorobyeva E. Nicholls R.J. Schusteritsch G. Pickard C.J. Thomas J.M. Pérez-Ramírez J. Ramasse Q.M. Midgley P.A.
P016	Gap Measurements via Monochromated Low-loss EELS on Atomically thin $Mo_xW_{(1-x)}S_2$ Nanoflakes Pelaez-Fernandez M. Suenaga K. Arenal R.

P017	Low dose acquisition of pseudo atomic column elemental map by 2D STEM moiré method Kondo Y. Fukunaga K. Okunishi E. Endo N.
P018	Quantifying the carrier distribution in hole-doped cuprates using atomic resolution near-edge structures: the case of $Ca_{11}Sr_3Cu_{24}O_{41}$ Bugnet M. Löffler S. Hawthorn D. Sawatzky G. Schattschneider P. Radtke G. Botton G.A.
P019	Distribution of hole in $La_{2-x}Sr_xCuO_4$ Haruta M. Fujiyoshi Y. Nemoto T. Ishizuka A. Ishizuka K. Kurata H.
P020	Dopant Size Effects on Interfacial Superconductivity in Lanthanum Cuprate Bilayers van Aken P. A. Suyolcu Y. E. Wang Y. Baiutti F. Gregori G. Cristiani G. Sigle W. Maier J. Logvenov G.
P021	Angular Resolved Electron Energy Loss Spectroscopy in hexagonal Boron Nitride Fossard F. Sponza L. Schué L. Ducastelle F. Barjon J. Loiseau A.
P022	Dimensionality effects in hBN probed by cathodoluminescence Schué L. Plaud A. Fossard F. Sponza L. Ducastelle F. Barjon J. Loiseau A.
P023	Unexpected huge atomic dimerization ratio in 1D carbon chains and atom-by-atom spectroscopy studies Lin Y.C. Morishita S. Koshino M. Yeh C.H. Teng P.Y. Chiu P.W. Sawada H. Suenaga K.
P024	Exciton and Plasmon Mapping at the Nanoscale Nerl H.C. Winther K.T. Hage F.S. Thygesen K.S. Houben L. Ramasse Q.M. Nicolosi V.
P025	Plasmonic nanowire arrays as a platform for photocatalytic testing Cottom J. Abellan P. Hage F. Ramasse Q. Critchley K. Brydson R.
P026	Mapping of Sn dopant in hematite photoanodes by STEM-EELS and atom probe tomography Zhang S. Li T. Gault B. Hufnagel A.G. Hoffmann R. Fattakhova-Rohlfing D. Bein T. Scheu C.
P027	Investigating molecular-plasmon interactions in chemically functionalized metal nanoparticles using monochromated EELS Abellan P. El-Khoury P.Z. Hage F.S. Cottom J. Joly A.G. Hess W.P. Brydson R. Ramasse Q.M.
P028	Near-Field Plasmon Resonances Near Poorly Plasmonic Materials Yazdi S. Swearer D.F. Daniel J.R. Boudreau D. Ringe E.
P029	Atomic-scale spectroscopic imaging of phase transformation in perovskite oxide heterostructures Baek D.J. Lu D. Hikita Y. Hwang H.Y. Kourkoutis L.F.
P030	Atomic-resolution STEM-EELS analysis of the interfaces in ferroelectric tunnel junctions Nagai T. Yamada H.
P031	Spatially resolved energy-loss mapping at magic angle conditions Alexander D.T.L. Fave L. Dennenwaldt T. Hébert C.

P032	Low-voltage Cc-corrected energy-filtered TEM: evaluation, first experiments and image simulation Mohn M.J. Biskupek J. Lee Z. Rose H. Kaiser U.
P033	EELS study of Nanocross: A super tunable plasmonic system Das P. Martins H.L. Tizei L. Kociak M.
P034	Extreme UV plasmonics: Localized surface plasmon resonances in 3D nanovoids Zhu Y. Nakashima P.N.H. Funston A.M. Bourgeois L.N. Etheridge J.
P035	Absolute Quantification of Nanoscale Precipitates in Steels MacLaren I. Sala B. Craven A.J.
P036	Surface plasmon resonances in crossed silver nano-rods by HREELS Fujiyoshi Y. Kurata H.
P037	Cathodoluminescence Measurements of CdTe in the Transmission Electron Microscope Yang W.D. Yoon Y. Gaury B.H. Haney P.M. Zhitenev N. Sharma R.
P038	Pseudo atomic column mapping of silicon using STEM-moiré method, reconstructed with K and L electrons detected by EELS & EDS Okunishi E. Kondo Y.
P039	Probing the internal atomic charge density distribution in real-space by aberration-corrected differential phase contrast. Sánchez-Santolino G. Lugg N. R. Seki T. Ishikawa R. Findlay S. D. Kohno Y. Kanitani Y. Tanaka S. Tomiya S. Ikuhara Y. Shibata N.
P040	Revealing more while damaging less: exploiting multi-frame EDX & EELS spectroscopy acquisition and post-processing tools. Jones L. Varambhia A. Wenner S. Holmestad R. Nellist P. D.
P041	Optimising the coupling a spectrometer to a TEM/STEM for high loss EELS MacLaren I. Black C. McFadzean S. Craven A.J. Sawada H.
P042	Orbital Angular Momentum in the Electron Microscope Hachtel J.A. Cho S.Y. Davidson II R.B. Haglund R.F. Pantelides S.T. Chisholm M.F. Lawrie B.J. Idrobo J.C.
P043	Advances in Electron Energy Filters and Spectrometers at Gatan Twesten R.D. Trevor C.G. Menon N.K. Barfels M.M.G. James E.M. Thomas P.J. Longo P. Gubbens A.J.
P044	2D detectors for electron energy loss spectroscopy and STEM imaging Krivanek O.L. Bleloch A.L. Bacon N.J. Corbin G.J. Dellby N. Hoffman M.V. Lovejoy T.C.
P045	Noise Reduction by Improving Dark-Reference Images Heil T. Tatlock G.J.
P046	Improvement of effective solid angle using virtual-pivot holder and large EDS detector Koshiya S. Kimoto K.
P047	Automatic spectral imaging analysis based on machine learning Shiga M. Muto S.
P048	Low-temperature study of interfacial coupling of octahedral distortions in $La_{0.5}Sr_{0.5}CoO_{3-\delta}$ /$SrTiO_3$ Rui X. Walter J. Leighton C. Klie R.F.

P049	Measuring Orbital Angular Momentum (OAM) and Torque Transfer from Polarization Vortices with a Pixel Array Detector Nguyen K.X. Purohit P. Yadav A. Tate M.W. Ramesh R. Gruner S.M. Muller D.A.
P050	ALS-MCR application for Diffraction imaging data Uesugi F. Koshiya S. Mitsuishi K. Kimoto K.
P051	Revisiting EELS Characterization and its Coupling with Raman Spectroscopy: Chemical Inhomogeneities at the Nanoscale of DLC Thin Films Lajaunie L. Pardanaud C. Arenal R.
P052	STEM SI Warp: a Digital Micrograph script tool for warping the image distortions of atomically resolved spectrum images Wang Y. Salzberger U. Srot V. Sigle W. van Aken P.A.
P053	Two-dimensional Gaussian Fitting for Accurate Lattice Constant Measurement from Selected Area Diffraction Map Bekarevich R. Mitsuishi K. Ohnishi T. Uesugi F. Takeguchi M. Inaguma Y. Ohno T. Takada K.
P054	Magnetic-field-free STEM tomography for ferromagnetic materials Hasezaki K.L. Saito H. Sannomiya T. Miyazaki H. Gondo T. Miyazaki S. Hata S.
P055	Bi-orthogonality allows observation of self-hybridization in plasmonic system Lourenço-Martins H. Das P. Tizei L.H.G. Weil R. Kociak M.
P056	The calculations of EELS and ion transfer properties based on the density functional theory for the degenerated layered rock salt cathode material of lithium ion battery. Segi T. Kano K. Takagishi Y. Tsubota T. Yamaue T.
P057	Multislice simulations for relativistic beam electrons incorporating atomic inner-shell ionizations Majert S. Kohl H.
P058	Reconstruction and interpretation of ELNES using sparse representation Kiyohara S. Mizoguchi T.
P059	Theoretical and numerical investigation of the interaction between phase-shaped electron probes and plasmonic modes Lourenço-Martins H. Guzzinati G. Verbeeck J. Kociak M.
P060	Hidden Antipolar Order Parameter: Structural Screening for the Charged Domain Walls in Hybrid Improper Ferroelectrics $(Ca,Sr)_3Ti_2O_7$ Lee M. H. Chang C.-P. Huang F.-T. Guo G. Y. Gao B. Chen C. H. Cheong S.-W. Chu M.-W.
P061	Strong excitonic interaction in O-K edge of Perovskite oxides Tomita K. Miyata T. Mizoguchi T.
P062	BN nanosheets: layer counting by EELS and stacking sequence determination by HAADF imaging Casillas G. Mitchell D.R.G. Khan M.H. Huang Z.
P063	Determination of the internal structure of a new line defect by EELS Jeong J. S. Topsakal M. Xu P. Jalan B. Wentzcovitch R.M. Mkhoyan K. A.

P064	EMCD : last developments for in situ magnetic transition and rare earth investigation Fu X. Serin V. Warot-Fonrose B.
P065	EELS Probing of lithium based 2-D battery compounds processed by liquid phase exfoliation Pokle A. Coelho J. McGuire E. Downing C. Casey P. Park S. Nicolosi V.
P066	Development of low dose cryo-EELS toward organic molecules structure analysis Maigné A. Schreiber M.T. Wolf M.
P067	Combined EELS/DFT characterization of the surface functionalization of Ti_3C_2 2D-sheets: from local coordination to optical properties. Magné D. Mauchamp V. Bugnet M. Célérier S. Chartier P. Botton G. Cabioc'h T.
P068	EELS as tool to assess microscopic properties of Bismuth Oxide Torruella P. Coll C. Martín G. López-Conesa L. Vila M. Díaz-Guerra C. Varela M. Ruiz-González M.L. Piqueras J. Estradé S. Peiró F.
P069	From Atomic-Scale Ordering to Materials Properties: Aberration-Corrected STEM, Spectroscopy, and Simulation Esser B. D. Smith T.M. Antolin N. Carlsson A. Williams R.E.A. Wessman A. Hanlon T. Fraser H.L. Windl W. Mills M.J. McComb D.W.
P070	Atomic Configuration of Functionalized Carbon Nanotubes probed via Spatially-Resolved EELS Arenal R.
P071	Momentum-resolved low-loss EELS of 2D heterostructures – experiments and simulations Mohn M.J. Hambach R. Wachsmuth P. Kaiser U.
P072	Probing emerging 2D transition metal dichalcogenides (TMDs) and integrated hetero-structures down to atomic scale Kim M.J. Wang Q. Oviedo J.
P073	The electronic structure of nanostructured bcc-CuCr thin films Liebscher C.H. Freysoldt C. Dennenwaldt T. Harzer T. Dehm G.
P074	Electron energy loss spectroscopy study of P-type doped MoS_2 with sub-angstrom beam and ab-initio simulations Nicotra G. Deretzis I. Fisichella G. Piazza A. Agnello S. Greco G. Bongiorno C. Spinella C. La Magna A. Roccaforte F. Giannazzo F.
P075	EELS analysis of rare earth elements in geological samples Dennenwaldt T. Piet H. Badro J. Hébert C.
P076	Study on the atomic and electronic structure in CrN/AlN multilayers Zhang Z.L. Gu X. Holec D. Bartosik M. Mayrhofer P.H.
P077	Surface probing of oxide catalysts, theory and experiment Tileli V. Ahmad E.A. Mallia G. Webster R. Stoerzinger K. Shao-Horn Y. Harrison N.M.
P078	Probing the local electronic configurations in original tubular thermoelectric cobaltates Bocher L. Pelloquin D. Hébert S. Stéphan O. Gloter A.

P079	Linear plasmonic resonators Sigle W. Schubert I. Talebi N. Guo S. Toimil-Molares E. Vogelgesang R. Esmann M. Becker S.F. Lienau C. van Aken P.A.
P080	Atomic-scale interactions of hydrogen with Aluminum nanoparticles at room temperature Wang C. Yang W. Sil D. Agrawal A. Sharma R.
P081	Room Temperature CO Dissociation on Selective Edges of Gold Nanoparticles Yang W.D. Wang C. Sharma R.
P082	Effect of Ir doping at the $LaAlO_3/SrTiO_3$ interface studied by combined EELS and XPS analyses Lee M. Warot-Fonrose B. Arras R. Lippmaa M. Daimon H. Casanove M.J.
P083	Cryo-analytical STEM of dispersed nanoparticles Hondow N. Matar O. Brown A. Brydson R.
P084	Grain boundary diffusion processed (Nd,HREs)-Fe-B magnets studied by combined STEM and quantitative EELS analysis Šturm S. Žužek-Rožman K. Mehmood F. Ikram A. Soderžnik M. Kobe S.
P085	Fundamental insights into the operation of new non-volative memory devices using in-situ and monochromated STEM-EELS Bernier N. Delaye V. Cooper D. Dewolf T. McDermott E. Berthier R. Audoit G.
P086	Advanced STEM-EELS for nanotechnology and renewable energy research and development Delaye V. Bernier N.
P087	STEM investigation of charge and strain distributions at the ferroelectric – doped Mott insulator interfaces Li X. Garcia V. Marinova M. Rault J. Barthélémy A. Bibes M. Stéphan O. Colliex C. Gloter A.
P088	STEM and EELS investigation of graphene nanoribbon epitaxially grown over SiC Gloter A. Palacio I. Celis A. Nair M. Zobelli A. Sicot M. Malterre D. Berger C. de Heer W. Conrad E. Taleb-Ibrahimi A. Tejeda A.
P089	Mapping of Local Bonding States at Intact Solid-Liquid Interfaces Enabled by Cryo-FIB Lift-Out and Cryo-STEM EELS Zachman M.J. Tu Z. Archer L.A. Kourkoutis L.F.
P090	The intermediate phase in Li-ion battery cathode material $Li_{1-x}FePO_4$ investigated by valence electron energy loss spectra Kobayashi S. Fisher C.A.J. Kuwabara A. Ukyo Y. Ikuhara Y.
P091	TEM-EELS study on photo luminescent multi-shell nanoparticles Sato Y. Nakahigashi N. Uehara M. Terauchi M.
P092	An investigation of interface interaction of Silver-Ceria core-shell nanoparticles via energy electron loss spectroscopy and X-ray absorption spectroscopy. Tseng E. Chen S.Y. Gloter A.

P093	O K-edge fine structures in highly strained $BiFeO_3$ thin films to probe local lattice distortions Pailloux F. Pacaud J.
P094	Combined STEM-HAADF/ABF and EELS study of the Mn-based spinel and birnessite insertion cathode materials for Mg-ion battery Tchernychova E. Robba A. Gaberšček M. Dominko R.
P095	Direct Imaging of single atoms in ionic liquids and observation of their dynamics Miyata T. Mizoguchi T.
P096	Observation of insulin amyloid fibrils on graphene supporting films with low-voltage STEM in SEM Ogawa T. Gang G. Thieu M. Ahn S. Ha T. Cho B.
P097	The studies of electronic excitations in MoS_2 by EELS Wu C.T. Huang J.H. Hou T.H. Lee Y.J. Chu M.W.
P098	Understanding Photoluminescence (PL) in porous anodic alumina (PAA) using Electron Energy Loss Spectroscopy Jang J.H. Lee S. Lee J. Kim H.J. Cho S.Y. Kim J.W. Kim J.H. Bu S.D.
P099	Electron energy loss spectroscopy of infrared plasmonic antennas Konečná A. Sarriugarte P. Neuman T. Damková J. Govyadinov A. Chuvilin A. Aizpurua J. Hillenbrand R.
P100	In-situ observation of binodal type phase coarsening in glass. Nakazawa K. Amma S. Miyata T. Mizoguchi T.
P101	Electron irradiation effects on lithium peroxides Kikkawa J. Shiotsuki T. Koshiya S. Nagai. T Shimo Y. Nito T. Kimoto K.
P102	Momentum resolved EELS at high energy resolution: applications and practical considerations Hage F.S. Nicholls R.J. Hardcastle T.P. Scott A.J. Brydson R. Yates J.R. Refson K. Ramasse Q.M.
P103	Layer-dependent EELS spectra of atomically thin h-BN sheet Kawasaki N. Otsuka Y. Kondo D. Hayashi K. Sato S.
P104	Study of nanometer-scale gas bubbles in zirconium alloys Dumbill S. Hernandez-Maldonado D. Blackmur M.S. Gass M. Ramasse Q.M.
P105	Atomic structural and chemical investigations of misfit layered nanotubes Lajaunie L. Panchakarla L.S. Ramasubramaniam A. Tenne R. Arenal R.
P106	Revisiting Graphene Oxide Chemistry via Spatially-Resolved Electron Energy Loss Spectroscopy Tararan A. Zobelli A. Benito A.M. Maser W.K. Stéphan O.
P107	Investigation of vibrational behavior of gas using ELNES Katsukura H. Miyata T. Shirai M. Matsumoto H. Mizoguchi T.
P108	Collateral beam damage in aromatic small molecules for organic devices Goode A.E. Ramasse Q. Heutz S.
P109	Crystal Structure Analysis of Two-Dimensional Materials using Quantitative Annular Dard-Field Imaging Yamashita S. Koshiya S. Ishizuka K. Kimoto K.

P110	Improvement of dielectric function measurements on α-Al_2O_3 by 60kV and 200kV TEM-EELS Sakaguchi N. Tanda L. Kunisada Y.
P111	Magnetism and morphology in faceted B2-ordered FeRh nanoparticles Warot-Fonrose B. Liu M. Benzo P. Tang H. Castiella M. Tarrat N. Gatel C. Respaud M. Morillo J. Casanove M.J.
P112	Characterization of the electron beam damage of $Li_4Ti_5O_{12}$/Li_2TiO_3 model interface by electron energy loss spectroscopy. Kitta M. Tanaka S.
P113	Noble metal salts on two dimensional materials studied by atomic resolution STEM imaging Okuno H. Kalita D. Alvarez C. Benayad A. Prestat E. Raux E. Le Poche H. Dah M.T. Vergnaud C. Jamet M. Marty A. Pochet P. Dijon J.
P114	Probing core electron orbitals by STEM-EDX mapping Jeong J.S. Odlyzko M.L. Xu P. Jalan B. Mkhoyan K.A.
P115	Convergent-Beam EMCD: Pitfalls and New Approaches Löffler S. Schachinger T. Hetaba W.
P116	Robust extraction of magnetic signals at sub-nanometer resolution Spiegelberg J. Muto S. Rusz J. Ohtsuka M.
P117	Surface Plasmon Resonance Modes of Upright Split Ring Resonators Probed by EELS and CL Bicket I.C. Bellido E.P. Meuret S. Polman A. Botton G.A.
P118	Implementing electron energy gain spectroscopy in STEM Das P. Blazit J.-D. Tencé M. Tizei L. Colliex C. Stéphan O. Kociak M.
P119	Time-Dependent Excited State Response in Nanostructures Batson P.E. Konečná A. Lagos M.J. Aizpurua J.
P120	Vibrational EELS probes confined Fuchs-Kliewer modes Lourenço-Martins H. Kociak M.

Orals

Structure Characterization of Electron-Beam-Sensitive One-Dimensional Nanomaterials

Sumio Iijima

Graduate School of Science and Technology, Meijo University, 1-501, Shiogamaguchi, Tenpaku, Nagoya, Aichi, 4688502 JAPAN.

Recent electron microscopes have been greatly improved in spatial resolution, electron beam energy resolution and temporal resolution in terms of the instrumentation such as lens aberration correction and monochromatization of electron beam. However from the point of view of EB sensitive materials the progress is less important than overcoming the specimen irradiation damage as demonstrated in protein structure investigations such as biological macromolecule particles.

Comparing with organic materials structure analysis of inorganic ones is much easier in TEM observations but certain clay minerals containing particularly water molecules have hindered detailed investigations by TEM. The situation becomes even serious for poorly crystalized materials such as nanometer-sized particles or fibers. Carbon nanotubes (CNT) [1], chrysotile asbestos, and imogolite [2] are quasi-one-dimensional and can stand reasonably with EB irradiation and so investigated successfully.

Pseudoboehmite is Aluminum oxy-hydroxide gamma-AlOOH which is said to be poorly crystalized boehmite. It is a typical EB sensitive material and many researchers have tried to know its crystal structure in the past without convincing results. XRD and NMR methods are not useful for this material because of its poor crystallization. Pseudoboehmite forms into a variety of morphologies from a fibril, low-dimensional sheet, platelets, to bulk crystal, depending on a synthesis process. The fibril one is a quasi-one-dimensional fibril structure, which grows in an aqueous solution as a sol form. We have studied detailed morphology of this fibril boehmite and found that the fibril grows selectively parallel to the c-axis and does not form in a tubular structure but a nanometer-sized ribbon [3]. The growth was not promoted by a particular catalytic substance like carbon nanotubes so that such an anisotropic growth should be originated from the boehmite structure itself. This is an interesting area for colloid science.

References

[1] S. Iijima, *Nature* , **345**, (1991) 56.
[2] K. Wada et al., *Amer. Min.*, **54**, (1969) 50.
[3] S. Iijima, T. Yumura and Zheng Liu, *PNAS*,**113**, (2016) 11759.

Pushing the limits: toward 5 meV EELS and 1Å probes at low kV

T.C. Lovejoy[1], A.L. Bleloch[1], N. Dellby[1], M.V. Hoffman[1], M.T. Hotz and O.L. Krivanek[1,2]

[1] Nion, 11511 NE 118th St, Kirkland, WA, 98034, USA
[2] Department of Physics, Arizona State University, Tempe AZ 85287, USA

The ground-potential monochromator and a new EEL spectrometer developed by Nion are allowing <10 meV energy resolution EELS. This has greatly extended the capabilities of vibrational spectroscopy in the electron microscope, introduced just 3 years ago [1], which can now perform:

- damage-free identification of different hydrogen bonds in a biological sample [2]
- vibrational spectroscopy with sub-nm spatial resolution [3]
- probing atomic vibration modes at surfaces and edges of nano-objects, with nm-level spatial resolution [4].

This talk will cover recent advances in the aberration corrector, the monochromator and the spectrometer, and show examples of applications.

For imaging with a cold-field emission source and an objective lens with a chromatic aberration coefficient C_c of ~1 mm, the chromatic aberration limits the optimal aperture half-angles to less than 35 mrad at 60 kV primary voltage and below. The Nion monochromated system allows two approaches to overcoming the chromatic limit: (a) reduction of the energy spread of the primary beam via monochromation, and (b) correction of the aberration by sextupoles acting on an energy dispersed beam [5]. The first approach is typically more useful, as it leads to improved EELS data at the same time. Once chromatic aberration is no longer limiting, major improvements in the spatial resolution require the correction of geometric aberrations to half-angles of 50 mrad and higher. This is a problem to which the latest design of the Nion aberration corrector is well suited, because it offers complete correction of all major as well as parasitic aberrations up to $C_{5,6}$ [6].

As the EELS energy resolution approaches 5 meV, the requirements on the spectrometer increase substantially: correction of spectrometer aberrations (and of the aberrations of pre-spectrometer coupling lenses) up to 50 mrad half-angle and beyond (in the sample plane), and stabilities such that the image of the source projected into the EELS detection plane (which becomes the Zero Loss Peak) remains stable to within a small fraction of its diffraction limit. Satisfying these constraints will lead to an era of *diffraction-limited EELS*, in which opening up the spectrometer entrance angle will lead to *better* energy resolution, with ~1 meV energy resolution ultimately becoming possible.

References

[1] Krivanek O.L., et al., Nature, 514, 209 (2014)
[2] Rez P., et al., Nat. Comms. 7, 10945 (2016)
[3] Batson P.E., Lagos M.J., *in preparation*
[4] Dwyer C., et al., Phys. Rev. Lett. 117, 256101 (2016).
[5] Krivanek O.L. et. al., Phil. Trans. R. Soc. **A367** (2009) 3683-3697.
[6] Dellby N. et al., Micr. Microanal. **20** (Suppl 3, 2014), 928-929.

5D Imaging of Multi-Element and Multi-Valence Material Evolution in In-Situ Environmental TEM by On-the-fly and *Quantitative* STEM-EELS Tomography

Lili Han[1], Ruoqian Lin[1], Weiwei Xia[1], and Huolin Xin[1]

[1] Center for Functional Nanomaterials, Brookhaven National Laboratory, Upton, NY 11973, USA.

The spatial, compositional, bonding, and time-domain complexity of materials transformation under the solid/gas reaction, particularly with heterogeneous nucleation involved [1], highlights the need to increase the dimensionality of electron microscopy data sets beyond conventional projection imaging and the acquisition of image series, i.e. x-y-t. Because projection images can be misleading or inconclusive for complex material systems, it is much desired to include all three spatial coordinates, x, y, and z, into the data set without losing the time and energy resolution. However, a key stumbling block that had held back progress in achieving this is the rather slow process in acquiring both regular and chemical- and bonding-sensitive tomography data for the retrieval of depth and chemical information. In this talk, I will report the realization of fully *quantitative* STEM-EELS tomography, on-the-fly reconstruction, and the first attempt to achieve 5-D electron microscopy data sets under reaction conditions. The five-dimensional data sets visualize the oxidation of a bimetallic catalyst with unprecedented 3-D and chemical/bonding details and transform our understanding of adsorbate induced segregation in bimetallic systems. [2]

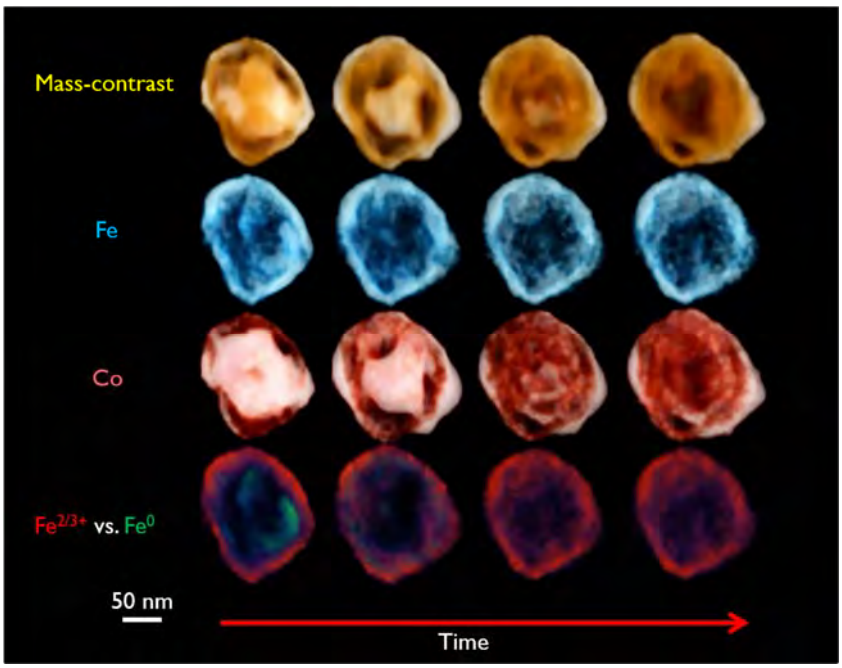

FIG. 1. 5D electron microscopy data (x, y, z, vs. Eloss vs. t) recorded in an environmental TEM tracking the oxidation process of a Co-Fe catalyst.

References

[1] L Han *et al*, HL Xin, Nature Communications, 7, 13335 (2016).

[2] Research carried out at the CFN/BNL, which is supported by the U.S. Department of Energy, Office of Basic Energy Sciences, under Contract No. DE-SC0012704.

Advantages of Direct Detection and Electron Counting for Electron Energy Loss Spectroscopy Data Acquisition

P. Longo[1], J.L. Hart[2], A.C. Lang[2], R.D. Twesten[1] and M.L. Taheri[2]

[1]Gatan Inc. 5794 W Las Positas Blvd, Pleasanton, CA, 94588, USA
[2]Drexel University, Philadelphia PA, 19104, USA

Transmission electron microscopes primarily employ indirect cameras (IDC) for electron detection in imaging, diffraction and EELS modes. Such cameras convert incident electrons to photons which, through a fiber optic network or lens, are coupled to a light sensitive camera. This indirect detection method typically has a negative impact on the point spread function (PSF) and detective quantum efficiency (DQE) of the camera. Over the last decade, radiation tolerant CMOS active pixel sensors, which directly detect high-energy incident electrons and have the speed to count individual electrons events, have been developed. These detectors result in greatly improved PSF and DQE in comparison to conventional IDCs. Such direct detection cameras (DDCs) have revolutionized the cryo-TEM field as well as have strong advantages for in-situ TEM in both imaging and diffraction applications.
EELS applications can benefit from the improved PSF and the ability to count electrons. The improved PSF allows spectra to be acquired over larger energy ranges while maintaining sharp features and greatly reduced spectral tails. The ability to count electrons nearly eliminates the noise associated with detector readout and greatly reduces the proportional noise associated with detector gain variations. This effectively leaves the shot noise as the limiting noise source present. The implication for EELS acquisition is that fine structure analysis becomes more straightforward for typical conditions and even possible for the case of low signal levels. To demonstrate, figure 1 shows a comparison between EELS spectra acquired using IDC and DDC detectors under identical probe, specimen and energy range conditions; the effect of the improved PSF and reduced noise are evident.
In this presentation, we will review the current state of electrons counting detectors for electron microscopy with an emphasis on system for EELS measurements.

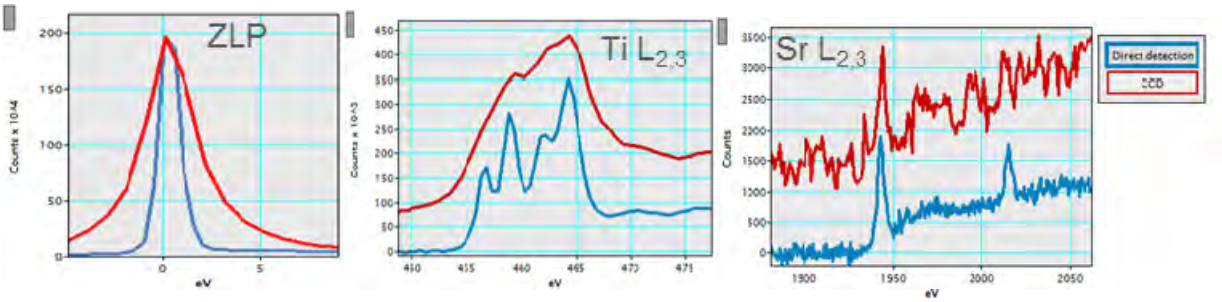

Figures. 1. a) ZLP spectra comparison. For both detectors, the spectrometer was setup with ~2000 eV energy range demonstrating the improved PSF and reduced tails; b) Ti $L_{2,3}$-edges comparison. The improved PSF is evident in the energy resolution of the DDC acquired spectrum allowing the observation of the fine structure present in the Ti edge which is typical of Ti in the oxidation state +4; c) Sr $L_{2,3}$-edges comparison. Due to the lower noise offered by electron counting, it is possible to observe both the L_2 and L_3 lines. Both the IDC and DDC sets of data were acquired from the same area in the specimen using identical microscope conditions and exposure time. (For all spectra, DDC is blue and IDC is red.)
NSF is greatly acknowledged for funding Drexel University for this project.

Hybrid transmission electron microscope: An integrated platform for in situ imaging and spectroscopies

Renu Sharma

Center for Nanoscience and Technology, National Institute of Standards and Technology, Gaithersburg, Maryland, USA

Environmental transmission electron microscopes (ETEM) and TEM holders with windowed reaction cells, both now commercially available, enable in situ measurements of the dynamic changes occurring during gas-solid and/or liquid-solid interactions. The combination of atomic-resolution images and high spatial and energy resolution has successfully revealed the nucleation and growth mechanisms for nanoparticles, nanowires, carbon nanotubes and the functioning of catalyst nanoparticles. While TEM-based techniques are ideally suited to distinguish between active and inactive catalyst particles and identify active surfaces for gas adsorption, we still must answer the following questions: (1) are our observations, made from an area a few hundred nanometers in extent, sufficiently representative to determine the mechanism for a particular reaction? (2) Is the reaction initiated by the incident electron beam? (3) Can we determine the sample temperature accurately enough to extract quantitative kinetic information? And (4), can we find efficient ways to make atomic-scale measurements from the thousands of images collected using a high-speed camera. The lack of global information available from TEM measurements is generally compensated for by using other, ensemble measurement techniques such as x-ray or neutron diffraction, x-ray photoelectron spectroscopy, infrared spectroscopy, Raman spectroscopy etc. However, it is almost impossible to create identical experimental conditions in two separate instruments to make measurements that can be directly compared.

We have designed and built a unique platform that allows us to concurrently measure atomic-scale and micro-scale changes occurring in samples subjected to identical reactive environmental conditions by incorporating a Raman Spectrometer into the ESTEM [1,2]. We have used this correlative microscopy platform i) to measure the temperature from a 60 μm^2 area using Raman shifts, ii) to investigate light/matter interactions in plasmonic particles iii) to act as a heating source, iii) to perform concurrent optical and electron spectroscopies such as cathodoluminescence, electron energy-loss spectroscopy (EELS) and Raman. We have developed an automatic image-processing scheme to measure atomic positions, within 0.015 nm uncertainty, from high-resolution images, to follow dynamic structural changes using a combination of algorithms publically available and developed at NIST. This method has been proven to capture the crystal structure fluctuations in a catalyst nanoparticle during growth of single-walled carbon nanotube (SWCNT). Details of the design, function, and capabilities of the optical spectrum collection platform and image processing scheme will be illustrated with results obtained during in situ measurements.

References

[1] Picher et al., *Ultramicroscopy.* 150 (2015) 10.
[2] Sharma and Mazzucco, US Patent:US9431211B2

Quantitative Experimental Determination of Site-specific Magnetic Structures and Magnetization Curve by Transmitted Electrons

X.Y. Zhong[1], Z.Q. Wang[1], H.B. Jiang[1], D. Pohl[2], V. Neu[2], R. Yu[1], Q. Zhan[3], H.G. Piao[4], J. Zhu[1], and B. Rellinghaus[2]

[1] National Center for Electron Microscopy in Beijing, School of Materials Science and Engineering, Tsinghua University, Beijing 100084, P.R. China
[2] IFW Dresden, Institute for Metallic Materials, Helmholtzstrasse 20, d-01069 Dresden, Germany
[3] Department of Material Physics and Chemistry, University of Science and Technology Beijing, Beijing 100083, China
[4] College of Science, China Three Gorges University, Yichang 443002, China

With the development of nanostructured magnetic materials and devices, the detection of magnetic information on the nanometer scale has increasingly become a major challenge. Electron Energy-loss Magnetic Chiral Dichroism (EMCD) technique is invented as a new route for detecting magnetic signals in a transmission electron microscope [1]. Compared with X-ray magnetic circular dichroism (XMCD), EMCD can easily achieve a higher spatial resolution down to the nanoscale [2,3].

Based on traditional EMCD, we developed site-specific EMCD method [3], and first experimentally demonstrate that the use of transmitted electrons allows us to quantitatively determine atomic site-specific magnetic structure information on a nanometer scale. From one $NiFe_2O_4$ nanograin in composite films, we extract its atomic site-specific magnetic circular dichroism spectra and achieve the quantitative magnetic structure information by constructively selecting the specific dynamical diffraction conditions in the experiments. We can reach a high spatial resolution, and get site-specific and element-specific magnetic information, as well as distinguish the orbital and spin magnetic moments. For example, we determined m_L/m_S ratios of Fe atoms in octahedral and tetrahedral sites. This work opens a door to meet the challenge of exploring the magnetic structures of magnetic materials at the nanoscale using transmitted electrons.

Recently, we have further achieved the measurement of magnetization curve in magnetic materials at a nanometer scale, using site-specific EMCD method. We have measured the magnetization curve of both iron and nickel atoms within an epitaxially grown $NiFe_2O_4$ nanograin that is laterally confined by neighboring $BiFeO_3$ grains. The magnetization data is shown to be in very good agreement with a simulated magnetization curve, which is calculated by micromagnetic simulation. The simulation took the structural details of the nanograin into account, thereby confirming the reliability of our method. Abundant information about microstructures, such as exchange bias effect, can be obtained and better understood based on our measurement. Our method thus has the potential to bridge the magnetization behavior and atomic structures of magnetic materials.

References

[1] P. Schattschneider et al., Nature 441 (2006) 486.
[2] J. Salafranca et al., Nano Lett. 12 (2012) 2499.
[3] Z. Q. Wang et al., Nat. Commun. 4 (2013) 1395.

Developments of cold field emission source (CFEG): from higher brightness to ultrafast emission

Florent Houdellier[1]

[1]CEMES-CNRS 29 Rue Jeanne Marvig, 31055 TOULOUSE, FRANCE, EU

Cold field emission gun are the brightest electron sources available for transmission and scanning electron microscopes, which exhibit the smaller intrinsic energy spread. Thanks to these properties, this well-known technology [1] remains the best choice when it come to deal with method requiring a high spatial or temporal coherence of the electron beam, like EELS, STEM or electron interferometry.
However, severe drawbacks are inherent to CFEG like the stability of the emitted current which, in the most favorable case, decreases by some 10%/hour, the beam noise (root mean square (rms) around 1%), etc. [2] To tackle these problems, the use of ultra high vacuum, careful high voltage conditioning and flash cleaning of the tip are mandatory.
By using a carbon cone nanotip (CCnT), we have succeeded to improve considerably the stability of the electron beam with almost no decay during 8 hours, and a noise rms lower than 0.5%, which avoids the use of flash cleaning [3]. An improvement of the reduced brightness has also been observed. I will present recent results, performed in close collaboration with Hitachi High Technology in Naka, and obtained using STEM and SEM equipped with this new source. Investigations of electron optical performance will also be discussed as well as the effect on the energy spread [4]. Finally, a new gun geometry specifically designed for this type of source will be presented.
Together with Arnaud Arbouet in CEMES, we have recently built a femtosecond time resolved CFE-TEM [5]. The biggest challenge of this project was the development of the ultrafast CFEG. I will show how CFEG technology needs to be deeply modified to achieve a femtosecond laser triggered emission of electrons, and present last results obtained with this modified CFE electron source.

[1] Crewe A.V., Eggenberger D.N.,Wall J., and Welter L.M. Electron Gun Using a Field Emission Source **Rev.Sci.Inst.** 39, 576–583, (1968).

[2] Shimoyama H., Ichihashi M., and Tonomura N. Emitter and electron gun. **J. Electron Microsc**. 38, S1–S9. (1989)

[3] Houdellier F., Masseboeuf A., Monthioux M., and Hÿtch M. J., New carbon cone nanotip for use in a highly coherent cold field emission electron microscope. **Carbon**, 50, 2037, (2012).

[4] Houdellier F., de Knoop L., Gatel C., Masseboeuf A., Mamishin S., Taniguchi Y., Delmas M., Monthioux M., Hÿtch M.J. and Snoeck E., Development of TEM and SEM high brightness electron guns using cold-field emission from a carbon nanotip. **Ultramicroscopy** , 151, 107-115, (2015)

[5] Arbouet A. and Houdellier F., USPTO No.US9,263,229 B2 of February 16.(2016)

Correction of the chromatic and spherical aberration in low-voltage TEM enabling EFTEM with large energy windows

H. Müller[1], M. Linck[1], F. Kahl[1], P. Hartel[1], J. Zach[1], S. Uhlemann[1], J. Biskupek[2], F. Börrnert[2], Z. Lee[2] , U. Kaiser[2], and M. Haider[1].

[1] Corrected Electron Optical Systems GmbH, D-69126 Heidelberg, Germany.
[2] Central Facility of Electron Microscopy, Ulm University, D-89081 Ulm, Germany.

The correction of the chromatic and the spherical aberration in low-kV TEM is useful to image beam sensitive materials consisting of light atoms [1,2]. Within the Sub-Ångstrøm Low-Voltage Electronmicroscopy (SALVE) project we have developed a novel dedicated low-voltage C_c/C_s-corrector. With this instrument at 40 kV an information limit of 90 pm could be achieved. This is only fifteen times the electron wavelength and corresponds to an effective optical aperture of 67 mrad [3].

Achromatic imaging in low-kV TEM enables the investigation of interface and defect structures with minimized knock-on specimen damage what was not possible before. For energy-filtered TEM it will enable large energy windows without noticeable degradation of optical resolution. This is encouraging for advanced EFTEM applications and in the near future may produce a demand for further improvements also in the area of in-column or post-column imaging energy filters.

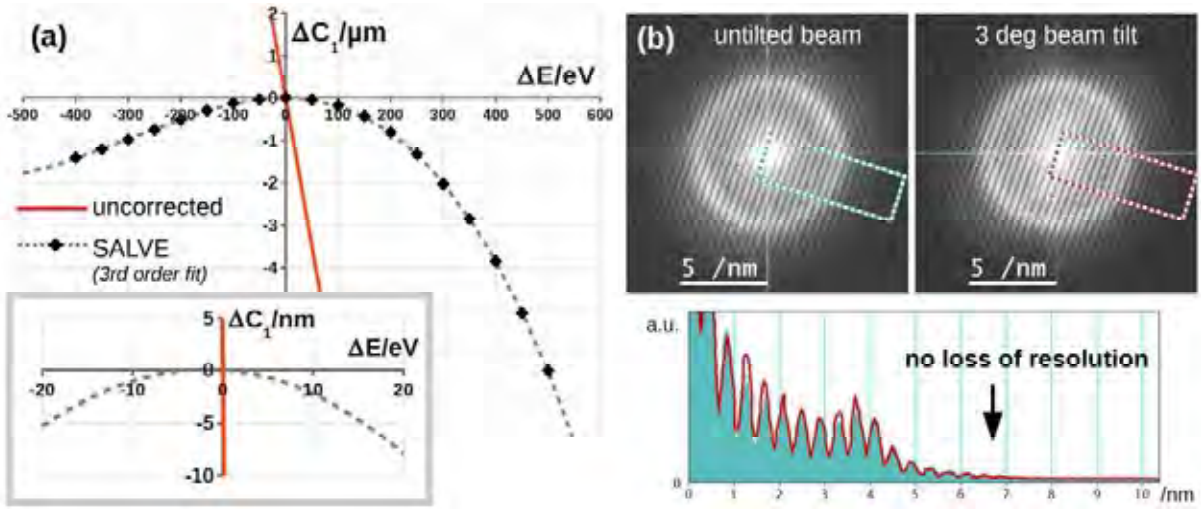

FIG. 1. (a) Change of defocus with energy for the Cc/Cs-corrected SALVE microscope (red line: uncorrected case, black dots: measured, dashed line: third-order fit). (b) Estimation of focus spread: The information transfer under axial illumination (solid profile) does not show any deterioration even under 3° (52.4 mrad) of beam tilt (red line in profile)

References

[1] Egerton, R. F., P. Li, and M. Malac. Micron 35.6 (2004): 399-409.
[2] Kaiser, U., et al. Ultramicroscopy 111.8 (2011): 1239-1246.
[3] Linck, M. et al. Physical Review Letters 117.7 (2016): 076101.

Opening up new paradigms for imaging in TEM & STEM through hybrid pixel detectors

D. McGrouther[1], M. Perreur-Lloyd[1], D. Maneuski[1], M. Nord[1], I. MacLaren[1], P.D. Nellist[2], R. Goldsbrough[3], A.I. Kirkland[2,4]

[1] School of Physics & Astronomy, University of Glasgow, G12 8QQ, United Kingdom.
[2] Department of Materials, University of Oxford,
[3] Quantum Detectors Ltd,
[4] Electron Physical Sciences Imaging Centre, Diamond Light Source Ltd, Didcot, Oxford, OX11 0DE.

Hybrid Pixel Detectors were developed to obtain high signal to noise detection of energetic particles in experiments at CERN. Implementations of this technology, such as Medipix3 [1], differ significantly from the current generation of direct imaging detectors. Comprising a thick (>100 µm) sensor and >1000 transistors per pixel, unambiguous on-chip counting and processing of single electron events is achieved with 1 MHz rate and zero detector noise.

We have investigated the application of hybrid pixel detection in three main areas of use. In TEM imaging we have assessed modulation transfer function (MTF) and detective quantum efficiency (DQE) response across a range of beam energies, finding that for 60-80 keV electrons the highest MTF and DQE response were achieved by on-chip Charge Summing Mode corrections [2]. We have applied the detector for 100-1000 fps filming dynamics of magnetic skyrmions. As a STEM detector, utilizing pixel dwell times 100-1000µs, 4D data sets have been routinely obtained allowing post-processing to reveal contrast from a multitude of detector geometries or via phase contrast (DPC/ptychographic). In a final theme, we have been investigating how detectors alone could enable imaging of material dynamics with timescales down to 10 ns in an otherwise unmodified instrument. In addition to research, we are collaborating with the electron Physical Sciences Imaging Centre & Quantum Detectors Ltd to develop this technology, via the MERLIN [3] platform.

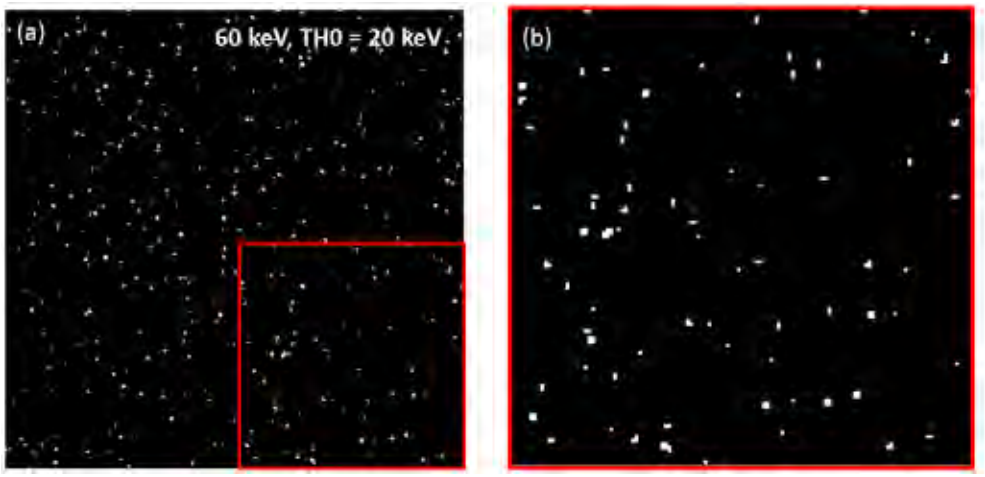

FIG. 1. (a) Single 60keV electron hits depositing energy above set threshold of 20keV (b) Enlarged detector region highlighting variation in hit shapes.

References
[1] R. Ballabriga et al., Nucl. Instr. Meth. Phys. Res. A **633** S15 (2011)
[2] J. A. Mir, et al., *submitted to Ultramicroscopy, December 2016*; arXiv:1608.07586
[3] http://quantumdetectors.com/merlin-for-em/

New Science Enabled by Recording Every Electron at STEM speeds with an Electron Microscope Pixel Array Detector (EMPAD)

David A. Muller[1], Kayla X Nguyen[1], Yimo Han[1], Zhen Chen[1], Michael Cao, Mark Tate[1] and Sol M. Gruner[1]

[1] Cornell University, Ithaca, NY 14853, USA

Complete information about the scattering potential of a sample is in principle encoded in the distribution of scattered electrons from a localized beam propagating through it. A new generation of high-speed, momentum-resolved electron microscope detectors brings us closer to realizing this general goal and in doing so enable new imaging modes spanning sub-Angstrom to multi-micron length scales. Most of these new detectors employ pulse counting architectures, designed for low-dose x-ray and biological imaging, but are poorly suited to diffraction applications, being limited to beam currents of less than ~0.1 pA/pixel by the transit time in the silicon sensor.

Our electron-microscope pixel array detector (EMPAD) developed at Cornell, overcomes this fundamental weakness of pulse counting with a high-speed, multiscale quantization architecture that preserves single electron sensitivity but in contrast also remains linear and unsaturated when exposed to the full electron beam [1]. Measuring complete diffraction patterns at 0.86 ms/frame with 30-bit dynamic range has proved useful for a wide range of quantitative applications including the imaging of strain fields in 2D materials, polarization vortices in ferroelectrics, and robust demonstrations of super-resolution imaging by full-field ptychography, where the full diffraction space is phased, not just the BF disk. This enables not only measurements of probability current flow that can be used to map electric and magnetic fields in the presence of diffraction contrast that foils DPC and earlier detectors, but also enables measurements of orbital angular momentum for any electron beam shape.

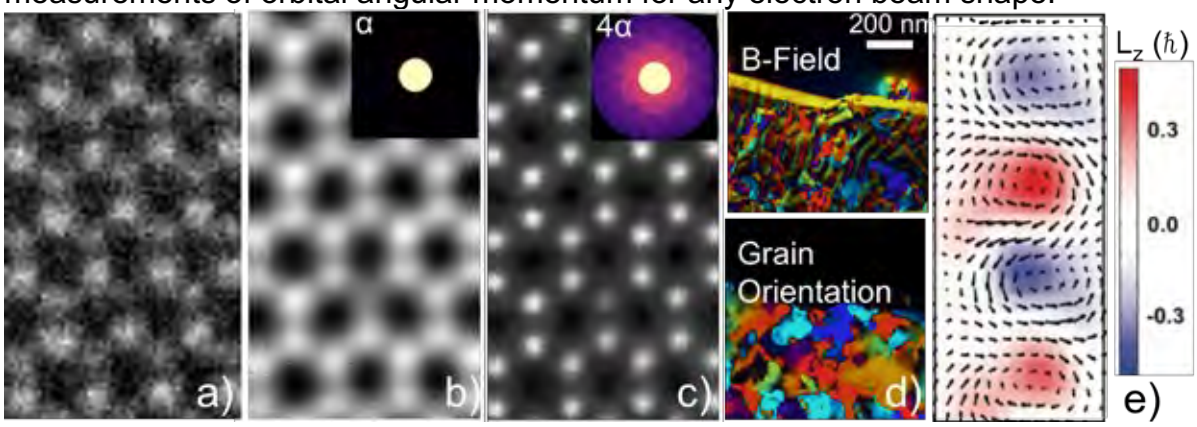

FIG. 1. Simultaneous a) ADF, b) BF-ptychography & c) Full-field pytochgraphy showing the resolution improvement in MoS_2 from using the full diffraction pattern. d) Separating magnetism & crystal structure for helices in FeGe at 100K. e) Orbital angular momentum changes from polarization vortices in a ferroelectric superlattice.

References

[1] M. W. Tate et al, "High Dynamic Range Pixel Array Detector for Scanning Transmission Electron Microscopy" *Micro. and Microanal.* **22**, 237-249 (2016)

[2] Research supported by US Dept of Energy, and Thermo Fisher Scientific. We thank E. Turgut, G. Fuchs, R. Ramesh, A. Yadav, S. Xie, J. Park for samples.

Free-electron Quantum Optics studied by Ultrafast Transmission Electron Microscopy

A. Feist, K. E. Priebe, S. V. Yalunin, S. Schäfer, and C. Ropers

4th Physical Institute – Solids and Nanostructures, University of Göttingen, Germany
Email: claus.ropers@uni-goettingen.de

Ultrafast Transmission Electron Microscopy (UTEM) is an emerging technique to study structural and electronic dynamics on the nanoscale. Besides its use as an analytical tool with simultaneous femtosecond temporal and nanometer spatial resolution [1], UTEM also provides for a unique test bench to study quantum optics phenomena with free electrons.

This talk will discuss several examples of free-electron beams interacting with optical near-fields at nanostructures, emphasizing quantum coherent processes. Specifically, for swift electrons traversing intense optical near-fields [2,3], we observe multilevel Rabi-oscillations on a ladder of quantized free-electron states [4], and implement Ramsey-type dual interactions in polarization-controlled, spatially separated near-fields [5]. Employing phase-locked two-color fields, coherent control of free-electron states is demonstrated [6], and we introduce a scheme to characterize the quantum state of such phase-modulated free-electron states in terms of their density matrix or Wigner function [6].

Finally, we demonstrate various new possibilities in the coherent manipulation of the longitudinal and transverse degrees of freedom of free-electron wave functions, including the optical preparation of attosecond electron pulses.

References

[1] A. Feist et al., “Ultrafast transmission electron microscopy using a laser-driven field emitter: Femtosecond resolution with a high coherence electron beam”, Ultramicroscopy (in press, 2016), http://dx.doi.org/10.1016/j.ultramic.2016.12.005
[2] B. Barwick, D. J. Flannigan, and A. H. Zewail, “Photon-induced near-field electron microscopy”, Nature **462**, 902 (2009).
[3] F. J. García de Abajo, Ana Asenjo-Garcia and Mathieu Kociak, “Multiphoton absorption and emission by interaction of swift electrons with evanescent light fields”, Nano Lett. **10**, 1859 (2010).
[4] A. Feist, K. E. Echternkamp, J. Schauss, S. V. Yalunin, S. Schäfer, and C. Ropers, “Quantum coherent optical phase modulation in an ultrafast transmission electron microscope”, Nature **521**, 200 (2015).
[5] K. E. Echternkamp, A. Feist, S. Schäfer, and C. Ropers, “Ramsey-type phase control of free electron beams”, Nature Phys. **12**, 1000 (2016).
[6] K. E. Priebe et al., unpublished.

SXES study of electronic structure of sodium borosilicide $Na_8B_{74.5}Si_{17.5}$

M. Terauchi[1], H. Morito[2], H. Yamane[1], S. Koshiya[3], and K. Kimoto[3]

[1] IMRAM Tohoku Univ., 2-1-1 Katahira, Aoba-ku, Sendai 980-8577, Japan.
[2] IMR Tohoku Univ., 2-1-1 Katahira, Aoba-ku, Sendai 980-8577, Japan.
[3] National Institute for Materials Science, 1-1 Namiki, Tsukuba 305-0044, Japan.

Sodium borosilicide $Na_8B_{74.5}Si_{17.5}$ is a new member of B_{12}-cluster network materials. The crystal structure determined by X-ray diffraction belongs to a space group of $P6_3/mmc$ (a=1.024nm, c=1.092nm) and has silicon chains of [-Si-(Si-Si)$_3$-Si-] along the c-axis [1]. The crystal structure projected along [11-20] is shown in Fig.1(a). The silicon atoms of the chain are connected by sp^3 bondings. Tetrahedral atomic arrangement and bonding distances are close to those in diamond. The stacking arrangement of sp^3 along c-axis is a mixture of diamond and wurtzite structures. To investigate the bonding character of the Si-chain, electron beam excited soft-X-ray emission spectroscopy (SXES) measurements, which can probe bonding states, were conducted by using a SXES instrument attached to a SEM [2]. Figure 2 shows Si-L emission spectra of Na-B-Si. A spectrum of Si wafer obtained at the same experimental condition is also shown for comparison. The top of the balance band of Na-B-Si indicated by a vertical line is lower than that of Si-wafer. A dominant peak is seen for Na-B-Si, but it is necessary to subtract 2nd order B-K emission spectrum intensity accidentally overlapped on Si-L emission. The 2nd order B-K emission spectrum is predicted from the 1st order B-K emission spectrum of Na-B-Si as shown at the top part in Fig.1(b). Spectrum intensity subtracted the overlapped B-K emission intensity, bonding electron states of Si-chain, will be compared with a theoretically calculated partial density of states by Wien2k and discuss the characteristics of the electronic structure of Si-chains in Na-B-Si.

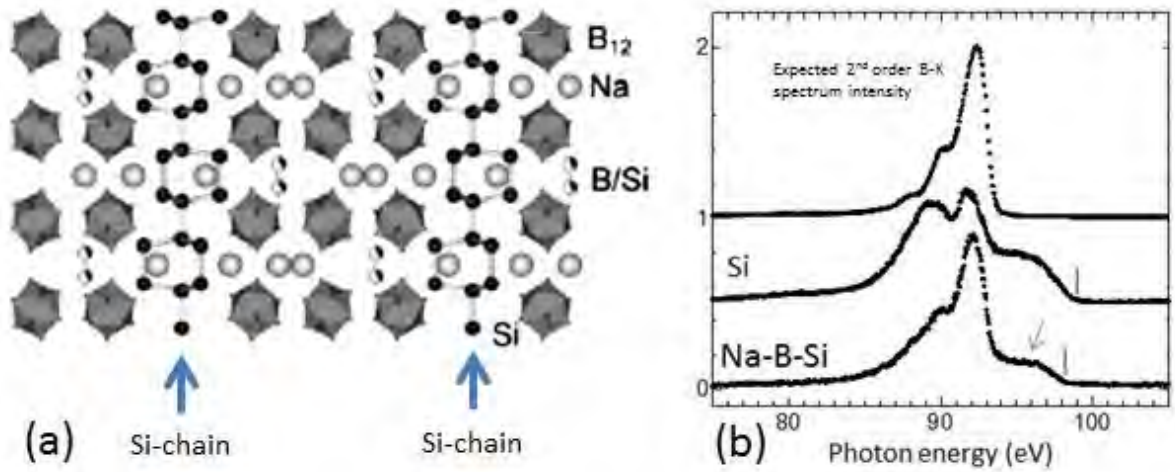

FIG. 1. (a) Crystal structure of $Na_8B_{74.5}Si_{17.5}$ [1] projected along [11-20] direction. (2) Si-L emission spectra of Na-B-Si and Si-wafer. 2nd-order B-K emission spectral intensity accidentally overlapped on Si-L spectrum, calculated from the 1st order B-K emission spectrum, is also shown at the top.

References

[1] H.Morito, *et al.*, *Dalton Transactions*, **12** (2012) 10197.
[2] M. Terauchi *et al., Microscopy and Microanalysis*, **20** (2014) 692.

Controlling the phase of electron beams for the (symmetry-)selective detection of plasmonic resonances.

G. Guzzinati[1], A. Béché[1], H. Lourenço-Martins[2], J. Martin[3], M. Kociak[2] and J. Verbeeck[1]

[1] EMAT, University of Antwerp, Antwerpen, Belgium.
[2] Laboratoire de Physique des Solides, Universite de Paris-Sud, Orsay, France
[3] Institut Charles Delaunay , Universite de Technologie de Troyes, France

Electronic spectroscopies are important in the study of localised surface plasmon resonances of metallic nanostructures, allowing to detect and image the strong spatial variations in the electrical field of the induced resonances of a single nanoparticle. These techniques do however present some drawback when compared to their optical counterparts. While optical spectroscopies can make use of polarisation to directionally probe the response of a nanoparticle, an electronic beam can't discriminate between energy-degenerate eigenmodes and is also blind to optical activity and dichroism. Here we present a radically new approach based on the idea of controlling, through phase manipulation techniques [1], the wave function of the electronic probe to fit the plasmonic modes under investigation, allowing to measure previously inaccessible properties. We show theoretically and experimentally how the phase in the electron beam's wave function couples to the electric potential of the plasmonic mode, allowing to selectively detect localised plasmonic excitations that possess the same symmetry as the electron probe [2]. Successful experimental tests focus on selectively detecting the dipolar mode of a nanorod with a two-lobed probe, which we successfully generate in a TEM by applying state of the art phase manipulation techniques. This demonstrates the viability of this new approach and opening the way to a new generation of plasmon-oriented TEM experiments, which will progress in parallel with the development of phase manipulation methods.

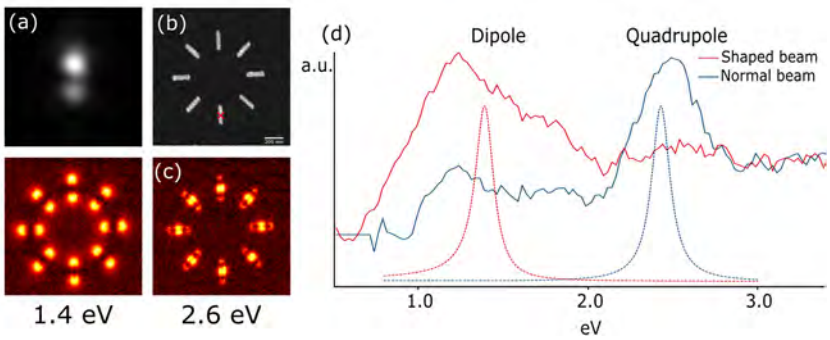

FIG. 1. A modified electron beam with a 2-lobed profile (a) is used to selectively detect dipolar modes. Plasmonic nanorods (b) which show clear dipolar and quadrupolar modes (c) are probed with the modified beam (a) and a normal one, in the position marked with a red cross (b). The modes are individually detected as shown in (d), also compared with simulations (dashed line).

References

[1] G. Guzzinati et al., Ultramicroscopy 151, 85 (2015).
[2] G. Guzzinati et al., Nature Communications, In Review / Arxiv:1608.07449
[3] G.G. acknowledges funding from FWO project 42/FA070100/6088 "Nieuwe eigenschappen in complexe oxides" and ERC starting grant 278510 VORTEX.

Time-resolved TEM-EELS using a pulsed beam extracted from a semiconductor photocathode

M. Kuwahara[1,2], K. Aoki[2], F. Ichihashi[2], T. Ujihara[1,2], N. Tanaka[1] and K. Saitoh[1,2]

[1] Institute of Materials and Systems for Sustainability, Nagoya University, Nagoya, 4648603, Japan.
[2] Graduate School of Engineering, Nagoya University, Nagoya, 4648603, Japan.

Narrow energy spread of probe beam contributes to higher energy resolution in electron energy-loss spectroscopy (EELS). Such energy spreads are also important for the temporal coherence of an electron wavepacket. A narrow electron beam linewidth is usually realized using a monochromatic filter applied to the illumination system of a transmission electron microscope (TEM) [1]. The narrowest achieved energy spread of 9 meV has been demonstrated by combining a cold field emission gun and an alpha-type monochromator, which improved the energy resolution of the EELS and allowed the observation of phonon scattering with fast electrons [2].

A spin-polarized electron beam emitted from a semiconductor photocathode with a negative electron affinity (NEA) surface has a narrow linewidth of below 0.24 eV due to the extraction process [3]. The spin polarized electron beam has also a very low initial emittance of 2.6×10^{-9} m rad. The reason for the low emittance is the small laser spot size and the small transverse momentum. The transverse momentum demonstrates a dependence on the wavelength due to the band structure of the conduction band of the semiconductor and the absolute value of NEA. The NEA is estimated to be 89 ± 32 meV [4]. The energy width of the electron beam is evaluated to be less than 116 meV at room temperature, which corresponds with a temporal coherence time of 34 fs.

In contrast, the space charge effect has also been observed in the energy distributions of picosecond pulse beams in a spin-polarized pulsed TEM (SPTEM), and was found to depend upon the quantity of charge per pulse. The non-linear phenomena associated with this effect have also been replicated in beam simulations that take into account of a three-dimensional space charge [5]. The results suggested that the narrow linewidth of 0.4 eV could be realized by a charge amount of several tens aC/pulse with a picosecond pulse duration. Time-resolved EELS (TR-EELS) was performed in the SPTEM using a picosecond pulsed probe beam with keeping the narrow energy width. A specimen and a pump laser were graphite and picosecond pulse laser of 780-nm wavelength, respectively. The delay time between probe and pump is set by controlling the traveling distance of pumping laser within an accuracy of 14 fs. We will report the development of the TR-EELS measurement system and the results of the time-resolved measurements.

References

[1] K. Kimoto, Microscopy **63**, 337-344 (2014).
[2] O. L. Krivanek, et al., Nature **514**, 209-212 (2014)
[3] M. Kuwahara, S. Kusunoki, et al., Appl. Phys. Lett. **105**, 193101 (2014).
[4] M. Kuwahara, S. Kusunoki, et al., Appl. Phys. Lett. **101**, 033102 (2012).
[5] M. Kuwahara, Y. Nambo, et al., Appl. Phys. Lett. **109**, 013108 (2016).
[6] The authors thank Drs. H. Shinada, M. Koguchi of Hitachi Central Research Laboratory for their helpful supports. This research was supported by JSPS KAKENHI Grant Numbers 25706031 and 15K13404.

Cathodoluminescence temporal statistics: single photon emitters and lifetime measurements at nanometer scales

Luiz H. G. Tizei[1], Sophie Meuret[1], François Treussart[2], Bruno Daudin[3], Bruno Gayral[3], Romain Brourellier[1], Anna Tararan[1], Alberto Zobelli[1], Odile Stéphan[1], Mathieu Kociak[1]

[1]Laboratoire de Physique des Solides, UMR 8502 CNRS and Université Paris-Sud, Orsay 91405, France
[2]Laboratoire Aimé Cotton, UMR 9188 CNRS, Université Paris Sud and ENS Cachan, Orsay 91405, France
[3]CEA, INAC-PHELIQS, « Nanophysique est semiconducteurs group », F-38000, Grenoble France

Spectroscopic techniques rely on the analysis of a system response function to external stimulus in frequency/energy or (photon) wavelength space averaged in time. For example, photoluminescence spectroscopy (PL) relies upon the excitation of a system by light and the observation of the intensity of light emitted as a function of wavelength (dispersed by a diffraction grating). Fundamentally, information is gained to the occupied and/or unoccupied energy levels of the system.
However, having access to the temporal information of the emission/absorption process gives important information about the system otherwise inaccessible in time-averaged measurements. For example, time-resolved PL allows one to follow the evolution of the emission spectrum due to the quantum confined Stark effect and Hanbury Brown and Twiss (HBT) intensity interferometry allows the detection of single photon sources.
In this contribution, we will describe experiments aimed at understanding the temporal statistics of light emitted from nanometer-wide objects excited by fast electrons (typically with 60 keV kinetic energy). The interest of these experiments are two-fold: 1) to benefit from electrons high localization (~1 nm in our current setup) and broadband excitation and 2) to borrow from all accumulated knowledge in light optics and quantum optics.
To start with, we will describe experiments performed with NV^0 centers in diamond [1] and point defects in hBN [2], which allowed the identification of single photon sources using fast electrons as excitation. These experiments used a standard HBT optical interferometer. Contrary to expectations, light intensity interferometry of the same defects at high concentrations shows light bunching (that is, higher probability of detecting two photons at zero time-delay than for a poissonian source) in the nanosecond time regime [3]. This effect is explained by a model taking into account the excitation dynamics due to individual electrons. As a side effect, this modes provides a way to measure an emitter's lifetime. This interesting effect has been used to measure lifetimes of emitters (GaN quantum disks) separated by a 15 nm [4].
Finally, we will briefly discuss how temporal correlation between EELS and CL signals may shine new light into how defects or nanostructures in semiconductor materials are excited by fast electrons.

References

[1] L. G. Tizei and M. Kociak, *Phys. Rev. Lett.* 110 (2013) 153604.
[2] R. Bourrellier *et al*, *Nano Lett.* 16 (2016) 4317.
[3] S. Meuret et al, *Phys. Rev. Lett.* (2015) 197401.
[4] S. Meuret et al *ACS Photonics* 3 (2016) 1157.

Nanoscale spectroscopy with low energy electrons

J. Jobst[1,2], D. Geelen[1], E.E. Krasovskii[3], R.M. Tromp[4,1] and S.J. van der Molen[1]

[1] Leiden Institute of Physics, Leiden University, Leiden, The Netherlands
[2] Department of Physics, Columbia University, New York, USA
[3] Universidad del Pais Vasco, San Sebastián, Spain
[4] IBM T.J.Watson Research Center, Yorktown Heights, USA

Spectromicroscopy (i.e. spectroscopy on microscopic length scales) is one of the most rapidly developing areas in materials analysis. Here we present two novel LEEM (Low Energy Electron Microscopy)-based spectromicroscopy techniques to study unoccupied bands and loss processes in materials, combining the high lateral resolution of state-of-the-art LEEM with detailed and in-depth spectroscopic analysis. Angle-Resolved Reflected-Electron Spectroscopy (ARRES) uses the energy- and k-vector-dependent specular *reflectivity* of the incident electron beam to map out the unoccupied band structure above the vacuum level [1]. This allows us to study the interaction in layered Van der Waals materials on the nanoscale [2]. With the introduction of an extra electron gun behind the sample, we are also able to study *transmission* properties of thin materials. With a demonstrated lateral resolution of ~10 nm, eV-TEM (i.e. Transmission Electron Microscopy with few eV electron energies) [3,4] will enable damage-free imaging of biological samples. Combining reflectivity and transmissivity data vs. electron energy, we determine the loss function of a material. Studying real-time electron energy loss enables us to better understand secondary electron generation and trap formation during low energy electron exposure of thin organic resist layers.

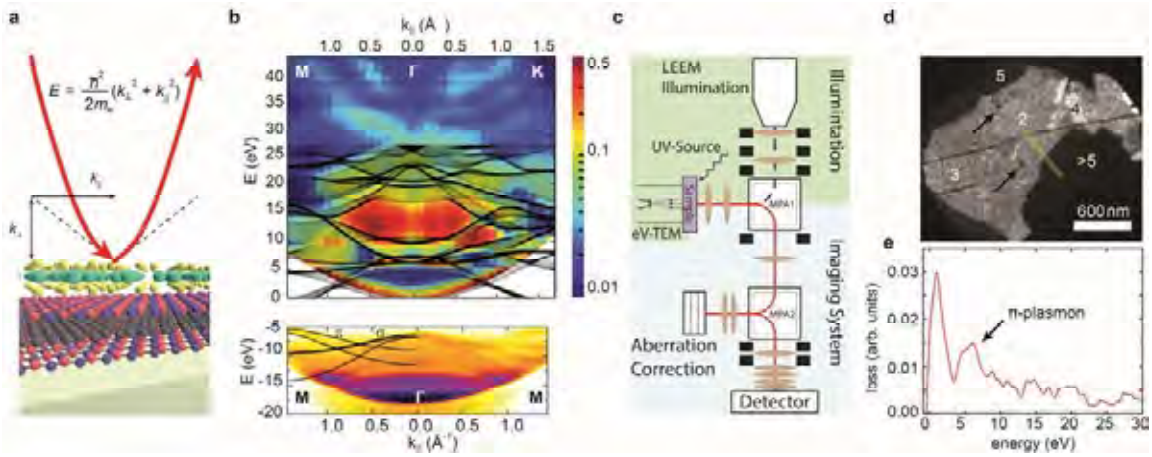

FIG. 1. **a,** Schematic of ARRES. **b,** Unoccupied (via ARRES) and occupied (via ARPES) bands of hexagonal boron nitride (from [2]). **c,** LEEM set-up with eV-TEM electron gun integrated. **d,** eV-TEM image of gold nanoparticles (arrows) on a few-layer graphene membrane (thickness indicated by layer numbers). **e,** Measured loss function from trilayer graphene.

[1] J. Jobst et al., *Nature Communications* 6 (2015) 8926.
[2] J. Jobst et al., *Nature Communications* 7 (2016) 13621.
[3] R.M. Tromp, US. Patent 8,586,923.
[4] D. Geelen et al., *Ultramicroscopy* 159 (2015) 482.

Mapping surface and bulk phonon modes in a single nanostructure

M. J. Lagos[1], A.Trugler[2], U. Hohenester[2], and P. E. Batson[1]

[1] Department of Materials, Science and Engineering; Department of Physics and Astronomy; IAMND, Rutgers University, USA.
[2] Institute of Physics, University of Graz, Austria.

At the nanoscale level, the surface, the shape and the size of a structure are tuning elements that play an important role for the design of plasmon and phonon properties. Typical energies of those collective excitations in matter span from the UV to infrared energy range. In 1980, Batson mapped, by the first time, UV-plasmon excitations in aluminum nanospheres using electron beams [1]. Later, similar imaging approaches were also used to map optical surface plasmons [2] and near-IR plasmons [3] in metallic particles. These EELS-spatially resolved results brought a lot of understanding about the surface plasmon properties at the nanoscale level, thus contributing to the fields of plasmonics and nanophotonics.

With further instrumentation development resulting in improvements of energy resolution [4], the doors for the phonon exploration using angstrom-sized electron beams were open. This is allowing us to address fundamental questions regarding the physical aspects of phonons at the nanoscale, such as: Can a nanosized object accommodate bulk modes? Are phonon modes highly localized? What is the spatial distribution of those phonon modes? What is the spatial variation of the vibrational scattering signal within atomic unit cells? Progress along this direction should bring insights into the understanding of nanoscale phonon properties.

In this work, we present a study of the spatial distribution of EELS excitations of vibrational modes in a single MgO nanocube (45 – 150 nm), aiming to determine the degree of localization of phonon modes and their spatial distribution [5]. We detected both optical (~ 90 - 50 meV) and acoustic (~ 40 – 50 meV) bulk modes, containing lattice contributions spanning the whole Brilloiun zone. These bulk vibrational excitations are mainly located in the inner regions of the nanocube. We also found size-dependent surface phonon modes (face, edge and corner) which are localized within the nanocube surfaces (~ 15 nm) and can extend into the vacuum. An interesting variation of the phonon bulk scattering in the presence of surface modes was also observed close to the cube surface. This scattering variation is similar to the Begrenzung effect observed in plasmon excitation and it points out that similar sum-rule might be active in the inelastic scattering from lattice vibrations.

References

[1] P. E. Batson, *Ultramicrospy* 9, 277 (1982).
[2] J. Nelayah *et al, Nature Physics* 3, 348 (2007);
M. Bosman, *et al*, *Nanotech*.18, 165505, (2007).
[3] D. Rossouw, *et al*, *Nanoletters* 11, 1499 (2011).
[4] O. Krivanek, *et al*, *Nature* 514, 209 (2014).
[5] M. J. Lagos, *et al*, *Nature* (2017) *to be published*
[6] This research was supported by D.O.E (#DE-SC0005132) and NSF (No. 0959905). The authors also acknowledge O. Krivanek, N. Dellby, T. Lovejoy, M. Saharan and C. Meyer for discussion regarding the instrumentation.

Sub 30meV in the monochromated Themis

P.C. Tiemeijer[1] and S. Lazar[1]

[1] Thermo Fisher Scientific, PO Box 80066, 5600 KA Eindhoven, The Netherlands

When we introduced the FEI monochromator in 2001 [1], the main application that we foresaw was unravelling the fine structure in EELS core losses. To this end, its design was optimized for an energy resolution of 0.1eV at HT= 200kV and probe current >100pA. Since then, applications of the monochromator have diverged to a wider range, such as bandgap measurements [2], reduction of chromatic blur [3], and plasmon mapping [4]. Improving the resolution of our monochromator to 0.05eV (for plasmon mapping) or reducing it to 0.2eV (for reduction of chromatic blur) was possible since the dispersion of our monochromator, being based on the Wiener filter principle, can be varied continuously.

However, stimulated by the recently generated interest for observing phonons in the electron microscope [5], which requires an even better energy resolution, we revisited the optics of our monochromator. We optimized the system (without compromising on standard performance of the Themis) to circumvent the resolution limits previously set by instabilities and aberrations. This resulted in an energy resolution between 25meV and 30meV. Figure 1 shows BN phonon peaks observed using this improved optics.

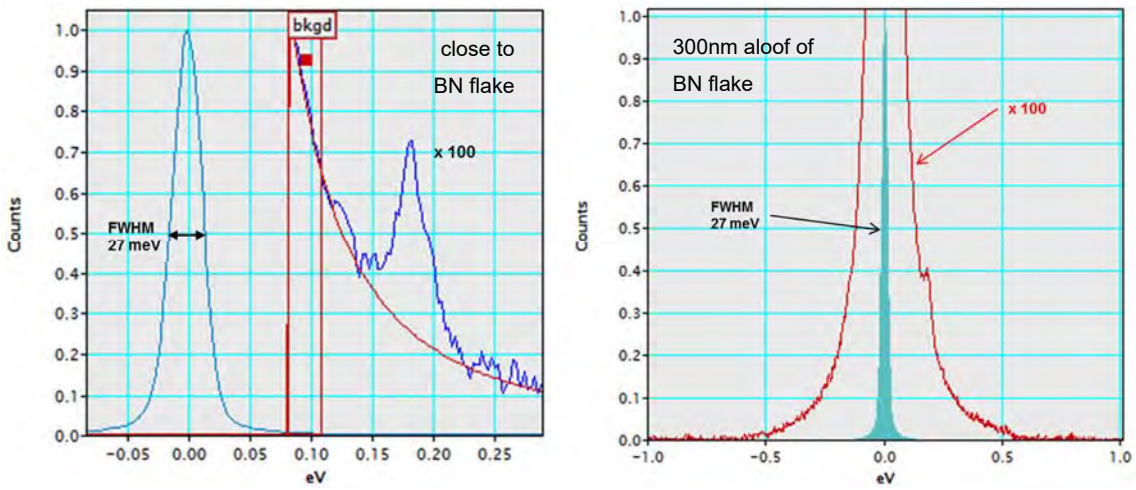

FIG. 1. Sub-30meV with a monochromated Themis with Quantum 966 at 60kV.
Left: BN phonon peak with FWHM of the ZLP and phonon peaks of 27meV. Collection time 25ms. The phonon peak is magnified 100 times.
Right: ZLP recorded in vacuum 300nm aloof of the specimen; the BN phonon is still observable. The spectrum is magnified 100x to show the tails of the ZLP. Collection time 300ms.

References

[1] P.C. Tiemeijer et al., Microscopy and Microanalysis 7, suppl 2 (2001) 1130
[2] S. Lazar et al., Ultramicroscopy 96 (2003) 535
[3] C. Girit et al., Science 323 (2009) 1705
[4] D. Rossouw et al., Nano Letters 11 (2011) 1499
[5] O. Krivanek et al., Nature 514 (2014) 209

Triple-axis vibrational spectroscopy in the electron microscope: theory and experiment

R.J. Nicholls[1], F.S. Hage[2], J.R. Yates[1], K. Refson[3], and Q.M. Ramasse[2]

[1] Department of Materials, University of Oxford, Oxford, UK
[2] SuperSTEM Laboratory, SciTech Daresbury Campus, Daresbury, UK.
[3] Department of Physics, Royal Holloway, University of London, Egham, UK.

Advances in high-resolution electron source monochromators have made it possible to routinely observe low energy vibrational signals from a variety of materials using a scanning transmission electron microscopy (STEM) [1]. Although the physical origin of these signals is very similar to that giving rise to low-energy phonon vibrations in neutron or inelastic X-ray scattering, differences in experimental geometries and selection rules, among other factors, have made the interpretation of phonon spectra in the STEM challenging. Here, we develop a methodology to calculate phonon spectra in a momentum-resolved STEM EELS experiment. This approach promises to provide data akin to triple-axis spectroscopy in neutron scattering, with the additional advantages of the higher spatial resolution and ability to correlate with chemical analysis. The theoretical formalism is based on that used by inelastic X-ray and neutron scattering [2] and it highlights the similarities as well as the differences between the techniques. We apply this framework to obtain a remarkable agreement with experimental data from two polymorphs of boron nitride, across different directions in the Brillouin zone. In particular, we demonstrate that acoustic branches of the phonon dispersion diagram can contribute to the observed spectra. The ability to assign the features in experimental spectra to specific phonon modes is predicted to greatly increase the applicability of this technique for materials science studies.

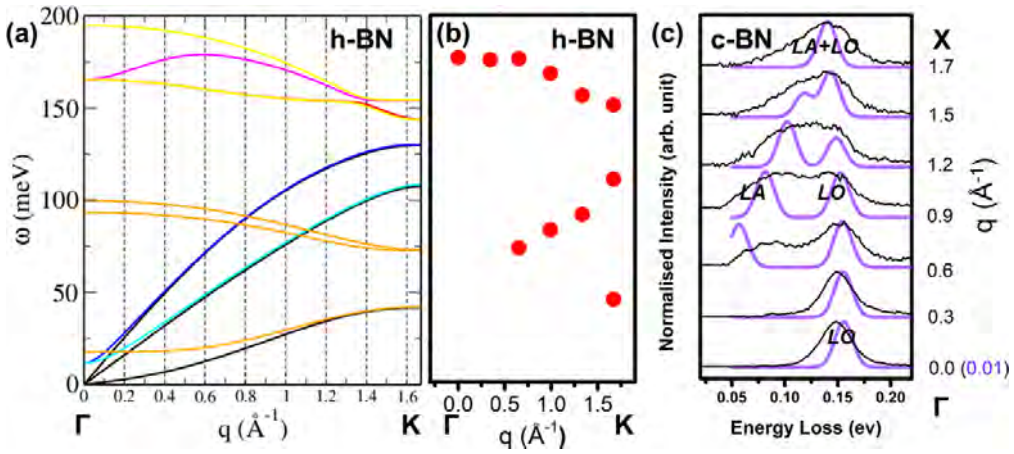

FIG. 1 Calculated phonon dispersion for h-BN (a) compared with experimental data obtained on a Nion UltraSTEM100MC (b). Background subtracted spectra can then be directly compared to simulations, here in the case of c-BN in the Γ→X direction (c): experiment, theory.

References
[1] O.L Krivanek et al., *Nature.* 514 (2014) 209.
[2] E. Burkel, *J.Phys.: Cond. Mat.* 13 (2001), 7627.
[3] SuperSTEM is the UK EPSRC National Facility for Aberration-Corrected STEM, supported by the UK Engineering and Physical Science Research Council.

Increasing the spatial resolution of vibrational EELS

C. Dwyer[1], T. Aoki[2], P. Rez[1], S.L.Y. Chang[2], T.C. Lovejoy[3], and O.L. Krivanek[3,1]

[1] Department of Physics, Arizona State University, Tempe, Arizona 85287, USA
[2] LeRoy Eyring Center for Solid State Science, Arizona State University, Tempe, Arizona 85287, USA
[3] Nion Company, 11511 NE 118th Street, Kirkland, Washington 98034, USA

Thus far, vibrational EELS experiments in the STEM have achieved a spatial resolution of only several tens of nm at best [1], which is a far cry from the sub-nm resolution routinely achieved in imaging and other forms of spectroscopy. This observation is often explained away using a v/ω "delocalization" argument, which predicts poor spatial resolution on account of the small energy losses $\hbar\omega \sim 100$ meV.

Here we demonstrate that it is possible to map the vibrational modes of a material with a spatial resolution of the order of one nanometer using an off-axial collection geometry in EELS. We use boron nitride, a polar dielectric which gives rise to both localized and delocalized electron-vibrational scattering, either of which can be selected in our experimental geometry. Our experimental results are well supported by quantum-mechanical calculations, and should reconcile current controversy regarding the spatial resolution achievable in vibrational EELS in the STEM [2].

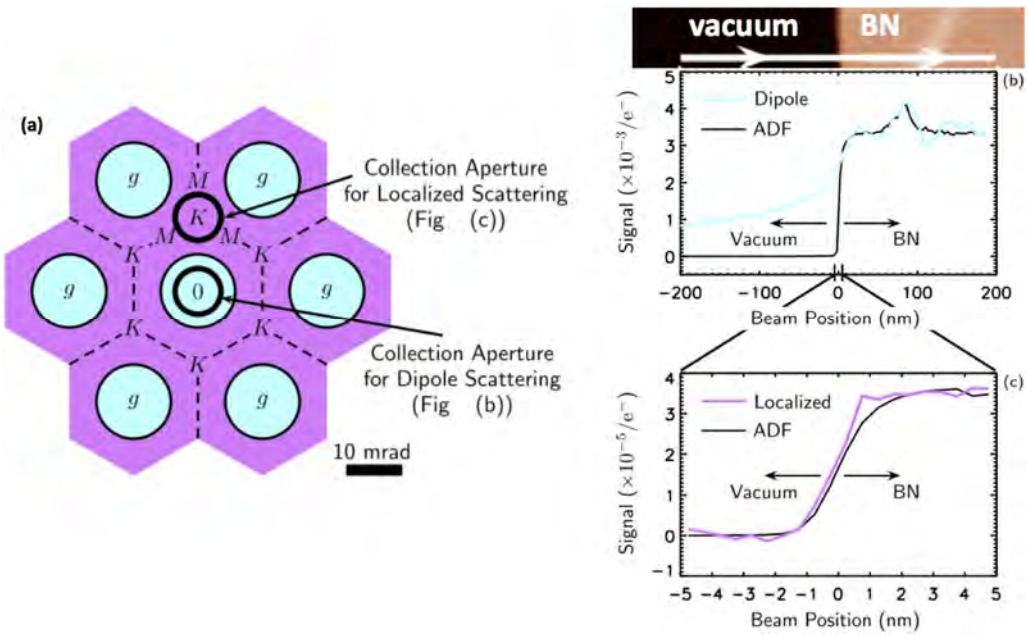

FIG. 1. (a) Schematic CBED pattern of BN, showing axial and off-axial collection. (c) the latter is used to acquire vibrational EELS with a spatial resolution of < 2 nm.

References
[1] O. L. Krivanek, T. C. Lovejoy, N. Dellby, T. Aoki, R. W. Carpenter, P. Rez, E. Soignard, J. Zhu, P. E. Batson, M. Lagos, R. F. Egerton, and P. A. Crozier, *Nature (London)* 514, 209 (2014); P. Rez, T. Aoki, K. March, D. Gur, O. L. Krivanek, N. Dellby, T.C. Lovejoy, S.G. Wolf, and H. Cohen, *Nat. Commun*. 7, 10945 (2016).
[2] C. Dwyer, T. Aoki, P. Rez, S.L.Y. Chang, T.C. Lovejoy, O. L. Krivanek, *Phys. Rev. Lett.* 117, 256101 (2016).

Spectroscopic mapping at cryogenic temperature

L.F. Kourkoutis[1,2], M.J. Zachman[1], B.H. Savitzky[3], I. El Baggari[3], D.J. Baek[1,4]

[1] School of Applied and Engineering Physics, Cornell University, Ithaca, NY, 14853, USA
[2] Kavli Institute at Cornell for Nanoscale Science, Cornell University, Ithaca, NY,14853, USA
[3] Department of Physics, Cornell University, Ithaca, NY, 14853, USA
[3] School of Electrical and Computer Engineering, Cornell University, Ithaca, NY, 14853, USA

Spectroscopic mapping by STEM/EELS has been proven to be a powerful technique for determining the structure, chemistry and bonding of interfaces, reconstructions, and defects. So far, most efforts in the physical sciences have focused on room temperature measurements where atomic resolution mapping of composition and bonding has been demonstrated [1-3]. For many materials, including those that exhibit electronic and structural phase transitions below room temperature and systems that involve liquid/solid interfaces, STEM/EELS measurements at low temperature are required. Operating close to liquid nitrogen temperature gives access to a range of emergent electronic states in solid materials and allows us to study processes at liquid/solid interfaces immobilized by rapid freezing [4,5]. Here, we will discuss progress, instrumentation requirements and current limitations in spectroscopic mapping of materials at cryogenic temperature.

References

[1] K. Kimoto, T. Asaka, T. Nagai, M. Saito, Y. Matsui, K. Ishizuka, *Nature* 450 (2007) 702.
[2] D.A. Muller, L.F. Kourkoutis, M. Murfitt, J.H. Song, H.Y. Hwang, J. Silcox, N. Dellby, O.L. Krivanek, *Science* 319 (2008) 1073.
[3] J.A. Mundy, Y. Hikita, T. Hidaka, T. Yajima, T. Higuchi, H.Y. Hwang, D.A. Muller, L.F. Kourkoutis, *Nat. Commmun.* 5 (2014) 3464.
[4] R. Hovden et al., *Proc. Natl. Acad. Sci.* 113 (2016) 11420.
[5] M.J. Zachman, E. Asenath-Smith, L.A. Estroff, L.F. Kourkoutis, *Microsc. Microanal.* 22 (2016) 1338.

Optoelectronic properties of organic photovoltaic materials determined via high-resolution monochromated electron energy-loss spectroscopy

Jessica A. Alexander[1], Frank J. Scheltens[1], Lawrence F. Drummy[2], Michael F. Durstock[2], Fredrik S. Hage[3], Quentin M. Ramasse[3], and David W. McComb[2]

[1] Center for Electron Microscopy and Analysis, Department of Materials Science and Engineering, The Ohio State University, Columbus, OH, United States
[2] Materials and Manufacturing Directorate, Air Force Research Laboratory, Wright Patterson Air Force Base, WPAFB, OH, United States
[3] SuperSTEM Laboratory, SciTech Daresbury Campus, Daresbury, United Kingdom

Organic photovoltaics (OPVs) show promise as an alternative to inorganic PVs. In order to improve their efficiency understanding the electronic structure at their acceptor/donor (A/D) interface vital. Utilizing monochromated electron energy-loss spectroscopy (EELS) in a scanning transmission electron microscope (STEM), the electronic structure can be obtained with nanometer spatial resolution [1]. In this contribution, EELS spectra were collected for four beam sensitive OPV materials – poly(3-hexylthiophene) (P3HT), [6,6] phenyl-C_{61} butyric acid methyl ester (PCBM), copper phthalocyanine (CuPc), and C_{60}. These spectra were collected on two STEMs: an FEI Titan^3 60-300 Image-Corrected S/TEM (ΔE=175 meV) and a Nion UltraSTEM 100 MC 'HERMES' (ΔE=35 meV). The large energy dispersions required that spliced datasets were used to extract the complex dielectric functions from the EELS data We will discuss the processing of the data for these materials and will show that ultra high-resolution is not necessary for studying the A/D interface in OPVs. We will demonstrate the quality of the extracted optical absorption coefficient (α) spectra (Fig. 1) to show how STEM-EELS can provide spatially resolved measurements of optical properties in these beam sensitive materials.

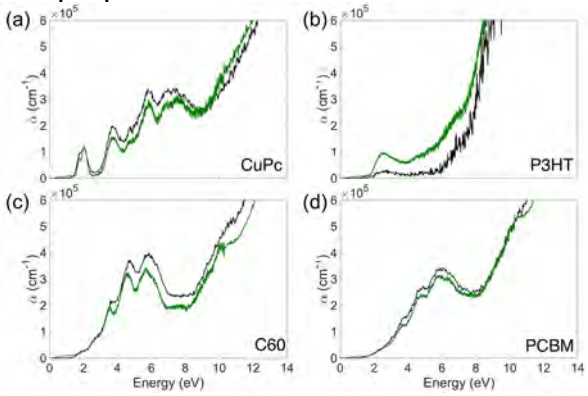

FIG. 1. The α spectra determined from EELS data collected on the Nion UltraSTEM (green) and the FEI Titan^3 (black) for (a) CuPc, (b) P3HT, (c) C_{60}, and (d) PCBM.

References

[1] R.F. Egerton. *Electron Energy-Loss Spectroscopy in the Electron Microscope* (Springer, 2011).

[2] This research was supported by the Air Force Office of Scientific Research, the Air Force Research Laboratory Materials and Manufacturing Directorate, the Dayton Area Graduate Studies Institute, and The Ohio State University.

Probing chemical pathways in polyamide reverse osmosis membranes

C.M. McGilvery[1], M.M. Kłosowski[1], P. Abellan[2], Q.M. Ramasse[2], A.G. Livingston[3] and A.E. Porter[1]

[1] Dept. of Materials, Imperial College London, London, SW7 2AZ, UK
[2] SuperSTEM Laboratory, SciTech Daresbury Campus, Daresbury, WA4 4AD, UK
[3] Dept. of Chemical Engineering, Imperial College London, London, SW7 2AZ, UK

Reverse Osmosis (RO) membranes are commonly used for sea water desalination. The membranes comprise of a polyester backing layer, a polysulfone support and a polyamide (PA) membrane layer (typically 100-500nm thick) which controls the salt selectivity and permeance of the membrane. Given the membrane's complex hierarchical structure, which spans different length scales, the controllability of ion selectivity remains unclear. Recently, a 10nm membrane has been grown.[1] leading to the hypothesis that the rougher, membranes are themselves formed by 'crumpling' of this thin film. We have performed structural characterization of both membranes by TEM. This presents a number of practical challenges, due to the poor image contrast from the amorphous material, the dynamic nature and size of the pores, and that sample preparation procedures and electron beam damage/sensitivity may produce artifacts.

Nanoparticle imaging experiments show that polarisation of ionic charge may control transport across the membrane [2]. This, combined with previous studies showing a difference in functional groups at the top and bottom surfaces of the membrane [3], suggests the existence of chemical pathways across the membrane by which ion transport may occur. The functional chemistry of similar membranes has previously been characterized using scanning transmission x-ray microscopy, x-ray photoelectron spectroscopy and small angle neutron scattering [1,4], but these techniques are limited in their spatial resolution. Spatially resolved electron energy-loss spectroscopy (EELS) is the only method available to investigate the distribution of these modulations in chemistry at the sub nanometer scale.

Here, for the first time, we use EELS spectrum imaging to map C, N and O, and specific C functional groups across the membranes with high spatial and energy resolution (1-3nm, 0.1-0.3eV). Here we show our most recent results demonstrating clear changes in elemental and functional chemistry across both flat in-house membranes and rough commercially available SW30HR (DowFilmtech) membranes. We discuss possible transport mechanisms taking place through the membrane.

References

[1] S. Karan *et. al. Science* 348 (2015) 1347-1351
[2] Y. Li *et al. (in submission, Journal of Membrane Science))*
[3] V. Freger, *Langmuir* 19 (2003) 4791-4797
[4] G. E. Mitchell *et al. Polymer* 52 (2011) 3956-3962
[5] This research was funded by BP and the BP International Centre for Advanced Materials (BP-ICAM). The work carried out at SuperSTEM was supported by the Engineering and Physical Sciences Research Council (EPSRC)

Investigation of sensitive hybrid organic-inorganic materials by analytical (S)TEM

V. Srot[1], B. Bussmann[1], M. Vittori[2], B. Pokorny[3,4] and P.A. van Aken[1]

[1]Stuttgart Center for Electron Microscopy, Max Planck Institute for Solid State Research, Heisenbergstr. 1, 70569 Stuttgart, Germany
[2]Department of Biology, Biotechnical Faculty, University of Ljubljana, Večna pot 111, 1000 Ljubljana, Slovenia
[3]Environmental Protection College, Trg mladosti 2, 3320 Velenje, Slovenia
[4]Slovenian Forestry Institute, Večna pot 2, 1000 Ljubljana, Slovenia

Many mineralized natural materials have a very complex structure where inorganic and organic components are closely intertwined and are forming exceptional constructions. Many of these bio-minerals are hybrid materials with excellent physical and mechanical properties [1] showing outstanding performance and fulfilling different functions in the animal bodies. Although the natural composite materials are often composed of relatively simple components, their sophisticated architectures are strongly influencing/controlling their properties. Therefore, the microstructure and local chemistry need to be characterized at the nanoscale level.

In our study, the microstructure and the chemical composition of continuously growing incisors from the coypu (*Myocastor coypus* Molina) [2] and of terrestrial isopod claws (Crustacea) [3] were studied using a combination of imaging and analytical transmission electron microscopy (TEM) techniques and compared to their mechanical properties. In the course of our work, energy-loss near-edge structures (ELNES) of several standard Ca and Fe based materials [2, 3, 4], that are often present in nature, were acquired and compared to the spectra from investigated material.

The presented studies will intensify the understanding of mechanisms controlling biomineralization processes, in order to identify details and recognize building strategies of functional natural composites.

References

[1] U.G.K Wegst and M.F. Ashby., *Philos Mag* 84 (2004) 2167-2186.
[2] V. Srot et al., *ACS Nano* (2016) DOI: 10.1021/acsnano.6b05297
[3] M. Vittori et al., *J Struct Biol* 195 (2016) 227-37.
[4] V. Srot et al., *Micron* 48 (2013) 54-64.

Low-dose EELS for 'thick' samples: Model-based and machine learning approaches to remove multiple scattering

S.M. Collins[1], T. Bennett[1], S. Fernandez-Garcia[2], J.J. Calvino[2], P.A. Midgley[1]

[1] Department of Materials Science and Metallurgy, 27 Charles Babbage Road, Cambridge CB3 0FS, United Kingdom
[2] Departamento de Ciencia de los Materiales, Ingeniería Metalúrgica y Química Inorgánica, Universidad de Cadiz, Campus Río San Pedro, Puerto Real (Cádiz) E-11510, Spain

Detailed chemical microanalysis of large sample volumes at high spatial resolution for diverse materials is a key target for analytical electron microscopy. However, the development of EELS, particularly for three-dimensional characterization of such samples, is challenging due to sample thickness and associated multiple inelastic scattering effects. Moreover, many radiation sensitive materials, from oxides to soft materials, suffer from deleterious electron beam damage during EELS acquisition, requiring unconventional approaches to EELS imaging and tomography for low-dose and limited exposure data recording strategies. In this presentation, machine learning and model-based techniques will be discussed for EELS analysis of beam-sensitive oxides and metal-organic frameworks. Model-based EELS tomography of lanthanum-doped cerium oxide nanoparticle aggregates making use of EELS acquired at a single sample orientation demonstrates an approach to multi-modal approaches with limited electron damage, while revealing orbital hybridization changes with sub-nanometer precision. Limitations and opportunities for machine learning-guided analysis in cerium oxide materials and in metal-organic frameworks will also be discussed, with particular emphasis on the role of multiple scattering contributions [1].

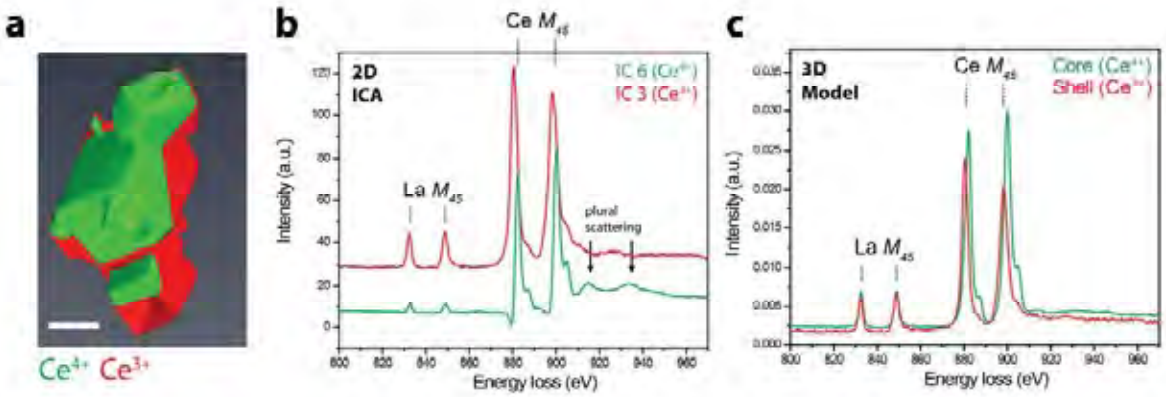

FIG. 1. (a) Three-dimensional visualization of the core and surface (1.5 nm) layers for a La-doped ceria aggregate, cropped at an oblique plane. The scale bar is 25 nm. (b) Machine learning and (c) model-based spectra for core and surface layers.

References

[1] This work has received funding from the European Research Council (No. FP7/2007-2013)/ERC Grant Agreement No. 291522-3DIMAGE and the European Union's Seventh Framework Program under a contract for an Integrated Infrastructure Initiative (Reference No. 312483-ESTEEM2).

Modelling imaging and energy-loss spectra due to phonon excitation

L.J. Allen[1], H.G. Brown[2], S. D. Findlay[2], B.D. Forbes[1], and N.R. Lugg[3]
[2]

[1] School of Physics, University of Melbourne, Parkville, Victoria 3010, Australia
[2] School of Physics and Astronomy, Monash University, Clayton, Victoria 3800, Australia
[3] Institute of Engineering Innovation, School of Engineering, University of Tokyo, Tokyo 113-8656, Japan

Recent developments have improved the attainable energy resolution in electron energy-loss spectroscopy in aberration-corrected transmission electron microscopy to the order of 10 meV [1]. In principle, this allows imaging and spectroscopy of crystals using the phonon sector of the energy-loss spectrum at atomic resolution, a supposition supported by recent simulations for molecules [2].

We show that the "quantum excitation of phonons" model [3] encapsulates the physics necessary to simulate the atomic resolution imaging of crystals based on phonon excitation and we discuss the predictions of such simulations [4].

We also discuss a fundamental theory of how to calculate the phonon-loss sector of the energy-loss spectrum for electrons scattered from crystalline solids based on transition potentials [5]. A correlated model for the atomic motion is used for calculating the vibrational modes. Spectra are calculated for crystalline silicon illuminated by a plane wave and also by an atomic-scale focused coherent probe, in which case the spectra depend on probe position. These spectra are also affected by the size of the spectrometer aperture. The correlated model is contrasted with and related to the Einstein model in which atoms in the specimen are assumed to vibrate independently. We then discuss how both the correlated and Einstein models relate to a classical view [6] of the energy-loss process.

Lastly we will discuss how so-called "aloof beam" imaging [7-10] arises within the context of the transition potential model.

References

[1] O.L. Krivanek et al., *Nature* 514 (2014) 209.
[2] C. Dwyer, *Phys. Rev. B* 89 (2014) 054103.
[3] B.D. Forbes et al., *Phys. Rev. B* 82 (2010) 104103.
[4] N.R. Lugg et al., *Phys Rev. B* 91 (2015) 144108.
[5] B.D. Forbes et al., *Phys Rev. B* 94 (2016) 014110.
[6] G. Argentero et al., *Ultramicroscopy* 151 (2015) 23.
[7] A. Howie, *Ultramicroscopy* 11 (1983) 141.
[8] P. Rez, *Microsc. Microanal.* 20 (2014) 671–677.
[9] R.F. Egerton, *Ultramicroscopy* 159 (2015) 95.
[10] P.A. Crozier et al., *Ultramicroscopy* 169 (2016) 30.
[11] This research was supported under the Australian Research Council's Discovery Projects funding scheme (Projects DP110102228 and DP140102538). N.R.L was supported by the Japan Society for the Promotion of Science (JSPS).

Addressing the accuracy of z-locality approximation in simulations of inelastic electron scattering

J. Rusz[1], A. Lubk[2], D. Tyutyunnikov[1]

[1] Department of Physics and Astronomy, Uppsala University, Box 616, Uppsala, SE-75 120, Sweden
[2] Leibniz Institute for Solid State and Materials Research, Helmholtzstraße 20, 01069 Dresden, Germany

The complex interplay of elastic and inelastic scattering, amenable to different levels of approximation, constitutes the major challenge for the computation and hence interpretation of TEM-based spectroscopic methods. The two major approaches to calculate inelastic scattering cross-sections of fast electrons on crystals – Yoshioka-based forward scattering approach and reciprocal wave method – are founded in two conceptually differing propagation schemes – a numerical forward integration of each inelastically scattered wave function, yielding the exit density matrix, and a computation of inelastic matrix elements using elastically scattered initial and final states (double channeling). We compare both approaches and show that the latter is computationally competitive to the former by exploiting analytical integration schemes over multiple excited states. Moreover, we show how to include full non-locality of the inelastic scattering event, neglected in the forward integration schemes, which comes at no additional computing costs in the reciprocal wave method. Detailed simulations show non-negligible errors due to the z-locality approximation and hence pitfalls in the interpretation of spectroscopic TEM results. [1]

References

[1] This research was supported by Swedish Research Council, STINT and Göran Gustafssons Foundation. The simulations were performed at the National Supercomputing Centra at Linköping University, under the Swedish National Infrastructure for Computing (SNIC).

Properties of the point-spread function for valence-electron and vibrational-mode inelastic scattering

R. F Egerton[1]

[1] Physics Department, University of Alberta, Edmonton, Canada T6G 2E1

Based on the angular dependence of scattered intensity, we calculate a point-spread function (PSF) to describe the spatial dependence of low-loss (< 50eV) inelastic scattering, which is delocalized on a scale much larger than atomic dimensions. Approximating this PSF as a Lorentzian with an exponential rolloff, we then compute a PSF for energy deposition, which characterizes the spatial extent of radiolysis damage produced by a small-diameter electron probe in a beam-sensitive specimen.

These PSFs allow us to explore the radiation damage involved in the measurement of valence-electron and vibrational-mode dipole scattering, based on aloof-beam or transmission-mode EELS. Following an initial rapid decay, the EELS signal produced by an intense small-diameter probe is proportional to the probe current but largely independent of the current density and beam diameter (see FIG. 1 below), in agreement with previous measurements on polymers [1].

The efficacy of a “leapfrog” coarse-scanning technique, as a means of controlling radiation damage in energy-selected imaging, will be discussed [2].

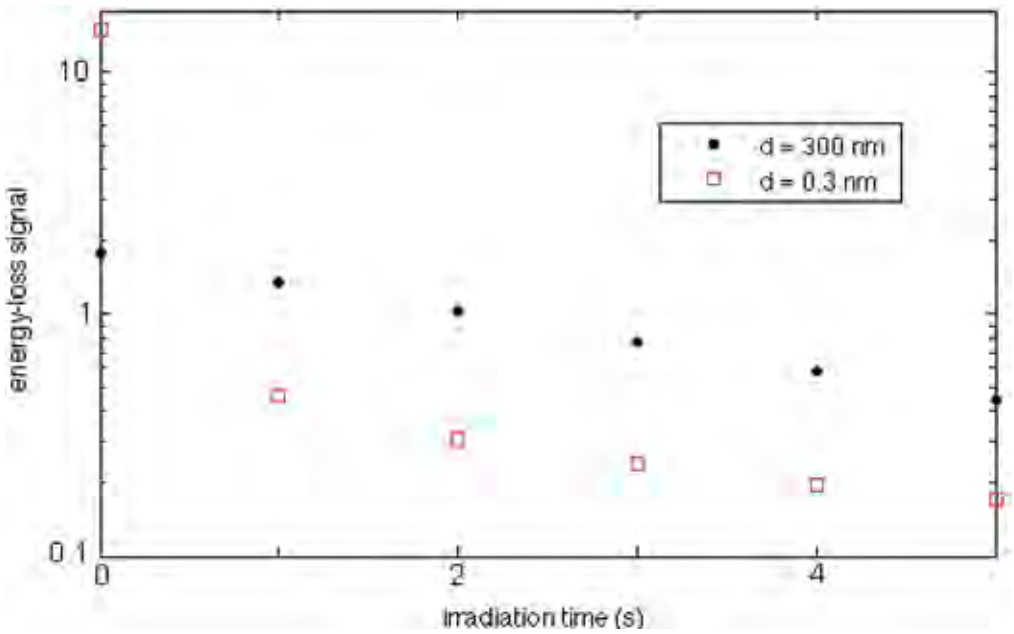

FIG. 1. Calculated time dependence of the 6eV π* energy-loss peak recorded from polystyrene, for 300keV incident energy and beam diameters of 300nm and 0.3nm.

References

[1] R.F. Egerton, S. Lazar, M. Libera, Micron 43 (2012) 2.

[2] This research was supported the Natural Sciences and Engineering Research Council of Canada. Critical comments from Chris Rossouw and Peter Crozier are gratefully acknowledged, as well as help from Peter Rez and Katia March.

Probing low-energy hyperbolic polaritons in van der Waals crystals with an electron microscope

A. Govyadinov[1], A. Konecna[1,2], A. Chuvilin[1,3], S. Vélez[1], I. Dolado[1], R. Hillenbrand[1,3], J. Aizpurua[2,4]

[1] CIC NanoGUNE, Donostia-San Sebastián, Spain
[2] Materials Physics Center CFM, CSIC-UPV/EHU, Donostia-San Sebastián, Spain
[3] IKERBASQUE, Basque Foundation for Science, Bilbao, Spain
[4] Donostia International Physics Center DIPC, Donostia-San Sebastián, Spain

Hexagonal Boron Nitride (hBN) is a representative material of a wide class of two-dimensional (2D) systems in which individual atomic layers are only weakly coupled by van der Waals interaction, resulting in extreme optical anisotropy. The latter gives rise to hBN's hyperbolic phonon polaritons (h-PhPs) [1,2] at mid-infrared (mid-IR) energies, in the range of 90-200 meV. Hyperbolic polaritons might be key to emerging technologies that rely on nanoscale light confinement and manipulation [3].

Here we perform an experimental mapping of the spectral signature of a 2D material by analyzing the electron energy loss spectroscopy (EELS) near a hBN edge, as a function of electron beam position (see Fig. 1a). We understand these excitations and the dispersion of the EELS peaks in terms of the excitation of surface h-PhPs. A theoretical description of the polaritonic losses that also considers the experimental resolution, provides an excellent agreement between theory and experiment (see Fig. 1b), proving that fast electrons can couple to hyperbolic polaritons. Further technical improvements might enable this tool to become a versatile technique for infrared vibrational spectroscopy of polaritons.

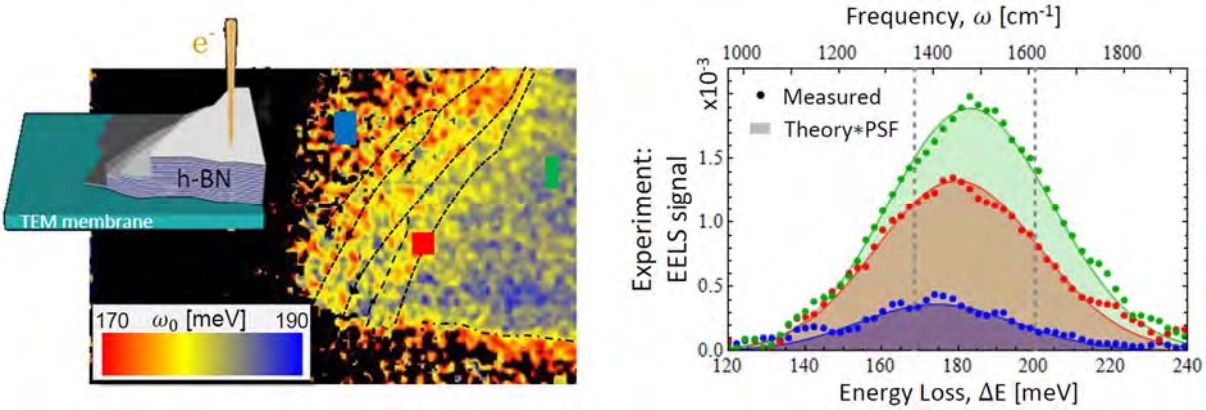

FIG. 1. Left: EEL-filtered map of a h-BN sample composed of different number of layers, as displayed in the schematics of the inset. The energy loss range is from 170 meV to 190 meV. Right: Experimental EEL spectra for different electron beam positions, as marked on the left side map (blue, red and green marks). Together with the measured dots, theoretical calculations of EELS for the different sample thickness after convolution with a 20 meV resolution is shown with lines.

References

[1] Dai S. et al. Science 343 (2014), 1125.
[2] Yoxall, E. et al. Nat. Photonics 9 (2015), 674.
[3] Li, P. et al. Nat. Commun. 6 (2015), 7507.
[4] Krivanek, O. L. et al. Nature 514 (2014), 209.

From orbital mapping to core and valence excitations: a theorist's perspective

Lorenzo Pardini[1], C. Cocchi[1], D. Nabok[1], C. Vorwerk[1], A. Manoharan[1], and C. Draxl[1,2]

[1] Physics Department and IRIS Adlershof, Humboldt-Universität zu Berlin
[1] Fritz Haber Institute of the Max Planck Society, Berlin

Ab initio spectroscopy is a powerful combination of quantum-based theories and computer simulations, covering a wide range of theoretical and computational methods that incorporate many-body effects and interactions showing up in the excited state. This framework, combining density-functional theory (DFT) with many-body perturbation theory, not only allows for analyzing data obtained by experimental probes, but also for shining light onto the underlying physics. I will demonstrate this for excitation processes from the core and valence regions and selected materials.

The first example concerns the possibility of mapping atomic orbitals. Transmission electron microscopy has been a promising candidate for a long time. Its capabilities in low-dimensional systems is explored with the prototypical example of graphene [1]. The ideal sp^2 hybridization is broken by introducing two different kinds of defects, namely a single isolated vacancy and a substitutional nitrogen atom. In this particular case, three different kinds of images are to be expected, depending on the orbital character of the conduction states. To judge the feasibility of visualizing orbitals in a real microscope, the effect of the optics' aberrations is simulated and it is finally demonstrated that a reasonable image resolution may be experimentally achieved with last-generation aberration-corrected microscopes.

The second example is dedicated to core spectroscopy. I will show how this process can be described fully from first principles including excitonic effects and spin-orbit coupling [2]. The mixing of the L_2 and L_3 edge will be demonstrated for selected materials. For the oxygen K-edge spectra from the wide-gap semiconductor Ga_2O_3 it will be shown how signals from atoms located in a particular environment can be selectively enhanced or quenched by adjusting the crystal orientation [3]. These results suggests ELNES, combined with *ab initio* many-body theory, to be a very powerful technique to characterize complex systems, with sensitivity to individual atomic species and their local environment.

References

[1] L. Pardini, S. Löffler, G. Biddau, R. Hambach, U. Kaiser, C. Draxl, and P. Schattschneider, Phys. Rev. Lett. 117, 036801 (2016).

[2] C. Vorwerk, C. Cocchi, and C. Draxl, submitted to Phys. Rev. B (2017).

[3] C. Cocchi, H. Zschiesche, D. Nabok, A. Mogilatenko, M. Albrecht, Z. Galazka, H. Kirmse, C. Draxl, and C. T. Koch, submitted to Phys. Rev. B (2016).

A hybrid method based on WIEN2k and VASP codes to calculate the complete set of EELS edges in a hundred-atoms system

G. Donval[1,2], J. Danet[3], S. Jouanneau-Si Larbi[2], P. Bayle-Guillemaud[3], F Boucher[1] and P. Moreau[1]

[1] Institut des Matériaux Jean Rouxel, Université de Nantes, CNRS, 2 rue de la Houssinière, BP 32229, 44322 Nantes Cedex, France.
[2] CEA-LITEN/DEHT SRGE, 38054 Grenoble Cedex 9, France
[3] Univ Grenoble Alpes, CEA, INAC-MEM, 38000 Grenoble, France

We present a hybrid approach well adapted to calculating the whole set of localized EELS core-loss edges on large systems using only standard tools based on Density Functional Theory, namely the WIEN2k and VASP codes. We first illustrate the usefulness of this method by applying it to a set of amorphous silicon structures (FIG 1, left) in order to explain, for amorphous silicon, the flattening of the $L_{2,3}$ EELS edge peak at the onset. We show that the peak flattening is actually caused by the collective contribution of each of the atoms to the average spectrum [1], as opposed to a flattening occurring on each individual spectrum. Furthermore, this method allowed us to reduce the execution time by a factor of 3 compared to a usual—carefully optimised—WIEN2k calculation. Then, this method is also applied to the study of the interface between crystalline silicon and Li_xSi created during lithiation of a silicon electrode for lithium batteries. Li K- and Si $L_{2,3}$ edges are calculated despite the large number of inequivalent atoms within the interphase. A graphical interface has also been developed to represent localized Li or Si edges of interest just by selecting the corresponding part of the atomic structure (FIG 1, right) [2].

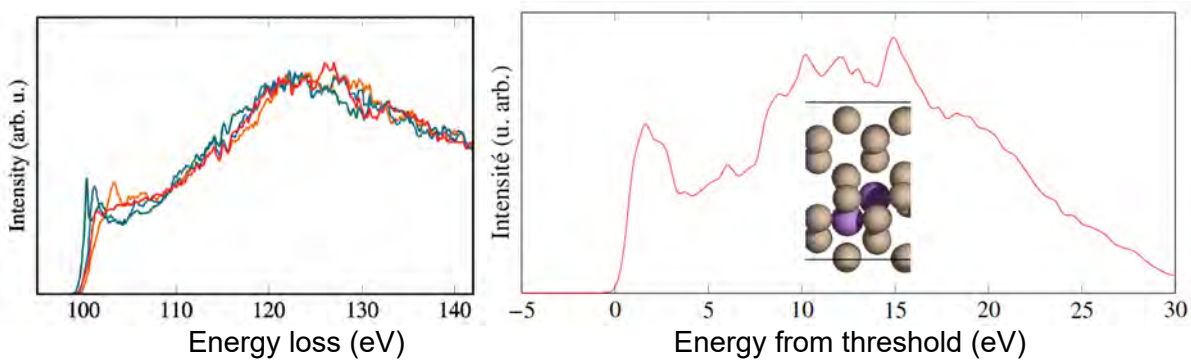

FIG. 1. (left) A few examples of amorphous silicon $L_{2,3}$ edges localized on each of the atoms of one amorphous silicon structure. (right) Extracted lithium K-edge of a Li atom in a Si/Li_xSi interface. The corresponding Li atom in the structure is shown in blue in the atomic representation.

.

References

[1] G. Donval et al.,*Phys.Chem.Chem. Phys.*(2017), DOI: 10.1039/C6CP06445K.
[2] G. Donval et al.,*to be submitted.*

Ab initio vibrational electron energy loss spectroscopy

G. Radtke[1]

[1] Institut de Minéralogie, de Physique des Matériaux, et de Cosmochimie (IMPMC), Sorbonne Universités - UPMC Univ Paris 06, UMR CNRS 7590, Muséum National d'Histoire Naturelle, IRD UMR 206, 4 place Jussieu, F-75005 Paris, France.

The infrared domain of frequencies has long remained inaccessible in electron energy loss (EEL) spectroscopy, both because of its poor energy resolution and because of the large tail of the zero-loss peak obscuring the weak inelastic signal arising in this energy range. With the recent advent of instruments able to overcome these limiting factors and pull the resolution down to less than 10 meV [1], it becomes possible to measure very low energy excitations with this spectroscopy and in particular, to detect lattice vibrations for a wide range of materials.

The emergence of this "new" vibrational spectroscopy also opens a very exciting field from a theoretical point of view. The development of tools based on first principle calculations, able to model the complex signatures [2] now accessible by this technique, are indeed mandatory to understand their physical origin and thus, to interpret the experimental data correctly. Here, I present different strategies employed to model electron energy loss spectra in the infrared range based on density functional calculations. The evaluation of the vibrational EEL scattering cross-section is carried out as a post-processing step following a harmonic phonon calculation [3], as implemented in the Quantum Espresso suite of codes [4]. Examples based on recently published experimental results [2] will be given to illustrate how *ab initio* calculations can clearly establish the origin of the different peaks forming the spectrum and reveal subtle effects, impossible to assess by a simple approach based on a fingerprint analysis. The approximations used to derive the main results will also be discussed.

References :

[1] O. L. Krivanek et al., *Nature* **514** (2014) 209.

[2] P. Rez et al., *Nature Comm.* **7** (2016) 10945.

[3] S. Baroni et al., *Rev. Mod. Phys.* **73** (2001) 515.

[4] P. Gianozzi et al., *J. Phys.: Cond. Mat.* **21** (2009) 395502.

First principles calculations of electron near edge structures of Li-ion battery materials

M. Saitoh[1], X. Gao[1], T. Ogawa[1], A. Kuwabara[1] and Y. Ikuhara[1,2]

[1] Nanostructures Research Laboratory, Japan Fine Ceramics Center, Atsuta, Nagoya 456-8587, Japan
[2] Institute of Engineering Innovation, The University of Tokyo, Bunkyo, Tokyo 113-8656, Japan

Electron energy loss (EEL) spectroscopy is a powerful method for investigating chemical states of materials. In this study we measured EEL spectra of Li-ion battery cathode material $LiCoO_2$ and compared the electron near edge structure (ELNES) with calculations using core-hole and Bethe-Salpeter equation (BSE) methods.

Experimental data were obtained using an EEL spectrometer (Tridiem ERS, Gatan, Inc.) attached to a Wien filter monochromated aberration corrected STEM (JEM-2400FCS, JEOL Ltd.) operated at 120 kV. DFT+*U* calculations were performed using the VASP code [1]. A hexagonal unit cell and *U* value of 4.9 eV were used for $LiCoO_2$. ELNES spectra were calculated using the WIEN2k code [2, 3]. Core hole calculations were carried out in a 4×4×1 supercell with the hole on one Li atom. BSE calculations were carried out using a primitive cell.

The results are summarized in Fig. 1. Calculated spectra are aligned at main peak B. Although peak intensities are not correct (peak B is underestimated by the BSE method, and peak C by the core-hole method), relative positions are in good agreement with experiment, with the BSE method the more accurate, especially for pre-edge A. By comparing the spectra with the partial density of states (PDOS) with a core hole, peak A can be attributed to hybridization of Li-*p* and Co-3*d* orbitals interposed by O-*p* orbitals, and peaks B~E result from hybridization of Li-*p* and O-*p* orbitals. The results show that both core-hole and BSE methods reproduce Li-*K* ELNES of $LiCoO_2$ well, and should be useful for ELNES analysis of other Li-ion battery materials.

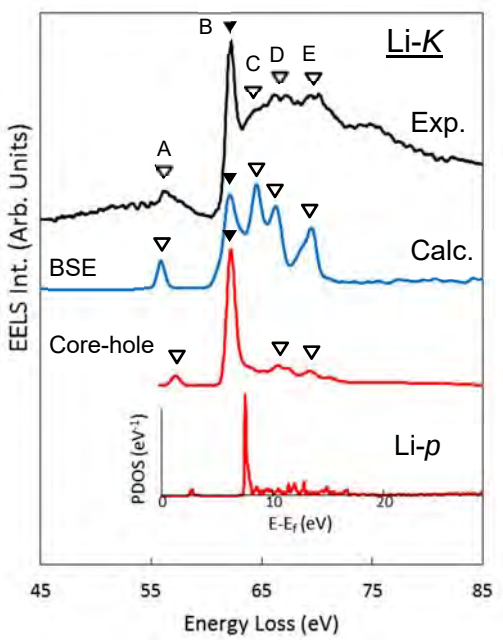

FIG. 1. Experimental and calculated Li-*K* ELNES of $LiCoO_2$, and PDOS of Li-*p* orbitals for a supercell with a core hole on one Li atom.

References

[1] G. Kresse et al., *Phys. Rev. B* 54 (1996) 11169.
[2] P. Blaha et al., *WIEN2k,* Vienna University of Technology (2001) ISBN 3-9501031-1-2
[3] R.Laskowski and P.Blaha, *Phys.Rev. B* 82 (2010) 205105.
[4] This work was supported by the Research and Development Initiative for Scientific Innovation of New Generation Batteries II (RISING II) project from the New Energy and Industrial Technology Development Organization (NEDO), Japan.

Understanding the Properties of Functional Materials with High-Resolution Electron Energy Loss Spectroscopy

G.A. Botton, E.P. Bellido, I.C. Bicket, M. Bugnet, H.S. Liu

Dept. of Materials Sci. & Eng., McMaster University, Hamilton, ON, Canada

Since the first international meeting dedicated to electron energy loss spectroscopy (EELS) in Lake Tahoe in 1990, this technique has entered new research fields and has been adopted by different research communities. Initially (and mostly) used as a method to detect “light elements” and complement X-ray microanalysis in the ‘90s, EELS has evolved from a microanalysis technique to a powerful tool to probe the electronic structure of materials. Over the years, the developments in electron microscopes and spectrometers have enabled the full potential of this technique, leading to improved spatial and energy resolution measurements. The international meetings have always showcased advances in EELS and have been setting trends of this technique and prospects for the future.

In this presentation, we will review recent applications of this technique in two fields of applications. First, we will show how EELS provides valuable information on the electronic structure and evolution of Li–based battery materials, demonstrating how the degradation and charge processes can be effectively probed to understand materials’ performance [1]. Secondly, we will show how EELS can be used effectively to understand the coupling of plasmonic excitations in metallic nanostructures [2-4]. We will highlight the flexibility of this technique due to the broad spectral range and the high spatial resolution.

The prospects for the near-future developments and the current limitations of the technique will be discussed [5].

References

[1] Liu, H.S.; Bugnet, M.; Tessaro, M. Z.; Harris, K. J.; Dunham, M. J. R.; Jiang, M.; Goward, G. R.; Botton, G. A., Spatially resolved surface valence gradient and structural transformation of lithium transition metal oxides in lithium-ion batteries, Physical Chemistry Chemical Physics 18, 29064-29075. (2016).

[2] Bellido, E.P.; Manjavacas, A.; Zhang, Y.; Cao, Y.; Nordlander, P.; Botton, G. A., Electron Energy-Loss Spectroscopy of Multipolar Edge and Cavity Modes in Silver Nanosquares, ACS Photonics 3, 428-433. (2016)

[3] Bellido, E.P.; et al. Electron Energy-Loss Spectroscopy of Fractal Structures, in submission (2017).

[4] Barrow, S.J.; Collins, S. M.; Rossouw, D.; Funston, A. M.; Botton, G. A.; Midgley, P. A.; Mulvaney, P., Electron Energy Loss Spectroscopy Investigation into Symmetry in Gold Trimer and Tetramer Plasmonic Nanoparticle Structures, ACS Nano 10, 8552-8563. (2016)

[5] This research was supported by the Natural Sciences and Engineering Research Council (NSERC). This work was carried out at the Canadian Centre for Electron Microscopy, a facility supported by the Canada Foundation for Innovation under the Major Science Initiative program, NSERC and McMaster University.

Oxygen sub-lattice ordering in A-site deficient perovskites through monochromated core-loss EELS mapping

D.M. Kepaptsoglou[1], T.Mizoguchi[2], D.Hernandez-Maldonado[1], F. Azough[3], R.Freer[3] and Q.M. Ramasse[4]

[1] SuperSTEM, Daresbury, WA4 4AD, U.K.
[2] Institute of Industrial Science, University of Tokyo, Tokyo 153-8505 Tokyo, Japan
[3] Materials Science Centre, University of Manchester, Manchester M13 9PL, U.K.

Perovskite oxides are widely studied for a variety of applications, from theromoelectrics to fuel cells. Part of the attraction lies in the fact that perovskite ceramics are relatively easy to dope chemically over a wide range of compositions, resulting in various degrees of structural ordering. As a consequence, the properties and functionalities of such materials can be readily tailored. Here, we investigate the effect of the A-site occupancy in the structure and electronic structure on an A-site deficient perovskite system based on the $Nd_{2/3x}TiO3$ double perovskite. This system, a candidate for thermoelectric applications [1], has attracted significant attention due to the presence of a peculiar superstructure [2] originating in part due to cation vacancy ordering of the A-site [3]. Using atomically resolved monochromated core loss Electron Energy Loss measurements, acquired with an energy resolution better than 90 meV, with the Nion UltraSTEM 100MC TM instrument, it is possible to map individual components of the Ti $L_{2,3}$ and O K near edge fine structures (ELNES). First-principles multiplet calculations [4] were used to explain subtle changes in the ELNES changes, and associate them predominantly with Coulombic interactions from the A-sites.

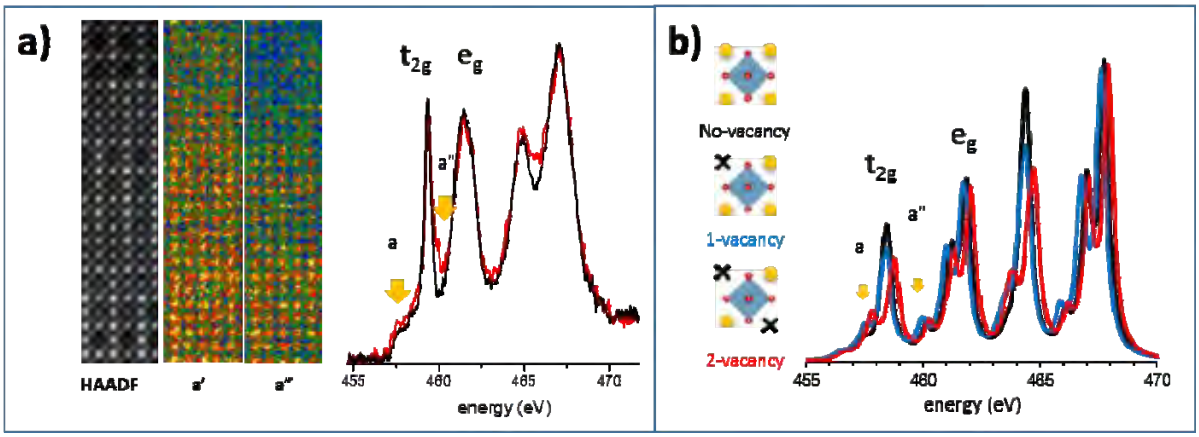

FIG. 1. (a) Atomically resolved monochromated core loss EELS measurements of the Ti $L_{2,3}$ edge in a $Nd_{2/3}TiO_3$ ceramic, showing predominantly changes in the pre- and post- intensity of the t_{2g} peak (a' and a'', respectively) and (b) theoretical spectra, associating the ELNES changes with the occupancy of the neighboring A-sites.

References

[1] S. Jackson, et al, J. Electron. Mater. 43 (2014) p.2331.
[2] A.M. Abakumov, et al Chem. Mater. 25 (2013) p. 2670.
[3] F. Azough, et al, Chem. Mater 27 (2015) p.497
[4] I. Tanaka, T. Mizoguchi, J. Phys. Cond. Matter , 21 (2009) p.104201

Applications of Electron microscopy imaging and spectroscopy to understand structure-properties relationships in complex functional materials

N. Gauquelin[1], G. Koster[2], M. Huijben[2], G. Rijnders[2], S. van Aert[1], and J. Verbeeck[1]
[1]EMAT, Department of Physics, University of Antwerp, Groenenborgerlaan 171, BE-2020, Antwerp, Belgium
[2] MESA+ Institute for Nanotechnology, University of Twente, P.O.BOX 217, 7500 AE, Enschede, The Netherlands

The study of novel physical properties appearing when two materials are interfaced has become one of the major fields of research in solid state physics over the last decade. As the materials involved in those new physical phenomena are often complex oxides, many factors (such as strain, oxygen stoichiometry, cation intermixing, electronic reconstructions) have to be considered when discussing their origin. If the two interfaced materials have different octahedral tilt systems, one has to adapt to the other [1]. Electron microscopy imaging (HAADF, ABF) and EELS spectroscopy are key tools for their study.
I will be reporting recent results enlightening the effect of this oxygen octahedral coupling on the change of the magnetic easy-axis in some ferromagnetic manganite films. [1] I will show how this change of magnetism can be related to a change in hybridization between the metal and the oxygen orbitals [2]. A second example using RNiO3 (R=Sm, Nd) superlattices will demonstrate the relationship between metal-oxygen hybridization, oxygen octahedral tilt and metal-insulator transition [3].

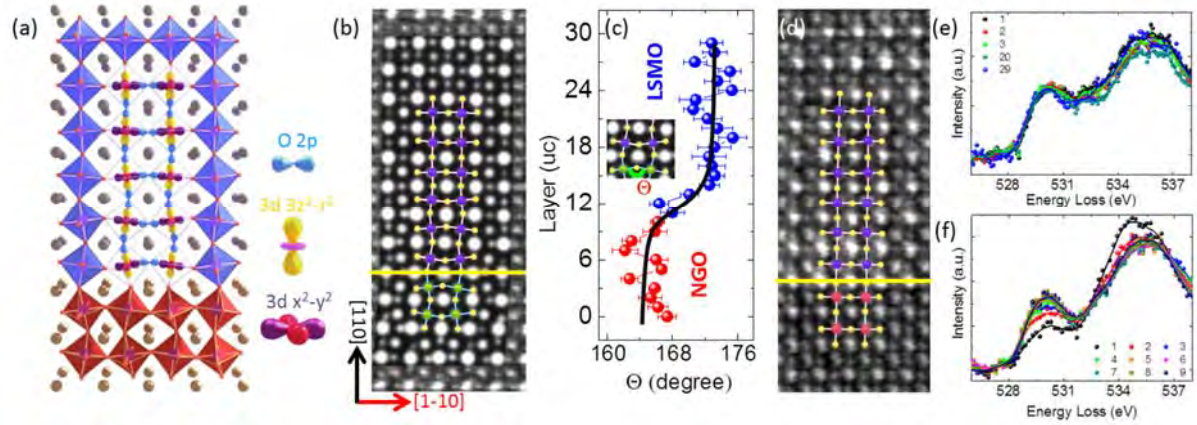

Fig1: (a) Structural model of the $NdGaO_3/La_{0.6}Sr_{0.4}MnO_3$ (NGO/LSMO) interface;(b) inversed contrast ABF image showing the tilt propagation and the corresponding BOB bond angle (c);(d) inversed contrast ABF image showing the absence of tilt when an $SrTiO_3$ (STO) buffer is intercalated; EELS O k edge fine structures of the STO buffered (e) and non-buffered (f) NGO/LSMO interface showing the change in Mn3d-O2p hybridization related to the change of BOB bond angle.

References

[1] Z. Liao, M. Huijben, Z. Zhong, **N. Gauquelin**, et al. Nat. Mater. 15 (2016), p.425-431; Z. Liao, R. Green, **N. Gauquelin**, S. Macke, et al., Adv. Funct. Mater. (2016)
[2] Z. Liao, **N. Gauquelin**, et al., *accepted,* Adv. Funct. Mater.
[3] N.G. acknowledges funding from the Geconcentreerde Onderzoekacties (GOA) project “Solarpaint” of the University of Antwerp and J.V. acknowledge funding from the Research Foundation Flanders (FWO, Belgium) project 42/FA070100/6088 “nieuwe eigenschappen in complexe Oxides”.

Hidden lattice instabilities as origin of the conductive interface between insulating $LaAlO_3$ and $SrTiO_3$

P. W. Lee[1,2], G. Y. Guo[2], H.-J. Liu[3], J.-C. Lin[4], Y.-H. Chu[3,4], C. H. Chen[1], and M.-W. Chu[1*]

[1] Center for Condensed Matter Sciences, National Taiwan University, Taipei 106, Taiwan
[2] Department of Physics, National Taiwan University, Taipei 106, Taiwan
[3] Department of Materials Science and Engineering, National Chiao Tung University, Hsinchu 300, Taiwan
[4] Institute of Physics, Academia Sinica, Taipei 105, Taiwan

The metallic interface between insulating $LaAlO_3$ and $SrTiO_3$ opens up the field of oxide electronics and displays order parameters absent in parent bulks such as superconductivity, ferromagnetism, and sensitivity to electromechanical stimuli like insulating ferroelectrics. With more than a decade of researches on this model oxide heterostructure, the fundamental origin of the interfacial conductivity is, by all means, unsettled, let alone why there shall be the collective properties. Here we resolve this long-standing puzzle of the interfacial metallicity by atomic-scale observation of electron-gas formation for screening hidden ferroelectric-like lattice instabilities, rejuvenated near the interface by epitaxial strain. Using atomic-resolution imaging and electron spectroscopy, the generally-accepted notions of polar catastrophe and cation intermixing for the metallic interface are discounted. Instead, the conductivity onset at the critical thickness of four unit-cell $LaAlO_3$ on $SrTiO_3$ substrate is structurally accompanied with head-to-head ferroelectric-like polarizations across the interface due to strain-rejuvenated ferroelectric-like instabilities in $LaAlO_3$ and $SrTiO_3$ (Fig. 1). The divergent depolarization fields of the head-to-head polarizations cast the interface into an electron reservoir, forming screening electron gas in $SrTiO_3$ with $LaAlO_3$ hosting complementary localized holes. The ferroelectric-like polarizations and electron-hole juxtaposition reveal the cooperative nature of metallic $LaAlO_3/SrTiO_3$ [1], shedding new light on the superconducting, ferromagnetic, and ferroelectric-like subtleties. This strain-hidden-lattice-instabilities interaction provides a new paradigm for novel physics at oxide interfaces.

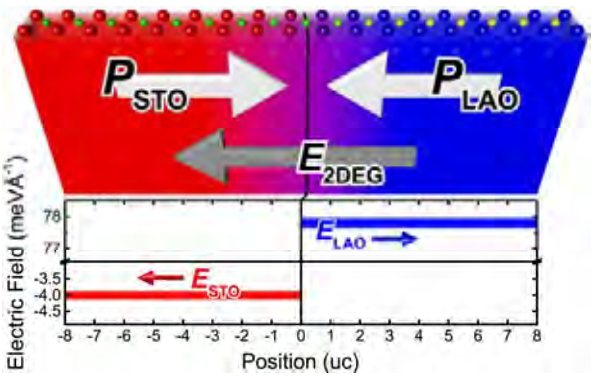

FIG. 1. Strain-rejuvenated head-to-head ferroelectric-like polarizations in metallic $LaAlO_3/SrTiO_3$ and the corresponding depolarization fields (E_{LAO}, E_{STO}, and E_{2DEG}).

References

[1] P. W. Lee *et al.*, *Nature Commun.* 7 (2016) 12773.

Carrier electron behavior of Cs doped WO_3 in NIR region studied by momentum transfer resolved EELS

Y. Sato[1], M. Terauchi[1], and K. Adachi[2]

[1] Institute of Multidisciplinary Research for Advanced Materials, Tohoku University, Sendai, 980-8577, Japan.
[2] Ichikawa Research Center, Sumitomo Metal Mining Co., Ltd., Ichikawa, Chiba 272-8588, Japan.

Near Infrared (NIR) scattering material, $Cs_{0.33}WO_3$ (CWO), which is applied for a heat-shielding filter [1], have carrier electrons (~10^{21} electrons/cm^3). The mechanism of heat-shielding (NIR EM wave scattering) is originated to plasmon resonance due to the carrier electrons [2]. However, an additional absorption structure, which cannot be explained only by plasmon, is observed in the optical scattering spectra. Polaron is a candidate of the origin of the absorption. But there is no report to show a feature of the absorption, experimentally. It is important to clarify the feature of the electron excitations of CWO in NIR region. We have adjusted a monochromator analytical TEM to conduct momentum-transfer (**q**) resolved EELS measurement. Using this technique, the q-dependence of the plasmon and the unknown excitation are investigated to reveal the origin of the NIR excitation.

Figures show E-q Maps obtained from CWO, where the **q** direction (a) is perpendicular to (b). The q-dependence of the plasmon dispersion is different between (a) and (b) (arrows). These results indicate that carrier electrons behave anisotropy in the crystal. Unfortunately, the plasmon and the additional excitation are not resolved in these E-q maps. To investigate the q-dependence of the NIR excitations in detail, the energy-resolution will be improved.

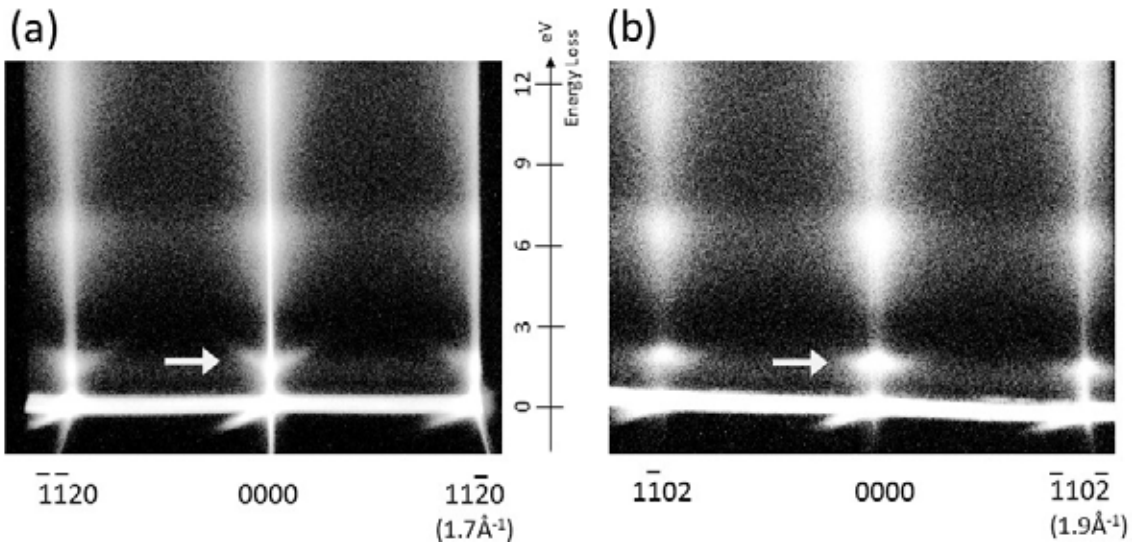

FIG. 1. E-q maps of $Cs_{0.33}WO_3$ crystal. **q** directions are along (a) $\bar{1}\bar{1}20$-0000-$11\bar{2}0$ and (b) $\bar{1}\bar{1}02$-0000-$\bar{1}10\bar{2}$.

References

[1] H. Takeda et al., J. Am. Ceram. Soc., **90** (2007) 4059-4061.
[2] Y. Sato et al., J. Appl. Phys. **112** (2012) 074308.

Is the atomic resolution monochromated EELS really useful?

K. Suenaga[1], Y.C. Lin[1], J. Lin[1], L. Tizei[1, 2] and R. Senga[1]

[1] National Institute of Advanced Industrial Science and Technology (AIST), Tsukuba 305-8565, Japan
[2] Laboratoire de Physique des Solides, Universite Paris-Sud, Orsay 91405, France

Despite of a lot of efforts (and investments) devoted to realize *both* high-spatial resolution and high-energy resolution at the same time in STEM-EELS experiments, the application of such wonderful equipment seems to be quite limited. In the low-loss regions, the EELS signal is intrinsically largely delocalized in comparison with the typical atomic size, and therefore it may not be useful to use an atomic-size probe to explore the spatial variations of low-loss spectra. On the other hand, though the EELS signal is enough localized at the targeted atom in the core-loss region, the fine structure of absorption edge (ELNES) at high-energy loss is considerably widened by a short relaxation time of the excited state. Therefore, the energy resolution required for core-loss spectroscopy is around 200 to 300 meV in FWHM for most cases, which is, sadly, within a reach of natural cold FEG and a subsequent software deconvolution. How can we then find relevant applications of the atomic resolution monochromated EELS?

We have installed a new instrument operable at low-accelerating voltages (15 - 60 kV) equipped with a double-Wien type monochromator and two DELTA correctors [1]. This machine enables us the atomic resolution STEM imaging *and* the high-energy resolution EELS better than 20 meV, both of which are, however, hardly used at the same time. Low-loss spectroscopy at optical regions in low-dimensional materials with interrupted periodicities [2, 3, 4] does not really require an atomic probe for spectroscopy but for imaging only. As a most successful example, a core-loss spectroscopy for C K-edge of carbon nanotube does identify the excitations to the van Hove singularities and show their spatial variations in connection with its atomic view in real space [5]. In this case, these peaks are non-dispersive and fully discrete in a molecular-type single quantum object, which implies sharper peaks in ELNES than those for bulk with band structures. Therefore we tentatively conclude that the atomic resolution monochromated EELS would be useful in very limited cases, where an atom or molecule is to be investigated in either fully isolated (freestanding) or very much confined (such as one-dimensional atomic chain) situation. A much confortable equipment to operate and stable specimens with perfectly immobile atoms will be needed for such extreme experiments.

References

[1] M. Mukai et al., (this conference)
[2] J. Lin et al., NanoLett., **16**, 2016, 7198-7202
[3] L. Tizei et al., Appl. Phys. Lett. **108**, 163107(2016) doi: 10.1063/1.4947058
[4] Y.C. Lin et al., (unpublished)
[5] R. Senga et al., NanoLett., **16**, 2016, 3661-3667
[6] This research was supported by JST Research Acceleration Programme and JSPS KAKENHI (JP16H06333 and JP25107003).

EELS and X-ray spectroscopic STEM imaging in 2D and 3D

G. Kothleitner[1], G. Haberfehlner[1], A. Meingast[2], H. Chan[3], F. Hofer[1] and B. Mendis[4]

[1] Institute for Electron Microscopy and Nanoanalysis, Graz University of Technology, and Graz Centre for Electron Microscopy, Graz, Austria
[2] Thermo Fisher Scientific (FEI), Eindhoven, The Netherlands
[3] Dep. of Mat. Science and Eng., Lehigh University, Bethlehem, U.S.A.
[4] Dep. of Physics, Durham University, Durham, UK

Atomic-resolution imaging with a spherical aberration-corrected (scanning) transmission electron microscope (STEM) has become widely used for the study of interesting, complex material systems. This is owed both to the flexibility in detection (annular bright [1]- and dark-field [2]) and processing (differential phase contrast, DPC [3,4]) of the scattered electrons, and to the improved efficiency of X-ray and electron energy-loss (EELS) detectors for acquiring simultaneous spectroscopic signals, ultimately even under tilting conditions, as in 3D spectroscopic STEM tomography [5]. While the principal acquisition of the data has become more straightforward, the data processing and the interpretation of the intensities appear more challenging.

In core-loss EELS imaging, for example, dynamical effects i.e. multiple elastic and inelastic scattering invoke time-consuming and computationally intense calculations, typically via Bloch-wave formalisms or multi-slice algorithms. Current studies emphasize the need for fewer simplifications in codes and for a proper treatment of the mixed dynamic form factor [6]. On the other hand, one might also benefit from “pragmatic” approaches that can quickly calculate defect structures (at least for elastic scattering) or are able to break down elastic scattering into contributions from geometric probe spreading and channeling, to support an experiment on-the-fly. In low-loss EELS, numerous applications are found that map surface plasmon resonances. Recently, a novel tomography scheme opened up new ways for characterizing the photonic environment of plasmonic nanoparticles and for computing the three-dimensional photonic local density of states [7].

Another powerful emerging combination is the linkage of integrated DPC [8] with X-ray spectroscopy. iDPC, being very dose-efficient and sensitive also to lighter elements, can complement EDX measurements and provides the projected electrostatic potential. This contribution gives recent examples for spectroscopic imaging in the mentioned areas.

References

[1] S.D. Findlay et al., *Appl. Phys. Lett.* 95 (2009) 191913.
[2] D. A. Muller et al., *Science* 319 (2008) 1073.
[3] H. Rose, *Optik* 39(4) (1974) 416.
[4] N. Shibata et al., *Nature Phys.* 8 (2012) 611.
[5] G. Haberfehlner et al., *Nanoscale* 6 (2014) 14563.
[6] Z. Lee et al., *Ultramicroscopy* 175 (2017) 58.
[7] A. Hörl et al., *ACS Photonics 2 (2015) 1429*.
[8] I. Lazić et al., *Ultramicroscopy* 160 (2016) 265.
[9] Financial support from the Austrian Research Promotion Agency (FFG) within the “Austrian Nanoinitiative” (ASTEM/COIN-821074)[1], by the EU within FP7 (FP7/2007-2013) under Grant Agreement No. 312483 (ESTEEM2)[1] and support of HMC by the US-Austria Fulbright Commission[3] is gratefully acknowledged.

Nanoscale Chemical Evolution of Silicon Negative Electrodes Characterized by Low-Loss STEM-EELS

Maxime Boniface[1], Lucille Quazuguel[2], Julien Danet[1], Dominique Guyomard[2],Philippe Moreau[2], Pascale Bayle-Guillemaud[1]

[1] Université Grenoble Alpes, CEA-INAC, F-38054 Grenoble, France
[2] Institut des Matériaux Jean-Rouxel, Université de Nantes, CNRS, F-44322 Nantes, France

Silicon represents one of the most promising anode materials for next generation lithium-ion batteries. Little is known about the Solid Electrolyte Interface (SEI) morphology at the particle scale. Attempts to characterize this system through transmission electron microscopy (TEM) have been severely limited by the radiolysis and sputtering damage respectively undergone by the SEI and lithium-silicon alloys (LixSi).

In this work [1] we demonstrate the possibility to map major SEI phases as well as quantifying Li_xSi compositions and Si crystallinity from a single dataset by combining scanning transmission electron microscopy and low-loss electron energy loss spectroscopy (STEM-EELS). The protocol we developed allows for large spectrum image acquisitions within short timeframes (~10 ms/voxel), making this method a robust and practical diagnostics tool for battery electrodes and other beam-sensitive nanostructured systems.
Results on silicon nanoparticle (SiNP)-based electrodes shed light on the SEI's deposition mechanism and morphological as well as chemical evolution along cycling (figure 1). Revealing the morphology of lithium fluoride (LiF) - large chunk-like deposits, lithium carbonates (such as Li_2CO_3) - thin conformal layers and carbon black allowed us to get unprecedented insight into the SEI's formation mechanism at the particle scale, while mapping lithium content in Li-Si alloys shed light on the lithiation mechanisms at the particle and aggregate scale.

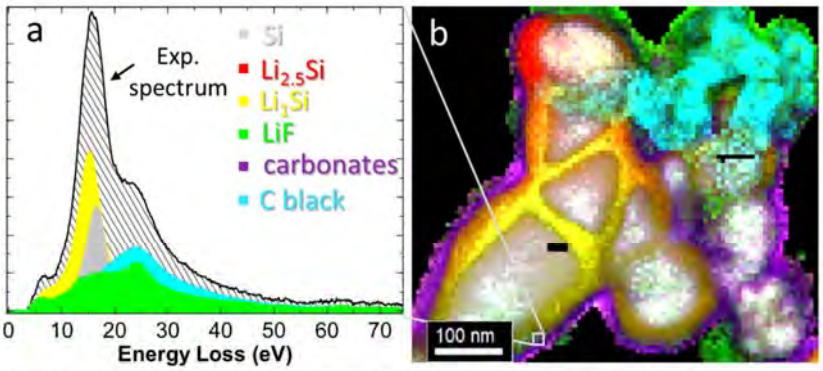

Figure 1: Analysis of silicon nanoparticles from an electrode at its 10th lithiation to 1200mAh.g^{-1}. a) Experimental low-loss EELS spectrum decomposed into reference SEI and Li_xSi compounds. b) Composite color map of the SEI and alloy morphology showing the c-Si/Li_xSi core-shell morphology, conformal carbonate coating, and LiF deposits.

References

[1] Boniface, M., Quazuguel, Danet J., Guyomard, D., Moreau, P., Bayle-Guillemaud, (2016). *Nano Lett.*, 2016, 16 (12), pp 7381–7388

STEM-EELS study of carbon doping in ferromagnetic Ge_3Mn_5 layers for spin injection

E. Prestat[1], Q. Ramasse[2], F. d'Acapito[3], S. Haigh[1], M. Jamet[4], M. Petit[5], and L. Michez[5]

[1] School of Materials, University of Manchester, Manchester, UK
[2] SuperSTEM Laboratory, Daresbury, United Kingdom
[3] European Synchrotron Radiation Facility (ESRF), 38043 Grenoble, France
[4] INAC and Université Joseph Fourier, 38054 Grenoble, France
[5] Aix-Marseille Université, CNRS CINaM-UMR 7325, F-13288 Marseille, France

Ge_3Mn_5 ferromagnetic layers are of great interest in spintronics application thanks to their compatibility with mainstream Si-based technologies [1]. While their Curie temperature (T_c) is close to room temperature, doping this material with light elements such as boron or carbon can increase the T_c [2]. Here, we study $Ge_3Mn_5C_x$ layers grown by solid phase epitaxy with carbon content ranging from x =0 to x= 0.8. Nanometric and atomic resolution EELS show that most of the carbon atoms are incorporated in the octahedral interstitial site of the Ge_3Mn_5 unit cell, with residual carbon segregation taking place at the nanometric scale. It means that not all interstitial sites are filled with carbon atoms and that there is a combination of interstitial and subtitutional Ge sites found in the high carbon concentration areas. Moreover, the fine structures of the C-K and Mn-$L_{2,3}$ edge change with carbon concentration, meaning that carbon and manganese atoms have different bonding environments [3]. Finally, we shows that correlative studies using X-Ray absorption near edge structure (XANES) and EELS techniques provide useful information in the growth mechanism of doped layers and lead to a better understanding of their physical properties.

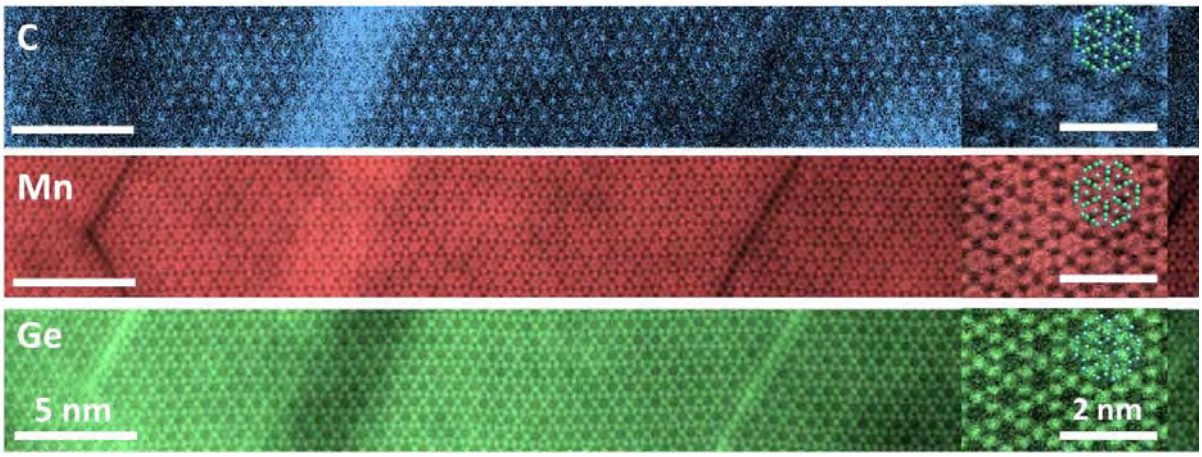

FIG. 1. Plan view atomic resolution STEM-EELS of C-doped Ge_3Mn_5 layers. (a) C, (b) Mn and (c) Ge maps showing nanoscale segregation and carbon incorporation in in octahedral interstitial site.

References
[1] A. Spiesser *et al.* Phys. Rev. B 84, 165203 (2011)
[2] I. Slipukhina *et al.* Appl. Phys. Lett. 89, 192505 (2009)
[3] D. H. Pearson *et al.* Phys. Rev. B 47, 8471 (1993)

Surface plasmon measurements using EELS – improving signal to noise ratio and revealing nanostructure coupling phenomena

A.B. Yankovich, R. Verre, E. Olsén, M. Käll, and E. Olsson

Department of Physics, Chalmers University of Technology, Göteborg, Sweden, 41296.

Metallic nanostructures support localized surface plasmons (SPs) with resonant energies that depend on the geometry and shape of the nanostructure, as well as the dielectric value of the nanostructure and surrounding medium. When bringing two nanoparticles close together (i.e. dimers), the plasmon resonances can couple and split through plasmon hybridization [1]. This plasmon coupling can produce strongly confined electromagnetic fields within the gaps that are of interest for multiple applications (i.e. bio-sensing).

Since first demonstrated [2], STEM EELS spectrum imaging (SPIM) has allowed the mapping of the plasmonic response of individual NPs with unprecedented spatial resolution [3]. However, even with state of the art equipment, the spectra often display a low signal to noise ratio (SNR) in the low energy region that can inhibit the detection of weak SPs. This is rooted in the low SP excitation cross sections and the low energy of SPs (e.g. 0.5-3 eV for Au). The zero-loss peak (ZLP) is usually >3 order of magnitude larger than SP signals, and their close proximity makes it is hard to acquire one without the other. Recording the ZLP is on the other hand often helpful for post-acquisition ZLP tail subtraction and zero energy calibration. Increasing exposure time is the simplest way to enhance SP SNR, but this is limited by saturation of the detector with the intense ZLP. Automatic spectrum summing tools that are integrated into microscope acquisition software enable better SNR but can also cause spectral blurring and reduced energy resolution due to time-varying energy instabilities. Extracting and summing multiple spectra from a SPIM can also improve SNR, but this is typically limited to tens of spectra in order to maintain nm spatial resolution.

Here, we present an EELS study of gold oligomers with controlled geometry, size, and gap distances. Samples were made using e-beam lithography. Monochromated STEM EELS experiments were conducted with ~1 nm spatial resolution and ~0.15 eV energy resolution. SPIM was used to map SP excitations and identify important electron beam impact parameters for understanding the whole set of the SPs hosted by a nanostructure. Then at each of the identified impact parameters, hundreds to thousands of fast exposure spectra were acquired using point spectral series acquisition. The spectral series were post-processed using dark spectrum subtraction, energy instability correction, Richardson-Lucy deconvolution, ZLP subtraction, and summing to improve SP SNR. STEM EELS simulations show excellent agreement with experiments and enabled the interpretation of the SP signals. These results reveal new insight into the nature of coupled plasmonic nanostructures.

References

[1] Koh et al., *ACS Nano* 3 10 (2009) 3015-3022.
[2] Nelayah et al., *Nature Physics* 3 (2007) 348.
[3] Colliex et al., *Ultramicroscopy* 162 (2016) A1-A24.
[4] This research was supported the Knut and Alice Wallenberg Foundation.

Angle-resolved cathodoluminescence spectroscopy for bandgap-based plasmonic structures

H. Saito[1], T. Sannomiya[2], and N. Yamamoto[2]

[1] Department of Electrical and Materials Science, Kyushu University, 6-1 Kasugakoen, Kasuga, Fukuoka 816-8580, Japan
[2] Department of Materials Science and Engineering, Tokyo Institute of Technology, Nagatsuta, Midori-ku, Yokohama, Kanagawa 226-8503, Japan

Confinement of surface plasmon polaritons (SPPs) using a plasmonic-crystal-based heterostructure (FIG. 1a) has been studied by angle-resolved cathodoluminescence spectroscopy (ARS) [1]. The heterostructure has a square lattice with a 600 nm period, and is composed of silver pillars with two different diameters D_1 = 250 nm and D_2 = 400 nm. Energy levels of new modes localized around the heterostructure were found in an energy range of a bandgap of the matrix lattice (FIG. 1b and 1c). Photon maps (FIG. 1d–1f) revealed that surface charge distributions of the new modes are similar to those of band-edge modes A and E in square lattice [2]. The A mode is a dark mode that does not form a surface parallel dipole moment on each pillar, and located at the lower band-edge in the square lattice with D_1 = 250 nm. Energy level of the A mode is elevated by the substituted pillar array with the larger diameter D_2 = 400 nm. On the other hand, the upper band-edge mode E is bright and doubly degenerate (E(1) and E(2)), and energy level of the E mode is lowered by the heterostructure. As a result, the new energy levels of A', E(1)', and E(2)' modes stand within the energy range of the bandgap.

A recent study about a plasmonic crystal waveguide will be also reported at the meeting.

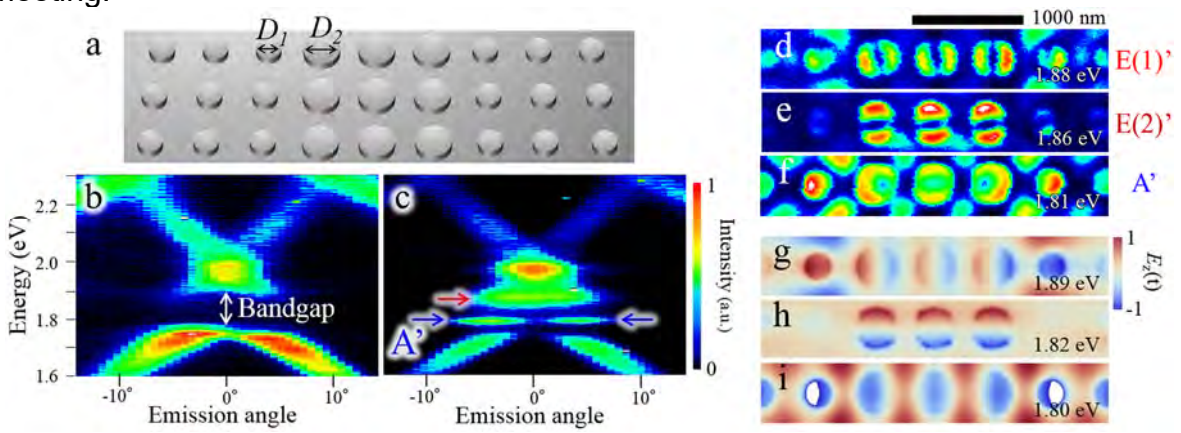

FIG. 1. (a) Illustration of the heterostructure. (b and c) ARS patterns taken from (b) the matrix and (c) the substituted rows. Photon maps of the (d) E(1)', (e) E(2)', and (f) A' modes taken using (d) s-polarized, (e) p-polarized, and (f) non-polarized light. Ez(t) of the (g) E(1)', (h) E(2)', and (i) A' simulated by the FDTD method.

References

[1] H. Saito, S. Mizuma, and N. Yamamoto, *Nano Lett.* 15 (2015) 6789–6793.
[2] N. Yamamoto, and H. Saito, *Opt. Express.* 22 (2014) 29761–29777.
[3] This work was supported by Kazato Research Foundation, and Tokyo Institute of Technology in "Nanotechnology Platform Project" sponsored by the Ministry of Education, Culture, Sports, Science and Technology (MEXT), Japan.

Nanofabrication and fast STEM-EELS for systematic studies of plasmon resonances and mode coupling in metallic heterodimers

V. Flauraud[1], G.D. Bernasconi[2], J. Butet[2], O.J.F. Martin[2], J. Brugger[1], and D.T.L. Alexander[3]

[1] Microsystems Laboratory, Institute of Microengineering, Ecole Polytechnique Fédérale de Lausanne (EPFL), 1015 Lausanne, Switzerland
[2] Nanophotonics and Metrology Laboratory (NAM), Ecole Polytechnique Fédérale de Lausanne (EPFL), 1015 Lausanne, Switzerland
[3] Interdisciplinary Centre for Electron Microscopy (CIME), Ecole Polytechnique Fédérale de Lausanne (EPFL), 1015 Lausanne, Switzerland

Advancing the applications potential of plasmonics relies on the ability to controllably tune the resonances of nanoscale antennas in order to achieve tailored near field and far field electromagnetic properties. Beyond well-known single metal structures, we explore new tuning concepts by selectively coupling the modes of nanoparticle pairs made from different materials. These “heterodimers” are made by novel wafer scale nanofabrication technology, which gives nanometric control over particle size, shape and separation, combined with a “TEM ready” sample geometry that can also be integrated into devices. The heterodimers, comprising of Au:Ag or Au:Al pairs, are systematically analyzed in function of particle shape, dimension and gap size by monochromated STEM-EELS on a FEI Titan Themis 60-300, using a specific setup to rapidly acquire high spatial statistic maps with ~110 meV energy resolution (e.g. 800 x 800 px in <10 minutes). A wide range of mode energy detuning and coupling conditions are studied by this near field imaging, supported by full wave analysis numerical simulations; see Fig. 1 for an example from a Au:Ag nanodisc pair. These results provide direct insights into the mode hybridization of plasmonic heterodimers, pointing out the influence of each dimer constituent in the overall electromagnetic response, which will lead to new design and applications possibilities.

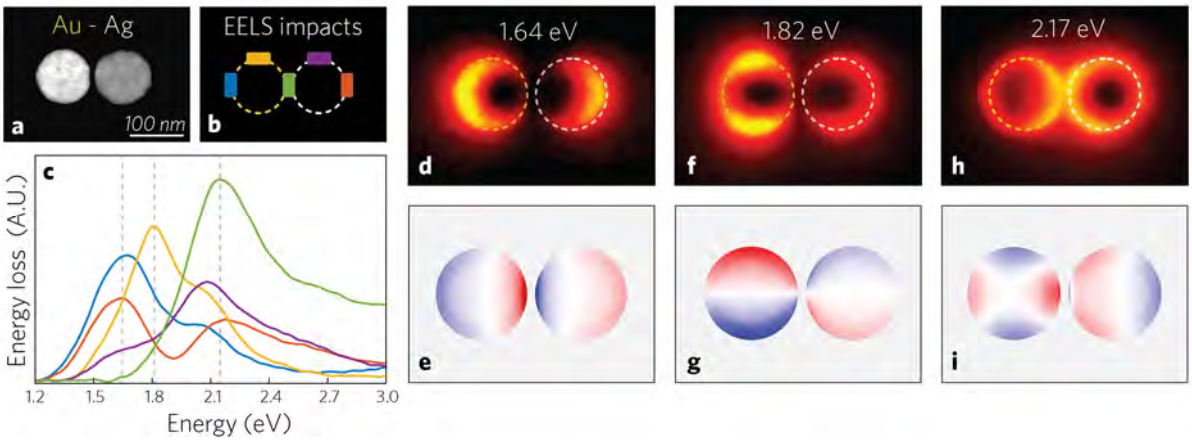

FIG. 1. Coupling of Au:Ag nanodisc pair showing: a) HAADF image; c) EEL spectra integrated from different impact positions b); d, f, h) EELS intensity maps for different plasmonic modes; with e, g, i) corresponding computed eigencharge distributions.

References

[1] Research in part supported by: European Commission; SNSF; CMi EPFL.

Hybrid plasmonics: From plasmon-plasmon to plasmon-exciton coupling

Franz-Philipp Schmidt[1,2], Harald Ditlbacher[1], Andreas Hohenau[1], Ulrich Hohenester[1], Ferdinand Hofer[2], and Joachim R. Krenn[1]

[1] Institute of Physics, University of Graz, 8010 Graz, Austria
[2] Institute for Electron Microscopy and Nanoanalysis, Graz University of Technology, 8010 Graz, Austria

The coupling of plasmonic nanoparticles can lead to extremely localized fields and is thus a central topic in nanooptics research and application. In our work, we show that the spectral response of a single rectangular plasmonic nanoparticle can be interpreted due to coupling of edge excitations, leading to bonding and antibonding modes (Fig.1a,b) [1]. On one hand, we rely on high-resolution experimental data from electron energy-loss spectroscopy, applied to a single lithographically prepared silver cuboid. On the other hand, we use numerical simulations by the boundary element method, finding excellent agreement with the experiment.

Going one step further we couple metallic with semiconducting nanostructures (Fig.1c) in terms of plasmon-exciton coupling [2]. The importance of high energy resolution to differentiate subtle energy shifts and splittings is demonstrated using a monochromated system in combination with advanced data post processing routines (Fig.1d) [3,4].

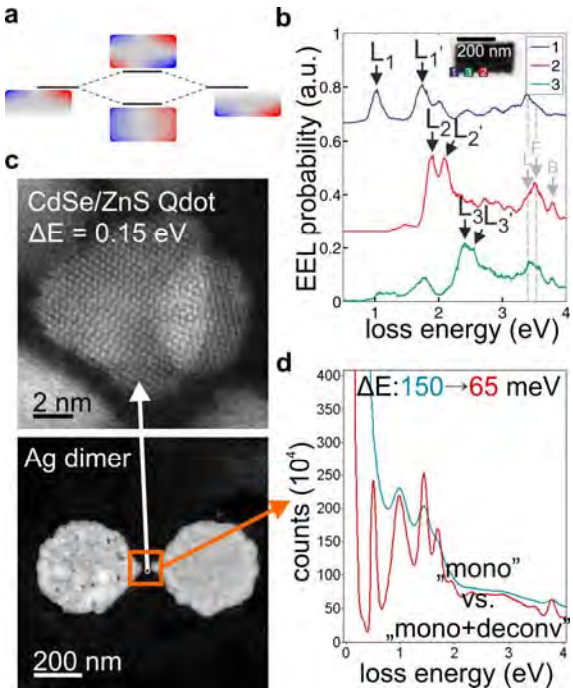

Fig. 1.
Plasmon-plasmon coupling:
(a) Simulated charge distribution of the dipolar plasmon edge mode along a 300 nm long silver edge, which splits up into a bonding and antibonding mode due to coupling of the opposite edge plasmons. (b) EEL spectra extracted from three different regions of a silver nanocuboid as indicated in the inset.
Plasmon-exciton coupling:
(c) (Monochromated) HAADF images of a silver dimer and CdSe/ZnS quantum dots and (d) corresponding EEL spectra in the gap region before (blue) and after (red) data post processing.

References

[1] F.-P. Schmidt et al., *Nano Lett.* 16 (2016) 5152.
[2] J. Wei et al., *Nano Lett.* 15 (2015) 5926.
[3] F.-P. Schmidt et al. *Micron* 93 (2017) 43.
[4] This research was supported by the Austrian Science Fund FWF (P21800-N20, SFB F49), NAWI Graz and the Graz Center for Electron Microscopy.

Probing the band structure modification in perovskite nanocrystals by low-voltage monochromatic electron energy loss spectroscopy

Junhao Lin[1], Leyre Gómez[2], Chris de Weerd[2], Yasufumi Fujiwara[3], Tom Gregorkiewicz[2,3], and Kazutomo Suenaga[1]

[1] National Institute of Advanced Industrial Science and Technology (AIST), AIST Central 5, Tsukuba 305-8565, Japan
[2] Institute of Physics, University of Amsterdam, Science Park 904, 1098 XH Amsterdam, The Netherlands
[3] Division of Materials and Manufacturing Science, Graduate School of Engineering, Osaka University, 2-1 Yamadaoka, Suita, Osaka 565-0871, Japan

The combination of monochromatic electron energy loss spectroscopy (EELS) with high spatial resolution provides the possibility to investigate the optical properties on nanometer-sized objects in parallel with their structural parameters. $CsPbX_3$ (X= Cl, Br and I) nanocrystals (NC) is an ideal platform for such EELS study due to their size-tunable optical properties, and also their promising applications in low-cost photovoltaic devices. We demonstrated the use of the valence-loss EELS n a state-of-the-art low-voltage monochromatic scanning transmission electron microscope (STEM) in probing the band structure modification in beam-sensitive $CsPbBr_3$ NCs. The beam damage is minimized by the optimized experimental conditions including lose acceleration voltage, low electron dose and low temperature so that a full EEL spectrum collection damage little to the NC. Explicitly, we demonstrate that the bandgap increase due to quantum confinement, and is governed by the smallest dimension of the cuboidal perovskite nanocrystal. We also discovered that the mutual coupling between neighboring NCs change the behavior of the quantum confinement effect (Fig. 1) [1]. These insights are uniquely enabled by the low-loss EELS techniques illustrating its potential for nano-optics research [2].

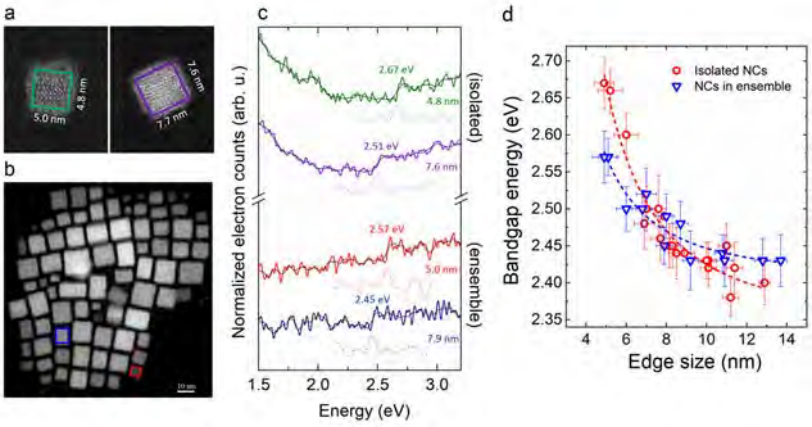

FIG. 1. (a, b) ADF images of individual NCs with a size of ~6 nm (green) and ~8 nm (purple) respectively, and an ensemble where two NCs with similar sizes as in (a) are indicated (red, blue). (c) The corresponding low-loss EEL spectra of the isolated (top) and in ensemble (bottom) NCs as shown in (a,b). (d) The bandgap energies of single NCs that are either isolated (red dots) or in an ensemble (blue triangles) as determined from low-loss EELS measurements on single NCs, plotted as a function of their sizes.

References

[1] Lin, J., et al., *Nano Letters.* 16, (2016) 7198

[2] We acknowledged JST-ACCEL and JSPS KAKENHI (JP16H06333 and P16382) for financial support.

Electronic excitations and molecular orientation in the charge density wave material 1T-TaS_2 intercalated with organic molecules.

M. K. Kinyanjui[1], J. Holzbock[2], J. Koster[1], M. Linden[2] and U. Kaiser[1]

[1] Central Facility of Electron Microscopy, Ulm University, Albert Einstein Allee 11, 89068 Ulm, Germany
[2] Institut für Anorganische Chemie II, Ulm University, Albert Einstein Allee 11, 89081 Ulm, Germany

We have investigated the electronic and atomic structures of charge density wave (CDW) material 1T-TaS_2 intercalated with Pyridine (C_5H_5N), and Triethylenediamine ($C_6H_{12}N_2$). Using momentum-resolved electron energy loss spectroscopy (EELS) we have determined the nature and dispersion of the plasmon and interband excitations along different directions of the Brillouin zones and at different CDW states. Figure 1 (a) displays the electron diffraction pattern of 1T-TaS_2 at 350 K showing the superlattice spots due to CDW distortion. The electron diffraction of 1T-TaS_2 intercalated with $C_6H_{12}N_2$ is shown in Fig.1 (b).The momentum resolved spectrum for CDW distorted 1T-TaS_2-$C_6H_{12}N_2$ along the Γ-M direction of the Brillouin zone is shown in Fig. 1(c). In addition we have determined the orientation of the intercalated C_5H_5N and $C_6H_{12}N_2$ molecules within the 1T-TaS_2 layers through orientation dependent EELS at the C-K and N-K edges. We demonstrate also first results using the new SALVE microscope [1].

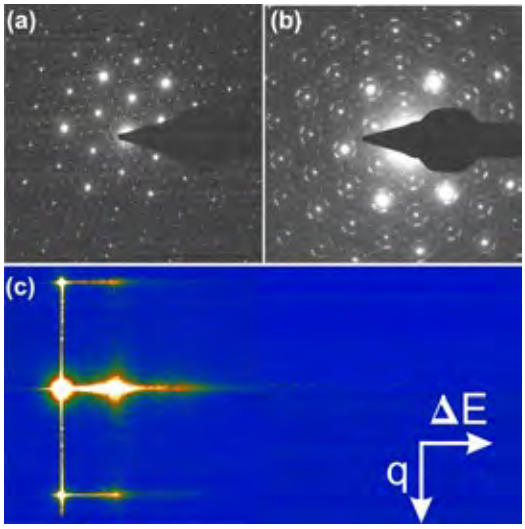

Figure. 1: Electron diffraction of (a) 1T-TaS_2 at 350 K showing the superlattice spots due to CDW distortion (b) 1T-TaS_2 intercalated with $C_6H_{12}N_2$ (c) Momentum-resolved EELS spectrum for CDW distorted 1T-TaS2- $C_6H_{12}N_2$ along the Γ- M direction of the Brillouin zone.

[1] www.salve-project.de
[2] This research was supported by the German Research Foundation (DFG) and the Ministry of Science, Research and the Arts (MWK) of the federal state of Baden-Württemberg, Germany in the frame of the SALVE project.

Combining EELS and HRTEM in operando analyses of ceria

M. Bugnet[1], F. J. C. S. Aires[2], M. Aouine[2], and T. Epicier[1,2]

[1] Laboratoire MATEIS, UMR 5510 CNRS – Université de Lyon – INSA Lyon
[2] Laboratoire IRCELYON, UMR 5256 CNRS – Université de Lyon – UCBL

Since the vast majority of materials are not used in moderate or high vacuum, investigating them *in situ* in the TEM in more realistic environmental conditions appears necessary to understand fundamental structural and chemical aspects in several fields of research such as catalysis or crystal growth. In this respect, control of the nature and the pressure of the atmosphere surrounding the specimen while allowing nanoscale down to atomic resolution analysis in a transmission electron microscope is of great importance. Oxidation and reduction phenomena at surfaces of catalysts such as ceria (CeO_2) can be induced and controlled by the partial pressure and temperature within a dedicated Cs-image corrected environmental TEM (ETEM) [1, 2]. Tracking the mobility of surface atoms using HRTEM and evaluating the reduction state of Ce using EELS (see FIG. 1a) at surfaces of ceria nanocubes under reducing and oxidizing conditions sheds light on the surface structure and chemistry of CeO_2. Beyond oxidation and reduction, both techniques are used to monitor CO_2 adsorption down to the atomic scale (see FIG. 1b). The combination of EELS and HRTEM is shown to be very powerful for ETEM studies, bringing new insights into the nature and structure of ceria surfaces in realistic conditions [3].

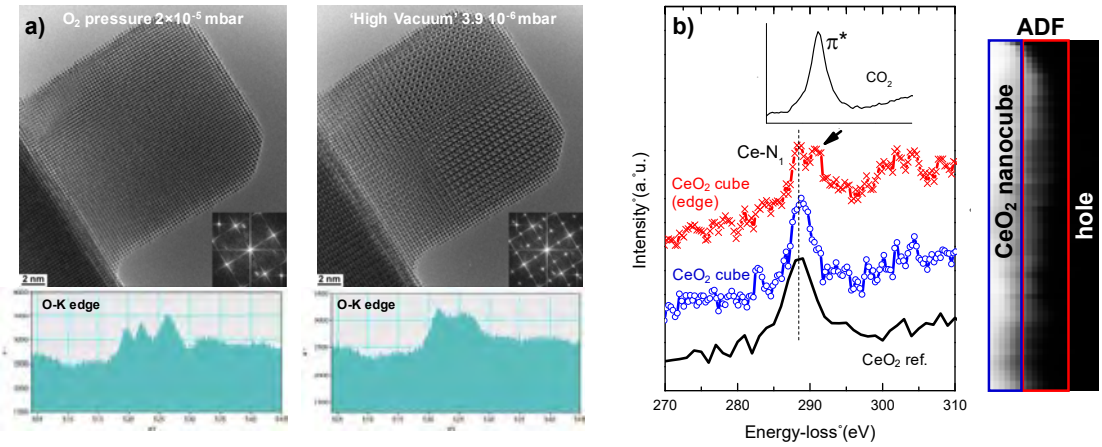

FIG. 1. a) HRTEM images of CeO_2 nanocubes as a function of O_2 partial pressure, and corresponding O-K edges. b) EEL spectra acquired at the edge of a CeO_2 nanocube (red crosses) and in the bulk of the same nanocube (blue crosses) during exposure to CO_2 (350ºC, $PCO_2 = 3.10^{-2}$ mbar) as shown in ADF. The peak indicated by the arrow can be related to the presence of adsorbed CO_2 at the surface of the nanocube (the very low pressure of CO_2(g) makes it undetectable in bulky areas).

References

[1] R. Wang et al., Nano Lett. 8 (2008) 962.
[2] F.J.C.S. Aires et al., *EMC 2016: Proceedings*. Wiley-VCH Verlag GmbH & Co.
[3] The authors thank A. K. P. Mann, Z. Wu, and S. H. Overbury from Oak Ridge National Laboratory for providing the ceria nanocubes. The electron microscopy presented here has been performed on a FEI Titan ETEM at the CLYM: Lyon-St-Etienne centre for electron microscopy (www.clym.fr).

In-Situ Materials Characterization at High Spatial Resolution: 2D Materials Based Liquid-Cell Microscopy

Xuan Hu, A. Mukherjee, J. Jokisaari, C. Wang and R.F. Klie[1]

[1] University of Illinois at Chicago, Dept of Physics, Chicago, IL 60607

The last few years have seen a paradigm change in scanning transmission electron microscopy (STEM) with unprecedented improvements in both spatial and spectroscopic resolution being realized by aberration correctors, cold-field emission guns and monochromators. Aberration correction also allows increased flexibility in choosing the appropriate electron energy to minimize beam-induced damage while maintaining atomic-resolution (e.g. 60 keV electrons for studying graphene with 1.3 Å resolution).[1] These developments have enabled a revolution in resolution, which now allows us to perform *in-situ* or *operando* measurements at, or close to, the limits dictated by sample properties rather than the instrumentation resolution. More specifically, direct imaging of electron-liquid interaction has become possible at the nanometer scale with the wide-spread availability of commercial liquid cells. While this enables thin liquid layers, and structures suspended in such layers, to be studied at atmospheric pressures, the imaging resolution and chemical quantification capabilities are still limited by the existing holder designs. Moreover, the electron dose rate required for atomic-resolution imaging is believed to be significantly higher than the damage threshold in conventional liquid-cell experiments.

We have recently developed a novel approach towards in-situ electron microscopy that allows the effects of radiolysis to be examined on the atomic-level scale and provides the required control over these effects to minimize beam-induced radiation damage. [2, 3] More specifically, we utilize a liquid cell, consisting of two graphene monolayers to encapsulate a small volume of liquid, as shown in Figure 1.[4] We will demonstrate that the creation of bubbles can be carefully controlled in graphene based liquid cells, and that the effects of heating and heat transfer can be measured using low-loss EELS.

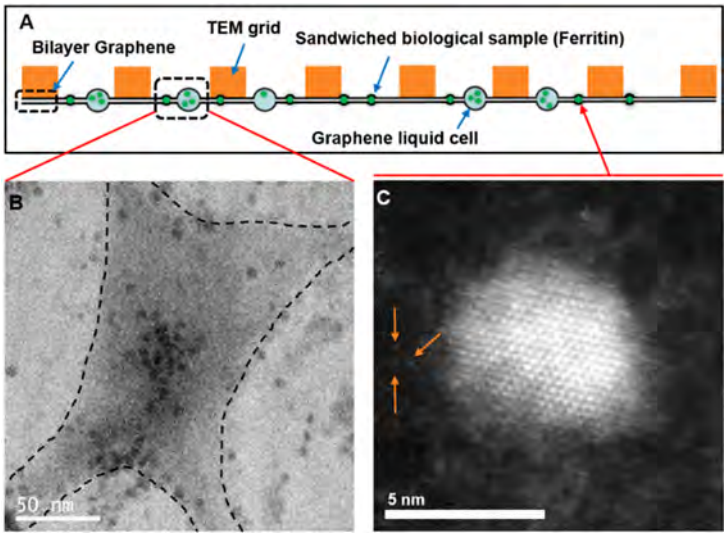

Figure 1: Schematic diagram (**A**), as well as STEM images (**B**) and (**C**) of ferritin molecules in a graphene liquid cell. (**B**) is an annular bright field (ABF) image showing ferritin molecules encapsulated in both a liquid pocket. The edges of the liquid are indicated by dashed lines. (**C**) is a high angle annular dark field (HAADF) image showing atomic-resolution image of a sandwiched ferritin molecule, with the 12nm in diameter protein shell and individual Fe atoms resolved.

References

[1] Zhou, W.et al. Nature Nanotechnology, 7(3),161-165 (2012)
[2] Wang, C., Q. et al., Advanced Materials, **26**,3410–3414 (2014)
[3] Wang, C., T. Shokuhfar, and R.F. Klie, Advanced Materials, **28**(35), 7716 (2016)
[4] This work in in part funded by the National Science Foundation (DMR-0959470).

Novel Spectroscopy in Aberration-Corrected and Monochromated STEM

J.C. Idrobo[1], J.A. Hachtel[1], J. Spiegelberg[2], J. Rusz[2], and A.R.Lupini[3]

[1] Center for Nanophase Materials Sciences, Oak Ridge National Laboratory, P.O.Box 2008, Oak Ridge, TN 37830
[2] Department of Physics and Astronomy, Uppsala University, P.O. Box 516, 75120 Uppsala, Sweden
[3] Materials Science and Technology Division, Oak Ridge National Laboratory, P.O.Box 2008, Oak Ridge, TN 37830

Until very recently, the goal of aberration-correction in STEM has been to produce the possible smallest electron probes. The reasoning is that smaller probes result in images and spectra with better spatial resolutions. However, it has been recently argued on theoretical grounds that in some cases it is desirable to have an atomic-size electron probe with customized aberrations [1]. In this talk we will discuss how one can use aberrated electron probes to detect magnetic ordering by observing a dichroic signal in the fine structure of an L-edge in a transition metal element, as shown in Figure 1 for the case of the antiferromagnetic LaMnAsO [2].

In this talk we will also present our recent spectroscopy results of plasmonic nanostructures using ORNL's recently acquired Nion's monochromated aberration-corrected STEM [3].

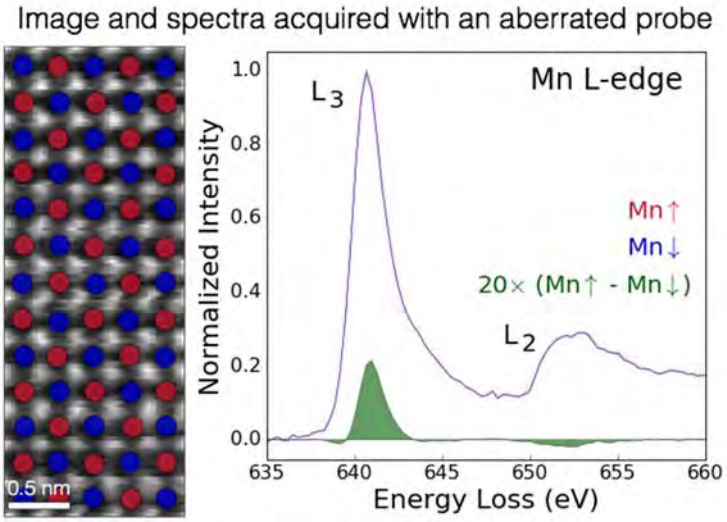

FIG. 1. Image and spectra acquired with an aberrated electron probe. The magnetic signal (green) arises from the subtraction of the spectra of all the Mn atomic columns with spin down (blue) from all the Mn atomic columns with spin up (red).

References

[1] J. Rusz, J. C. Idrobo, and S. Bhowmick, *Phys. Rev. Lett.* **113** (2014) 145501
[2] J. C. Idrobo et al., *Advanced Structural and Chemical Imaging* **2** (2016) 1
[3] This research was partially supported by the Center for Nanophase Materials Sciences (CNMS), which is sponsored at ORNL by the Scientific User Facilities Division, Office of Basic Energy Sciences, U.S. Department of Energy (JCI, JAH), by the Swedish Research Council and Swedish National Infrastructure for Computing (NSC center) (JR), and by the Materials Sciences and Engineering Division Office of Basic Energy Sciences, U.S. Department of Energy (ARL).

The Universe is my nano-fab: STEM-EELS-EDX analysis of planetary materials and synthetic analogs

R.M. Stroud[1], B.T. De Gregorio[1], K.D. Burgess[1]

[1]Materials Science and Technology Division, U.S. Naval Research Laboratory, 4555 Overlook Ave. SW, Washington, DC, 20375.

Analytical electron microscopy of planetary materials enables researchers to constrain astrophysical processes ranging from the evolution of stars to the delivery of carbon to the early Earth. Many of the planetary materials of interest, such as nanodiamond and SiC, are also of interest for technological applications. Questions that can be addressed with STEM-EELS and EDX that are common to both planetary materials and materials science research include incorporation of Si, N and other impurities into nanodiamonds (Fig. 1A) [1], and the distribution of Al and N in SiC grains. Questions more specific to planetary science include the use of EELS to quantify the implanted solar wind H and He content of exposed lunar soil and asteroid particles (Fig. 1B). This presentation will discuss use of the Nion UltraSTEM-200X with a Gatan Enfinium ER EEL spectrometer and Bruker 0.7 sr windowless, SDD EDX system for high-spatial resolution, high sensitivity analysis of both planetary materials, and laboratory analogs.

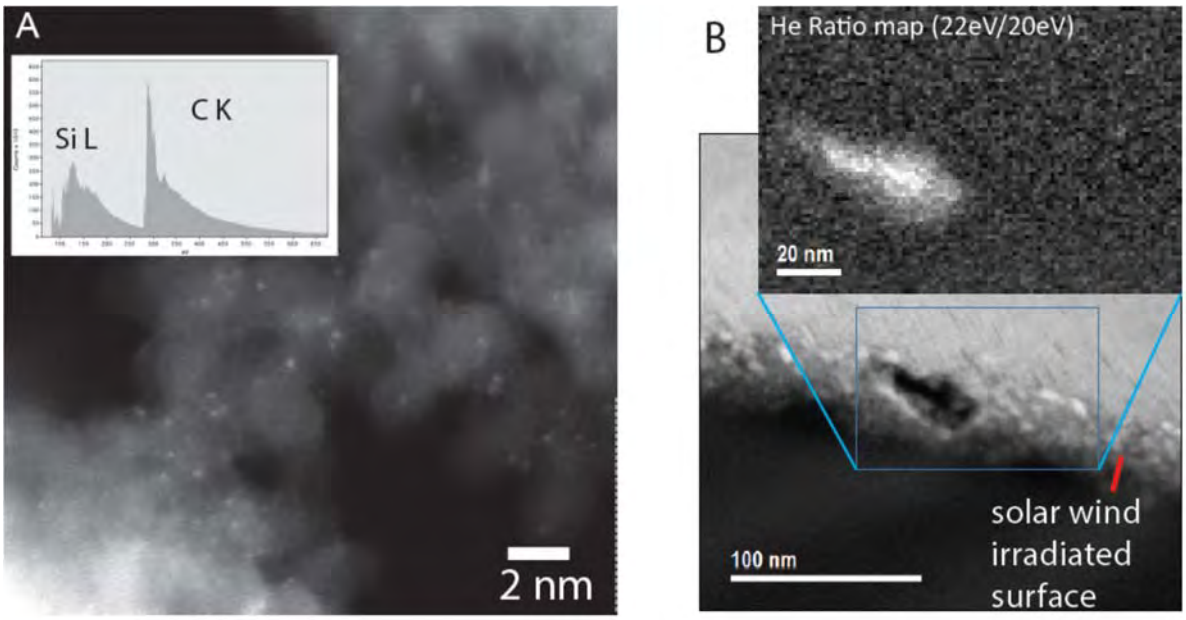

FIG. 1. A. HAADF image and core-loss EELS of Si ad atoms on nanodiamond aerogel. B. HAADF and EELS map of solar wind implanted He in a lunar illemenite grain.

References

[1] Stroud, R.M., et al., *Individual heteroatom identification with X-ray spectroscopy.* Applied Physics Letters, 2016. **108**(16).

[2] This research was the NRL 6.1 basic research program and the NASA Emerging World and SSREVI programs. Diamond aerogel samples provided by M. J. Crane and P. J. Pauzauskie. Lunar soil samples provide by NASA JSC.

Aberration-Corrected Differential Phase Contrast Scanning Transmission Electron Microscopy

N. Shibata

Institute of Engineering Innovation, The University of Tokyo

Understanding the structures of interfaces even down to atomistic scales is essential to design and control the functional properties of nanomaterials and devices. Scanning transmission electron microscopy (STEM) boosted by aberration-correction technology has made possible the direct imaging and characterization of atomic and electronic structures at localized volumes of many materials and devices, especially at interface regions where very interesting properties emerges. In STEM imaging, a very finely focused electron probe is scanned across the specimen and the transmitted and/or scattered electrons at each raster position are detected by the post-specimen detector(s) to form images. It is well known that the STEM image contrast is strongly dependent on the detector geometries, and in turn we gain flexibility in determining the contrast characteristics of the STEM images by controlling the detector geometry. In recent years, we have developed segmented type STEM detectors which divide the detector plane into 16 segments [1]. Using these segmented type STEM detectors, we have shown differential phase-contrast (DPC) imaging [2,3] can be very powerful tool for characterizing local electromagnetic field structures in materials and devices. For example, DPC STEM can clearly visualize the local electric field variation due to the abrupt potential change within a p-n junction in a GaAs semiconductor [4]. Imaging of magnetic structures, such as skyrmions, is also very effective using DPC STEM [5,6]. Moreover, real-time imaging of electromagnetic structures can now be realized through very fast data processing and reconstruction algorithms [7]. In this talk, the current status of aberration-corrected DPC STEM along with some applications in materials studies will be reported. New prospects for atomic-resolution DPC imaging [8] will be also discussed.

References

[1] N. Shibata *et al.*, *J. Electron Microscopy*, **59**, 473-479 (2010).
[2] N.H. Dekkers and H. de Lang, *Optik*, **41**, 452 (1974).
[3] H. Rose, *Ultramicroscopy*, **2**, 251 (1977).
[4] N. Shibata *et al.*, *Sci. Rep.*, **5**, 10040 (2015).
[5] T. Matsumoto *et al.*, *Sci. Adv*, **2**. e1501280 (2016).
[6] T. Matsumoto *et al.*, *Sci. Rep.*, **6**, 35880 (2016).
[7] R. Close *et al.*, *Ultramicroscopy*, **159**, 124-137 (2015).
[8] N. Shibata *et al.*, *Nature Phys.*, **8**, 611-615 (2012).

New STEM strategies at FEI

E. Van Cappellen[1], I. Lazić[2], E. Bosch[2], S. Lazar[2] and E. Yücelen[2]

[1] Thermo Fisher Scientific Hillsboro;
5350 NE Dawson Creek Drive, Hillsboro OR 97124; USA
[2] Thermo Fisher Scientific Acht;
Achtseweg noord 5, P.O. Box 80066, 5600 KA, Eindhoven; The Netherlands

Annular Dark Field (ADF) is the technique of choice for HR-STEM imaging because of some well-established properties. ADF images are directly interpretable, atomic columns are always white and there's only one unmistakable focus. The only drawbacks of ADF imaging are that it's not sensitive to light elements and that fairly long acquisition times (several seconds to a minute) are required to achieve good signal-to-noise images. "Bright" Field (BF) techniques have a clear advantage when it comes to signal-to-noise and light element sensitivity but BF imaging saw little acceptance until Annular Bright Field (ABF) was introduced [1].

The above "conventional" techniques use disc and annulus shaped STEM detectors but the new trends are to change these geometries. The simplest non-conventional geometry is a segmented disc or annulus and the most complex one is a pixelated detector capable of mimicking any shape but as always there are trade-offs between complexity and usability and they'll be discussed.

The most promising technique using segmented detectors is iDPC or integrated Differential Phase Contrast [2] and the many desirable properties of iDPC will be presented. The main benefits are that all elements, light and heavy can be imaged simultaneously and that the interpretation is straightforward as no contrast reversals occur (atom columns are always white). The latest iDPC application results will be shown including, but not limited to, low-dose and low-Z elements imaging.

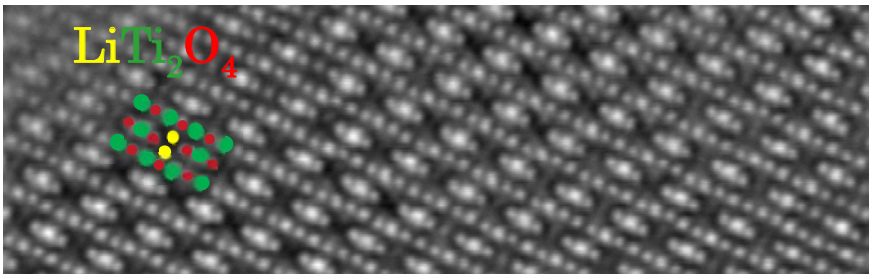

FIG. 1. Imaging of the lithium columns in $LiTi_2O_4$

The options for pixelated STEM detectors will be revealed and the trade-offs between the different techniques will be discussed.

References

[1] S.D. Findlay et al. *Ultramicroscopy* 110 (2010) 903–923
[2] I. Lazić, E. Bosch & S. Lazar, *Ultramicroscopy* 160 (2016) 265-280

Mapping the Angular and Spatial Dependence of Phonon Scattering using LACBED

J. Etheridge[1], C.J. Rossouw[1], K. Tsuda[2] and C.L. Zheng[1]

[1] Monash Centre for Electron Microscopy, Monash University, Australia.
[2] Frontier Research Institute for Interdisciplinary Sciences, Tohoku University, Japan.

LACBED patterns provide a map of scattered intensity as a function of incident angle and specimen position for a specific scattering vector, **s** [1]. Normally, the scattering vector is chosen to be a Bragg vector, **g**, and the LACBED patterns then map the intensity scattered into **g**. This intensity is due primarily to elastic scattering [2].

Here, we consider zero-loss energy filtered LACBED patterns where the scattering vector, **s**, is chosen *not* to equal a Bragg vector. Then the intensity scattered into the pattern derives almost entirely from electrons that have scattered from phonons because of the energy filtering action of the selected area aperture and the imaging filter. These patterns map the angular and spatial dependence of scattering from all phonon modes with wave vectors, **q**, where **s**=**g**+**q**, and **g** can be any Bragg vector.
We map the scattering from the low energy transverse acoustic mode in Si with wave vectors in the planes {011} [3] with an angular resolution within 0.01Å^{-1}. We also map phonon scattering in spatially inhomogeneous materials.

If this approach were executed in an ultrahigh energy resolution STEM, such as have recently become available [4], it may help to resolve the currently elusive low energy transverse acoustic phonon modes.

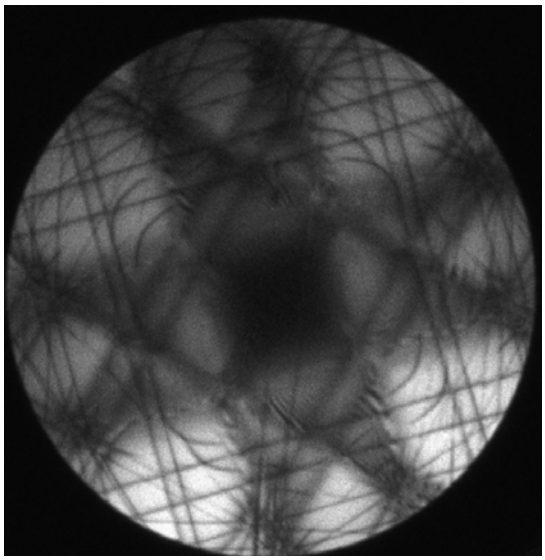

FIG.1. LACBED pattern generated almost exclusively by phonon-scattered electrons with scattering vector, $\mathbf{s}\sim\mathbf{1/5g}_{-2-20}+\mathbf{1/2g}_{2-20}$, in <100> Si at 300keV.

References
[1] M. Tanaka et al. *J. Elect. Micro.*, 29 (1980) 408
[2] I.K. Jordan et al. *Ultramic.* 35 (1991) 237
[3] G. Honjo et al. *J Phys Soc Jap* 19 (1964) 351
[4] O. Krivanek et al. *Nature* 514 (2014) 209.

Posters

Influences of geometric aberrations in post-specimen lens system on energy resolution of monochromated EELS

Masaki Mukai[1, 2], Shigeyuki Morishita[1], Hidetaka Sawada[1], Shigeo Maruyama[2], and Kazu Suenaga[3]

[1] JEOL Ltd., 3-1-2 Musashino, Akishima, Tokyo 196-8558, Japan
[2] The University of Tokyo, 7-3-1 Hongo, Bunkyo-ku, Tokyo 113-8656, Japan
[3] AIST, Central 5, 1-1-1 Higashi, Tsukuba, Ibaraki 305-8565, Japan

The monochromated low-voltage analytical electron microscope equipped with delta-type aberration correctors for probe- and image-forming lens system was developed under the project “Triple-C” [1]. The ultimate energy resolutions at 30 kV of this microscope were 14 meV and 20 meV for 2 ms and 100 ms acquisition. These results were obtained with an acceptance-angle of 15 mrad. Since the delta-type aberration corrector enables us to correct up to fifth-order geometric aberrations, the uniformed phase area in a Ronchigram is extended to be 58.6 mrad at 30 kV. The large convergence angle by the aberration correction reduces a diffraction limit, which enables us to obtain an atomic resolution STEM imaging at low voltage [2].

FIG. 1 compares the zero-loss peaks obtained with and without aberration correction in image-forming lens system in STEM mode at 30 kV. The convergent- and acceptance- angles were 57.2 mrad. The zero-loss peak in FIG. 1(a) shows sharp peak shape and the full width of half maximum was measured to be 20 meV, while the peak in FIG. 1(b) shows caustic surface shape. Due to the aberrations in the image-forming lens system, the energy resolution deteriorated and the tail of zero-loss peak was expanded. Thus, high spatial- and high energy-resolution STEM-EELS with a large convergent- and acceptance-angle requires not only a monochromator and a probe-forming aberration corrector but also an image-forming aberration corrector.

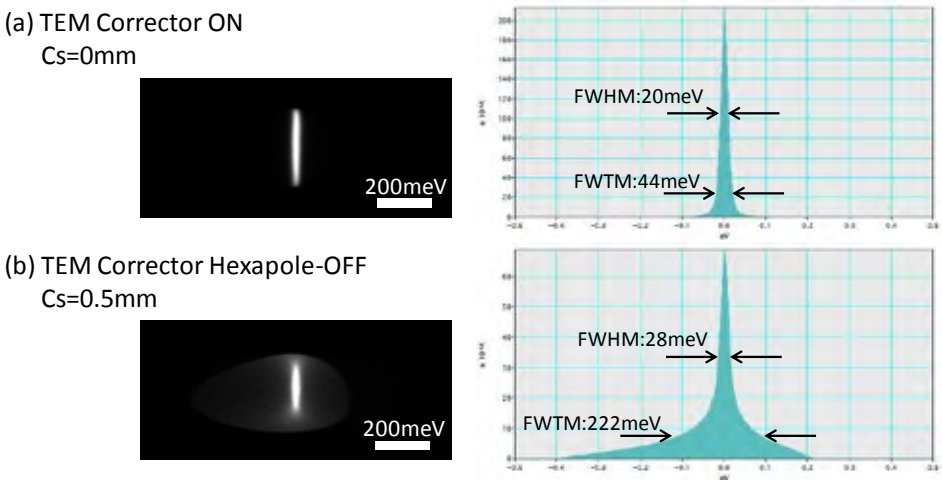

FIG. 1. Zero-loss spectra and their profiles at 30 kV. They obtained with acquisition time of 100 ms, camera length of 1.0cm, convergent- and acceptance-angle of 57.2 mrad. With (a) and without (b) aberration corrected image-forming lens system.

References

[1] M. Mukai et al.: Proc. EMC2016, Vol.1, 338-339 (2016)
[2] H. Sawada et al., Phys. Rev. Lett., 114 (2015) 166102

Valence EELS investigation on $GeSe_xTe_{1-x}$ phase change material

S. Zhang[1], A. Mio[2], M. Cagnoni[2], O. Cojocaru-Mirédin[2], M. Wuttig[2], C. Scheu[1]

[1] Max-Planck-Institut für Eisenforschung GmbH, Max-Planck-Straße 1, Düsseldorf, 40239, Germany
[2] Institute of Physics (IA), RWTH Aachen University, Sommerfeldstraße 14, Aachen 52074, Germany

Phase change materials are widely applied in optical storage, making use of the sensitivity of their dielectric properties on their crystallinity [1]. Miniaturizing of such devices requires characterization of the dielectric properties on the nanoscale. In this study, we apply valence EELS to study $GeSe_xTe_{1-x}$ phase change material (Fig. 1a). Monochromated electron beam was utilized to reveal band onset of ~1 eV (Fig. 1b). However, the high dielectric response of $GeSe_xTe_{1-x}$ (ε_r > 20) makes it impractical to get rid of the Cerenkov and surface losses by lowering the incidence energy. To get a proper model of the dielectric function, we extract the bulk energy loss function using the method introduced by Stöger-Pollach and Schattschneider [2] and develop a linear fitting scheme (Fig. 1c,d) to make the method more resilient to noise.

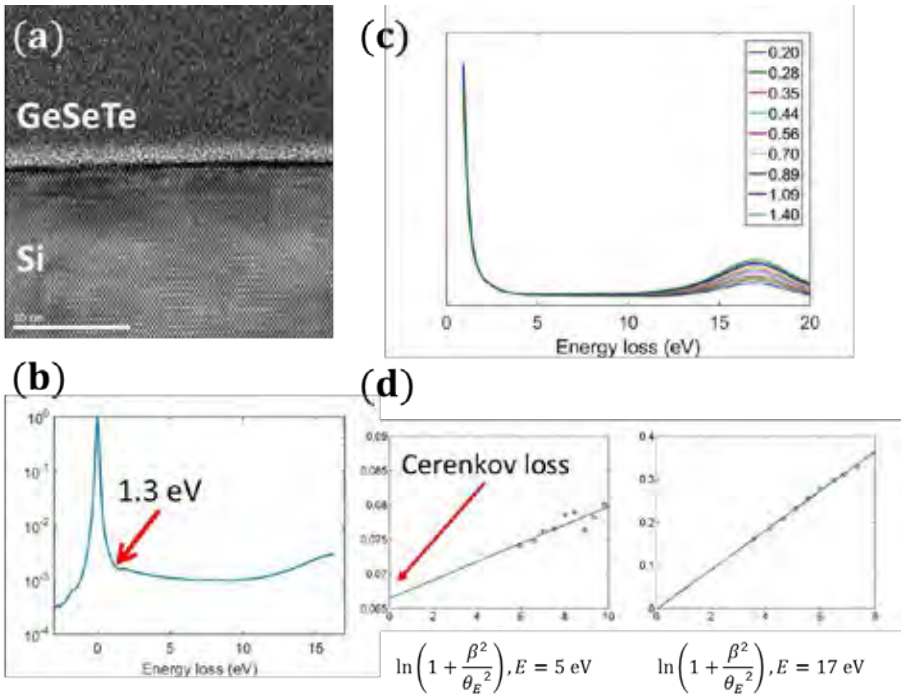

FIG. 1. (a) Amorphous $GeSe_xTe_{1-x}$ film deposited on Si substrate, (b) monochromated valence EELS spectrum (in log scale) of amorphous $GeSe_xTe_{1-x}$ showing a 1.3 eV band onset, (c) a set of valence EELS spectra collected using near parallel beam and various collection angles (in mrad), and (d) their fitting to extrapolate the Cerenkov loss and the bulk energy loss function at different energy losses.

References

[1] K. Shportko et al., *Nat. Mater.* 7 (2008) 653.
[2] M. Stöger-Pollach, P. Schattschneider, *Ultramicroscopy* 107 (2007) 1178.
[3] MW gratefully acknowledges support by the ERC within Advanced Grant 340698 (Disordered Control).

Monochromated STEM-EELS as a THz electrical probe

M. Bosman[1]

[1] Institute of Materials Research and Engineering, A*STAR (Agency for Science, Technology and Research), 2 Fusionopolis Way, 138634, Singapore.

This paper introduces a method for measuring the electrical resistance and capacitance of noble metals at optical frequencies using monochromated STEM-EELS.

An earlier-developed method [1] quantifies the surface plasmon damping parameters from monochromated EELS measurements. These parameters are here used as input into our optical conduction model that accounts for the frequency-dependence of materials parameters. This is an important refinement of electrical circuits that are used as models at DC or sub-THz AC frequencies. After all, physical quantities such as resistance and resistivity that are considered constant at standard operating conditions are strongly frequency-dependent in the THz regime [2].

Fig. 1 shows an example from a series of measurements on ~18 nm wide gold rods with different lengths. As the surface plasmon energy and damping vary for differently-sized rods, the resistance and capacitance are strongly dependent on the plasmon energy—and therefore on the resonance frequency.

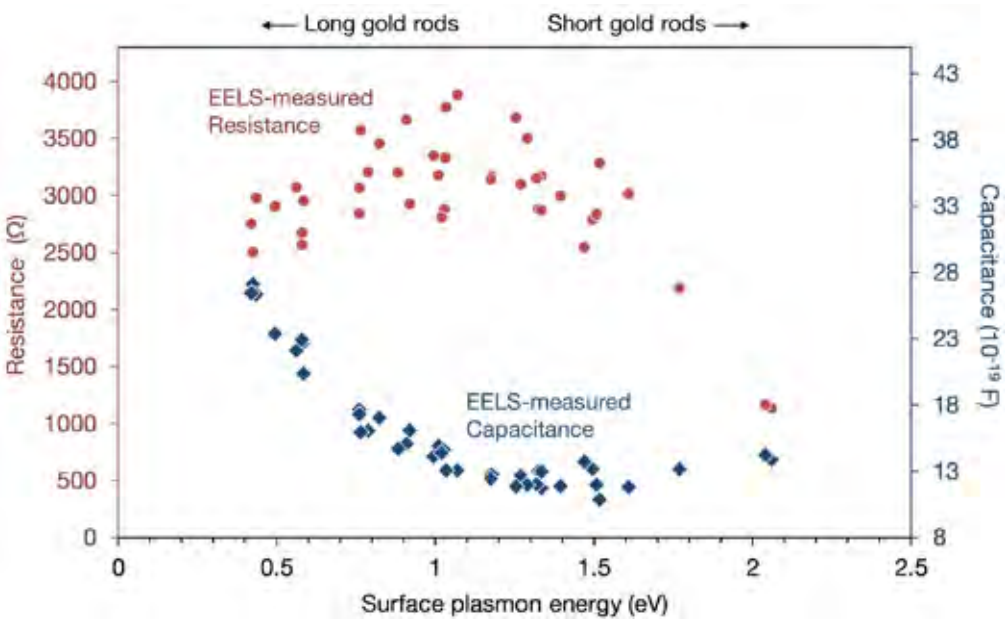

FIG. 1. Electrical Resistance (red, left axis) and Capacitance (blue, right axis) from a series of monochromated EELS measurements on polycrystalline ~18 nm wide gold nanorods with different lengths on a 30 nm thick SiN_x film [3].

References

[1] M. Bosman et al., *Scientific Reports* 3 (2013) 1312.
[2] D. Zhu et al., *Optics Express* 22 (8) (2014) 9809.
[3] Technical and intellectual support from the group of Joel K.W. Yang (Singapore University of Technology and Design) is gratefully acknowledged.

Scattering-vector dependent EELS of $LiCoO_2$

J. Kikkawa[1], T. Mizoguchi[2], T. Nagai[1], and K. Kimoto[1]

[1] National Institute for Materials Science, 1-1 Namiki, Tsukuba, Ibaraki 305-0044, Japan
[2] Institute of Industrial Science, The University of Tokyo, 4-6-1 Komaba, Meguro, Tokyo 153-8505, Japan

Identification of anisotropy in electronic structure and electron excitation is a significant subject in a wide range of research fields. Probing Li *K* edge using EELS is one of the powerful methods for directly observing anisotropic properties at Li [1]. However, the anisotropy of electronic structure at Li in $LiCoO_2$, an electrode material for lithium ion batteries, has never been identified experimentally because the Li *K* edge in EELS overlaps completely with the Co $M_{2,3}$ edge. In this study, we overcome this issue by the probing profiles and anisotropy of the Co $M_{2,3}$ edge using $Na_{0.72}CoO_2$ with a structure similar to $LiCoO_2$ (Fig. 1(a)). We achieved scattering-vector (***q***) dependent EELS with a monochromated electron source. Figure 1(b) shows the ***q***-dependent EELS spectrum (i.e., superposition of Li *K* and Co $M_{2,3}$ edges) from $LiCoO_2$ when the electron incident direction is [001] and the transverse (i.e., perpendicular to the electron incident direction) component of ***q***, $\boldsymbol{q}_T$ is parallel to $\boldsymbol{a}^*+\boldsymbol{b}^*$ direction. By comparing this result with ***q***-dependent EELS spectrum of Co $M_{2,3}$ edge for $Na_{0.72}CoO_2$, we found that the variation of EELS spectrum (Fig. 1(b)) originates mainly from the ***q***-dependence of Li *K* edge. We present that Li $1s \rightarrow 2p_c$ excitation is significantly different from Li $1s \rightarrow 2p_{ab}$ excitation in $LiCoO_2$, with support of first principles Bethe–Salpeter Equation calculation results.

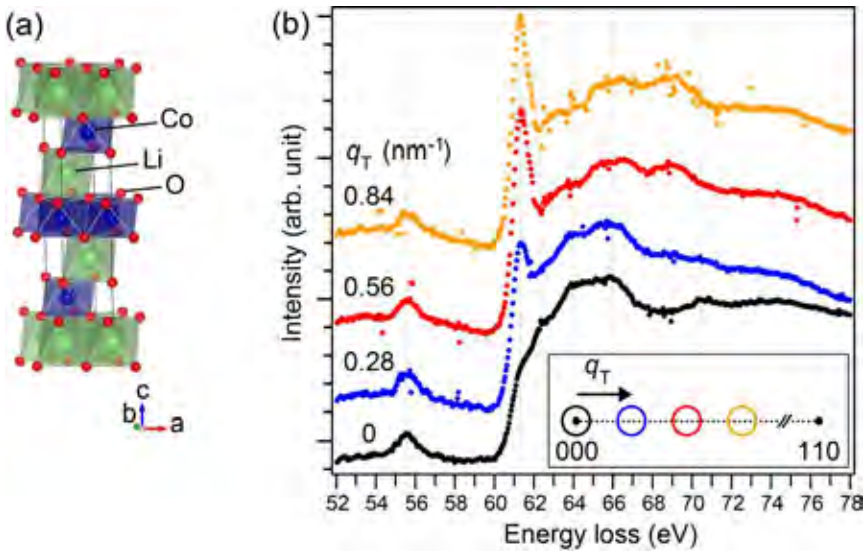

FIG. 1. (a) Drawings of crystal structure of $LiCoO_2$. (b) The ***q***-dependent EELS spectrum for $LiCoO_2$, acquired with [001] electron incident direction from circled areas with radius of 0.070 nm^{-1} and step increment of 0.28 nm^{-1} along $\boldsymbol{a}^*+\boldsymbol{b}^*$ direction.

References

[1] J. Kikkawa et al., *J. Phys. Chem. C* 119 (2015) 15823.
[2] J. Kikkawa et al., submitted for publication (2016).

Probing graphitic carbon nitrides via monochromated EELS

D.M. Haiber[1], T. Aoki[2], P.A. Crozier[1]

[1]School for Engineering of Matter, Transport & Energy, Arizona State University, PO Box 876106, Tempe AZ, 85287
[2]LeRoy Eyring Center for Solid State Science, Arizona State University, Tempe AZ, 85287

Polymeric graphitic carbon nitride (g-CN_xH_y) and poly(triazine imide) with intercalated Li and Cl ions (PTI/LiCl) have potential application for visible light water splitting [1,2]. They are planar materials that often possess a high degree of disorder making it challenging to characterize aspects of their physical and electronic structure. We have employed monochromated EELS to explore the vibrational, valence and inner-shell excitations in graphitic carbon nitrides ("g-CN's") to investigate their composition and bonding. By implementing an aloof-beam configuration, we show that structural "fingerprinting" of different g-CN's can be obtained through the vibEELS signal (FIG.1a). Local variations in the vibEELS signal, characterized by the presence of an extra peak at 265 meV (FIG.1a, spectra 2 and 4) indicates structural inhomogeneity on the nanoscale. Comparison between bulk optical vibrational spectroscopies (FT-Raman, FT-IR spectroscopy) vs. aloof-beam EELS can provide insights in spectral interpretation (FIG. 1b and c). The valence-loss region has also been measured to quantify bandgaps and its correlation with the vibEELS signal is highlighted.

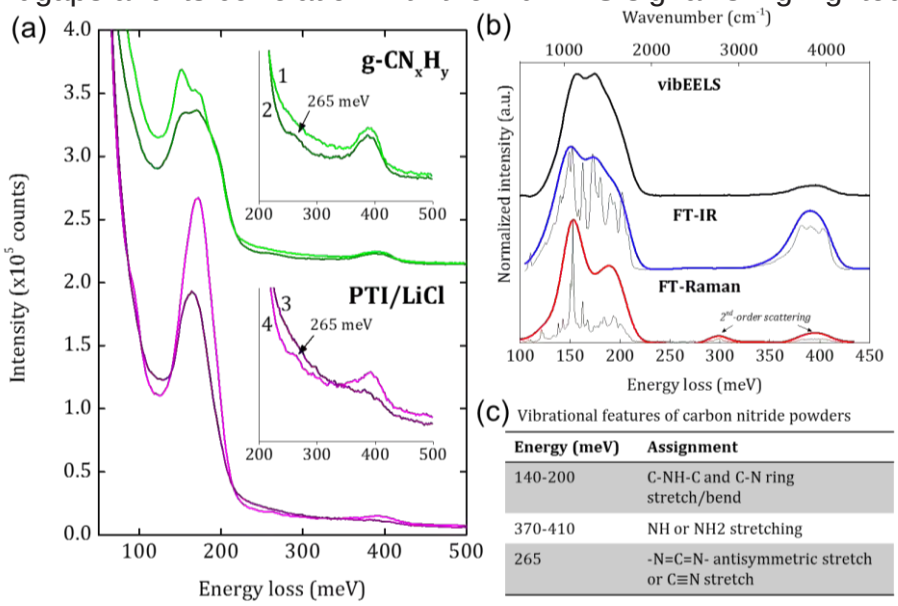

(c) Vibrational features of carbon nitride powders

Energy (meV)	Assignment
140-200	C-NH-C and C-N ring stretch/bend
370-410	NH or NH2 stretching
265	-N=C=N- antisymmetric stretch or C≡N stretch

FIG. 1. (a) Aloof-beam vibEELS spectra from g-CN_xH_y and PTI/LiCl. (b) vibEELS, FT-IR, and FT-Raman from g-CN_xH_y (thin, grey curves) also convolved with a Gaussian function of FWHM = 16 meV (thick colored lines). (c) Table of vibrational features.

References

[1] Wang et al. *Nat. Mater.* 2009, **8**, 76-80.
[2] Schwinghammer et al. *J. Am. Chem Soc.* 2014, **136**, 1730-1733.
[3] The support from the US Department of Energy (DE-SC004954) and the use of facilities within the LeRoy Eyring Center for Solid State Science at Arizona State University are gratefully acknowledged.

Retrieving the chemical composition of transition metal oxide core/shell nanoparticles

A. Ruiz-Caridad.[1,2], P. Torruella[4], L. López-Conesa[4], A. Gómez-Roca[3], J. Nogués[3], S. Estradé[4], F. Peiró[4] , M.G. Walls[2].

[1] Institut Laue-Langevin, BP 156, 38042 Grenoble, FRANCE.
[2] Laboratoire de Physique des Solides (LPS), UMR 8502 Université Paris-Sud bât 510, 91405 Orsay Cedex, FRANCE.
[3] Institut Català de Nanociència i Nanotecnologia, Bellaterra, 08193 Barcelona, SPAIN.
[4] Laboratory of Electron Nanoscopies (LENS-MIND-IN^{2}UB), Departament d'Electrònica, Universitat de Barcelona, Martí i Franquès 1, 08028 Barcelona, SPAIN.

Antiferromagnetic-ferromagnetic (AFM-FM) surfaces in core/shell nanoparticles based in metal oxides are proposed for applications in different fields as in recording media, magnetoresistive devices, catalysis, ferrofluids, pigments, biomedicine and spintronic devices due to its outstanding superparamagnetic properties [1,2].

Metal oxides spinels are ferrimagnetic materials that shows a general formulation of $A^{2+}B^{3+}{}_2O^{2-}{}_4$ in which A and B cations take the octahedral and tetrahedral sites of the structure. Mn_3O_4 ($Mn^{2+}Mn^{3+}{}_2O_4$) and Fe_3O_4 ($Fe^{2+}Fe^{3+}{}_2O_4$) are formed by a tetragonal structure in which, the A and B cations correspond to two different oxidation states. In this work we present the structural and chemical study of iron oxide/manganese oxide core/shell nanoparticles by means of High Resolution (HR), High Angular Annular Dark Field (HAADF) and Electron Energy Loss Spectroscopy (EELS). Experiments were carried out in a non-aberration corrected (JEOL2010F) microscope and in a probe-corrected (Nion USTEM200) microscope.

Polydisperse iron oxide/manganese oxide nanoparticles presenting spinel structure could be observed by HRTEM. Further experiments by EELS allowed identifying a much higher concentration of iron oxide at the nanoparticle core, surrounded by a manganese oxide shell. In addition, the EELS mapping characterization of the oxidation states of the manganese oxide also provided unambiguous confirmation of a spinel structure ($Mn^{2+}Mn^{3+}{}_2O_4$) located at the nanoparticle shell. Oxidation state information which leads to identify Fe_3O_4 in the core was also obtained thorough chemical shift of the Fe-L(2,3) edges. In this work we take advantage of EELS spectroscopy as an efficient tool to characterize the full structure and local chemical composition of oxide nanoparticles with a complex morphology. [3]

REFERENCES

[1] López-Ortega, A. et al., Size-Dependent Passivation Shell and Magnetic Properties in Antiferromagnetic/Ferrimagnetic Core/Shell MnO Nanoparticles. Journal of the American Chemical Society 132(27): 9398-9407 (2010).
[2] Estrader, M., et al., Robust antiferromagnetic coupling in hard-soft bi-magnetic core/shell nanoparticles. *Nature Communications, 4,* [2960] (2013). 10.1038/ncomms3960
[3] This research was supported by the LENS group of Universitat de Barcelona and the STEM group of Université Paris-Sud. Author wants to specially thank the MATRIX group in the Laboratoire de Physique des Solides and the Institute Laue-Langevin.

Nanoscale probing of bandgap states from oxide particles using monochromated STEM EELS

Q. Liu[1], W.J. Bowman[1], K. March[1], and P.A. Crozier[1]

[1] School for the Engineering of Matter, Transport and Energy, Arizona State University, 501 E. Tyler Mall, Tempe, AZ 85287-6106 United States.
[2] Laboratoire de Physique des Solides, Université Paris-Sud, CNRS, UMR 8502, 91405 Orsay Cedex, France.

Electronic states within the bandgap of an oxide are usually associated with defects, dopants, or extrinsic species in the bulk or on the surface, which may have significant impact on its optical, electrical and/or catalytic properties. Monochromated electron energy-loss spectroscopy (EELS) in a scanning transmission electron microscope (STEM) is a unique tool for probing local bandgap electronic structures, as the ultra-high energy resolution and greatly suppressed zero loss peak tail makes it possible to detect subtle features in the bandgap region (a few eV) of oxides. In one example, Pr doped ceria (PCO) showed a plateau feature before the conduction band onset, whereas pure CeO_2 showed no bandgap plateau. This feature can be modeled by adding an empty Pr 4f state 1.4 eV above the valence band to the projected density of states (PDOS) of ceria. In addition, surface states were detected on MgO nanocubes by comparing transmission and aloof EELS spectra from the same cube. Only when the beam was positioned outside the cube (aloof-beam geometry), was significant intensity observed within the bandgap, suggesting this state is localized at the surface. PDOS calculations showed a broad filled state at 1.1 eV above the MgO valence band. Simulation based on dielectric theory was also performed and this surface state was found to be associated with a ~2 nm hydroxide layer on MgO. More results will be discussed [1,2].

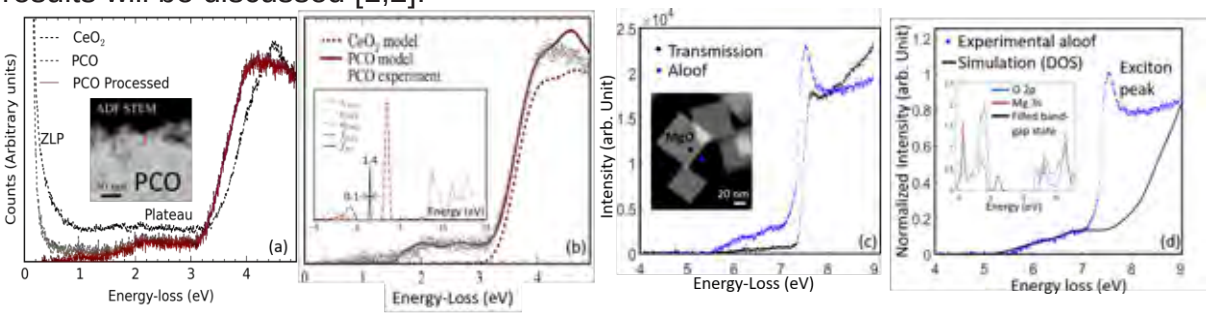

FIG. 1. (a) Valence-loss spectra from PCO and CeO_2. Insert is ADF image of PCO with beam position. (b) Calculated CeO_2 and PCO spectra overlaid with PCO EELS. Insert shows CeO_2 PDOS with a Pr bandgap state. (c) Background subtracted transmission and aloof spectra from MgO. Insert is ADF image of MgO cubes with beam positions. (d) Calculated MgO spectrum with a filled bandgap state shown in insert overlaid with MgO aloof spectrum.

References

[1] W.J. Bowman et al., *Ultramicroscopy* 167 (2016) 5-10.
[2] Q. Liu et al., *Ultramicroscopy* (in press).
[3] US Department of Energy (DE-SC0004954), NSF's Graduate Research Fellowship (DGE-1211230), NSF Grant DMR-1308085 and the use of NION microscope at John M. Cowley Center for HR Microscopy at Arizona State University.

Particle Shape Effects in Vibrational EELS

David D. Kordahl[1], Christian Dwyer[1]

[1] Department of Physics, Arizona State University, Tempe, Arizona 85287, USA

One initially perplexing fact of vibrational EELS, which we explain here, is the apparent absence of certain long-wavelength optical vibrational excitations—excitations that are easily observed with infrared and Raman spectroscopy. Previously established theory [1] predicts that the long-wavelength excitations in nanoscale particles depend not only on the particle's composition, but also on its size and shape. The strong influence of particle shape and size distinguishes vibrational EELS in the STEM from the well-established forms of vibrational spectroscopy.

Modelling an isotropic dielectric with the phenomenological equations of Born and Huang [2], we investigate simple shape effects, including the limiting cases of foil-shaped and spherical particles, and the intermediate case of ellipsoidal particles. We also show how the vibrational states predicted by the classical Born-Huang equations can be used in a quantum-mechanical description of the inelastic electron-vibration scattering. The Møller potential formalism allows us to calculate sample energy-loss spectra, and thus to identify the qualities of our limiting cases.

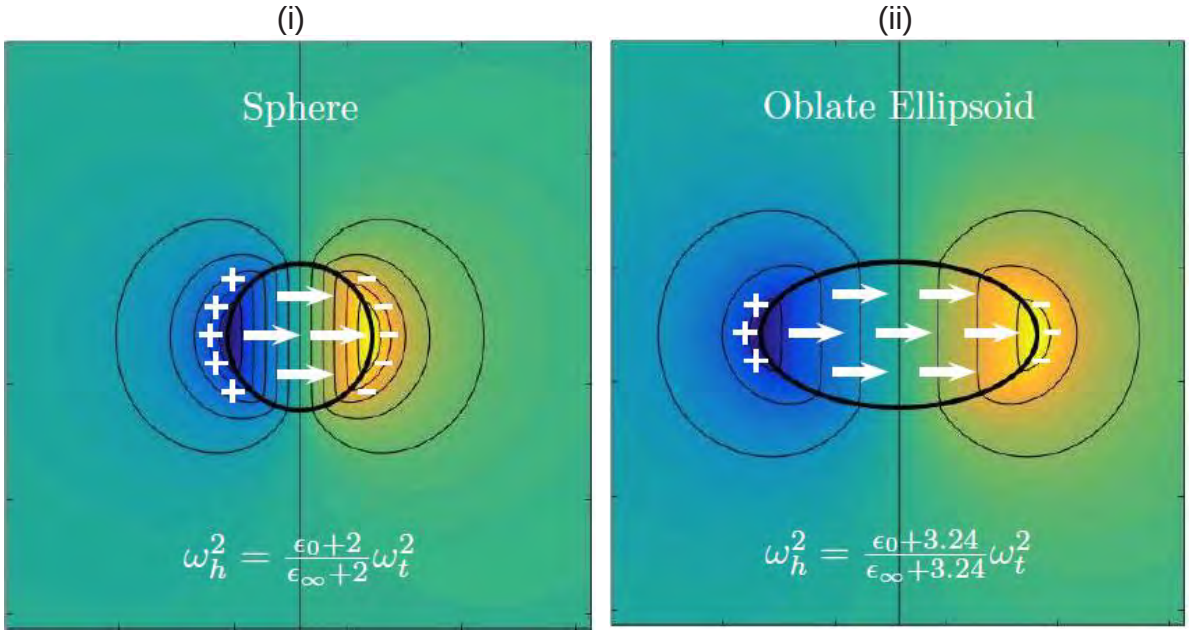

FIG. 1. A simple shape effect. The electrical potentials generated by a uniform ionic displacement across particles are shown for (i) a sphere and (ii) an oblate ellipsoid (a=b=2c). The reduced charge density on the surface of the ellipsoid also reduces the magnitude of the ellipsoid's electric field, relative to that of the sphere. Hence for corresponding harmonic states, an ellipsoid's vibrational frequency and excitation energy are both lower than those for a sphere of the same material.

References

[1] R. Englman, R. Ruppin, Phys. Rev. Lett. 16, 898 (1966).
[2] M. Born and K. Huang, *Dynamical Theory of Crystal Lattices* (1954).

Characterization of individual 1D materials by monochromated STEM

Ryosuke Senga[1], Thomas Pichler[2], Kazu Suenaga[1]

[1] Nanomaterial research institute, AIST, Tsukuba 305-8565, Japan
[2] Faculty of Physics, University of Vienna, Vienna, Austria

Physical properties of low-dimensional materials are strongly governed by their atomic structures. Therefore a sophisticated instrument which can directly correlate the physical properties to the atomic structures has been desired. Herein, we successfully demonstrate highly-localized electronic properties of individual carbon nanotubes [1] and related 1D materials such as fullerene peapods or ionic crystals inside nanotubes with precise atomic structures by a monochromated TEM. We have used a JEOL TEM (TripleC#2) consisting of a Schottky field emission gun (15-60 kV), a double Wien filter monochromator and delta type correctors. The energy resolution is adjustable from 30 to 200 meV with the slits in the monochromator. A Gatan Quantum spectrometer modified for low primary energy operation (15-60 kV) has been used for EELS.
Fig. 1 shows the EEL spectra for an elastically bent single-wall carbon nanotube (SWNT). The well-separated sharp peaks at the carbon K-edge correspond to the van Hove singularities (Fig. 1(c)). When the EELS line scan at STEM mode starts on the tensioned side of the SWNT following a broken arrow (i→ii) in (a), the π^* peak downshifts as the electron probe moves to the compressed side, whereas the σ^* peak slightly upshifts, as shown in Figs. 1(b and c). Note that the spectral image is calibrated by zero-loss peak positions which are simultaneously recorded with a Gatan dual EELS option. These shifts presumably reflect the quite small distortion in the bond length. Such a local absorption spectroscopy will contribute to understand the unique properties caused by non-periodic structures of low-dimensional materials, which is not possible with conventional absorption spectroscopy by using photons as probe.

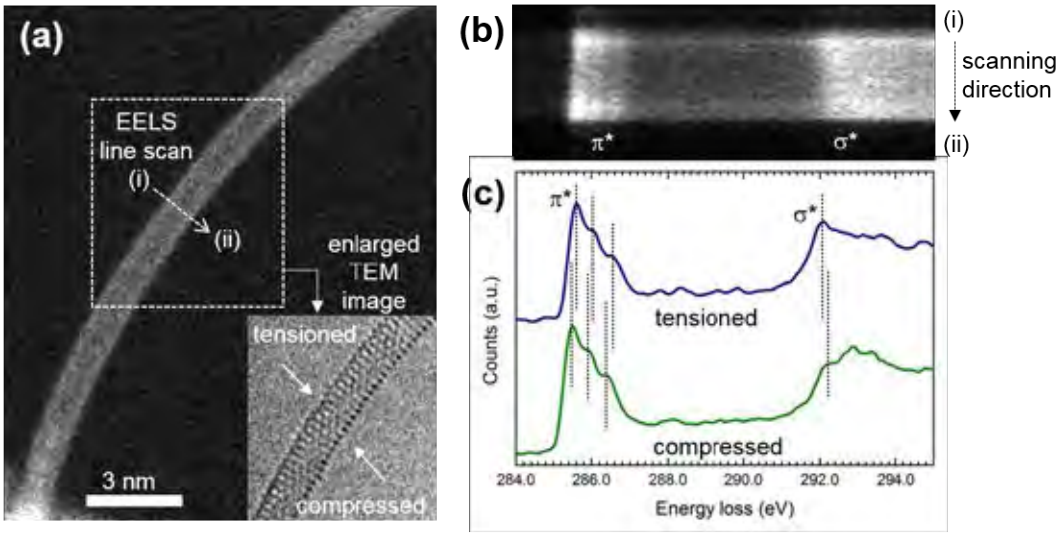

FIG. 1. (a) STEM and TEM (inset) images of an elastically bent SWNT. (b) The core-loss spectra images for the SWNT during the line scan (i→ii) in (a). (c) The carbon K-edge spectra at the tensioned region (blue) and the compressed region (green).

References

[1] R. Senga et al., *Nano Letters,* 16 (2016) 3661.
[2] Supported by JST Research Acceleration Program and JSPS KAKENHI.

EELS analysis of bonding in quantum computing materials

B. M. Hudak[1], J. Song[1], P. C. Snijders[1], and A. R. Lupini[1]

[1] Materials Science and Technology Division, Oak Ridge National Laboratory, 1 Bethel Valley Rd, Oak Ridge, TN, 37830

The widespread application of silicon in electronics makes it an ideal material for quantum computing due to existing infrastructure for the production, study, and use of Si-based devices. Group V elements are promising candidates for use as single-atom qubit dopants in Si [1]. Bi, in particular, has a large atomic number relative to Si, making it an ideal candidate to study using *Z*-contrast scanning transmission electron microscope (STEM). For quantum computing applications, it is of utmost importance to fully understand the coordination of these dopants atoms and relationship to vacancies within the Si matrix, which can be investigated through the use of atomically-resolved electron energy loss spectroscopy (EELS) in addition to *Z*-contrast imaging. Shifts and splitting in the Si $L_{2,3}$ edges as the Si atoms come into close contact with the Bi dopants provide information necessary to understanding how the Bi incorporates into and interacts with the Si crystal [2].

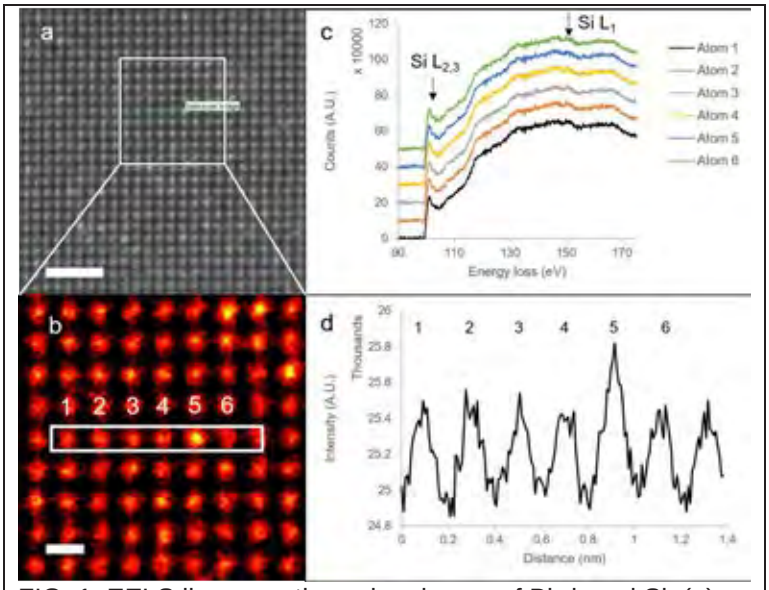

FIG. 1. EELS line scan through columns of Bi-doped Si. (a) Raw data showing the position of the line scan. Scale = 1 nm (b) Zoomed-in region with white box highlighting the scanned atoms. Scale = 2 Å (c) EELS signal extracted from the six atoms in the line scan. (d) Position and relative intensities of the atomic columns that were scanned.

Figure 1 shows data acquired from an EELS line scan across a row of Bi-doped Si columns. The raw *Z*-contrast image is shown in (a). In (b), the image is zoomed in and false-colored, with the white box indicating the columns from which EELS was recorded. Position 5 appears significantly brighter than the others, indicating that a Bi atom is located in that column. The intensity profile map displayed in (d) confirms the location of the Bi dopant. The EELS data in (c) shows Si $L_{2,3}$ and L_1 edges, with no detectable change in the edge structures or position as the probe approaches the Bi-doped column. However, the new monochromated, aberration-corrected STEM capabilities now available at ORNL will provide the means to collect and analyze the subtle shifts in peak positions necessary to provide a complete picture of the Si-Bi interaction in these materials. [3]

References

[1] B.E. Kane, *Nature* 393 (1998) 133.

[2] J.F. Morar et al., *Phys. Rev. B.* 47 (1992) 4107.

[3] Research sponsored by the Laboratory Directed Research and Development Program of Oak Ridge National Laboratory, managed by UT-Battelle, LLC, for the U. S. Department of Energy.

HIGH RESOLUTION SPECTROSCOPY OF LITHIUM FLUORIDE

K. March[1], P. Rez[2]

[1]LeRoy Eyring Center for Solid State Science, Arizona State University, Tempe, AZ 85287-1704
[2]Department of Physics, Arizona State University, Tempe, AZ 85287-1504

LiF is an alkali halide that is used as a detector of ionizing radiation. Similar to the other alkali halides radiation causes ejection of the anion. In the initial stages a single F center is formed, an electron trapped at the site of a missing fluorine atom. As dose accumulates F2 and F3 centers, clusters of 2 and 3 missing fluorine atoms, are created. In the final stage large regions are depleted of fluorine ions and what remains is Li metal. LiF has the NaCl structure and it is possible to find cubic nanoparticles 80nm across. To follow the damage process we defocused the probe so its diameter was comparable to the size of the nanoparticle. The electron exposure was then 450 e-/Å^2/sec. The acquisition time was 4 sec for successive spectra. Fig 1(a) shows a peak at 3 eV which has been attributed to F2 and F3 centers. The peak grows with increasing exposure. The exciton marking the conduction band onset at 13 eV is also apparent from the spectrum, as is the core exciton on the Li-K edge shown in Fig 1(b). Further exposure results in a peak at 7.5 eV which we attribute to the Li metal plasmon. As the regions of Li metal grow the plasmon increases in strength compared to the band onset exciton, and the Li-K edge shape changes to that characteristic of the metal. This behavior is similar to what was observed in fluorite [1].

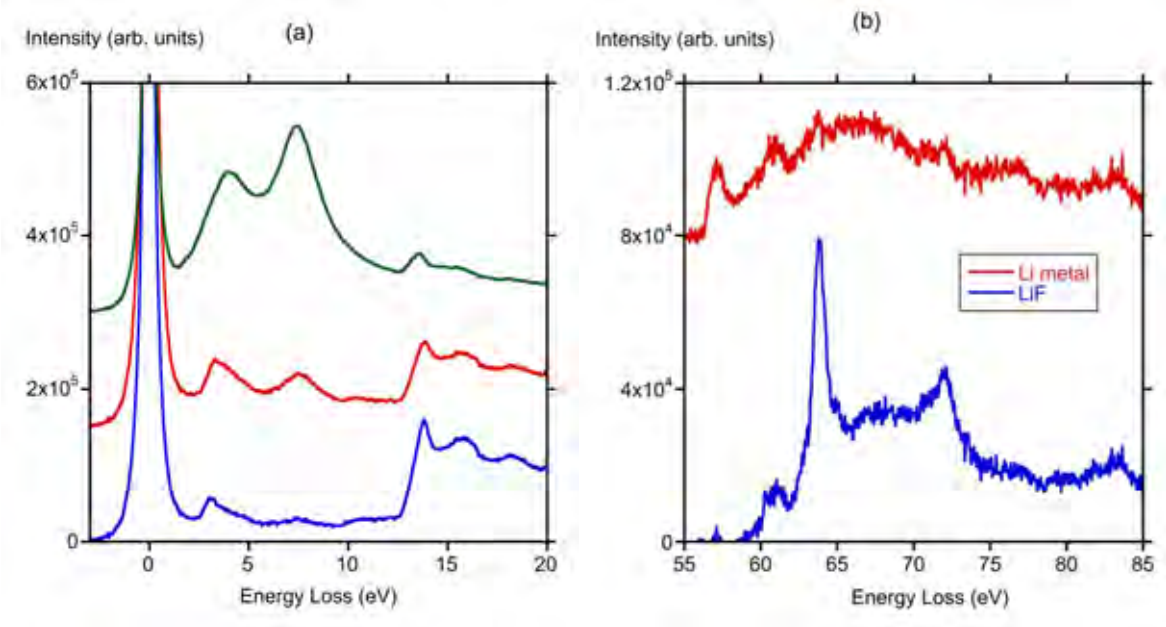

FIG 1 (a) Evolution of damage (bottom to top) (b) Li-K edge

References
[1] T. Aoki et al., *Ultramicr*. 153 (2015) 40.
[2] We thank Dr. Nigel Browning for the specimen. Use of facilities in the LeRoy Eyring Center for Solid State Science at Arizona State University is gratefully acknowledged.

Probing Interfacial Effects with Vibrational Electron Energy-Loss Spectroscopy

Kartik Venkatraman[1], Qianlang Liu[1], Katia March[2], Toshihiro Aoki[2], Peter Rez[3], Peter A. Crozier[1]

[1]School for the Engineering of Matter, Transport and Energy, Arizona State University, Tempe, Arizona 85287-6106, USA
[2]LeRoy Eyring Center for Solid State Science, Arizona State University, Tempe, Arizona 85287-1704, USA
[3]Department of Physics, Arizona State University, Tempe, Arizona 85287-1704, USA

We are investigating the spatial variation in the Si-O vibrational stretch at a Si/SiO_2 interface using monochromated electron energy-loss spectroscopy (EELS) in the Nion UltraSTEM 100 operated at an accelerating voltage of 60kV. The bulk Si-O vibrational stretch signal, observed at ~144 meV, decreases in intensity as the probe moves towards the interface, dropping to a background level exactly at the interface. The spatial variation inside the SiO_2 can be accurately modeled using a non-relativistic dielectric theory [1]. The SiO_2/Si interfacial vibrational stretch signal, observed at ~136 meV, starts to appear at ~5 nm from the interface and increases to a maximum intensity exactly at the interface. As expected, the relativistic theory [2] incorporates Cerenkov losses and gives a better estimate of the intensity in the Si.

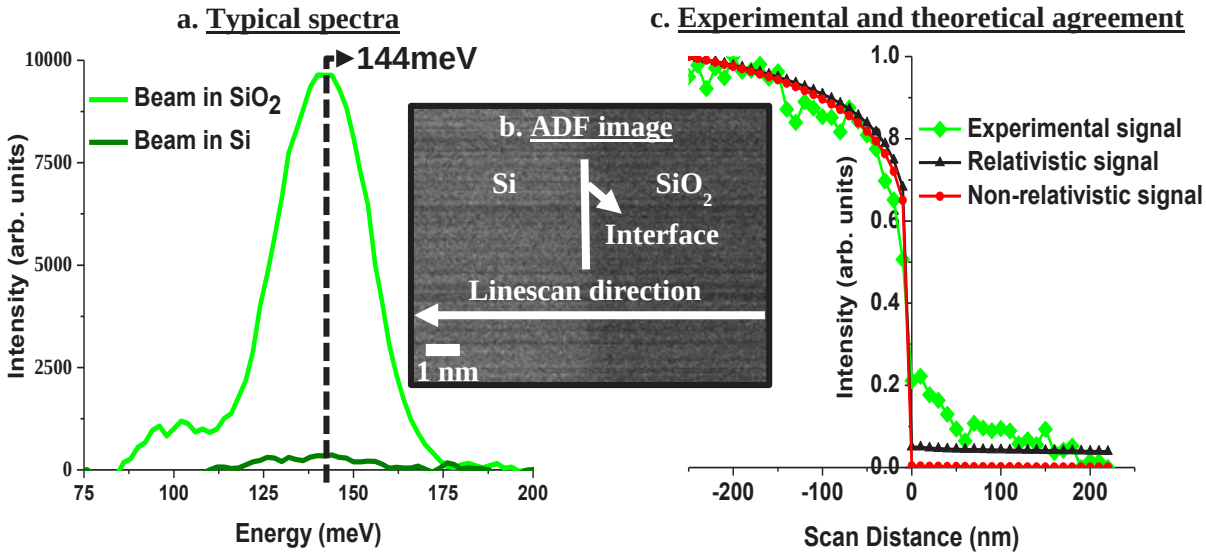

FIG. 1. (a) shows the typical Si-O vibrational stretch signal observed when the beam is in SiO_2 and Si far away from the Si/SiO_2 interface shown in the ADF image in (b). A typical linescan direction is also shown in (b). (c) shows the agreement between the experimental linescan profile and simulations based on relativistic and non-relativistic dielectric theory.

References

[1] A. Howie and R.H. Milne, *Ultramicroscopy* 18 (1985) 427.
[2] Z.L. Wang, *Micron* 27 (1996) 265.
[3] The support from National Science Foundation CHE-1508667 and the use of TEM at John M. Cowley Center at Arizona State University is gratefully acknowledged.

Understanding guided light modes in oxide nanoparticles with monochromated EELS

Q. Liu[1], S.C. Quillin[2], D.J. Masiello[2] and P.A. Crozier[1]

[1] School for the Engineering of Matter, Transport and Energy, Arizona State University, 501 E. Tyler Mall, Tempe, AZ 85287-6106 United States.
[2] Department of Chemistry, University of Washington, Seattle, Washington 98195-1700, USA

Monochromated electron energy-loss spectroscopy (EELS) is a potentially powerful technique for exploring bandgap states within insulators [1]. However, it is also important to understand losses associated with Cherenkov radiation and guided light modes because they can also give rise to intensity in the bandgap region of the spectrum [2]. Here we perform an experimental and theoretical investigation of these effects on the transmission and aloof beam EELS from oxide particles. Monochromated EELS in a Nion UltraSTEM was used to reveal guided light modes in MgO, TiO_2 and CeO_2 nanoparticles. Classical electrodynamic modelling was employed to simulate and interpret the bandgap features. Fig. 1a demonstrates the cavity modes detected from a pair of CeO_2 nanocubes in close proximity: 2 cubes ~110 nm in size generate a broad 2.6 eV peak and a sharp 3.3 eV peak, which were in qualitative agreement with preliminary calculations. A series of more complex peaks were present in the bandgap region of anatase spectra recorded with 60 kV electrons. Interestingly, decreasing the voltage to 40 kV (corresponding to a 16% of beam velocity drop) significantly reduced the overall intensities of these cavity modes. Both experiment and simulation show that the energy and strength of the modes are related to the material's complex dielectric, particle size and shape, speed of the fast electron as well as beam positions relative to the particle.

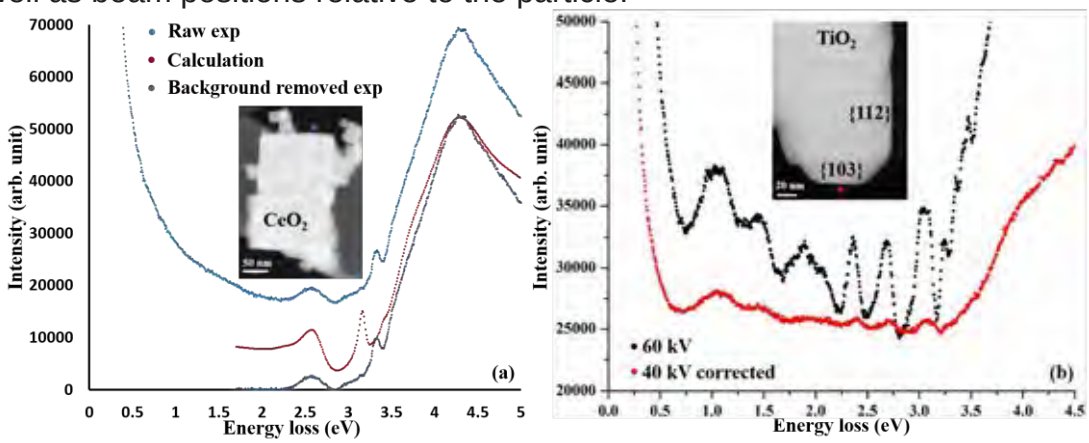

FIG. 1. (a) Raw and background removed aloof spectra from CeO_2 cubes, overlaid with normalized calculated spectrum. Insert is an image of the cubes with beam position. (b) Aloof EELS spectra acquired at 60 and 40 kV from the same facet of a TiO_2 particle. Insert is an image of the TiO_2 particle with beam position.

References

[1] Q. Liu et al., *Ultramicroscopy* (in press).
[2] J.D. Jackson, Classical Electrodynamics, *Wiley*, (1999).
[3] Funding from DOE (DE-SC0004954) and NSF CHE-1253775 and the use of NION microscope at John M. Cowley Center for Microscopy at Arizona State University.

Detection of Hydrogen-Oxygen Bonds with Vibrational EELS

P.A. Crozier[1], Q. Liu[1], and Toshihiro Aoki[2]

[1]School for the Engineering of Matter, Transport and Energy, Arizona State University, 501 E. Tyler Mall, Tempe, AZ 85287-6106 United States.
[2]LeRoy Eyring Center for Solid State Science, Arizona State University, Tempe, Arizona 85287-1704, USA

High spatial resolution detection of hydrogen-oxygen bonds is important for many materials systems including catalysts, proton conductors, minerals, clays, aerosols as well as life science systems. Here we show that vibrational electron energy-loss spectroscopy (EELS) in the scanning transmission electron microscope can be employed to locally detect hydrogen-oxygen bonds. To investigate the feasibility of OH detection, a series of hydroxides and hydrates have been investigated [1]. The OH stretch mode varied from 430 to 452 meV depending on the local molecular environment around the OH species. For catalytic applications, it is important to detect water and hydroxide species on nanoparticle surfaces. The delocalized nature of the vibrational spectrum also makes it possible to use the aloof beam acquisition mode to probe bonding while reducing electron beam damage. FIG 1a shows an annular dark-field image of ~60 nm MgO cubes that have been exposed to water vapor. FIG 1b is the aloof beam vibrational spectrum showing a peak at 430 meV indicating the presence of water species on the surface of the nanoparticle. Factors affecting the sensitivity and radiation damage for OH detection in materials will be discussed.

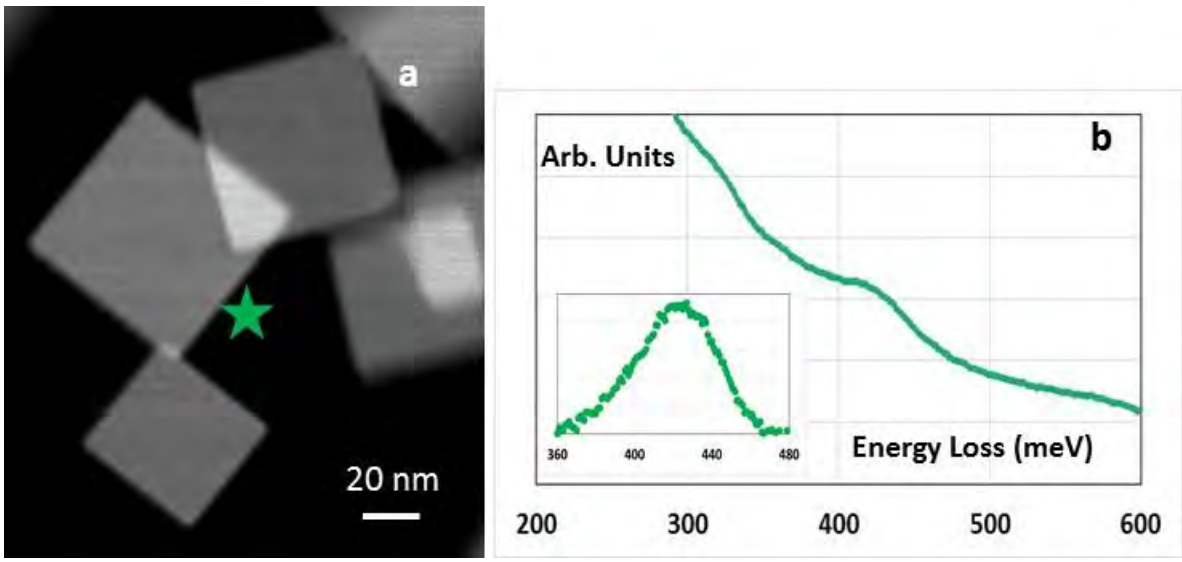

FIG. 1. Surface analysis of (100) facets of MgO nanocubes. (a) Annular dark-field image of MgO cubes. (b) aloof beam vibrational spectrum showing peak at 430 meV associated with surface hydrate layer (insert shows the background subtracted peak).

References

[1] P.A. Crozier et al, *Ultramicroscopy*, 169 (2016) 30.
[2] The support from US DOE (DE-SC0004954) and ASU's John M. Cowley Center for High Resolution Electron Microscopy is gratefully acknowledged.

Characterisation of graphitic carbon nitride single-atom catalysts across the energy loss spectrum, real space and reciprocal space

R.K. Leary[1], S.M. Collins[1], D.N. Johnstone[1], T. Furnival[1], Z. Chen[2], S. Mitchell[2], E. Vorobyeva[2], R.J. Nicholls[3], G. Schusteritsch[1], C.J. Pickard[1], J.M. Thomas[1], J. Pérez-Ramírez[2], Q.M. Ramasse[4] and P.A. Midgley[1]

[1] Department of Materials Science and Metallurgy, University of Cambridge, UK.
[2] Department of Chemistry and Applied Biosciences, ETH Zurich, Switzerland.
[3] Department of Materials, University of Oxford, UK.
[4] SuperSTEM Laboratory, SciTech Daresbury Campus, Daresbury, UK.

Single-atom catalysts (SACs) offer a means to achieve efficient and environmentally less harmful chemical conversions in processes that are used throughout modern society, such as industrial hydrogenations. The 'holy-grail' is to achieve stable single-atom dispersions where the active sites are precision-tuned for a target reaction. This requires identification of atomic-scale structures that are capable of strongly anchoring catalytic metal atoms, and that provide structural and chemical environments that can choreograph a catalytic process.

Our recent work has shown that entrapping catalytic metal atoms in the cavities of a nano-porous polymeric graphitic carbon nitride (GCN) (that is cheap and readily synthesized) is a promising approach to stable SAC anchoring [1]. To develop a deeper understanding of these SACs, we have employed high-energy-resolution monochromated EELS, using machine learning and selected area spectra to reveal the local structure and chemistry from core-loss, low-loss and vibrational spectrum images. The vibrational EELS offers particular insights into the local bonding of the GCN, including significant N-H groups and changes in the layer structure seen as a separate spectral component (Fig. 1). Coupled with high-resolution STEM and scanning electron diffraction, the multi-dimensional analysis provides a fresh avenue for unravelling complex GCN structures on the nanoscale, which continue to be much debated.

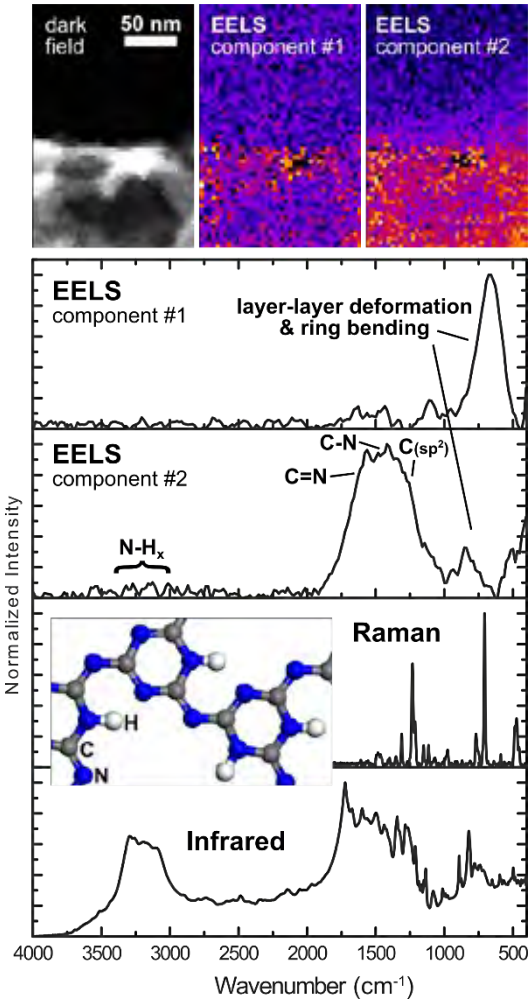

FIG. 1. STEM-EELS, Raman and infrared spectra revealing the vibrational modes of an exfoliated GCN SAC support. Using machine learning, the EELS spectrum image has been separated into two spectrally and spatially distinct 'components'.

References

[1] Z. Chen et al., *Adv. Funct. Mater.* DOI: 10.1002/adfm.201605785

[2] This work is supported by ERC grant agreement 291522–3DIMAGE, the EPSRC UK SuperSTEM Facility and a Junior Research Fellowship at Clare College.

Gap Measurements via Monochromated Low-loss EELS on Atomically thin $Mo_XW_{(1-X)}S_2$ Nanoflakes

M. Pelaez-Fernandez[1], K. Suenaga[2], and R. Arenal[1,3]

[1] Instituto de Nanociencia de Aragon, Univ. Zaragoza, Zaragoza - Spain
[2] National Institute of Advanced Industrial Science and Technology, Tsukuba - Japan
[3] Fundacion ARAID, Zaragoza – Spain

For the past years, layered semiconductors of the TX_2 type (T=Mo, W; X=S, Se, Te) have been drawing an increasing amount of attention due to their many interesting properties [1,2]. In this context, and due to the possibility of tailoring their band gap, $Mo_xW_{(1-x)}S_2$ alloys have been reported lately, but some of its properties remain undiscussed yet.
In this study, monochromated low-loss EELS has been used to examine the bandgap behavior as well as two features, α and β, that have been reported to Van Hove singularities [3]. This study has been performed for different alloying degrees (x=0, 0.3, 0.5, 0.7 and 1) and different few-layer stacks within each alloying degree [4]. The results yielded by this study will be discussed with regard to recent experimental (photoluminescence) and theoretical (DFT calculations) works [1,2]. This provides a broader vision of the potential applications of these materials.

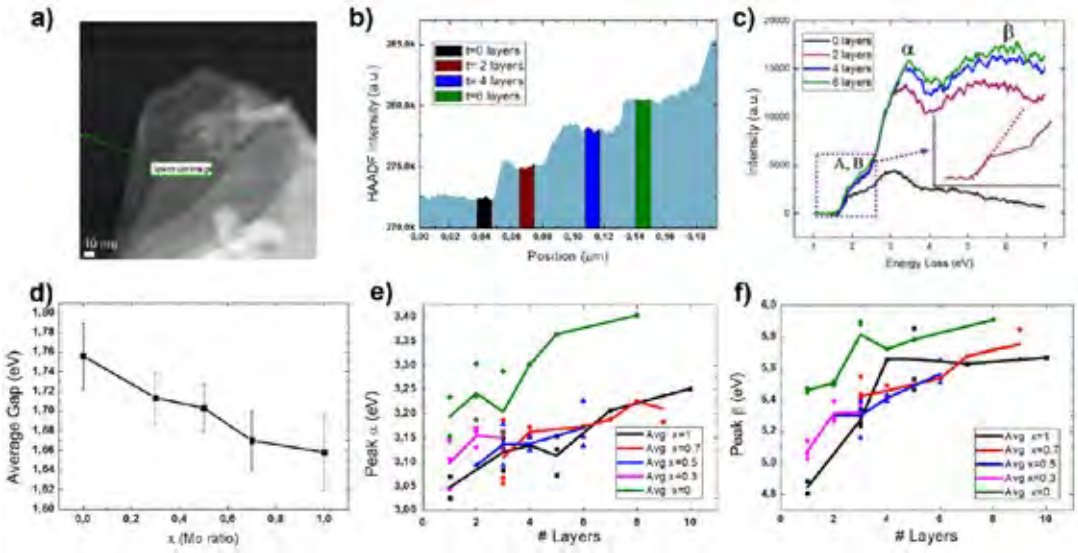

FIG. 1. (a) STEM-HAADF micrograph of a region showing an example spectrum-line on a flake of $Mo_{0.5}W_{0.5}S_2$. (b) HAADF intensity along the aforementioned spectrum-line. (c) Integrated low-loss EEL spectra on the areas marked in figure 1b after zero loss peak removal. Three features are shown, corresponding with the bandgap/A-B exciton region, the α peak and the β peak. (d), (e) and (f) show each the average band gap, α peak and β peak values for various Mo ratios and thicknesses.

[1] D.O. Dumcenco *et al*, Nature Comm. 4, 1351 (2013).
[2] Y. Chen *et al*., Acs Nano 7, 4610-4616 (2013).
[3] K. Dileep, *et al*, J. App. Phys 119, 114309 (2016)
[4] M. Pelaez-Fernandez, K. Suenaga, R. Arenal, to be submitted
[5] This work was supported by the Spanish MINECO (MAT2016-70776-P) and by the EU, under Grant Agreements 604391 and 696656. The low-loss EELS studies were developed at the LMA of the INA - U. of Zaragoza (Spain).

Low dose acquisition of pseudo atomic column elemental map by 2D STEM moiré method

Y. Kondo[1], K. Fukunaga[1], E. Okunishi[1], and N. Endo[1]

[1] JEOL Ltd., 3-1-2 Musashino, Akishima, Tokyo, 196-8558, Japan.

Atomic column elemental mapping, by EELS and/or EDS, is useful, since elemental species and atomic sites are determined simultaneously [1]. The sample damage limits applicable samples for this method, because it requires high dose density. We recently succeeded in displaying the pseudo atomic column elemental map utilizing a 2D STEM moiré method, under the low dose condition [2]. This method allows the atomic column mapping with the dose density less than 1 % of that taken with the conventional method, since a pixel interval to draw the pseudo lattice fringe is sparser than that for a real lattice. This paper reports the results obtained by the method for beam sensitive materials.

Figure 1 shows the atomic column elemental maps of Si_3N_4 taken by the 2D moiré and conventional methods. The total dose densities for the 2D moiré and direct methods were 2.33 x 10^8 and 7.43 x 10^{10} electrons /nm^2, respectively. The reduced rate of the dose density was ≈ 1/320. The peak positions in the Si maps accord well with the atomic sites in both methods. However, the positions in N map accord with the atomic sites only in the map by 2D moiré. The reason of this disagreement is thought to come from the difference of the dose densities. The results clearly show that maps by the pseudo 2D moiré atomic column elemental mapping do not suffer damage by electron beam irradiation.

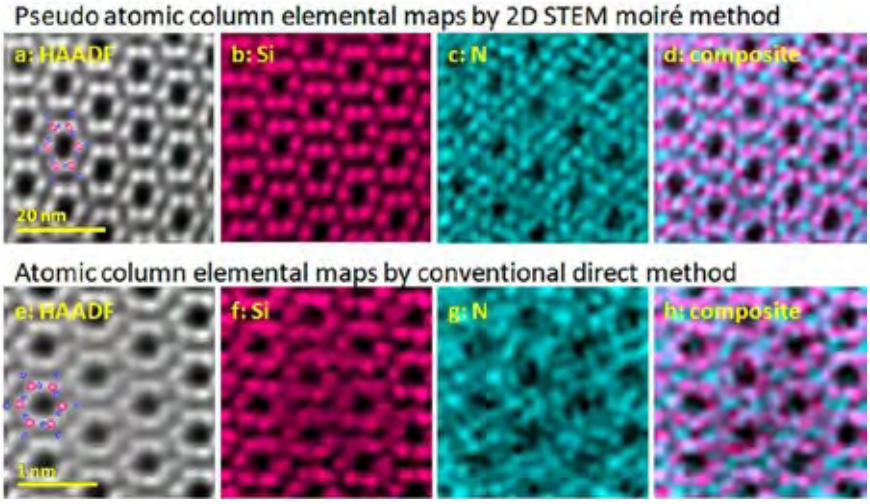

FIG. 1. (a-d) maps by 2D moiré method: (a) the HAADF image, (b-d) Si, N and composite maps, and (e-h) are those by direct mapping. The elemental signals were collected by EDS. The acquisition conditions: Acc. Volt. = 120 kV, probe current = 38 pA, probe size = 0.2 nm, accumulated frames = 508, dwell time = 1 ms. The instrumentation was JEM-ARM200CF with two SDDs (total solid angle = 1.75 sr)

References

[1] E. Okunishi et al, Microsc. Microanal. **12 (S2)** (2006) 1150.
[2] Y. Kondo and E. Okunishi, Microscopy **63 (5)** (2014) 391.

Quantifying the carrier distribution in hole-doped cuprates using atomic resolution near-edge structures: the case of $Ca_{11}Sr_3Cu_{24}O_{41}$

M. Bugnet[1,2], S. Löffler[1,3], D. Hawthorn[4], G. Sawatzky[5], P. Schattschneider[3], G. Radtke[6], G. A. Botton[1]

[1] Department MSE, McMaster University, Hamilton, ON, Canada
[2] Laboratoire MATEIS, UMR 5510 CNRS – Univ. Lyon – INSA Lyon, France
[3] Institute of Solid State Physics and USTEM, Vienna Univ. of Technology, Austria
[4] University of Waterloo, Waterloo, ON, Canada
[5] University of British Columbia, Vancouver, BC, Canada
[6] IMPMC, UMR 7590 CNRS – UPMC – IRD – MNHN, Paris, France

A central issue to understand the mechanisms leading to superconductivity in cuprates is to measure accurately the carrier distribution among Cu-rich planes in the structure. Here, the chain-ladder hole-doped superconductor $Ca_{11}Sr_3Cu_{24}O_{41}$, the only known superconductor with a non-two-dimensional CuO_2 plane structure, which consists of CuO_2 chains and Cu_2O_3 ladders, is investigated using STEM-EELS at the atomic level [1]. The hole distribution is studied from the O-K pre-edge Energy Loss Near Edge Structures (ELNES), composed of the O-2*p* hole band, and the upper Hubbard band [2]. Mapping the O-K pre-edge ELNES demonstrates that the holes are mostly concentrated within the CuO_2 chains of the structure. Furthermore, quantification of the relative hole concentration within the chains and the ladders is performed by evaluating the O-K pre-edge intensity and using inelastic channeling simulations. This work illustrates how atomic-resolution ELNES can improve the understanding of the electronic properties of complex oxides, and highlights the necessity of inelastic channeling calculations to validate the quantitative analysis of high resolution STEM-EELS on $Ca_{11}Sr_3Cu_{24}O_{41}$ [3].

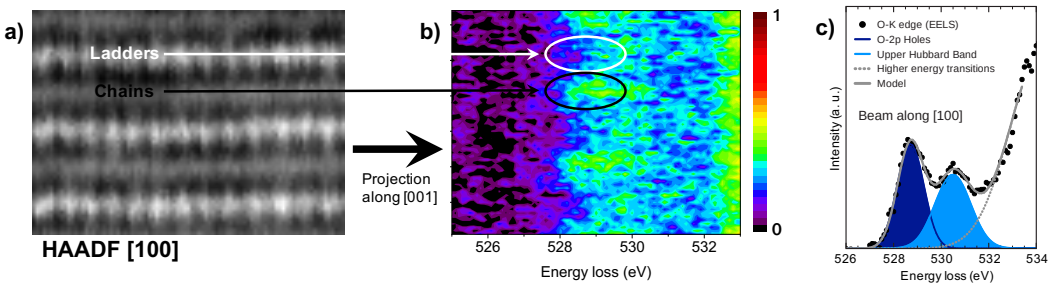

FIG. 1. Spectrum image data set of $Ca_{11}Sr_3Cu_{24}O_{41}$ recorded in [100] zone axis illustrating simultaneously acquired STEM-HAADF image (a) and O-K pre-edge ELNES projected along [001] (b). Modulations in the intensity of the pre-edge fine structures show a dominant localization in the chains CuO_2. (c) Monochromated O-K edge of $Ca_{11}Sr_3Cu_{24}O_{41}$. Pre-edge fine structures are fitted with Gaussian functions.

References

[1] M. Bugnet et al., *Sci. Adv.* 2 (2016) e1501652.
[2] A. Rusydi et al., *Phys. Rev. B* 75 (2007) 104510.
[3] The electron microscopy work presented here has been performed at the Canadian Centre for Electron Microscopy, a national facility supported by CFI, NSERC and McMaster University. G.R. acknowledges funding from CNRS PICS. This work was supported by the FWF (grants I543-N20, J3732-N27).

Distribution of hole in $La_{2-x}Sr_xCuO_4$

M. Haruta[1], Y. Fujiyoshi[1], T. Nemoto[1], A. Ishizuka[2], K. Ishizuka[2], and H. Kurata[1]

[1] Institute for Chemical Research, Kyoto University, Uji, Kyoto, 611-0011, Japan.
[2] HREM Research Inc., 14-48 Matsukazedai, Higashimatsuyama, Saitama 355-0055, Japan.

Since advanced STEM-EELS analysis provides the electronic structure of unoccupied states with atomic scale, it can potentially analyze the distribution of hole as typified by cuprate high-T_c superconductor [1]. However, it is difficult to obtain the high S/N spectrum for low cross-section edge from each atomic column. This means that such a spectrum needs a high total electron dose that introduces damages even to an oxide. A well-known high-T_c superconductor material, $La_{2-x}Sr_xCuO_4$ (Fig. 1(a)), is also sensitive to heavy electron irradiation which leads to the spectrum change. In many cases, electron damage prevents atomic resolution spectroscopy. Low voltage is not always the answer to this problem.

In this study, the distribution of hole in $La_{2-x}Sr_xCuO_4$ is investigated with an atomic-resolution by summing many spectra obtained from crystallographically equivalent sites with a low-dose condition. Figure 1(b, c) shows experimental atomic resolution O K-edge spectra from apical (O1) and planar (O2) oxygen sites. It is well known that the substitution of Sr^{2+} induces hole in O 2p state and the new electronic state generated by hole doping is observed above the Fermi level as a pre-peak in O K-edge. The results show that the induced hole distribution is clearly different between under ($x \leq 0.15$) and over ($0.15 < x$) dope conditions, where $x = 0.15$ is optimum and highest-T_c condition. In the over dope samples, hole is induced not only O2 site but also O1 site. Such experimental evidences are firstly measured.

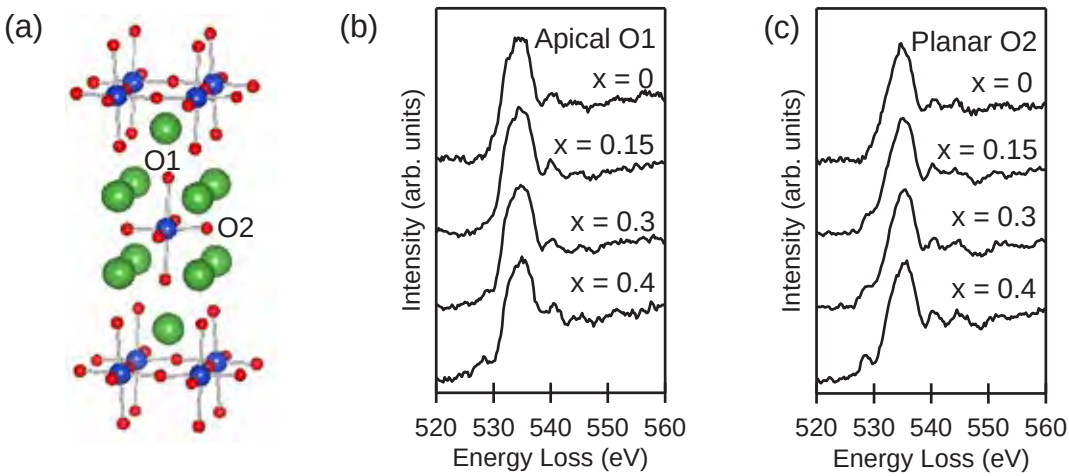

FIG. 1. (a) Crystal structure of $La_{2-x}Sr_xCuO_4$ wigh the different type of oxygen (apical O1 and planar O2) indicated. Experimental oxygen K-edge spectra from (b) apical O1 and (c) planar O2.

References

[1] N. Gauquelin et al., *Nature communications.* 5 (2014) 4275.
[2] This work was supported by JSPS KAKENHI Grant Number 26706015. The aid of sample synthesis by Dr. Kimoto, Dr. Nagai, and Dr. Nagao is gratefully acknowledged.

Dopant Size Effects on Interfacial Superconductivity in Lanthanum Cuprate Bilayers

P. A. van Aken[1], Y. E. Suyolcu[1], Y. Wang[1], F. Baiutti[1], G. Gregori[1], G. Cristiani[1], W. Sigle[1], J. Maier[1], G. Logvenov[1]

[1] Max Planck Institute for Solid State Research, Heisenbergstr.1, 70569 Stuttgart, Germany

Epitaxial interfaces in oxide systems have been extensively studied in the last years and unexpected local properties (such as magnetism, electronic and ionic redistribution, superconductivity) have been highlighted [1-8]. Highly adaptable crystal structures of oxide materials enable changes in composition and thus provide the opportunity of fabricating them in different forms.

In this study, lanthanum cuprate-based bilayers grown by atomic layer-by-layer oxide molecular beam epitaxy (ALL oxide MBE), consisting of a metallic (M) and an insulating (I) phase, are considered. Remarkably, the structures exhibit high-temperature interfacial superconductivity (up to $T_c \approx 40$ K). With the aim of assessing the role of the dopant size on the interface structure (chemistry and lattice distortions) and functionalities (interfacial superconductivity), different dopants (Ca^{2+}, Sr^{2+} and Ba^{2+}) have been employed in the M-phase, and the M-I bilayers have been investigated by complementary techniques, including analytical spherical-aberration-corrected scanning transmission electron microscopy. A series of exciting findings are highlighted: (i) overdoped $La_{2-x}Ca_xCuO_4$ (x up to 0.4) is successfully grown for the first time, (ii) the out-of-plane lattice parameter of the bilayers is linearly dependent on the dopant ionic size while each dopant redistributes at the interface with a characteristic diffusion length, and (iii) superconductivity is highly dependent on the dopant of choice.

References

[1] A. Frano, E. Benckiser, Y. Lu, M. Wu, M. Castro-Colin, M. Reehuis, A.V. Boris, E. Detemple, W. Sigle, P.A. van Aken, G. Cristiani, G. Logvenov, H.-U. Habermeier, P. Wochner, B. Keimer, V. Hinkov: *Adv. Mater.* 26 (2014) 258

[2] F. Baiutti, G. Logvenov, G. Gregori, G. Cristiani, Y. Wang, W. Sigle, P.A. van Aken, J. Maier: *Nature Comm.* 6 (2015) 8586

[3] C. Woltmann, T. Harada, H. Boschker, V. Srot, P.A. van Aken, H. Klauk, J. Mannhart: *Phys. Rev. Appl.* 4 (2015) 064003

[4] F. Bern, M. Ziese, I. Vrejoiu, X. Li, P.A. van Aken: *New J. Phys.* 18 (2016) 053021

[5] Y. Wang, F. Baiutti, G. Gregori, G. Cristiani, U. Salzberger, G. Logvenov, J. Maier, P.A. van Aken: *ACS Appl. Mater. & Interfaces* 8 (2016) 6763

[6] F. Baiutti, G. Gregori, Y. Wang, Y.E. Suyolcu, G. Cristiani, P.A. van Aken, J. Maier, G. Logvenov: *ACS Appl. Mater. Interfaces* 8 (2016) 27368

[7] A. Frano, S. Blanco-Canosa, E. Schierle, Y. Lu, M. Wu, M. Bluschke, M. Minola, G. Christiani, H.-U. Habermeier, G. Logvenov, Y.Wang, P. A. van Aken, E. Benckiser, E. Weschke, M. Le Tacon, B. Keimer: *Nature Mater.* 15 (2016) 831

[8] X. Li, I. Lindfors-Vrejoiu, M. Ziese, A. Gloter, P.A. van Aken: *Sci. Rep.* 7 (2017) 40068, DOI: 10.1038/srep40068

Angular Resolved Electron Energy Loss Spectroscopy in hexagonal Boron Nitride

F. Fossard[1], L. Sponza[1], L. Schué[1,2], F. Ducastelle[1], J. Barjon[2] and A. Loiseau[1]

[1] Laboratoire d'Etude des Microstructures, ONERA-CNRS, UMR104, Université Paris-Saclay, BP 72, 92322 Châtillon Cedex, France
[2] Groupe d'Etude de la Matière Condensée, UVSQ-CNRS, UMR8635, Universit é Paris-Saclay, 45 avenue des Etats-Unis, 78035 Versailles Cedex, France

Core and low energy electronic excitations have been studied in hexagonal boron nitride (h-BN). Angular resolved electron energy loss spectra have been measured using a transmission electron microscope equipped with a monochromator and an in-column filter. Energy filtered diffraction patterns have been recorded and provide us with a global view of anisotropic effects in reciprocal space. From combined angular and energy resolved measurements, we analyze the symmetry of the losses as a function of the energy transferred to the material. We show how easily the core loss spectra at the K edges of boron and nitrogen can be measured and imaged. Low losses associated to interband and/or plasmon excitations are also measured and discussed from ab initio calculations. We show that RPA based simulations correctly describe the angular dependence of the dielectric response [1].

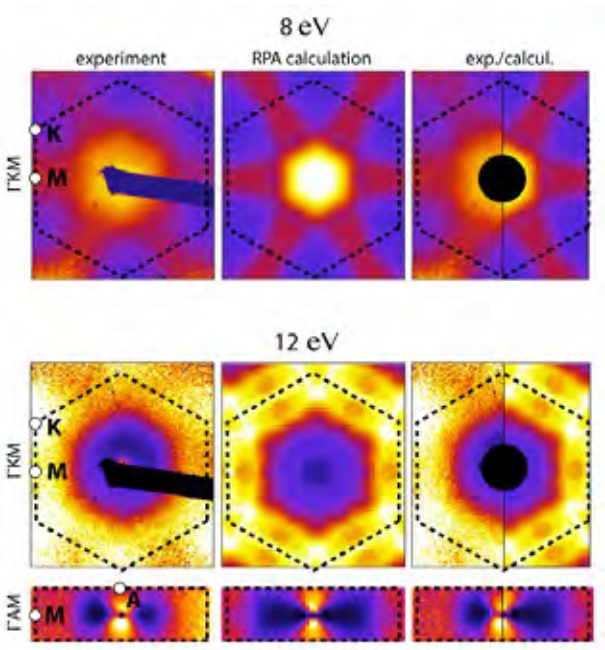

FIG. 1. Experimental and calculated loss functions (scattered intensities multiplied by q^2) at 8 eV for the ΓKM plane and at 12 eV for the ΓKM and ΓAM planes. Dashed lines delimitate the Brillouin zone of h-BN.

References

[1] F. Fossard, L. Sponza et al., ArXiv:1701.05119v1

[2] This research was supported by European Union H2020 Programme Programme (Flagship Graphene Core1,N° 696656) and by the French National Research Agency. P. Wachsmuth, G. Benner and U. Kaiser are warmly acknowledged.

Dimensionality effects in hBN probed by cathodoluminescence

L. Schué[1,2], A. Plaud[1,2], F. Fossard[1], L. Sponza[1], F. Ducastelle[1]
J. Barjon[2] and A. Loiseau[1]

[1] Laboratoire d'Etude des Microstructures, ONERA-CNRS, UMR104, Université Paris-Saclay, BP 72, 92322 Châtillon Cedex, France
[2] Groupe d'Etude de la Matière Condensée, UVSQ-CNRS, UMR8635, Université Paris-Saclay, 45 avenue des Etats-Unis, 78035 Versailles Cedex, France

Hexagonal boron nitride is a wide band gap semiconductor (6.4 eV), which can be synthesized, as graphite, its carbon analog, as bulk crystallites, nanotubes and layers. These structures meet a growing interest for deep UV LED and graphene engineering [1]. We attempt to have a better comprehension of the optical and electronic properties of thin BN layers, in correlation with their structural properties and to better know how electronic properties of graphene can be impacted by underlying BN layers. In this work, we investigate by cathodoluminescence (CL) the optical properties of various hBN bulk sources in the 5-6 eV energy range. Then, thin h-BN layers have been obtained by mechanical exfoliation from a commercial powder and a single crystal. We focused on the D series (5.2-5.7 eV) on folded flakes and measured a strong enhancement of defects lines along the fold axis. Finally, we analyzed defect free hBN flakes with various thicknesses from 100ML to 6ML and observed a significant effect of the confinement on the luminescence [2,3].

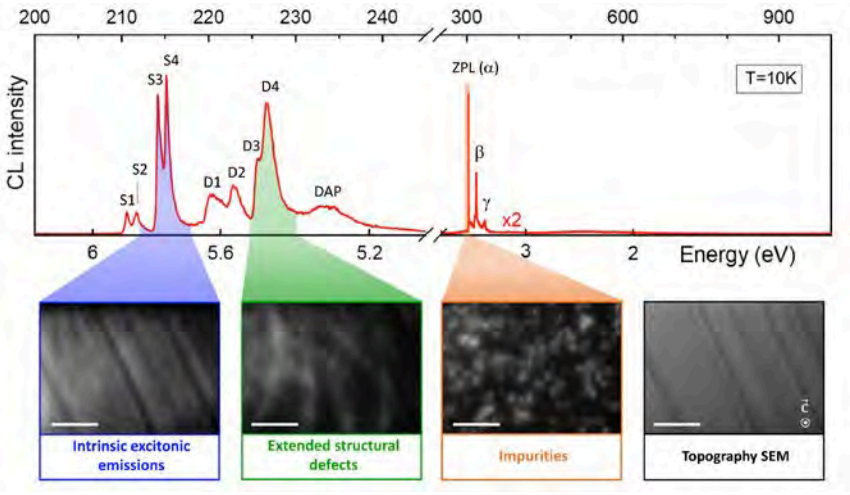

FIG.1: Typical CL spectrum of hBN in the 200–1000 nm range acquired at 10 K on a FIB preparation of the HPHT-grown crystal. Lower: SEM image (black) and the corresponding monochromatic CL images. Scale bar: 1 µm.

References

[1] C.R. Dean et al., Nature Nanotechnology, 5, 722-6 (2010)
[2] Léonard Schué et al., Nanoscale 8, 6986-6993 (2016)
[3] Léonard Schué et al., *2D Mater.* **4** 015028 (2017)

This work was supported by European Union H2020 Program and by the French National Research Agency (ANR).

Unexpected huge atomic dimerization ratio in 1D carbon chains and atom-by-atom spectroscopy studies

Y.C. Lin[1], S. Morishita[2], M. Koshino[3], C.H. Yeh, P.Y. Teng, P.W. Chiu, H.Sawada, and K. Suenaga[4]

[1] National Institute of Advanced Industrial Science and Technology (AIST), Tsukuba 305-8565, Japan
[2] JEOL Ltd., 3-1-2 Musashino, Akishima, Tokyo 196-8558, Japan.
[3] Department of Electrical Engineering, National Tsing Hua University, Hsinchu 30013, Taiwan
[4] Department of Mechanical Engineering, The University of Tokyo, 7-3-1 Hongo, Bunkyo-ku, Tokyo 113-8656, Japan

Single-atomic carbon chain is the last missing puzzle of the carbon families. The sp^1-hybridized carbon chain is believed to form two possible chemical structures with distinct electronic properties, i.e., metallic Cumulene (periodic double bonds, =C=C=) and semiconducting Polyyne (alternating single and triple bonds, ─C≡C─). These two phases have been calculated to transform alternatively by controlling the boundary condition, atomic number, strain, and temperature [1], but the related atomic configuration have not been experimentally corroborated so far. In this presentation, we will show a systematic study of suspended carbon atomic chain sculpted from graphene by using transmission electron microscopy (TEM) and scanning TEM at various temperatures ranging from 773K to 97K. Carbon chains were found more preferable Polyyne-like at high temperature, but more Cumulene-like at cryogenic temperature. The atomic structure of carbon chain at 773K shows unexpected huge dimerization ratio which is 10 times larger than the theoretical value of infinity long Polyyne and 2 times larger than short Polyyne under a strain. We will show the EELS fingerprints of sp^1-carbon chain at various temperatures. We will also describe how two carbon chains interact and switch between sp^1 and sp^2 bonding configurations by using fast monochromated TEM imaging.

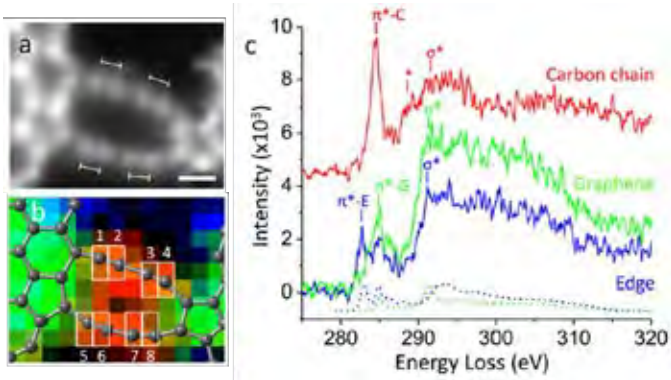

FIG. 1. (a) ADF image of two parallel carbon chains with huge atomic alternation. (b) The corresponding 2D EELS color mapping overlapped with the atomic model. (c) The carbon chain (red), graphene (green) and graphene edge (blue) spectra extracted from (b). Scale bar is 2Å.

References

[1] V.I. Artyukhov et al., Nano Lett. 14 (2014) 4224-4229.
[2] Y.C. Lin et al., *Nano Lett.* 17 (2017) 494-500.

Exciton and Plasmon Mapping at the Nanoscale

H. C. Nerl[1], K. T. Winther[3], F. S. Hage[2], K. S. Thygesen[3], L. Houben[4], Q. M. Ramasse[2] and V. Nicolosi[1,5]

1 CRANN & AMBER and School of Physics, Trinity College Dublin, Dublin 2, Ireland

2 SuperSTEM Laboratory, STFC Daresbury Campus, Keckwick Lane, Daresbury WA4 4AD, UK

3 Center for Atomic-Scale Materials Design, Department of Physics, Technical University of Denmark, Fysikvej, 2800, Kgs. Lyngby, Denmark

4 Ernst Ruska Center for Microscopy and Spectroscopy with Electrons, Research Center, Juelich, Germany & Weizmann Institute of Science, Israel

5 School of Chemistry, Trinity College Dublin, Dublin 2, Ireland

Excitons and plasmons are the two most fundamental types of collective electronic excitations occurring in solids. Traditionally, they have been studied separately using bulk techniques that probe their average energetic structure over large spatial regions. However, as the dimensions of materials and devices continue to shrink, it becomes crucial to understand how these excitations depend on local variations in the crystal- and chemical structure on the atomic scale.

Due to recent technical improvements we can now access parts of the low loss electron energy-loss (LL EEL) spectra which had previously been inaccessible. This opens up new possibilities to study nanomaterials not only at unprecedented energy but also with a spatial resolution at the nanoscale [1]. Although some significant progress has been made recently in unravelling the physical origins of the LL EEL features as shown by Tizei, Lin [2], significant gaps in our understanding of the signals and their origins remain. In the study presented here, we used a combination of experimental monochromated LL STEM EEL spectroscopy and theoretical calculations using time-dependent density functional theory (TDDFT) as well as the Bethe-Salpeter equation (BSE) to study the optical properties of MoS2 at the nanoscale with the aim to understand the origins of the peaks and regional variations of the complete LL EEL spectrum.

Using first-principles many-body calculations we confirm the excitonic nature of the peaks at ~2eV and ~3eV in the experimental EEL spectrum and the plasmonic nature of higher energy-loss peaks. Furthermore, we observed great spatial variations in the LL EELS signal when comparing the edge to inner regions of a flake, i.e. with increasing number of layers, and we show how these can be largely attributed to beam geometry effects. Moreover, we show that the excitonic features are dominated by the long wavelength (q=0) components of the probing field, while the plasmonic features are sensitive to a much broader range of q-vectors, indicating a qualitative difference in the spatial character of the two types of collective excitations. Our work provides a template protocol for mapping the local nature of electronic excitations that open new possibilities for studying photo-absorption and energy transfer processes on a nanometer scale.

1. Zhou, W., et al., Monochromatic STEM-EELS for Correlating the Atomic Structure and Optical Properties of Two-Dimensional Materials. Microscopy and Microanalysis, 2014. 20(S3): p. 96-97.
2. Tizei, L.H.G., et al., Exciton Mapping at Subwavelength Scales in Two-Dimensional Materials. Physical Review Letters, 2015. 114(10).

Plasmonic nanowire arrays as a platform for photocatalytic testing

J. Cottom[1], P. Abellan[2], F. Hage[2], Q. Ramasse[2], K. Critchley[3], and R. Brydson[1]

[1] School of Chemical & Process Engineering, University of Leeds, Leeds LS2 9JT, U.K.
[2] SuperSTEM Laboratory, SciTech Daresbury Campus, Daresbury, U.K.
[3] School of Physics and Astronomy, University of Leeds, Leeds LS2 9JT, U.K.

We report the fabrication of two dimensional metallic nanowire arrays over mm-sized areas on an electrode using templated electrodeposition and subsequent post-processing (see Fig. 1 a). This approach allows control of the metal (Au, Ag, or a combination of both), the nanowire length, aspect ratio and inter-wire separation in the array can be controlled. These are characterized in terms of their structure by SEM (see Fig. 1 b) and cross-sectional TEM [1]. The plasmonic response was investigated using finite element modeling and monochromated electron energy low loss spectroscopy. Of special interest are the different coupled modes, the effect of the substrate (Figs. 1c,d) and modes detected at very low energy. Subsequent atomic layer deposition of a thin layer of semiconductor photocatalyst onto the array permits photocatalytic testing under controlled conditions [2] in order to identify any effects of plasmonic enhancement.

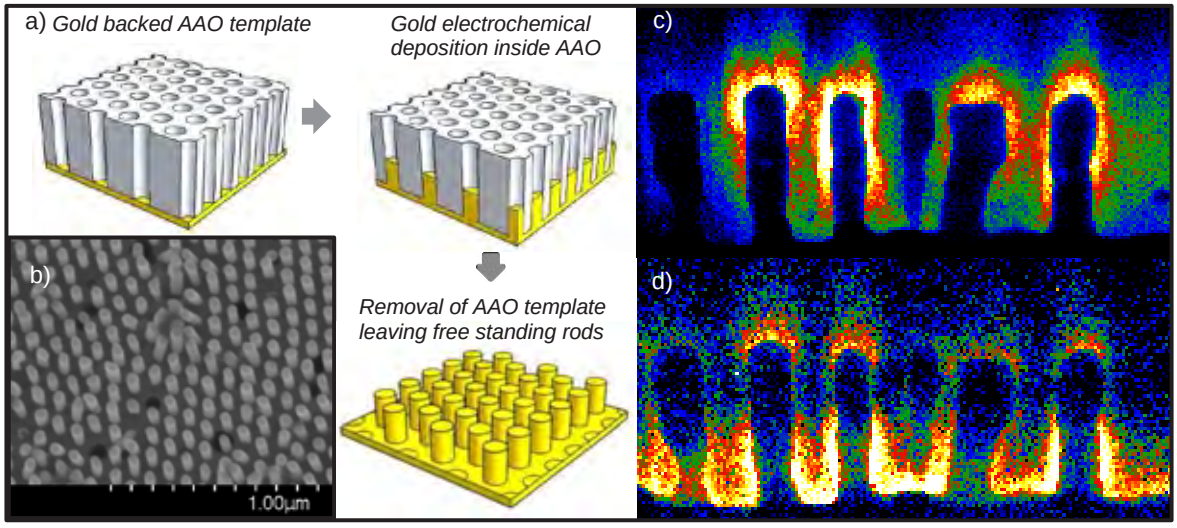

FIG. 1. a) Schematic diagram showing fabrication of a regular Au nanowire array supported on an Au substrate, b) Tilted SEM image of fabricated Au nanowire array, c-d) EELS plasmon maps between 0.7-0.8eV and 1.9-1.95eV, respectively (ZLP FWHM is 35meV) showing two different coupled modes of the array. EELS data acquired using a Nion UltraSTEM 100MC Hermes microscope at SuperSTEM.

References

[1] S.J. Hurst et al., *Angewandte Chemie International Edition* (2006) 2672.
[2] J. Lee et al., *Nano Lett.* (2012) 5014.
[3] This work was financially supported by the EPSRC through the University of Leeds Centre for Doctoral Training in Low Carbon Technologies (Grant No.: EP/G036608/1). The SuperSTEM Laboratory is the U.K. National Facility for Aberration-Corrected STEM, supported by the EPSRC.

Mapping of Sn dopant in hematite photoanodes by STEM-EELS and atom probe tomography

S. Zhang[1], T. Li[1], B. Gault[1], A.G. Hufnagel[2], R. Hoffmann[2], D. Fattakhova-Rohlfing[2], T. Bein[2], C. Scheu[1]

[1] Max-Planck-Institut für Eisenforschung GmbH, Max-Planck-Straße 1, 40237 Düsseldorf, Germany
[2] Department of Chemistry and Center for NanoScience (CeNS), University of Munich (LMU), Butenandtstraße 5-13, 81377 Munich, Germany

Photoelectrochemical water splitting is a promising technology for H_2 fuel production. To optimize hematite (α-Fe_2O_3) photoanodes for water oxidation, doping with Sn can improve the photocurrent by orders of magnitude [1]. A non-uniform distribution of Sn within the nm to sub-µm sized photoanodes further opens up the design space, and demands chemical characterization at nm-resolution. We showcase the analysis on atomic layer deposited hematite photoanodes with different doping profiles (Fig. 1a).

The usual STEM-EDS analysis is not applicable due to the fluorescence artefacts from the conductive SnO_2 substrate. While the delayed Sn-$M_{4,5}$ EELS edge is difficult to quantify (Fig. 1b), multivariate analysis on STEM-EELS spectrum imaging was developed to model the signal (Fig. 1c). Furthermore, atom probe tomography was employed to study the distribution of Sn in the hematite layer (Fig. 1d), which corroborates the observation from EELS analysis.

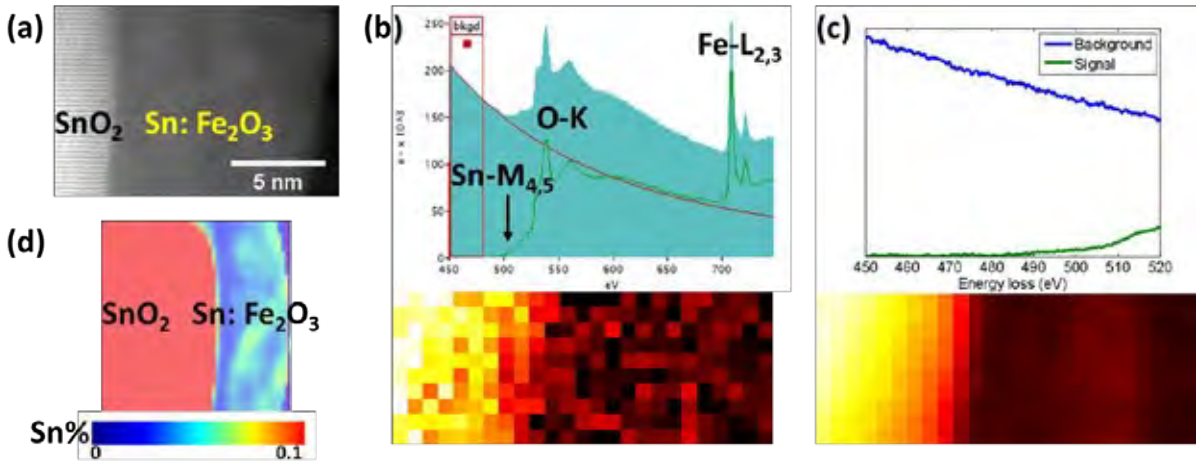

FIG. 1. (a) STEM micrograph of a Sn doped Fe_2O_3 photoanode on SnO_2 substrate; (b) Sn-$M_{4,5}$ edge and its signal integration map analyzed by standard routine (each pixel is 1 nm * 1 nm); (c) Sn-$M_{4,5}$ signal extracted from multivariate analysis of the same area and its corresponding signal integration map; (d) A cross-sectional 2D concentration map of Sn, plotted from an atom probe tomography reconstruction.

References

[1] H.K. Dunn, et al., *Phys. Chem. Chem. Phys.* 16 (2014) 24610.
K.D. Malviya et al., *J. Mater. Chem. A* 4 (2016) 3091.
[2] This research is funded by DFG under the priority programme SPP 1613.

Investigating molecular-plasmon interactions in chemically functionalized metal nanoparticles using monochromated EELS

P. Abellan[1], P.Z. El-Khoury[2], F.S. Hage,[1] J. Cottom,[3] A.G. Joly,[2] W.P. Hess,[2] R. Brydson[3] and Q.M. Ramasse[1]

[1] SuperSTEM Laboratory, SciTech Daresbury Campus, Daresbury, U.K.
[2] Physical Sciences Division, Pacific Northwest National Laboratory, Richland, U.S.A.
[3] School of Chemical and Process Engineering, University of Leeds, Leeds, U.K.

Metal nanostructures can be used to detect, image, and identify molecules with high sensitivity and selectivity using tools of (non)linear optical spectroscopy [1]. The interplay and coupling of molecules to plasmons is known to be complex and, indeed, the exact mechanisms behind a plethora of phenomena of mixed molecular-metallic/plasmonic origin are not well understood. We use monochromated EELS to detect aromatic thiols in chemically functionalized metal particles, to visualize the local electric fields associated with plasmonic excitation and to explore the interaction between the molecules and plasmons on the nanoscale. Specific aims of this work have been to find conditions for identifying molecular reporters (eg. DMS – see Fig. 1A), for simultaneously mapping vibrational and plasmonic modes (Fig. 1B) and to study the resonances due to molecule-plasmon coupling and their spatial variances (peaks at ~1eV in Fig. 1C) [2].

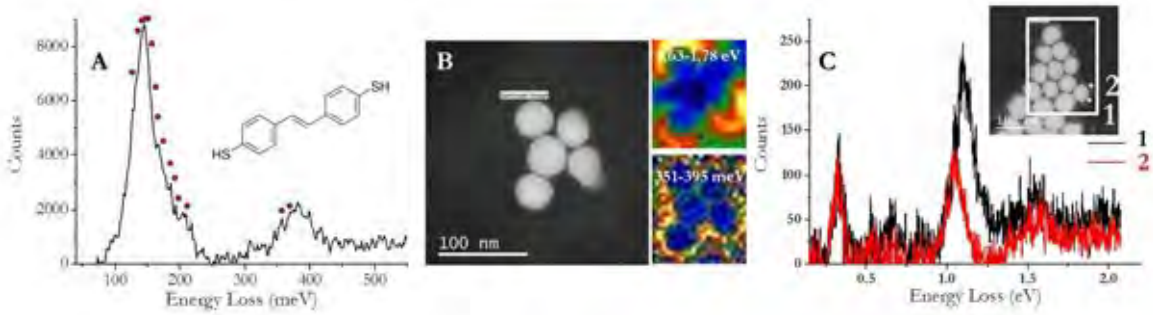

FIG. 1. A) Vibrational modes of DMS, with vibrations (IR and Raman active) indicated by red circles. The most intense peak is assigned to the C-S stretching (134meV) and aromatic C-H in-plane rocking (147meV) vibrations. B) Simultaneous mapping of aromatic C-H (360meV) from surface bonded molecules and Ag nanoparticle surface plasmon modes. C) Vibrational response and plasmonic resonances measured in aloof geometry from locations 1 and 2 (see inset). The energy resolution was 12 meV (FWHM of ZLP through support).

References

[1] Pettinger et al., N. *Annu. Rev. Phys. Chem.* 63 (2012) 379; Le Ru & Etchegoin, *Annu. Rev. Phys. Chem.* 65 (2012) 65.

[2] SuperSTEM is the UK EPSRC National Facility for Aberration-Corrected STEM, supported by the Engineering and Physical Science Research Council. PZE acknowledges support from the Laboratory Directed Research and Development Program at Pacific Northwest National Laboratory (PNNL). WPH and AGJ are supported by the US Department of Energy (DOE), Office of Science, Office of Basic Energy Sciences, Division of Chemical Sciences, Geosciences & Biosciences.

Near-Field Plasmon Resonances Near Poorly Plasmonic Materials

S. Yazdi,[1] D. F. Swearer,[2] J. R. Daniel,[3] D. Boudreau,[3] and E. Ringe[1,2]

[1] Department of Materials Science and NanoEngineering, Rice University, 6100 Main Street, Houston, TX 77005
[2] Department of Chemistry, Rice University, 6100 Main Street, Houston, TX 77005
[3] The Center for Optics, Photonics and Lasers (COPL), Department of Physics, Laval University, 2325 Rue de l'Université, Ville de Québec, QC G1V 0A6, Canada

The catalytic and optical properties of metal nanoparticles can be combined to create platforms for light-driven chemical energy storage and enhanced in-situ reaction monitoring. However, the heavily damped plasmon resonances of many catalytically active metals (e.g., Pt, Pd) prevent this dual functionality in pure nanostructures. The addition of catalytic metals at or close to the surface of efficient plasmonic particles thus presents a unique opportunity *if* the resonances can be conserved after coating.

Here, electron-based techniques (electron-energy loss, cathodoluminescence, and energy dispersive X-ray spectroscopy) are used to characterize bimetallic plasmonic-catalytic systems such as Pt-decorated Au prisms [1], transition metal-decorated Al nanocrystals [2], and semi-hollow, liquid-filled Ag-M (M=Pd, Pt, Au) nanorods [3]. We show that these plasmonic nanomaterials incorporating catalytically active but heavily damped metals sustain multiple size-dependent LSPRs that are strongly localized at the particle tips or edges, depending on the mode energy. Tomography and composition mapping unravels the availability of catalytic metal at the surface of the nanoparticles, and catalytic studies unravel their potential as light-enhanced catalysts. [4]

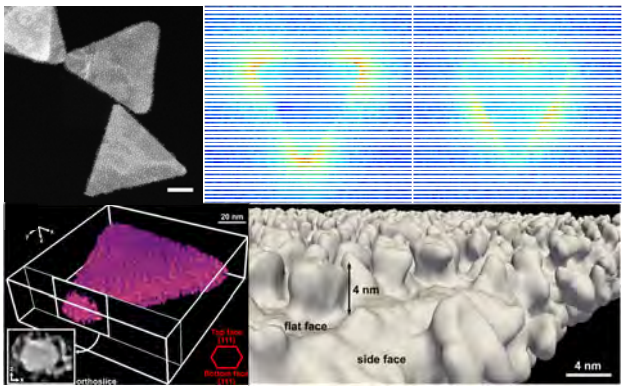

FIG 1. HAADF-STEM (top left, scalebar is 50 nm), plasmon maps (top middle and right) and tomographic reconstructions for Pt-decorated Au nanoprisms (bottom), an example of nanomaterial incorporating plasmonic and catalytic elements [1].

References

[1] R. K. Leary, A. Kumar, P. Straney, S. M. Collins, S. Yazdi, R. E. Dunin-Borkowski, P. A. Midgley, J. E. Millstone, E. Ringe, *J. Phys. Chem. C* (2016), 120, 20843.
[2] D. F. Swearer, H. Zhao, L. Zhou, C. Zhang, H. Robatjazi, J. M. Martinez, C. M. Krauter, S. Yazdi, M. J. McClain, E. Ringe, E. Carter, P. Nordlander, N. J. Halas, PNAS (2016), 113, 8916
[3] S. Yazdi, J. R. Daniel, N. Large, G. C. Schatz, D. Boudreau, E. Ringe, Nano Lett. (2016), 16, 6939
[4] This research was supported by the ACS-PRF (# 56256-DN15), NSF (GRFP #1450681), and FRQNT International Internship Programs.

Atomic-scale spectroscopic imaging of phase transformation in perovskite oxide heterostructures

D.J. Baek[1], D. Lu[2], Y. Hikita[3], H.Y. Hwang[3,4], and L.F. Kourkoutis[5,6]

[1] School of Electrical and Computer Engineering, Cornell University, Ithaca, NY 14853, USA
[2] Department of Physics, Stanford University, Stanford, CA 94305, USA
[3] SLAC National Accelerator Laboratory, Menlo Park, CA 94025, USA
[4] Department of Applied Physics, Stanford University, Stanford, CA 94305, USA
[5] School of Applied and Engineering Physics, Cornell University, Ithaca, NY 14853, USA
[6] Kavli Institute at Cornell for Nanoscale Science, Ithaca, NY 14853, USA

With recent advances in aberration correction, electron energy loss spectroscopy (EELS) in combination with scanning transmission electron microscopy (STEM) has proven to be a powerful tool to study materials at the atomic scale. Here, using aberration-corrected STEM-EELS, we present atomic-resolution spectroscopic mapping conducted on thin films of $La_{0.7}Sr_{0.3}MnO_3$ (LSMO) grown on top of a water-soluble perovskite-like buffer layer, $Sr_3Al_2O_6$ (SAO). Its unique properties enable fabrication of freestanding 2D oxide membranes, but critically depend on SAO's inherent structure. [1] Any structural or chemical modification of the buffer layer during subsequent growth, therefore, has to be avoided.

Spectroscopic imaging performed on a 5th order aberration-corrected Nion UltraSTEM reveals that Mn and La from the LSMO film can diffuse fully into the SAO buffer layer, thereby creating a new phase. The Mn elemental map shows that this phase consists of a characteristic double-layer ordering of the Mn atoms. Interestingly, multivariate curve resolution (MCR) further suggests the presence of two distinct Mn valence states, Mn^{2+} and Mn^{3+}. The relative difference in ionic radii between the two drives an atomic reconstruction, which stabilizes this new phase. [2]

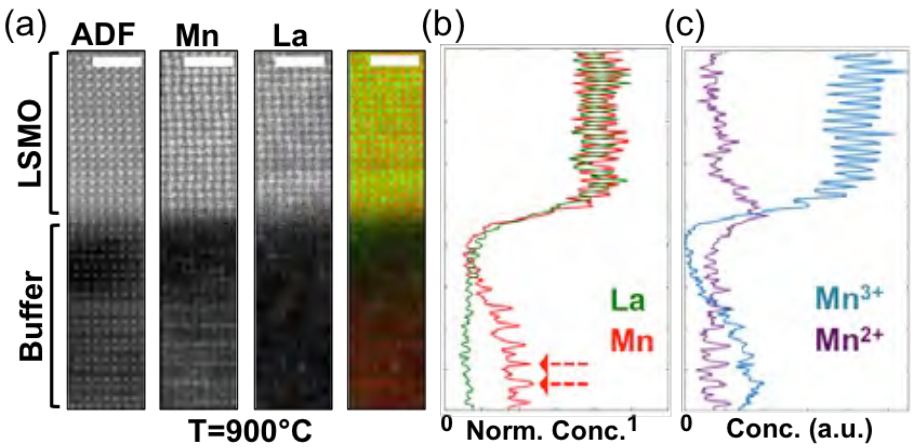

FIG. 1. **(a)** Atom-resolved EELS maps acquired from an LSMO film grown atop SAO at a growth temperature of T=900 °C. **(b)** Concentration profiles of Mn and La. **(c)** Concentration profiles of the two Mn valence states extracted from MCR.

References

[1] D. Lu et al., *Nature Mater.* 15 (2016) 1255.
[2] D. J. Baek et al., *ACS Appl. Mater. Interfaces* 9 (2017) 54.
[3] This work was supported by the Cornell Center for Materials Research with funding from the NSF MRSEC program (DMR-1120296).

Atomic-resolution STEM-EELS analysis of the interfaces in ferroelectric tunnel junctions

T. Nagai[1] and H. Yamada[2,3]

[1] National Institute for Materials Science (NIMS), Tsukuba, Ibaraki 305-0044, Japan
[2] National Institute of Advanced Industrial Science and Technology (AIST), Tsukuba, Ibaraki 305-8562, Japan
[3] Japan Science and Technology Agency (JST) PRESTO, Kawaguchi , Saitama 332-0012, Japan

Tunnel electroresistance (TER) in ferroelectric tunnel junctions (FTJs) has attracted large interest due to the potential application to nonvolatile memories. The importance of the electrode-insulator interface has been pointed out for TER. We performed aberration-corrected STEM-EELS analysis of the interfaces in $BaTiO_3$ (BTO)-based FTJs, Co/BTO/(La,Sr)MnO_3 (LSMO) junctions [1].

An ultrathin BTO film and an LSMO bottom-electrode layer were deposited on a TiO_2 (*B*-site)-terminated $SrTiO_3$ (STO) (001) substrate by pulsed laser. Cross-sectional TEM specimens of a BTO/LSMO/STO heterostructure (Sample 1) and a water-agitated BaO_x/BTO/LSMO/STO heterostructure (Sample 2) were prepared by Ar ion milling, and observed using FEI Titan Cubed at 300 kV. The aberration-corrected STEM-EELS analysis revealed the atomic arrangement of TiO_2–BaO–MnO_2–(La,Sr)O, that is, *B*–site (MnO_2) termination of LSMO at the BTO/LSMO interface in Sample 1 (FIG. 1). Additionally, the STEM observation confirmed *B*–site (TiO_2) termination of the BTO surface. On the other hand, the STEM analysis revealed *A*–site (BaO) termination of the surface in Sample 2. The two heterostructures showed opposing relationships between the polarization direction and the resistance state. These results indicate that the sign of TER depends on the surface termination of the BTO layers.

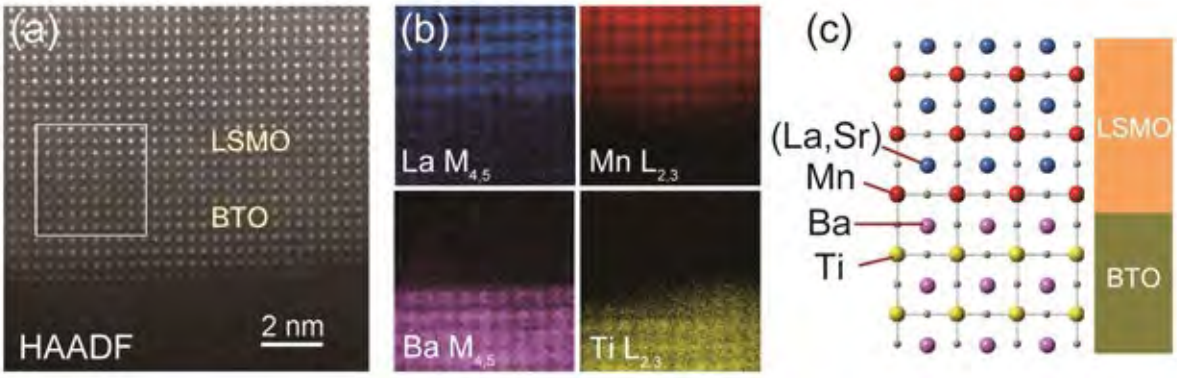

FIG. 1. (a) HAADF-STEM image, (b) EELS map, and (c) atomic arrangement of the interface in a Co/$BaTiO_3$ (BTO)/(La,Sr)MnO_3 (LSMO) ferroelectric tunnel junction.

References

[1] H. Yamada et al., *Adv. Funct. Mater.* 25 (2015) 2708.
[2] This work was partly supported by the Nanotechnology Platform (Grant No. A-14-NM-0075) of MEXT, Japan.

Spatially resolved energy-loss mapping at magic angle conditions

D.T.L. Alexander[1], L. Fave[2], T. Dennenwaldt[1,3], and C. Hébert[1,3]

[1] Interdisciplinary Centre for Electron Microscopy (CIME), Ecole Polytechnique Fédérale de Lausanne (EPFL), 1015 Lausanne, Switzerland
[2] Laboratory for Nuclear Materials, Paul Scherrer Institut, Villigen, Switzerland
[3] Electron Spectroscopy and Microscopy Laboratory (LMSE), Institute of Physics, Ecole Polytechnique Fédérale de Lausanne (EPFL), 1015 Lausanne, Switzerland

"Magic angle" conditions provide a way to cancel the orientation dependence of energy-loss near edge structure measurements in materials with anisotropy in the band structure, and so are useful for fingerprinting their electronic structure. Here, in order to map the C sp^2/sp^3 ratio in carbonaceous materials that are chemically or structurally inhomogeneous, we implement approaches for spatially resolved mapping of the carbon ionization K-edge under magic angle conditions. The first method utilizes energy-filtered (EF-) TEM on a JEOL 2200FS operated at 200 kV. While successfully acquired data are demonstrated in Fig. 1a, the demands of recording EFTEM image series with a small 2 eV energy selecting slit and a collection semi-angle of just ~1 mrad (obtained with a 5 µm objective aperture) bring inherent challenges related to microscope alignment, data signal-to-noise, dark noise thermal drift, and spectrum image data processing. The second approach is instead based on STEM EELS mapping, implemented on a FEI Titan Themis 60-300 with a GIF Quantum ERS spectrometer. The instrument is operated at 80 kV, which both "relaxes" the angular requirements of the magic angle condition, and reduces beam damage. The flexible condenser lens optics of the microscope, combined with the GIF's capabilities, lead to a more robust data acquisition and processing; example results are illustrated in Fig. 1b. Other aspects of data acquisition time and electron dose efficiency are compared between the two methods.

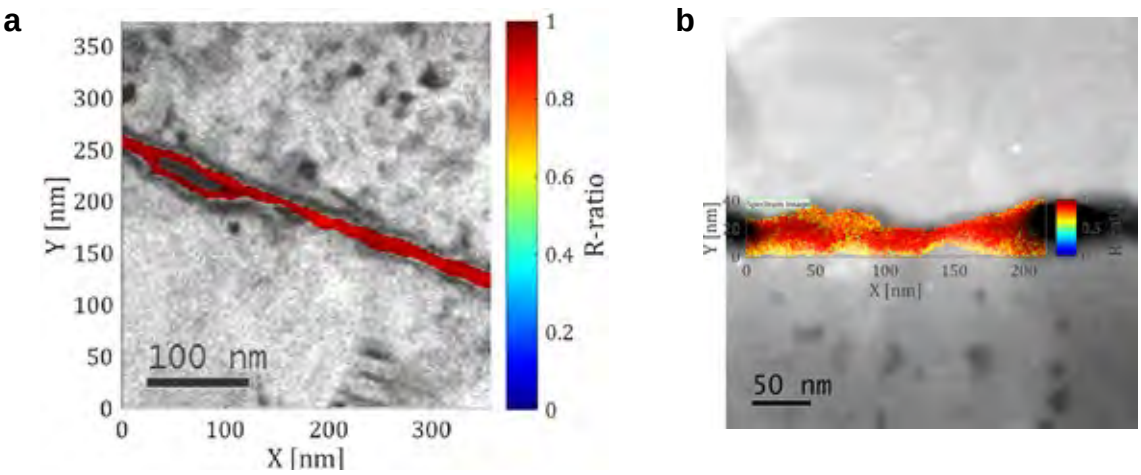

FIG. 1. sp^2/sp^3 "R-ratio" intensity maps of: (a) pristine pyrolytic carbon interlayer in SiC/SiC composite acquired using EFTEM-based mapping; (b) same type of carbon interlayer after ion irradiation, acquired using STEM-EELS based method.

References

[1] C. Hébert et al., *Ultramicrosc.* 106 (2006) 1139.

Low-voltage Cc-corrected energy-filtered TEM: evaluation, first experiments and image simulation

Michael J. Mohn, Johannes Biskupek, Zhongbo Lee, Harald Rose, and Ute Kaiser

Central Facility of Electron Microscopy, University of Ulm, D-89081 Ulm, Germany

The SALVE (Sub-Ångstroem Low-Voltage Electron Microscopy) instrument is equipped with an imaging energy filter and corrected for geometric and chromatic aberrations [1, 2]. According to these properties the instrument provides the possibility to form high-resolution images by inelastically scattered electrons of different energy losses.

Here we characterize the performance of our Cc/Cs-corrected EFTEM system, show first experimental results and compare them with simulations obtained with our novel image calculation routine which includes inelastic scattering.

In particular, we (a) discuss the effects of chromatic aberrations induced by the imaging energy filter in the voltage range between 20kV and 80kV and (b) show first atomically resolved experimental images of 2D materials such as graphene and boron nitride obtained by plasmon-loss electrons and by high-energy-loss electrons. For the latter case we present images formed by electrons which have excited the carbon K-edge (graphene) and the Ti $L_{2,3}$ edge (TiO_2, $TiSe_2$), respectively.

Our experiments are accompanied by image calculations that involve inelastic scattering. In order to simplify the calculations, we have developed a method to represent the mixed dynamic form factor (MDFF) by its two-dimensional eigenvectors [3]. This method reduces the 4D problem to a set of 2D problems whose numbers are minimized. These improvements enable a more precise comparison between experiments and calculations than previously.

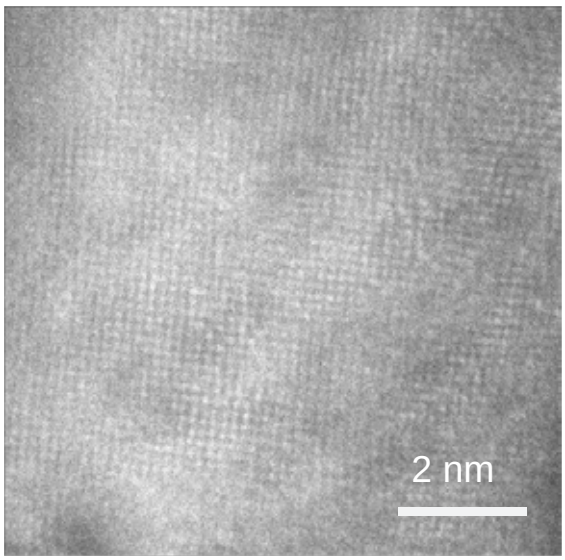

FIG. 1. 80 kV C_C and C_S corrected energy-filtered TEM image of TiO_2 at an energy loss of 463 eV using an 8 eV energy window.

[1] M. Linck et al. (2016). *Physical Review Letters*, 117(7), 1–5.
[2] U. Kaiser et al. (2011). *Ultramicroscopy*, 111(8), 1239–1246.
[3] Z. Lee et al. (2017). *Ultramicroscopy,* 175, 58-66.

EELS study of Nanocross: A super tunable plasmonic system

P. Das[1,*], H. L. Martins[1,*], L. Tizei[1], and M. Kociak[1]

[1] Laboratoire de Physique des Solides, Université Paris Sud - ORSAY - FRANCE

Although a significant amount of research has been devoted to the study of plasmonic properties of metal nanoparticles, spectral tunability still remains one of the key issues. Especially when it comes to application, e.g. in sensing, surface enhanced spectroscopy or photo-thermal therapy, precise spectral tunability is a very important factor. It is now well known that higher order surface plasmon modes can be better utilized in various applications due to their higher Q factor and ability to achieve strong field confinement. However it is not easy to tune higher order plasmon modes in a systematic manner.

In this work, with the help of electron energy loss spectroscopy (EELS) in a scanning transmission electron microscope (STEM) and boundary element method (BEM) simulations, we have shown that a silver nanocross can be used to tune the plasmon modes and especially the higher order modes in a very controlled manner. Morphing a nanorod to a nanocross can lead to a spectacular evolution of various order modes in the EEL spectra (Figure 1(a, b), geometry in middle panel). The higher order modes (S2, S4) come closer in energy with S1 and S3 respectively as the length of the short arm of the cross increases slowly. They can even cross each other in energy (S3, S4 in (b)). Hence a higher order mode can be placed at a lower energy compared to a lower order mode (S3). Apart from this manipulation of different order modes, we have also studied the coupling of two nanocross separated by a small gap of ~ 30 nm ((c), (d)). It gives us more tunability of plasmon modes in a wide range of energy.

We will discuss the evolution of modes based on a first order perturbation theory approach.

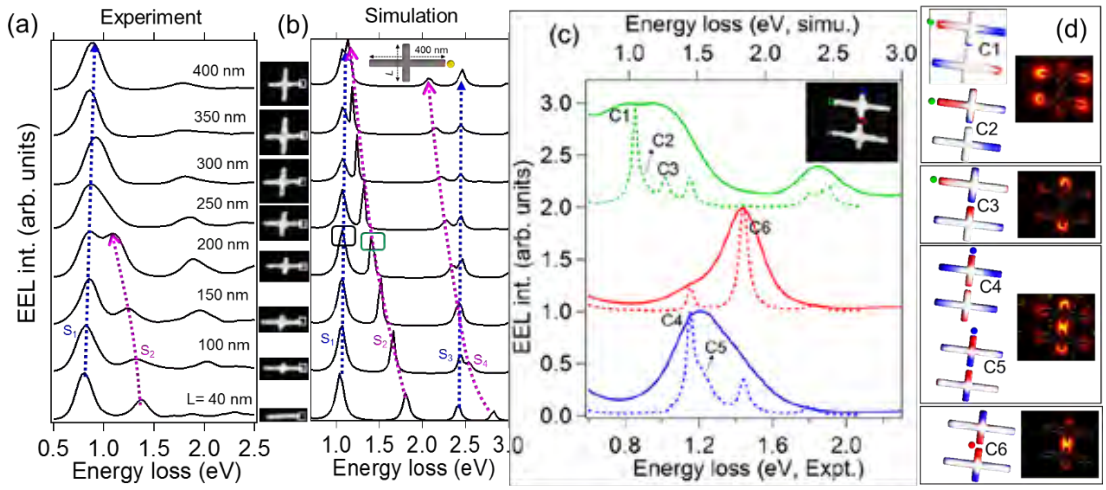

FIG. (a,b) Morphing nanorod to a nanocross and evolution of modes. The crosses have been prepared with e-beam lithography. (c) EEL spectra corresponding to different location of coupled cross (simu. dotted) (d) Simulated charge maps and experimental EEL maps.

* These authors have contributed equally to the work to be presented.

Acknowledgement: PD wants to thank the ESTEEM 2 project and the French ANR FEMTOTEM project for funding.

Extreme UV plasmonics:
Localized surface plasmon resonances in 3D nanovoids

Y. Zhu[1], P.N.H. Nakashima[1], A. M. Funston[2], L. N. Bourgeois[1,3], J. Etheridge[1,3]

[1] Dept of Materials Science and Engineering, Monash University, VIC 3800, Australia
[2] School of Chemistry, Monash University, VIC 3800, Australia
[3] Monash Centre for Electron Microscopy, Monash University, VIC 3800, Australia

In the last decade, the ability to synthesise and fabricate metallic nanoparticles with chosen geometries has greatly advanced the field of plasmonics. However, the complementary system - the inverted nanostructure or nano-void - has so far been limited to either 2D holes or spherical voids, due to the difficulty in creating voids with well-defined 3D geometries. Here we present the first localized surface plasmon resonance (LSPR) study of nano-voids fully encapsulated in a matrix.

Nano-voids were created in high-purity aluminium [1] and the LSPRs were characterized using electron energy-loss spectroscopy (EELS) in an aberration-corrected FEI Titan^3 80-300 S/TEM with a Schottky field emission gun at 80 kV. To compare with experimental observations, electrodynamic EELS simulations were performed based on electron-driven discrete dipole approximation (*e*-DDA) [2].

The Al nano-voids exhibit strongly localized field enhancements, with the LSPR energies in the extreme UV region, 10.7 -13.3 eV (116-93 nm, Fig. 1), well beyond the conventional LSPR spectrum range, and hence are promising for applications such as LSPR-enhanced UV photoemission spectroscopy and photoionization. The nanovoids are also free from surface oxides, unlike their Al nanoparticle counterparts.

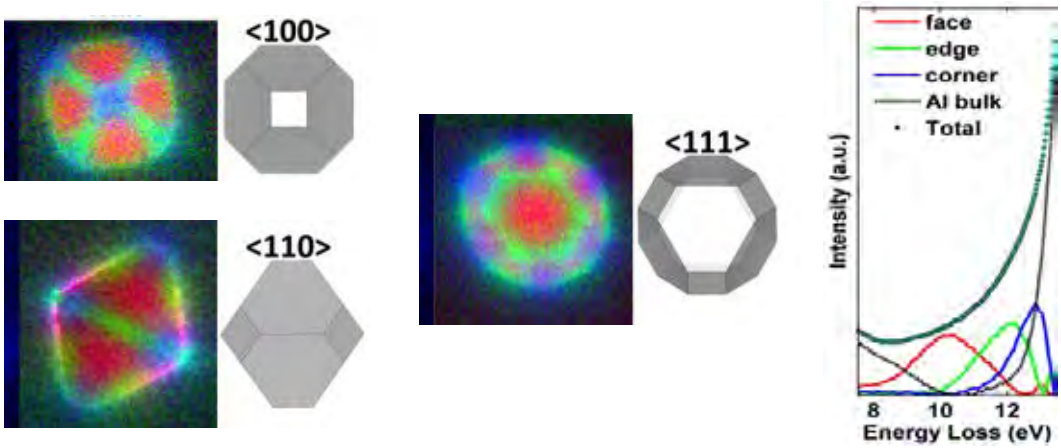

FIG. 1. STEM-EELS mapping of surface plasmon resonances (SPR) on a 17 nm Al nano-void in the shape of a truncated-octahedral at <100>, <110>, and <111> zone axes, with face LSPR modes in red, edge modes in green, corner modes in blue.

References

[1] Z. Zhang. et al, *J. Appl. Crystal.* 49 (2016) 1459.
[2] N. W. Bigelow et al., *ACS Nano.* 6 (2012) 7497.
[3] This work was supported by the Australian Research Council (ARC) grants DP110104734 and DP150104483. The FEI Titan^3 80-300 S/TEM at Monash Centre for Electron Microscopy was funded by the ARC Grant LE0454166.

Absolute Quantification of Nanoscale Precipitates in Steels

I. MacLaren[1], B. Sala[1], A.J. Craven[1]

[1] SUPA School of Physics and Astronomy, University of Glasgow, Glasgow G12 8QQ, UK

It is shown that accurate and precise quantification of the chemistry of few nm carbonitride precipitates in steels is possible. In order to do this, DualEELS is essential [1, 2], and three steps are then required to make this quantitative:

1. The contribution of the steel matrix and any surface layers needs to be subtracted, leaving a precipitate-only spectrum image. [3]
2. Accurate cross sections for each edge used in the quantification need to be determined from suitable standards of well-known composition. [4]
3. A suitable procedure has to be developed to then use the calculated cross sections in the most effective way to quantify the precipitate dataset.

Spectrum images were recorded from nanoscale carbide precipitates in a vanadium microalloyed high-Mn steel and extracted from their matrix contributions as in Bobynko *et al.* [3]. These were found to contain significant Ti and N impurities.

Cross sections were determined from highly pure and homogeneous standards of $VC_{0.83}$, $VN_{0.97}$, $TiC_{0.98}$, and $TiN_{0.87}$. Differential cross sections for each elemental edge were determined from spectrum images covering a large thickness range using least squares fitting. The resulting cross sections only approach the Hartree-Slater H-S cross sections at > 100 eV above the edge onset.

These experimental cross sections were used for the quantification of the precipitates using multiple linear least squares fitting of the whole spectrum from before C-K to beyond V-$L_{2,3}$. The traditional method of background subtraction and edge integration does not work due to the failures of background subtraction with closely spaced edges (such as N-K and Ti-$L_{2,3}$ just 50 eV apart). The results allow high absolute accuracy concentration analysis in precipitates as small as 6 nm, and show the ability to detect N concentrations as low as 2 atoms per atomic column.

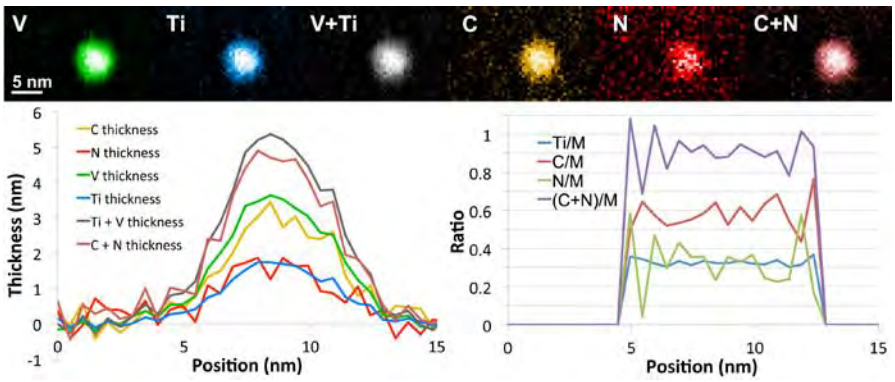

Fig. 1: Quantified maps of the different elements, together with plots of the elemental profile and the stoichiometry ratios.

References

[1] J. Scott *et al.*, *Ultramicroscopy*, **108** (2008) 1586-1594.

[2] A. Gubbens et al., *Ultramicroscopy*, **110** (2010) 962-970.

[3] J. Bobynko, I. MacLaren, A. J. Craven, *Ultramicroscopy* **149** (2015) 9-20.

[4] A J Craven *et al.*, *Ultramicroscopy* **170** (2016) *113-127.*

Surface plasmon resonances in crossed silver nano-rods by HREELS

Y. Fujiyoshi[1], H. Kurata[1]

[1] Institute for Chemical Research, Kyoto University, Uji, Kyoto 611-0011, Japan

The surface plasmon resonances (SPRs) excited in a single nanorod (NR) are understood as standing wave modes of Fabry–Pérot type resonator. The nodes of standing wave modes increase with the increase of its mode order [1].
In this study, the behavior of the SPR excited in crossed silver NRs composed of a long NR (1280 nm) and a short NR (169 nm) shown in FIG. 1(a) were examined using a spherical aberration-corrected STEM (JEM-ARM200F) equipped with a monochromator.
Fig. 1 (b) shows the summed EELS spectrum obtained from the whole area of the crossed NRs (Fig. 1(a)). The EELS maps extracted at 1st to 5th resonance energies are shown in FIG.1(c). In the crossed silver nanorods, the positions of node observed in the EELS maps are similar to those in a single nanorod except for the 4 th mode. The EELS map extracted at 4th resonance energy shows the unique distribution having a weak intensity of the right side from the cross position of nanorods. The blocking of the surface plasmon propagation in the long NR is related to the position relation of branch and the length of short NR relative to the long NR.

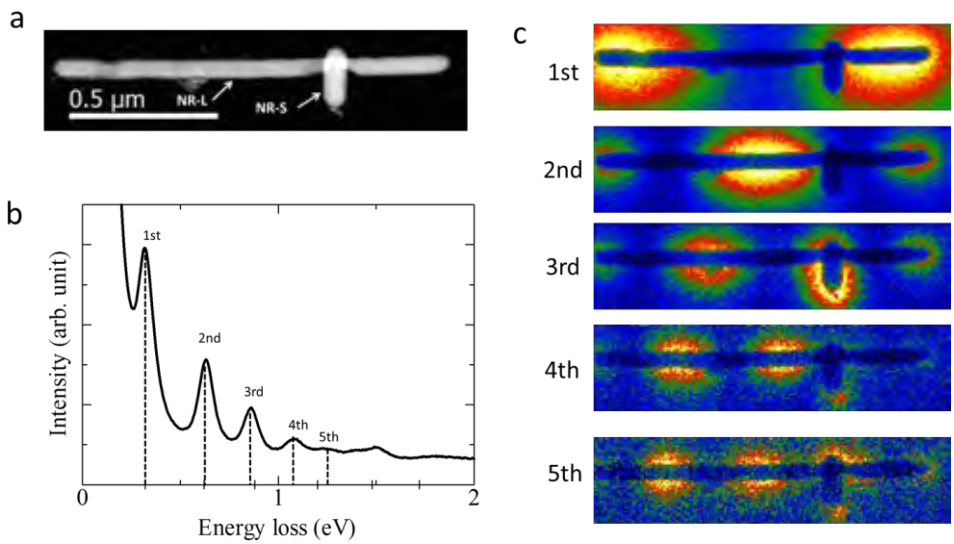

FIG. 1. Experimental data obtained from the crossed nanorods. (a) HAADF image (b) EELS spectrum (c) EELS maps extracted at 1st (0.32 eV), 2nd (0.63 eV), 3rd (0.86 eV), 4th (1.08 eV) and 5th (1.23 eV) resonance energies.

References

[1] D. Rossouw et al., Nano Lett. 11, (2011) 1499-1504.

Cathodoluminescence Measurements of CdTe in the Transmission Electron Microscope

W.D. Yang[1,2], Y. Yoon[1,2], B.H. Gaury[1,2], P.M. Haney[1], N. Zhitenev[1], and R. Sharma[1]

[1] Center for Nanoscale Science and Technology, National Institute of Standards and Technology, Gaithersburg, Maryland 20899 (USA)
[2] Maryland NanoCenter, University of Maryland, College Park, MD 20742 (USA)

Cathodoluminescence (CL) is an important spectroscopic method for characterizing photovoltaic materials in the electron microscope. It provides spectroscopic information that can be used to reveal features of the electronic structure, such as the band gap and defect states near the band edge. Ultimately, this knowledge can be used to develop processing schemes that optimize material structure and performance. As nanostructures are widely employed in quantum-dot and thin-film solar cells, it is necessary to use high-spatial-resolution CL so that the effects of interfaces, e.g. grain boundaries, can be characterized. However, the spatial resolution of CL in the scanning electron microscope) is limited by the lateral size of the interaction volume (at least 250 nm). Much higher resolutions are needed to extract quantitative information from nanostructured materials.

We use a home-built CL spectroscopy set-up integrated with a transmission electron microscope (TEM) to measure CL spectra of polycrystalline CdTe with interaction volumes of ≈ 10 nm in diameter, as shown by Monte Carlo simulations. We find that the improved spatial resolution allows TEM-CL to distinguish CL emission peaks from grain interiors and grain boundaries. A spectral redshift (≈ 0.01 ± 0.0015 eV) in the CL peak location and a reduction in intensity are both observed at the grain boundaries with respect to that of the grain interiors (Fig. 1), suggesting an increased concentration of non-radiative recombination centers. Using an energy-dispersive X-ray spectroscopy (EDX) system attached to the same microscope, chlorine – a dopant that improves CdTe solar cell performance, is found to segregate at the grain boundaries (Fig. 1c) and may be responsible for the shallow defect states that lead to the redshift. A systematic CL measurement as functions of the sample lamella thickness and electron beam current have been performed for building numerical models that can be used to evaluate the competition between non-radiative surface recombination against radiative bulk recombination. Such information will enable an estimate of the grain boundary recombination velocity based on the decreased CL intensities at the grain boundaries.

In sum, TEM-CL enables the measurement of CL spectra with high spatial resolution which can be used to compare the radiative recombination rates in grain interiors and at grain boundaries. This can be extended to characterize polycrystalline photovoltaic materials and to provide guidelines to improve solar cell efficiency.

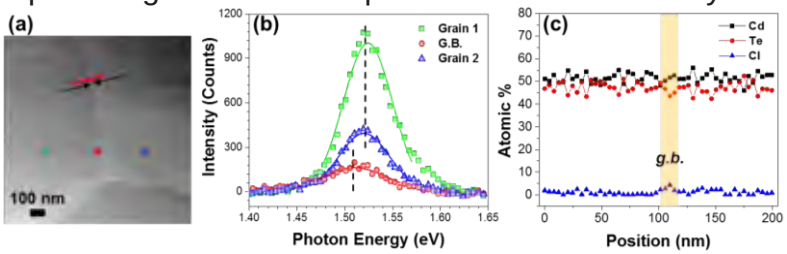

FIG. 1. (a) Annular dark-field (ADF) image of a CdTe lamella. (b) CL spectra of grains 1 (green), 2 (blue) and the grain boundary in between (red). (c) EDX line-scan showing the elemental distributions of Cd, Te and Cl.

Pseudo atomic column mapping of silicon using STEM-moiré method, reconstructed with K and L electrons detected by EELS & EDS

E. Okunishi[1] and Y. Kondo[1]

[1] JEOL Ltd., 3-1-2 Musashino, Akishima, Tokyo, 196-8558, Japan.

The characteristics of the atomic column elemental mapping, such as spatial resolution or quantitative capability, have been requested to clarify experimentally, since it is important to estimate its advantages and disadvantages of the method [1]. For example, delocalization of analysis, which is one of the important physical parameter, is determined by accelerating voltage of a primary electron and an energy at the absorption edge of a sample. For measurement of such physical parameter, it is ideal to perform under the condition with no sample damage, because the damage makes displacement of atoms, resulting in a large measurement error.
With the 2D STEM moiré method, which is already succeeded to display the pseudo atomic column elemental map, under low dose condition [2, 3] was used to examine the delocalization of elemental signal on the pseudo atomic column elemental maps.

Figures 1(a~e) shows the simultaneously obtained pseudo atomic column maps of Si (110) with HAADF signal (a), $L_{2,3}$ and K signal by EELS (b, c) and K signal by EDS(d). The pseudo dumbbell by moiré method in Si (110) sample is clearly shown as in HAADF image. The peaks in elemental maps also show the atom sites of Si atoms. Figure 1(f) shows the intensity profiles of Si K by EDS, $L_{2,3}$ electrons by EELS and HAADF along a yellow region shown in Figures 1(a~d), after background subtraction and normalization. Comparing these intensity profiles, those show little difference. The profiles of HAADF and Si-K(EELS and EDS) have consistent shape. Profile of Si-L(EELS) has wider peaks than another profiles (see dips of dumbbell). We suppose that it is due to delocalization effect. We are obtaining similar results from thinner and thicker region as well.

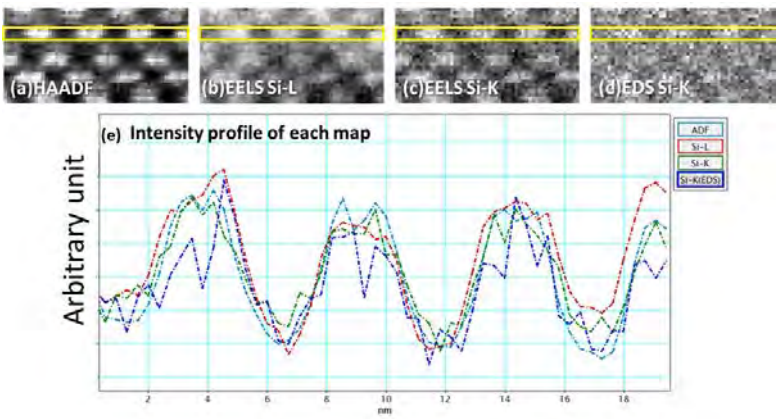

FIG. 1(a~d). simultaneously obtained pseudo moiré atomic column maps of Si. Fig. 1(e) show the profiles of signals from yellow region in Fig. 1 (a-d).
Used microscope was JEM-ARM200F with cold FEG, working at 200 kV. The sample thickness was estimated to be ≈ 250 nm.

References
[1] L. J. Allen et al, MRS Bulletin. 37 (2012), 47.
[2] Y. Kondo and E. Okunishi, Microscopy **63 (5)** (2014) 391.
[3] E. Okunishi et al, Microsc. Microanal. **12 (S2)** (2006) 1150.

Probing the internal atomic charge density distribution in real-space by aberration-corrected differential phase contrast.

G. Sánchez-Santolino[1], N. R. Lugg[1], T. Seki[1], R. Ishikawa[1], S. D. Findlay[2], Y. Kohno[3], Y. Kanitani[4], S. Tanaka[4], S. Tomiya[4], Y. Ikuhara[1] and N. Shibata[1]

[1] Institute of Engineering Innovation, School of Engineering, The University of Tokyo, Yayoi 2-11-16, Bunkyo-ku, Tokyo 113-8656, Japan
[2] School of Physics and Astronomy, Monash University, Victoria 3800, Australia
[3] JEOL Ltd., 1-2, Musashino 3-chome Akishima, Tokyo 196-8558, Japan
[4] Advanced Materials Laboratories, SONY Corporation, 4-14-1, Asahi, Atsugi-shi, Kanagawa, 243-0014, Japan

Differential phase contrast imaging in the aberration corrected scanning transmission electron microscope brings the possibility to probe the electric field distribution in a material down to the atomic scale [1]. Furthermore, recent studies have shown how to quantify these fields using both pixelated [2] and segmented detectors [3]. Here we obtain the atomic total charge density distribution for a crystalline GaN thin specimen from the experimental measurements of the atomic electric fields, revealing both the positively charged nucleus and the surrounding negative electron cloud. The experimental results acquired using a new generation segmented annular all field detector, composed of 16 segments and installed in a JEOL JEM-ARM300F, will be discussed in comparison with full dynamical scattering simulations.

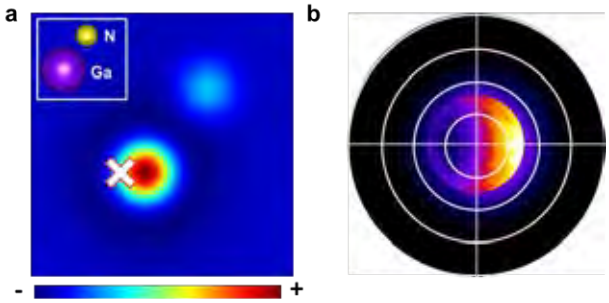

FIG. 1. **a** Ideal total charge density distribution for GaN convolved with a 60pm FWHM electron probe. **b** Simulated diffraction pattern depicting the intensity distribution acquired by a segmented detector when the electron probe is placed at the position marked in **a**.

References

[1] N. Shibata et al., Nature Physics, 8 (2012) 611.
[2] K. Müller et al., Nature Communications, 5(2014) 5653.
[3] R. Close et al., Ultramicroscopy, 159 (2015), pp. 124–137.
[4] This work was supported by SENTAN, JST, and the JSPS KAKENHI Grant number 26289234. A part of this work was supported by Grant-in-Aid for Scientific Research on Innovative Areas (25106003). A part of this work was conducted in the Research Hub for Advanced Nano Characterization, The University of Tokyo, under the support of "Nanotechnology Platform" (Project No.12024046) by MEXT, Japan. This research was supported under the Discovery Project funding scheme of the Australian Research Council (Project No. DP160102338).

Revealing more while damaging less: exploiting multi-frame EDX & EELS spectroscopy acquisition and post-processing tools.

L. Jones[1], A. Varambhia[1], S.Wenner[2], R. Holmestad[2], and P. D. Nellist[1]

[1] Department of Materials, University of Oxford, Parks Rd. Oxford, OX13PH, UK.
[2] Department of Physics, NTNU – Trondheim, NO-7491 Trondheim, Norway.

Obtaining high quality atomic resolution chemical maps is a compromise between collecting sufficient signal, while minimising sample damage from the electron dose. Classically the experimentalist has had only one parameter, beam current, to do this. Recently with the advent of fast and robust software tools for the non-rigid registration (scan-distortion correction) of multi-frame data [1], a new regime has opened up for the operator where both dose-per-frame and total-dose can be varied independently. Several studies now propose dose-rate as the critical parameter in minimising sample damage.

Here we exploit this ability to re-register multiple spectrum-image volumes, to share our total electron budget over tens of faster scans, reducing damage and improving chemical map quality. New scripted data-acquisition tools will be presented along with recent developments in processing multi-frame SI; including, digital super-resolution, template-matching and feature-averaging; and for EELS, noise reduction from channel-shifting, custom gain-reference acquisition, energy-drift compensation, and conversion of EELS data to fractional-beam-current units. As a case study, the imaging of rod-like precipitates in Al-alloys are presented for improved understanding of light-alloy heat-treatment design (Figure 1).

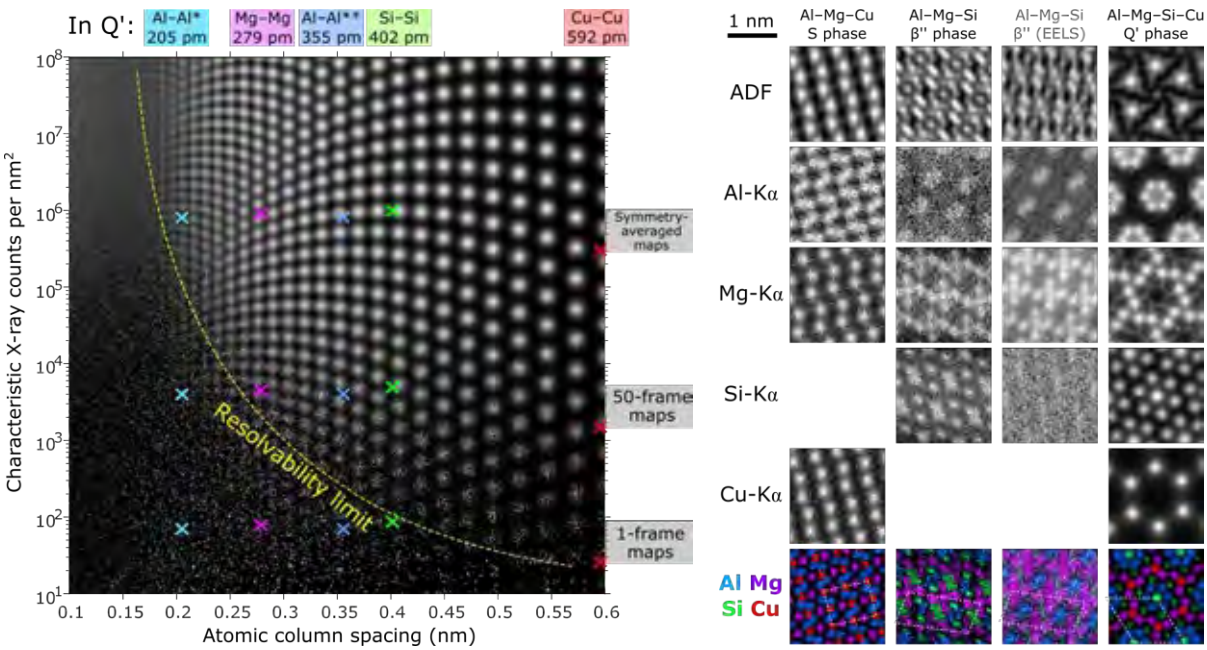

FIG. 1. Left) experiment design planning for a JEOLARM200CF using a 155pA beam current, 500µs dwell-time and 0.98sr Centurio EDX detector. Right) experimental atomic-resolution EDX maps from a range of Al-Mg based rod-like precipitates.

References:
[1] L. Jones et al. *Adv. Struct. Chem. Imaging*, 1, (2015).
[2] This work was funded by the EU-FP7 Programme, Grant 312483: ESTEEM2.

Optimising the coupling a spectrometer to a TEM/STEM for high loss EELS

I. MacLaren[1], C. Black[1], S. McFadzean[1], A.J. Craven[1], and H. Sawada[2]

[1] SUPA School of Physics and Astronomy, University of Glasgow, Glasgow G12 8QQ, UK
[2] JEOL UK Ltd., JEOL House, Silver Court, Watchmead, Welwyn Garden City, Herts., AL7 1LT, UK

We demonstrate how the post-specimen lens setup can be modified in a modern aberration-corrected TEM/STEM with 4 post-specimen lenses to provide optimal coupling of the microscope to the spectrometer with a collection angle of > 30 mrad. This is done by explicit consideration of the ray paths for electrons of different energy losses in a manner based on the earlier work of Craven and Buggy [1] for a two-lens system. The calculations are backed up by EFTEM imaging of the diffraction patterns at different energy losses. It is found at 200 kV that an almost constant collection angle (within 5% variation) can be maintained to 4.7 keV loss. This has many benefits for EELS at high losses including reduced background under the edges with a more predictable shape due to the elimination of aberration fold-over of high-angle rays.

It is demonstrated that the new setting allows for the acquisition of high loss data of unprecedented quality and a number of examples are demonstrated including:

- ELNES changes on oxidation on the L-edges of Zr, Mo and Sn
- High quality K-edges for first row transmission elements such as Ti, Fe and Mn
- EELS edges at over 10 keV loss using the L_3 and L_2 edges of Ta.

It is expected that such advances will be especially important in extending the energy range of EELS for low voltage STEM at 80 kV and below. Preliminary results from 80 kV will also be shown.

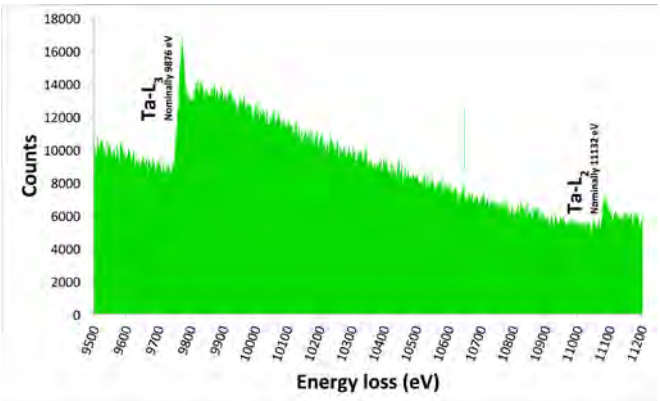

FIG. 1. Ta L_3 and L_2 edges from an amorphous Ta_2O_5 film.

References

[1] A.J. Craven, T.W. Buggy, *Ultramicroscopy*, 7 (1981) 27-37

Orbital Angular Momentum in the Electron Microscope

J.A. Hachtel[1], S.Y. Cho[2], R.B. Davidson II[3], R.F. Haglund[3], S.T. Pantelides[3,4], M.F. Chisholm[4], B.J. Lawrie[5], and J.C. Idrobo[1]

[1] Center for Nanophase Materials Sciences, Oak Ridge National Laboratory, P.O.Box 2008, Oak Ridge, TN 37830
[2] Klipsch School of Electrical and Computer Engineering, New Mexico State University, NM 88003
[3] Department of Physics and Astronomy, Vanderbilt University, Nashville, TN 37203
[4] Materials Science and Technology Division, Oak Ridge National Laboratory, P.O.Box 2008, Oak Ridge, TN 37830
[5] Computational Sciences and Engineering Division, Oak Ridge National Laboratory, P.O. Box 2008, Oak Ridge, TN 37830

Orbital angular momentum (OAM) is an intrinsic property possessed by both electrons and photons that can be utilized to measure chiral magnetic and optical [1,2] signals. Recently, scanning transmission electron microscopy (STEM) has been used to explore OAM in nanostructures using high-resolution spectroscopy.

Optical OAM effects such as plasmonic vortices in spiral holes can be directly observed via cathodoluminescence (CL) spectroscopy within STEM. Figure 1a shows a spiral hole milled in a silver film, fabricated such that the surface plasmon polaritons (SPPs) coherently interfere to form a plasmonic vortex at the origin of the spiral at a wavelength 660 nm. The spiral intensity pattern can be seen in Fig. 1b.

Furthermore, advanced electron microscopy OAM experiments can be performed with a holographic aperture. The aperture can either be inserted into the column of a monochromated aberration-corrected STEM to form electron vortex probes with selectable OAM. Alternatively, it can be used to disperse the CL signal into discrete beams of differing OAM to study the luminescent response of chiral structures. These two techniques that promise high spatial- and spectral-resolution insight into a wide range of complex materials will be discussed in this talk.

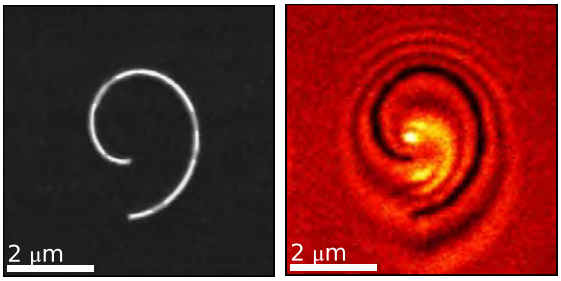

FIG. 1. (a) BF image of spiral hole. (b) STEM-CL response of the plasmonic vortex at 660 nm.

References
[1] J. Verbeeck *et al., Nature* **464** (2010) 737
[2] M. Padgett and R. Bowman, *Nat. Photonics* **5** (2011) 343
[3] Research sponsored by the Laboratory Directed Research and Development Program of Oak Ridge National Laboratory, managed by UT-Battelle, LLC, for the U.S. Department of Energy (JAH, JCI, RBD, BJL), and the Department of Energy, Office of Science, Basic Energy Sciences, Materials Sciences and Engineering Division (JAH, STP, MFC).

Advances in Electron Energy Filters and Spectrometers at Gatan

R.D. Twesten, C.G. Trevor, N.K. Menon, M.M.G. Barfels, E.M. James, P.J. Thomas, P. Longo and A.J. Gubbens[1]

[1] Gatan Inc., 5794 W. Las Positas Blvd., Pleasanton, CA 94588, USA

Since the EDGE 2013 conference in Sainte-Maxime, France, Gatan has contributed to progress in EELS and Energy Filter technology on several fronts: on the low voltage front with the TripleC#1 [1] and SALVE [2] projects, on the energy resolution fronts with the ASU group [3, 4] and TripleC#2 [5] projects, and on the sensitivity front with the Drexel group counting mode EELS project [6]. For data acquisition and analysis, efforts in reducing the complexity, increasing throughput and improving quality have been paramount. The user interface to the spectrometer and spectrum imaging has been refactored in the fully scriptable yet stream-lined GMS3 platform; EELS analysis has been completely rebuilt based on the Antwerp model based EELS approach [7]. To make this more assessable to the community, many of these new features are included in the freely available GMS 3.2 offline version [8].

In this talk, we will present the latest developments in EELS instrumentation and technique with a particular focus on improvements in system integration, simplicity of operation and acquisition automation. These improvements have the promise of extending the highest levels of filter functionality to the mainstream.

References

[1] K. Suenaga et al., *Nature 468* (2010) 1088-1090
[2] U. A. Kaiser, Project homepage (SALVE) project (Ulm University, Germany, 2016), http://www.salve-project.de/home.html.
[3] P.A. Crozier et al., *Ultramicroscopy 169* (2016) 30.
[4] O.L. Krivanek et al., *Nature 514* (2014) 209.
[5] K. Suenaga et al., *Microscopy and Microanalysis 22* (2016) 950.
[6] J.L. Hart et al., *Microscopy and Microanalysis 22* (2016) 336.
[7] J. Verbeeck et al., *Ultramicroscopy, 101* (2004) 207.
[8] Gatan Microscopy Suite Software (Gatan USA, 2017) http://www.gatan.com/products/tem-analysis/gatan-microscopy-suite-software/.

2D detectors for electron energy loss spectroscopy and STEM imaging

O.L. Krivanek, A.L. Bleloch, N.J. Bacon, G.J. Corbin, N. Dellby, M.V. Hoffman and T.C. Lovejoy

Nion R&D, 11515 NE 118th St., Kirkland, WA 98034, USA

There are many different applications for 2D detectors in EELS and STEM imaging, including detecting a) EEL spectra, b) Ronchigrams/shadow images for autotuning, c) Ronchigrams/shadow images for ptychography, and d) point diffraction patterns for structure analysis. The general characteristics of the ideal 2D detector are the same for all the applications:

a large number of independent pixels,
single electron sensitivity,
wide dynamic range,
fast read-out,
zero or minimal radiation damage,
minimum dark current,
uniform gain,
vacuum-compatibility, and ideally also being bakeable.

The specific requirements for the above-listed applications are nevertheless different, and there is no single technology that is likely to be best at meeting all of them.

For the detection of EEL spectra, a rectangular format detector or a rectangular sub-area of a square detector are typically chosen, and the intensity ranges from $>10^5$ e^-/s (at the zero loss peak) to a few e^-/s (at high energy losses). Read-out speeds rarely need to be higher than 1000 spectra per second, because EELS cross-sections are much weaker than elastic ones. Two types of detectors are likely to come out on top: fast, low noise SCMOS cameras coupled to a scintillator, which can provide single electron sensitivity, wide dynamic range, freedom from radiation damage, and speeds of around 400 (detector) Mpixels/s, which gives 2000 unbinned spectra per second if a 1000x200 pixel area of the detector is used for spectrum-imaging. Another promising possibility is a multiply stacked Medipix detector (e.g. in a 4x1 configuration giving a 1024x256 pixels sensor), which will perform more reliably when detecting single electrons, but may not be able to handle the full intensity of the zero loss beam.

The requirements for the detection of point diffraction patterns are similar to the EELS case, but the detector needs to be square, and the frame speed can be lower. For ptychography, a 128x128 or 256x256 pixel detector is typically sufficient, and a very high read-out speed (ideally 10,000 frames per second) and single electron sensitivity are paramount. Ronchigram detection for autotuning is possibly the least challenging application: the data needs to have high SNR and therefore cannot be recorded much faster than about 20 frames per second, the dynamic range is not large, and 2kx2k pixels are typically more than enough.

Nion is developing detectors for all the above applications. The designs will be reviewed, and preliminary results discussed.

Noise Reduction by Improving Dark-Reference Images

Tobias Heil[1], Gordon J. Tatlock[2]

[1] Max Planck Institute of Colloids and Interfaces, Department of Colloid Chemistry, 14424 Potsdam, Germany
[2] Centre for Materials and Structures, School of Engineering, University of Liverpool, United Kingdom

The quality of TEM CCD measurements is not only influenced by the investigated sample and the utilised instrument, but also by the noise that is acquired together with the signal. This becomes especially apparent when dealing with a low signal-to-noise ratio, which is often countered by merging several images into one, thus ideally increasing the signal while flattening the random noise at the same time. However, in order to generate the best results, it is important to ensure that the dark-reference image, which is subtracted from the raw CCD image, is free of any excessive noise. This is often neglected, although creating a dark-reference by simply averaging over just a small number of images can already have significant effects.

Furthermore, having access to a stack of dark-reference images offers the possibility to apply routines to separated intense one-shot noise like cosmic rays or x-ray spikes from wanted features like hot pixels and remove their influence on the merged image altogether, instead of only diminishing it by the merging alone (figure 1).

While this procedure is only applied to dark-reference image so far, it should also be possible to utilise it to improve the quality of other series of CCD acquisitions, like gain-reference images, multi-frame EELS or drift-corrected images of static objects.

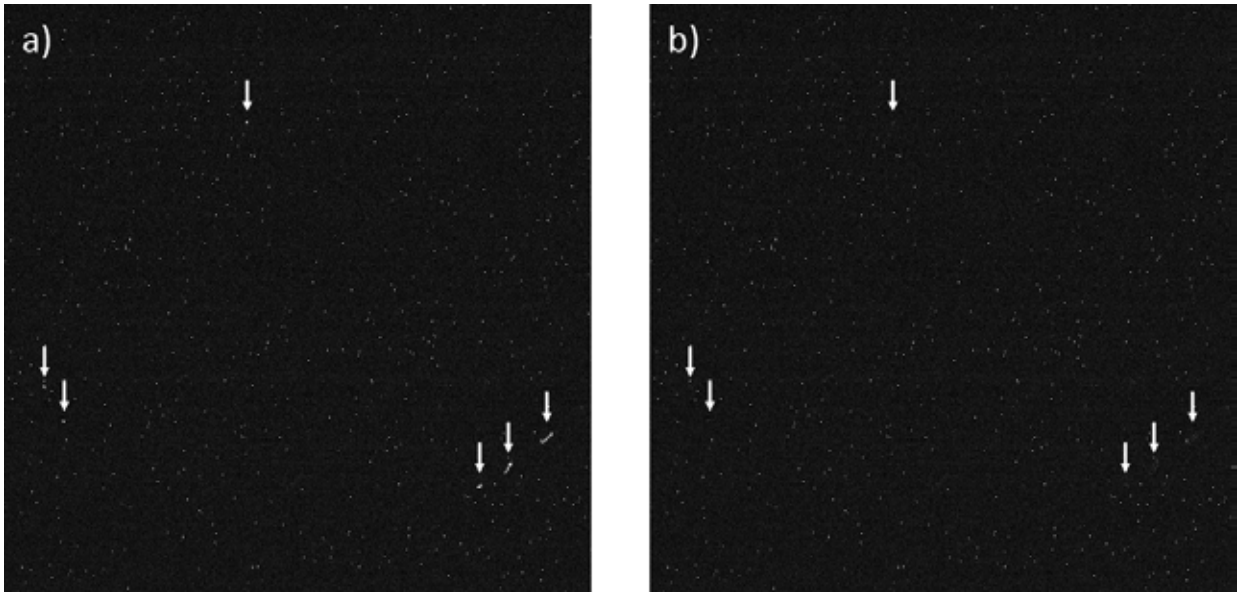

FIG. 1. Section of a dark reference image created by averaging over 3 images without (a) and with (b) using cosmic ray correction. Note that the indicated cosmic ray events are removed, while the hot pixels are preserved.

Improvement of effective solid angle using virtual-pivot holder and large EDS detector

Shogo Koshiya[1], Koji Kimoto[1]

[1] National Institute for Materials Science (NIMS), Tsukuba, Ibaraki 305-0044, Japan

Energy-dispersive X-ray spectroscopy (EDS) combined with scanning transmission electron microscopy (STEM) is a standard technique for high-spatial-resolution elemental analysis. Although large solid angle can be realized by a large-area detector or a multi-detector system, the effective solid angle is often reduced due to shadowing by a specimen holder or a specimen itself. Pioneering studies on EDS detector solid angle assessment have been conducted [1,2], and shadowing remains the main obstacle preventing high-efficiency analyses.

In this study, the combination of a large-area silicon drift detector (SDD) and a virtual-pivot double-tilt specimen holder [3] is demonstrated to improve the effective solid angle. The X-ray shadowing and system noise were measured using a few different designs and specimen shapes [4].

FIG. 1. shows an effective solid angle Ω_{eff} for various specimen holder and specimen combinations. For the standard holder (●), Ω_{eff} becomes almost zero for $-25^{\circ} < \alpha < -15^{\circ}$. On the other hand, Ω_{eff} decreases only to 60% of the nominal solid angle for the virtual-pivot holder (■) at $\alpha = -10^{\circ}$. The X-ray self-absorption of the NiO_x specimen (×) is about two times larger than that of the single-crystal NiO specimen (■), because of the shadowing of the TEM-grid. Besides, there is no absorption in the NiO_x cut in half specimen (▲, see an inset of FIG. 1). It can be concluded that X-ray detection in a wide α range and with a large effective solid angle is achievable by combining a large-area detector with a virtual-pivot holder and optimal shape of the specimen. We will also demonstrate the decreasing of system peaks by using the plastic [4] as an analytical specimen holder.

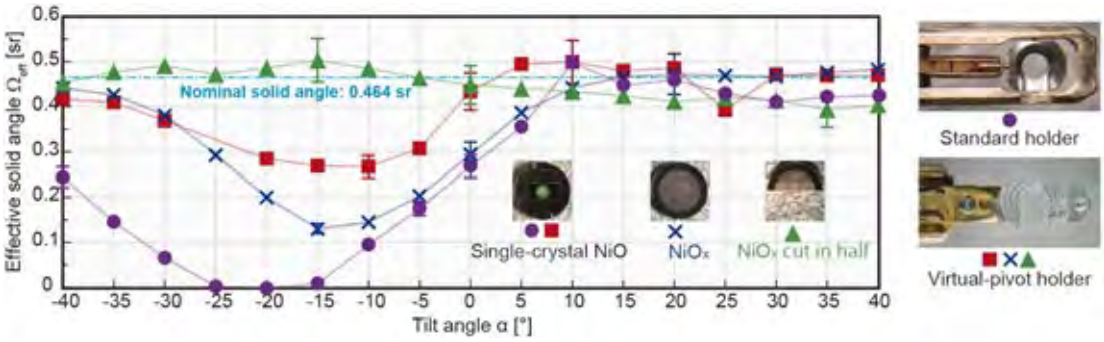

FIG. 1. Effective solid angle for various specimen holder and specimen combinations.

References

[1] R.F. Egerton and S.C. Cheng, *Ultramicroscopy* 55 (1994) 43.

[2] J.C. Bennett and R.F. Egerton, *Microscopy and Microanalysis* 1 (1995) 143.

[3] S. Hata et al., *Ultramicroscopy* 111 (2011) 1168.

[4] S. Koshiya and K. Kimoto, *Micron* 93 (2017) 52.

[5] This research is supported by the JST Research Acceleration Program and the Nanotechnology Platform of MEXT, Japan. The authors thank Prof. R. F. Egerton, Prof. M. Malac, Prof. M. Watanabe, and Dr. J. Sagar for invaluable discussions. The aid of Mr. Miyazaki, Prof. Hata and Mr. K. Watanabe is gratefully acknowledged. They also thank Dr. Suenaga for encouragement.

Automatic spectral imaging analysis based on machine learning

Motoki Shiga[1,2], and Shunsuke Muto[3]

[1] Department of Electrical, Electronic and Computer Engineering, Gifu University, 1-1 Yanagido, Gifu, 501-1193 Japan
[2] PRESTO, Japan Science and Technology Agency, 4-1-8, Honcho, Kawaguchi, Saitama, 332-0012 Japan
[3] Advanced Measurement Technology Center, Institute of Materials and Systems for Sustainability (IMaSS), Nagoya University, Nagoya, 464-8603, Japan

With the development of microscopy technologies and the first principles calculations, the size of datasets to be analyzed in materials science has been rapidly increasing. Against such a large size of datasets, informatics technologies such as machine learning and data mining have become more important. In scanning transmission electron microscopy (STEM) with comprehensive electron energy-loss (EELS) and energy-dispersive X-ray (EDX), the spectrometers collect a set of spectra called spectral imaging (SI), each from the sub-nanometer area of the sample by the fine incident electron probe consecutively scanning over the two-dimensional region. An important task on SI data analysis is to automatically identify both spectra and spatial distributions of chemical components on a specimen. We have developed a Nonnegative Matrix Factorization (NMF), in which both spectra and intensities of chemical components are non-negative. Our method has two useful features: 1) a spatial orthogonal penalty to clearly resolve EELS/EDX-SI into each component and 2) an automatic determination of the number of components using only a given SI dataset. Analysis results such as FIG. 1, will be demonstrated in our presentation.

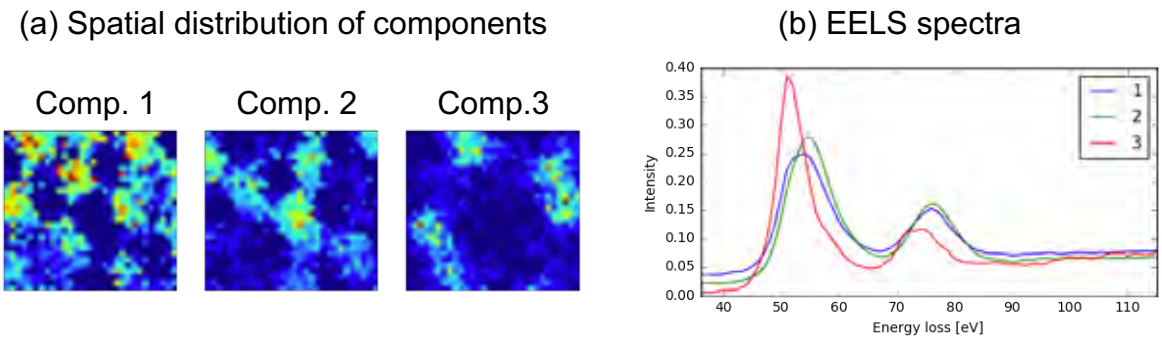

FIG. 1. Automatic component decomposition of spectral imaging of Mn_3O_4.

References
[1] M. Shiga, *et al.*, *Ultramicroscopy*, 170, 43-59 (2016).
[2] This research was supported by JSPS KAKENHI #16H02866, #16H00736, #25106004 and JST PRESTO.

Low-temperature study of interfacial coupling of octahedral distortions in $La_{0.5}Sr_{0.5}CoO_{3-\delta}$ /$SrTiO_3$

X. Rui[1], J. Walter[2], C. Leighton[2], and R.F. Klie[1]

[1] Department of Physics, University of Illinois at Chicago, Chicago, 60607.
[2] Department of Chemical Engineering and Material Science, University of Minnesota, Minneapolis, 55455

$La_xSr_{1-x}CoO_{3-\delta}$ thin films have been studied for years due to their rich magnetic phase behavior and interesting interplay between strain, defects, and magnetism. [1] For $La_{0.5}Sr_{0.5}CoO_{3-\delta}$ (LSCO) films grown on $SrTiO_3$ (STO) substrates, the phase transition of $SrTiO_3$ from cubic to tetragonal at around 105 K can further modify the magnetic/transport properties of the films due to coupling of the out-of-phase TiO_6 octahedral tilt with the CoO_6 octahedral network. [2]

Here, we utilize atomic-resolution imaging and spectroscopies in a scanning transmission electron microscope to study the coupling of the STO substrate and the oxygen vacancy ordering in the $La_{0.5}Sr_{0.5}CoO_{3-\delta}$ thin films using in-situ cooling experiments. While both high-angle annular dark field (HAADF) and annular bright field (ABF) images of the STO/LSCO interface show clear signs of oxygen vacancy ordering in LSCO at both room temperature and 90 K (Figures 1a and b), the oxygen *K*-edge pre-peak intensity in STO increases below 105 K, reflecting the tilt of TiO_6 octahedral (Figure 1c). The corresponding O *K*-edges taken from LSCO show a shift and increase in the pre-peak intensity (Figure 1e) at low temperature; the Ti and the Co L-edge remain largely unchanged (Figure 1d and f). These changes in the EELS fine-structure will be correlated with the octahedral tilts and the corresponding structure symmetry breaking, as well as the electrostatic balance disruption at the STO/LSCO interface. The formation of magnetic domains will be studied using angular-resolved EELS in TEM. [3]

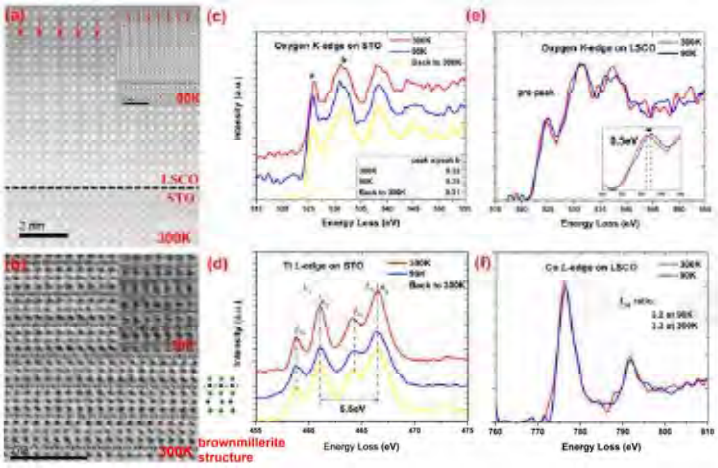

FIGURE 1: (a) Representative HAADF image of the LSCO/STO interface viewed along the (100) directions at both 300K and 90K. (b) ABF image of LSCO thin film along (110) at both 300K and 90K, consistent with the brownmillerite structure. (c) and (d) Oxygen *K*-edge and Ti *L*-edge of the STO substrate above and below the anti-ferrodistortive transition temperature. (e) and (f) Oxygen *K*-edge and Co *L*-edge acquired within 3.3nm area off the interface.

References:
[1] M. A. Torija et al, J. Appl. Phys. 104 (2008) 023901
[2] T. Hidaka, Phys. Rev. B 17(1978) 4363
[3] This research was supported by National Science Foundation (Grant No. DMR-1408427). Help from A.W. Nicholls and F. Shi is gratefully acknowledged.

Measuring Orbital Angular Momentum (OAM) and Torque Transfer from Polarization Vortices with a Pixel Array Detector

Kayla X Nguyen[1], Prafull Purohit[2], Ajay Yadav[3], Mark W. Tate[2], Ramamoorthy Ramesh[3], Sol M. Gruner[2], and David A. Muller[1]

[1] School of Applied Physics and Engineering, Cornell University, Ithaca NY, USA.
[2] Department of Physics, Cornell University, Ithaca NY, USA.
[3] Department of Material Science and Engineering, UC Berkeley, Berkeley, CA, USA.

While orbital angular momentum (OAM) and torque transfer play central roles in a wide range of physical processes and devices ranging from skyrmions to spin torque transfer electronics, recent experimental realization [1] of polarization vortex arrays in ferroelectric materials offers analogous roles for topological structures encoded in polarization fields. Here, we demonstrate a new phase-sensitive detection method for measuring the OAM of an electron beam where its shape and resolution are not compromised. In addition, measurements extracted from this method can range over five orders of magnitude in length scales, making it well suited for measuring polarization fields and torque transfer in complex, extended patterns. The starting point is a new generation of high-speed, momentum-resolved electron microscope detectors; from which, we highlight the electron microscope pixel array detector (EMPAD) [2], whose high dynamic range makes it possible to record the complete angular distribution of all transmitted electrons from a focused electron beam at every scanned position, building up a 4-dimensional phase space. Here, we present how the OAM of the scattered beam can be recovered exactly and apply this technique to measure the torque transfer from a polarization vortex lattice formed in superlattices of $PbTiO_3$ and $SrTiO_3$. Although this imaging method should work equally well for electric and magnetic structures, we observed that this technique is uniquely well suited for imaging the toroidal order parameter of ferroelectric polarization vortex arrays.

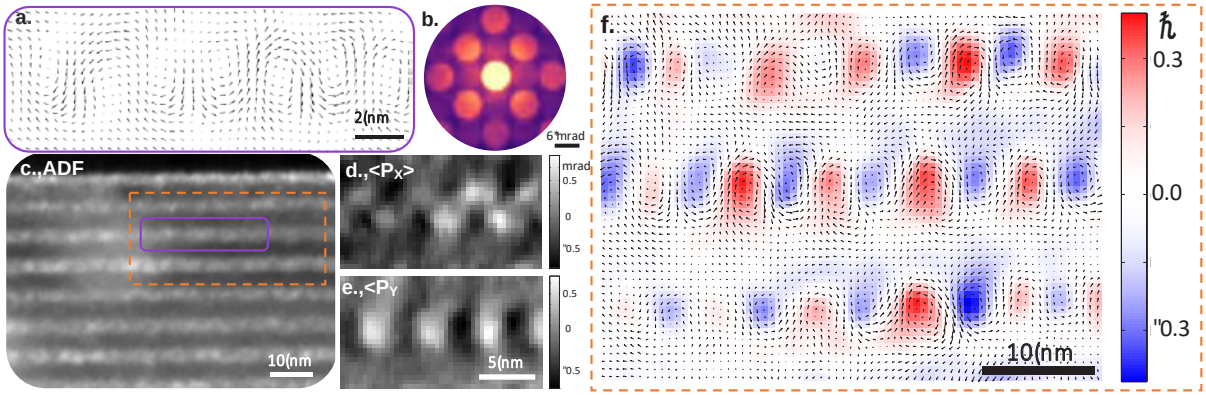

FIG. 1. Analysis of (a) polarization vortices from [200] and [020] diffracted disks using (b) CBED pattern shown. Vortices reconstructed from purple boxed region of (c) ADF, using (d) <Px> and <Py>. (f) Torque transfer measurements extracted from orange boxed region in (c).

References

[1] Yadav, A. K. et al., *Nature*, 530, (2016) 198-201.
[2] Tate W. M. et al., *Microscopy and Microanalysis.* 22 (2016) 237-249.
[3] Supported by NSF MRSEC program (DMR 1120296),Kavli Institute at Cornell.

ALS-MCR application for Diffraction imaging data

F. Uesugi[1], S. Koshiya[1], K. Mitsuishi[1], K. Kimoto[1],

[1] National Institute for Materials Science (NIMS), Tsukuba, Ibaraki, Japan

Recently, owing to development of detector devices and the PC to control them, we can take a vast data from nano area with sub-nano meter resolution using Cs-corrected S/TEM. Although the acquired data should be analyzed by human, human can not analyze those data in the same time scale in most cases. It is a big and annoying problem for experimental scientists.

As a solution to this problem, statistics techniques are often used and are effective. Some microscopists use the multivariate analysis, which is one of the statistics techniques, to extract characteristic spectra and density distributions to them from a spectrum imaging of EDS or EELS. We can also take a diffraction imaging (DI) which is a set of 4 dimensional data, but there is no multivariate analysis application to it yet. So, we examined to apply multivariate analysis to a DI.

We used *Alternating Least Square-Multivariate Curve resolution* (ALS-MCR) to extract characteristic diffraction patterns and corresponding density distribution from a DI. The present DI is acquired from a titanium oxide nano-sheet. We will show how to deal with the DI and the results.

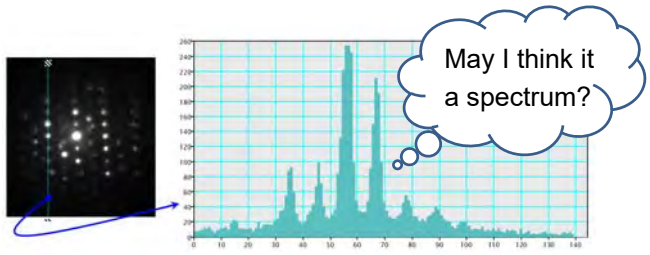

Figure 1. Start point of fancy (or motivation) that apply multivariate analysis to Diffraction imaging

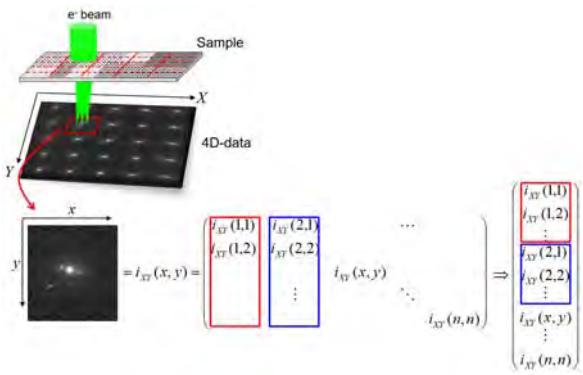

Figure 2. Data handling

References

[1] J.-H. Wang, P. K. Hopke, T. M. Hancewicz, S. L. Zhang, Anal. Chimi. Acta 476 (2003) 93-109

Revisiting EELS Characterization and its Coupling with Raman Spectroscopy: Chemical Inhomogeneities at the Nanoscale of DLC Thin Films

L. Lajaunie[1], C. Pardanaud[2] and R. Arenal[3,4]

[1] Laboratorio de Microscopías Avanzadas, Instituto de Nanociencia de Aragón, Universidad de Zaragoza, 50018 Zaragoza,
[2] Aix-Marseille Université-CNRS, PIIM, 13397 Marseille cedex 20, France
[3] ARAID Foundation, 50018 Zaragoza, Spain

The long-term stability of the properties of hydrogenated amorphous carbon (a:C-H) thin films makes them very promising materials for numerous applications, including coatings for spatial applications [1]. For improving their performances, a full understanding of their local chemistry is highly required. Fifteen years ago, according to the seminal work of Ferrari et al., [2] EELS was the most used technique to get such kind of quantitative information on these materials. Nowadays, the complexity of the physics phenomena behind EELS is well known [3], but this technique is regarded as time-consuming and difficult to interpret properly. Other optical techniques, such as Raman spectroscopy, are now clearly favored by the scientific community. However, these macroscopic techniques still lack the high spatial resolution. This limitation can be overcome by STEM-EELS, which offers the possibility of getting direct chemical information at the local (atomic) scale.

In this contribution, we will revisit the procedures to extract proper and reliably quantitative chemical information from EELS spectra. In addition, the coupling of multi-wavelength Raman and EELS spectroscopies to obtain a wealth of chemical information will be discussed. Our results provide a complete combination of C-hybridization, spatial elemental analyses and structural defects studies for shedding light on these complex materials. In particular, we will show how the deposition process induces a gradient of sp^2 ratio in the thin films and how this gradient is modified as a function of the annealing time [4]. In addition, recent results on nanocrystalline and microcrystalline CVD diamond films will be presented [5]. Surprisingly, strong in-depth inhomogeneities of the local chemistry has been highlighted and the evolution of the morphology, nanostructure and composition of the films, as a function of methane in excess of hydrogen, will be discussed [6].

References

[1] A. Rusanov et al., Carbon 81, 788–799 (2015).
[2] A.C. Ferrari et al., Phys. Rev. B 62 (16), 11089 (2000)
[3] P. Schattschneider et al., Phys. Rev. B 72, 045142 (2005)
[4] L. Lajaunie, C. Pardanaud, C. Martin, P. Puech, C. Hu, M.J. Biggs and R. Arenal, Carbon 112, 149-161 (2017)
[5] J.G. Buijnsters, C. Pardanaud, L. Vázquez, R. Gago, J.L. Endrino, L. Lajaunie and R. Arenal, In Preparation
[6] We acknowledge funding from the EU under Grant Agreement 312483-ESTEEM2, Grant Agreement 696656 Graphene Flagship and the Spanish Ministerio de Economia y Competitividad (MAT2016-79776-P).

STEM SI Warp: a Digital Micrograph script tool for warping the image distortions of atomically resolved spectrum images

Yi Wang, Ute Salzberger, Vesna Srot, Wilfried Sigle, and Peter A. van Aken

Stuttgart Center for Electron Microscopy, Max Planck Institute for Solid State Research, Heisenbergstr. 1, 70569 Stuttgart, Germany

The marked progress of scanning transmission electron microscopy (STEM) configuration has made the chemical analysis at atomic resolution readily possible nowadays. Generally, STEM SI requires higher electron dose and longer dwell time than STEM imaging. As a consequence, scanning distortion becomes more serious in spectrum imaging. At atomic resolution, instabilities combined with long dwell times may create substantial image distortions that limit the interpretability of the spectrum image (SI).

In this contribution, we present a software tool, written in Digital Micrograph scripting language [1], to post correct the image distortion of atomically resolved spectrum images. Two methods have been implemented to correct these distortions, pure pixel shift and bilinear interpolation [2]. With the prior knowledge of the crystal structure, the diagnosis of the image distortion was performed on the annular dark field (ADF) image. Then the correction of image distortion was applied to ADF, SI and/or elemental maps. As shown in Fig.1, using a practical example, we demonstrate that the script can correct the image distortion and warp the deformed SI back, and finally ending up in a refined color elemental map can be constructed. This plugin is available by request to the authors.

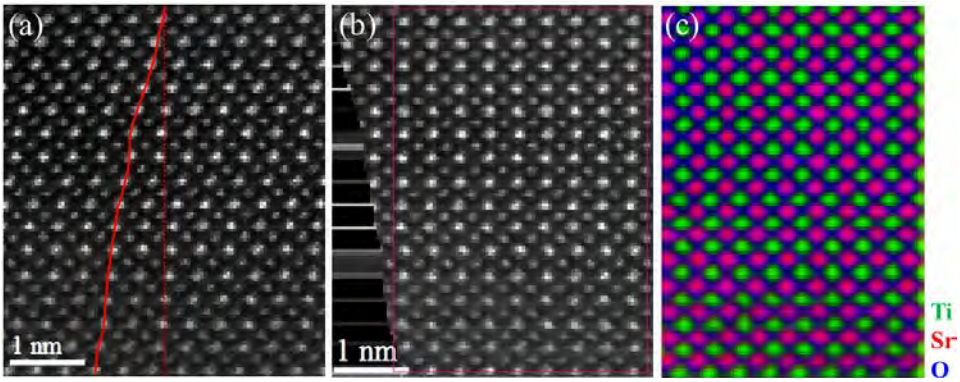

FIG. 1. (a) Nonlinear image distortions in the spectrum image. The straight lattice (indicated by the dotted lines) has been distorted to a curve. (b) Nonlinear image distortion minimized by STEM SI Warp. (c) Final warped and cropped RGB color figure of the overlaid elemental maps, Sr (Red), Ti (Green), and O (Blue).

References

[1] D R G Mitchell, B Schaffer, Ultramicroscopy 103 (2005), 319.
[2] https://en.wikipedia.org/wiki/Bilinear_interpolation [Accessed 20 January2017]

Two-dimensional Gaussian Fitting for Accurate Lattice Constant Measurement from Selected Area Diffraction Map

R. Bekarevich[1], K. Mitsuishi[1,2], T. Ohnishi[1], F. Uesugi[2], M. Takeguchi[2], Y. Inaguma[3], T. Ohno[1], and K. Takada[1]

[1] Global Research Center for Environment and Energy based on Nanomaterials Science, National Institute for Materials Science, Tsukuba, 305-0047 Japan
[2] TEM station, National Institute for Materials Science, Tsukuba, 305-0047 Japan
[3] Department of Chemistry, Faculty of Science, Gakushuin University, 1-5-1 Mejiro, Toshima-ku, Tokyo 171-8588, Japan

Transmission electron microscopy (TEM) is a powerful tool for observing the microstructure of materials. Particularly, it is possible to determine the lattice constant at the local region of material by using selected-area electron diffraction (SAED). However, because of hysteresis and drift of magnetic lens the accuracy of SAED is lower than that using X-ray diffraction, and is usually considered to be several percent. Uesugi [1] proposed a strain mapping method combining nanosized SAED with a two dimensional sample scanning system developed by Takeguchi et al. [2] In this method the optical system of the TEM is fixed at the certain position and less susceptible by magnetic lens issues, therefore relative lattice constant change can be detected with high accuracy by scanning the sample and measurements of the inter-spot distances at different locations. In this study a method for diffraction pattern analysis is presented. Two dimensional Gaussian function fitting with Levenberg-Marquardt method is applied to measure the relative lattice constant change by determination of subpixel displacement of diffraction spot at different positions on the specimen. The Si sample was measured by an aberration corrected TEM (JEOL JEM-ARM200F) equipped with SA aperture with diameter corresponding to 10 nm at the sample plane. 25 diffraction patterns (matrix 5x5) were acquired from the scanned area (300x300 nm) were acquired with a 2048x2048 pixel CCD camera (Gatan Orius). The camera length, intermediate and projector lenses were adjusted so that the Si 111 diffraction spots were spaced as far as possible (Fig. 1a). The measured spot displacement was within 0.04% (Fig. 1b) with standard deviation of 0.0157%. This value corresponds to 0.6 pixels of CCD camera, which means that fitting with a two-dimensional Gaussian function allows the determination of the spot position in the subpixel order.

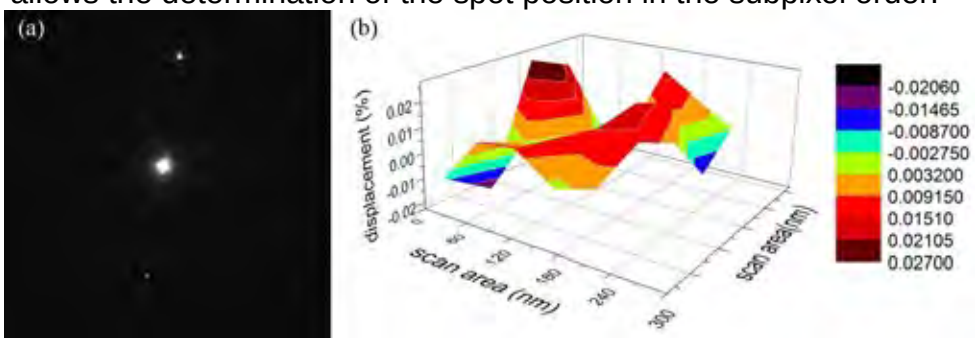

FIG. 1. (a) A typical diffraction pattern, (b) the relative spot displacement at different positions on the specimen

References
[1] F. Uesugi, *Ultramicroscopy* 135 (2013) 80–83
[2] M.Takeguchi et al, *J. Electron Microsc.* 57 (2008) 123

Magnetic-field-free STEM tomography for ferromagnetic materials

K.L. Hasezaki[1], H. Saito[1], T. Sannomiya[2], H. Miyazaki[3], T. Gondo[3], S. Miyazaki[4], and S. Hata[1]

[1] Department of Electrical and Materials Science, Kyushu University, 6-1 Kasugakoen, Kasuga-shi, Fukuoka 816-8580, Japan
[2] Department of Materials Science and Engineering, Tokyo Institute of Technology, Nagatsuta, Midori-ku, Yokohama-shi, Kanagawa 226-8503, Japan.
[3] Mel-Build Corporation, 3-1-15, shimoyamato, Nishi-ku, Fukuoka 816-0052, Japan
[4] Materials and Structural Analysis, Thermo Fisher Scientific (FEI Japan), 4-12-2 Higashi-Shinagawa, Shinagawa-ku, Tokyo 140-0002, Japan

Three-dimensional (3D) observation of dislocations is one of the successful applications of electron tomography (ET) for crystalline materials research [1]. However, ET applications to ferrous steels have barely been reported before because steels, except for austenite-based ones, are ferromagnetic at room temperature. A ferromagnetic specimen magnetized by the objective lens field about 2 T causes undesirable problems especially for ET such as out of focus, anisotropic defocus, deformation of the specimen and change of the electron beam path when the specimen is tilted [2]. Fortunately, a high spatial resolution around 1 nm has been achieved by aberration correction performed for objective lens-free scanning transmission electron microscopy (STEM) [3]. This method seems to be suitable for ET observation of dislocations in a ferromagnetic materials because STEM with a convergent electron probe can suppress diffraction contrast other than dislocations. In this study, a STEM tomography method without magnetizing a ferromagnetic specimen has been developed for three-dimensional visualization of dislocation arrangements in α-Fe. For realizing a magnetic-field-free environment, the objective-lens current was reduced to zero in a demagnetization manner. The achievable lowest magnetic field was 0.38±0.07 mT in the objective lens polepiece of a commercial electron microscope (FEI Titan 60-300), which was measured by a Hall element built into a specimen holder (Mel-Build Corporation). A large spherical aberration (Cs) of a condenser mini-lens was reduced by using a Cs corrector (CEOS DCOR). An electron channeling contrast imaging (ECCI) using inelastically-scattered electrons [4] was effectively employed to emphasize the dislocation-line contrast up to large specimen-tilt angles. As a result, a tilt-series data set was acquired without any problems mentioned above over -70° to 70° of the tilt angle range. The present magnetic-field-free STEM tomography is available to visualize a three-dimensional dislocation arrangement in ferromagnetic materials with about 10^{15} m^{-2} of dislocation density.

References

[1] J. S. Barnard et al., *J. Phys. Conference Series* 26 (2006) 247.
[2] S. Hata et al., *ISIJ Int.* 55 (2015) 623.
[3] S. McVitie et al., *Ultramicroscopy* 152 (2015) 57.
[4] N. Kuwano et al., *J. Electron Microsc.* 59 (2010) S175.
[5] This work was supported by the Japan Science Technology Agency ‘Development of systems and technology for advanced measurement and analysis’ program and Research and Education Center for Advanced Energy Materials, Devices and Systems, Kyushu University.

Bi-orthogonality allows observation of self-hybridization in plasmonic system

H. Lourenço-Martins[1], P. Das[1], L.H.G. Tizei[1], R. Weil[1] and M. Kociak[1]

[1] Laboratoire de Physique des Solides, Université Paris-Sud, CNRS UMR 8502, Orsay, France.

Surface plasmons resonances occur when a metallic nano-particle is excited by an external electric field. Ouyang and Isaacson [1] have shown that the plasmon modes are the solutions of an eigenproblem. Depending on the geometry of the particle, the solutions can form a bi-orthogonal basis in which left and right eigenvectors are different. This particularity of the plasmonic eigenproblem has always been considered as a mere computation detail [2]. In the present work, we will demonstrate that, on the contrary, plasmonic bi-orthogonality has dramatic physical consequences. Relying on the perturbation theory introduced by Trügler et al [3-4], we will show that the bi-orthogonality can trigger the interaction between plasmon modes of different orders within a single particle. Moreover, we will relate the splitting energy of this self-hybridization phenomenon to the overlap matrix of the system, allowing a direct measurement of the degree of bi-orthogonality of the plasmonic system. We will then unambiguously determine the role of the particle symmetries in the apparition of bi-orthogonality and design a model system (dagger) in which the bi-orthogonality is expected to strongly express. We will theoretically and numerically describe the physics of plasmonic bi-orthogonality, and demonstrate through EELS that its manifestation is large enough to be observed experimentally (Fig 1). Finally, we will discuss how our findings may be applied to other fields of physics, in particular that of the open quantum systems [5].

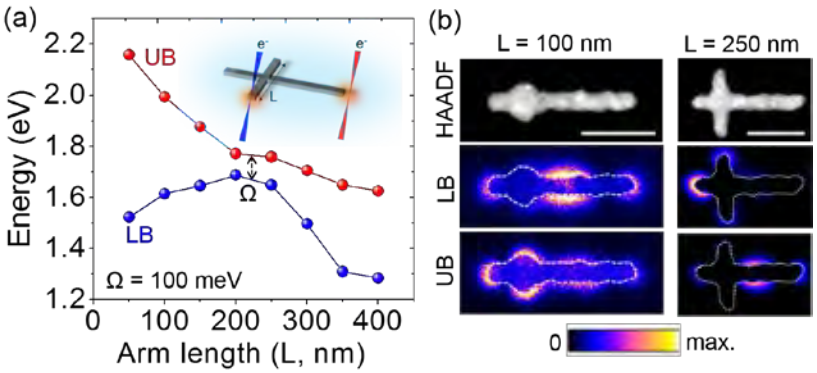

FIG. 1. (a) Experimental plasmon resonance energies dispersion of two dagger modes as a function of the short arm length L, as measured by EELS. A strong strong anti-crossing due to bi-orthogonality, is evidenced. (b) EELS energy filtered maps corresponding to the upper (UB) and lower branches (LB) for L=100, 250 nm.

References

[1] F. Ouyang et al., Philo. Mag. Part B 60, 481–492 (1989).
[2] I. D. Mayergoyz et al., Phys. Rev. B, 72 (2005)
[3] A. Trügler et al., Phys. Rev. B, 83 (2011)
[4] F. P. Schmidt et al., Nano Lett. 14, 4810–4815 (2014).
[5] D.C. Brody, Journal of Physics A 47, 035305 (2014).

The calculations of EELS and ion transfer properties based on the density functional theory for the degenerated layered rock salt cathode material of lithium ion battery.

T. Segi, K. Kano, Y. Takagishi, T. Tsubota and T. Yamaue
KOBELCO RESEARCH INSTITUTE, INC., Takatsuka-dai, Nishi-ku, Kobe, Hyogo 651-2271, Japan

Layered rock salt (LRS) materials like $LiCoO_2$ and Li(Ni, Mn, Co)O_2 with an α-$NaFeO_2$-type structure are widely used as the cathode in lithium ion rechargeable batteries. The cubic phase develops at the surface of the degenerated LRS particles because of the charge–discharge cycle test [1]; therefore, the relation between the ion transfer properties and the cubic phase is of interest to many investigators.

The O *K* edge TEM-EELS spectra obtained on the inside and at the surface of the aged particles are depicted in the FIG. 1. The fine structure of BULK can be explained by the calculated spectrum of LRS, which is obtained by density functional theory (DFT) using the super-cell model based on the same crystallographic data. On the contrary, because the intensity peaks of the SURFACE and NiO appeared at ~538 eV, the SURFACE spectrum is presumed to result from the cubic NaCl-like atomic structure.

To determine the ion transfer properties of the interfacial structure based on the aforementioned results, the DFT and the nudged elastic band method were performed using the super-cell models of the heterojunction of LRS and NaCl type.

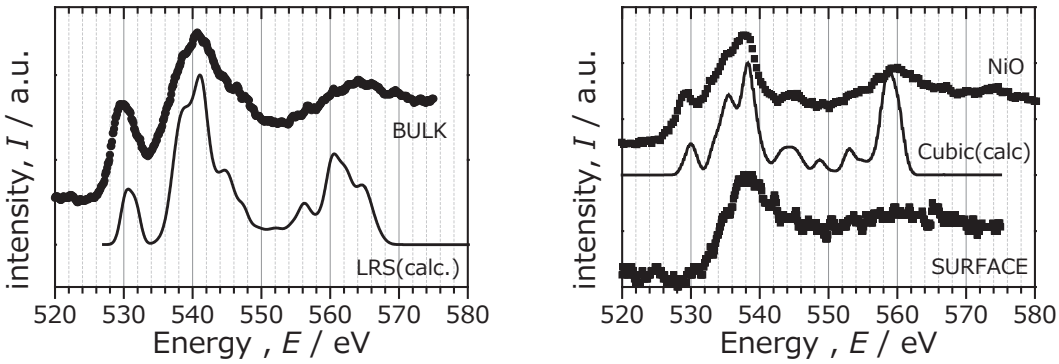

FIG. 1. The experimental and calculated O *K* edge EELS spectra. The BULK and SURFACE correspond to the inside and surface of the typical degenerated LRS cathode particles. The NiO is obtained from the commercially supplied reagent. The solid line of LRS and Cubic are estimated using DFT.

References

[1] T. Segi, R. Syu, T. Tsubota and T. Yamaue, JPS Conf. Proc. **5**, 011014 (2015).

[2] The presented research employed the K-computer computational resources provided by the RIKEN Advanced Institute for Computational Science through the HPCI System Research project (Project ID: hp140095).
PHASE and PHASE/0 are program packages for first-principles calculations based on the density functional theory, developed within the RISS project supported by MEXT of the Japanese government. See the website Research and Development of Innovative Simulation Software,
URL: http://www.ciss.iis.u-tokyo.ac.jp/riss/english/.

Multislice simulations for relativistic beam electrons incorporating atomic inner-shell ionizations

S. Majert[1] and H. Kohl[1]

[1] Physikalisches Institut, WWU Münster, Münster, Germany

Depending on the acceleration voltage, the speed of a beam electron in a Transmission Electron Microscope (TEM) can be in the relativistic regime. Relativistic corrections can therefore become important for image calculations, as seen for example in simulations of electron energy loss images [1,2]. To estimate the influence of relativistic effects on the TEM image, we developed a program which can perform conventional (i.e. based on the Schrödinger equation) multislice calculations [3] as well as multislice calculations where the scattering process is described within a completely relativistic framework [4,5].

The program incorporates atomic inner-shell ionizations into the multislice algorithm by use of projected matrix elements. Utilizing Darwin wave functions [6], we can obtain the matrix elements for the relativistic multislice algorithm without directly calculating the Dirac spinors of the ejected atomic electrons, leading to a comparatively simple formalism.

Our preliminary simulations indicate that, while negligible for the image formed with elastically scattered electron, relativistic corrections lead to a higher intensity in the electron energy loss image of certain transitions (see fig. 1).

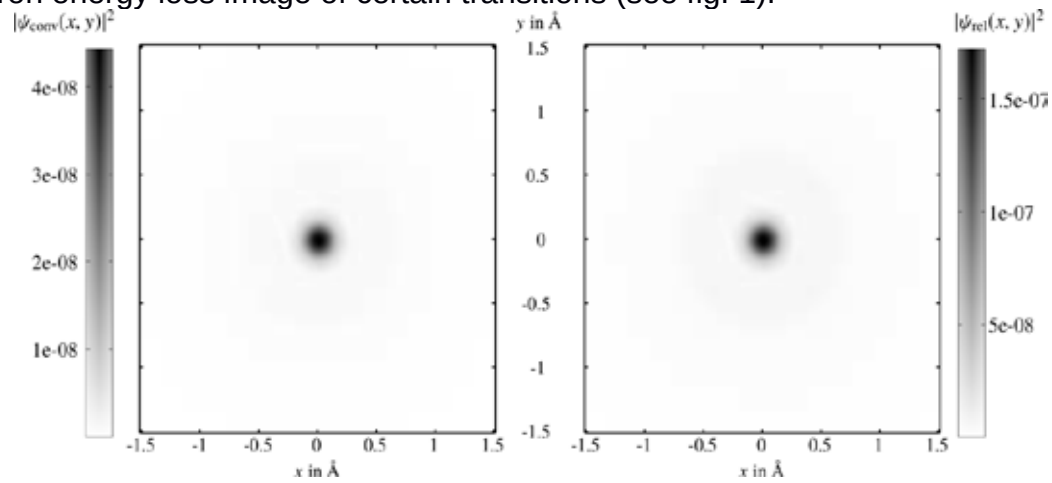

FIG. 1. Exit surface intensity due to the excitation of atomic electrons from the silicon K-shell to a free state with an energy of 10 eV above the ionization threshold and the quantum numbers l=1, m=0. Depicted are the results from the conventional multislice algorithm (left) and the relativistic multislice algorithm (right) for a specimen consisting of ten silicon atoms stacked on top of each other at the image center and an acceleration voltage of 300 kV.

References
[1] R. Knippelmeyer et al., J. Microsc. 194 (1999) 30
[2] C. Dwyer, Phys. Rev. B 72 (2005) 144102
[3] E. J. Kirkland “Advanced Computing in Electron Microscopy” (Springer, New York, 2010)
[4] A. Rother, Ultramicroscopy 109 (2009) 154
[5] A. Lubk, PhD thesis, TU Dresden (2010)
[6] C. G. Darwin, Proc. Roy. Soc. A 118 (1928) 654

Reconstruction and interpretation of ELNES using sparse representation

S. Kiyohara[1] and T. Mizoguchi[1]

[1] Institute of Industrial Science, The University of Tokyo, 4-6-1, Meguro, Tokyo 153-8505, Japan

Near edge structure of electron energy loss spectroscopy (ELNES) observed with TEM can identify the atomic and electronic structures at a localized area, and thus it is an indispensable tool for modern materials investigation. To find logical connections between the spectral features and atomistic and electronic structures theoretical calculations of ELNES have been performed [1-2]. On the other hand, even though the theoretical calculation was performed and the experimental spectrum was reproduced, interpretation of the spectrum is usually difficult. Here, we demonstrated the application of an informatics approach, non-negative matrix factorization, to reconstruct and interpret the ELNES.

As model case, ELNES of five polymorphs of SiO_2, α-, β-quartz, α-, β-cristobalite and tritymite were considered. A first principles pseudopotential calculation based on the density function theory was performed. The plane waves within 500 eV were used as the basis functions, and exchange-correlation functional was treated under the generalized gradient approximation with Perdew-Burke-Ernzerhof functional. The Monkhorst-Pack k-point density in reciprocal space was set to approximately 0.003 points/Å. The intensity matrix composed by five polymorphs were decomposed to three basis spectra. The ELNES spectrum were reproduced using these three basis spectra and their weights.

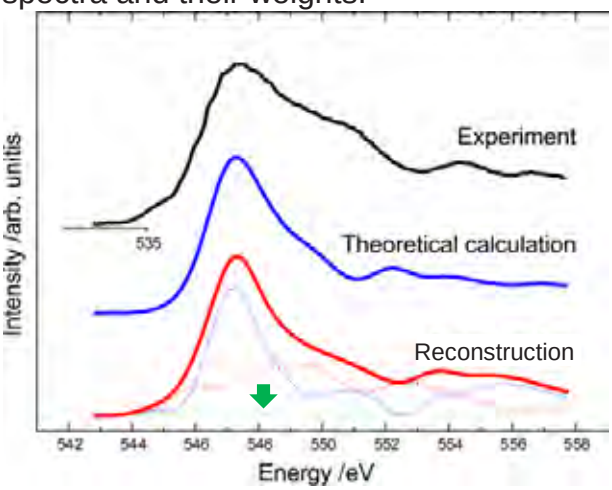

Figure 1 The experimental, calculated and reproduced spectrum of α-quartz.

The experimental[3], theoretical, and reconstructed spectra of α-quartz are shown in Fig. 1. The reconstructed spectrum is composed of the three basis spectrum (dashed lines). It is seen that the spectrum for the α-quartz is made by the two basis spectra (red and blue dashed lines), whereas the weight of the green arrowed basis spectrum is almost zero. Since the arrowed basis spectrum corresponds to that of the β-cristobalite, this result indicates that the electronic structure of α-quartz is far from that of the β-cristobalite. More details will be discussed on my presentation.

References

[1] T. Mizoguchi et al, *Micron*, 41 (2010) 695–709.
[2] M. Wu et al, *Sci. Rep.* 2 (2012)
[3] T. Sharp et al, *Phys. Chem. Miner.* 23 (1996) 17–24.

Theoretical and numerical investigation of the interaction between phase-shaped electron probes and plasmonic modes

H. Lourenço-Martins[1], G. Guzzinati[2], J. Verbeeck[2] and M. Kociak[1]

[1] Laboratoire de Physique des Solides, Université Paris-Sud, CNRS UMR 8502, Orsay, France.
[2] EMAT, Antwerp University, Belgium.

Electron energy loss spectroscopy (EELS) in the low-loss region has attracted a large interest due to its efficiency in resolving plasmonic resonance at the nanometer scale [1]. However, standard low-loss EELS remained intrinsically unable to detect plasmonic optical activity. Nevertheless, phase shaped electron probes constitute a perfect candidate to overcome this limitation and measure the dichroic behavior of plasmons in an electron microscope - as recently pointed out through simulations by Asenjo-Garcia and García de Abajo [2]. Moreover, it has been recently demonstrated that such probes can be created in an electron microscope by tailoring the phase of the beam [3]. In the present work [4], we developed a semiclassical formalism describing the interaction between an electron probe with an arbitrary phase profile and a plasmonic mode. We showed that the equation ruling this interaction takes the elegant form of a transition matrix between two electron states mediated by the eigenpotentials of the plasmon modes. Important experimental inputs, such as convergence and collection angles, were considered. In this contribution, we will present the theoretical formalism and a wide variety of numerical studies of interactions between different nano-structures (e.g. helix, rod) and phase shaped electron probes (e.g. vortex beams, HG-like beams...), with a special emphasis on the experimental feasibility of the proposed geometries (see FIG. 1.)

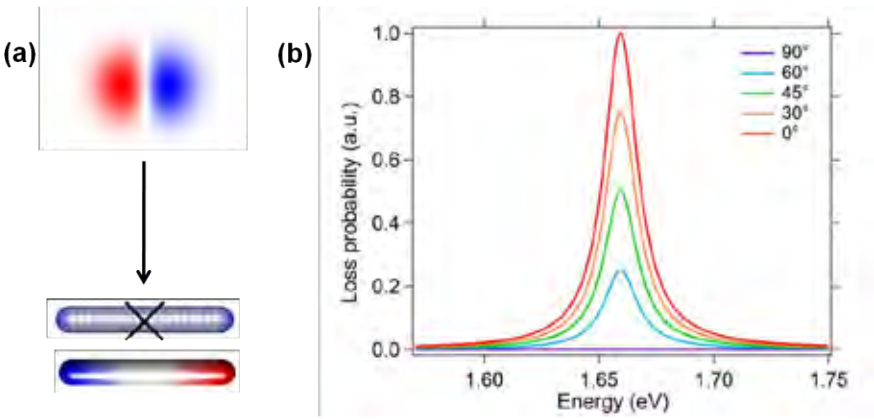

FIG. 1. (a) Schematic representation of the simulation: a HG-beam is sent on the dipolar plasmon mode of a silver rod. (b) Corresponding EELS spectra for different orientations of the probe with respect to the rod showing a polarizer effect.

References
[1] Nelayah et al, Nature Physics 3, 348-353, 2007.
[2] Asenjo-Garcia, García de Abajo, Phys. Rev. Lett. 113, 066102, 2014.
[3] Verbeeck et al, Nature 467, 301-304, 2010.
[4] Guzzinati et al., Nature Com., accepted (2017).

Hidden Antipolar Order Parameter: Structural Screening for the Charged Domain Walls in Hybrid Improper Ferroelectrics $(Ca,Sr)_3Ti_2O_7$

M. H. Lee,[1] C.-P. Chang,[1] F.-T. Huang,[2] G. Y. Guo,[3] B. Gao,[2] C. H. Chen,[1,2] S.-W. Cheong[2,4], and M.-W. Chu[1*]

[1]Center for Condensed Matter Sciences, National Taiwan University, Taipei 106, Taiwan

[2]Rutgers Center for Emergent Materials and Department of Physics and Astronomy, Rutgers University, Piscataway, New Jersey 08854, USA

[3]Department of Physics, National Taiwan University, Taipei 106, Taiwan

[4]Laboratory for Pohang Emergent Materials and Max Planck POSTECH Center for Complex Phase Materials, Pohang University of Science and Technology, Pohang, Korea

Hybrid improper ferroelectrics is recently established in the layered Ruddlesden-Popper oxides of $Ca_3Ti_2O_7$ and $(Ca,Sr)_3Ti_2O_7$, with the ferroelectric order parameter being the hybrid product of two non-polar lattice instabilities that condensate at two-dimensional irreducible representations (irreps). Within the framework of related two-dimensional order-parameter space, the ferroelectric domain in the materials have been extensively studied, while the abundant coexistence of head-to-head (a) and tail-to-tail (b) domains (head and tail, polarizations pointing to and away from each other) therein remains puzzling considering the respective domain walls have to be stabilized by screening electrons and holes, yet holes inaccessible in the n-type oxides. Using group-theoretical analysis and microscopic structural, electronic characterizations though electron microscopy and spectroscopy, we established the existence of hidden antipolar order parameter in $(Ca,Sr)_3Ti_2O_7$ due to the condensation of an unexpected antipolar lattice instability that transforms like four-dimensional irrep. This exploration turns the order-parameter space to be multidimensional, leading to intertwined polar and antipolar order parameters. The corresponding domain topology is characterized by sandwiched antipolar domains between the head-to-head and tail-to-tail domains, indeed observed in our atomic-resolution imaging of the domain walls.

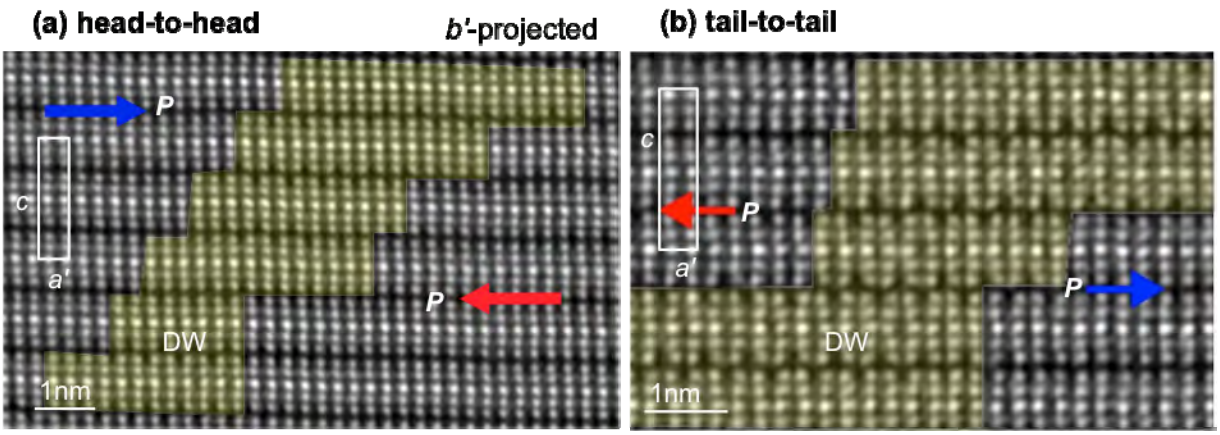

Strong excitonic interaction in O-K edge of Perovskite oxides

K. Tomita[1], T. Miyata[1], and T. Mizoguchi[1]

[1] Institute of Industrial Science, University of Tokyo, 153-8505, Japan

Theoretical methods for calculating ELNES have advanced in parallel with the development of experimental STEM/TEM/EELS facilities. ELNES calculations have been categorized into three theoretical frameworks: the one-particle method, the two-particle method and the multi-particle method. However, an important open question is still present in the ELNES calculation. That is, the effect of the excitonic interaction at high-energy ELNES is not sufficiently discussed. The exciton in the ELNES is a core exciton between the excited electron and the core hole. The excitonic interaction is approximated using the DFT–LDA/GGA framework in the one-particle calculation. If the energy distance between the electron and hole is large, such as the case in high-energy ELNES, the one-particle approximation works well.

In semiconductor optics, on the other hand, it is known that exciton behavior is strongly dependent on the electronic structure of material. For example, excitonic interaction at the band gap, i.e., the "band gap"-exciton, is affected by the size of the band gap and band dispersion. Furthermore, it is known that low-dimensional materials show strong excitonic interaction because of their confined electronic structure. Contrary to the band gap exciton, the possibility of the presence of a strong "core"–excitonic interaction in high-energy ELNES has not been sufficiently discussed.

In this study, we report unusually strong excitonic interaction in high energy ELNES. Figure 1 shows the experimental and calculated O-K edge of $CaTiO_3$. Both one-particle and two-particle calculations are shown. Although both theoretical methods reproduce the experimental spectrum satisfactorily, the one-particle calculation cannot reproduce the position of the peak A, whereas it is well reproduced by the two-particle calculation. The same trend was observed in other perovskite materials.

In the poster, the details of the results and the origin of this strong excitonic interaction at the O-K edge will be discussed [1,2].

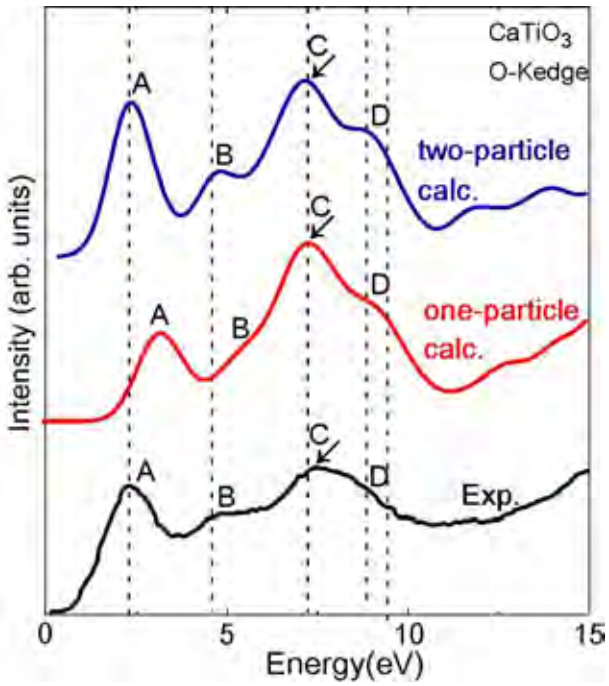

Figure 1: Calculated and experimental O-K edge of $CaTiO_3$.

References

[1] K. Tomita, T. Miyata, W. Olovsson, and T. Mizoguchi, Ultramicroscopy, in press. DOI:10.1016/j.ultramic.2016.04.006i

[2] K. Tomita, T. Miyata, W. Olovsson, and T. Mizoguchi, J. Phys. Chem. C, 120 (2016) 9036-9042. DOI: 10.1021/acs.jpcc.5b12389

BN nanosheets: layer counting by EELS and stacking sequence determination by HAADF imaging

G. Casillas[1], D.R.G. Mitchell[1], M.H. Khan[2], and Z. Huang[2]

[1] Electron Microscopy Centre, University of Wollongong, Wollongong, NSW 2500, Australia
[2] Institute for Superconducting and Electronic Materials, University of Wollongong, Wollongong, NSW 2500, Australia

2-D materials have been the subject of intense research in the last decade. One such material is boron nitride nanosheets (BNNS). BNNS structural similarity with graphene (hexagonal atom-thick layers) makes it a suitable substrate for graphene-based electronics. It also shows promise in anti-corrosion, nano and optoelectronics applications [1]. The properties of the material depend~~s~~ on the number of layers, hence, in this work we present a methodology based on Electron Energy Loss Spectroscopy to quantify the number of layers in CVD grown BNNS. We also applied atomic resolution High Angle Annular Dark Field (HAADF) imaging combined with image simulation to identify the stacking order up to 3 layers.

BN sheets were grown by CVD [2] and analyzed in a JEOL ARM200FC equipped with a Quantum 963 SE GIF. Line scans were acquired across triangular pyramids. Single layer BNNS were identified by a distinctive N K edge as shown in Fig. 1a. Moreover, the B and N K edges were quantified to determine the number of layers. The sheet stacking sequence for ensembles up to 3 sheets in thickness, as shown in Fig. 1b, and energetically non-favored stacking sequences were identified.

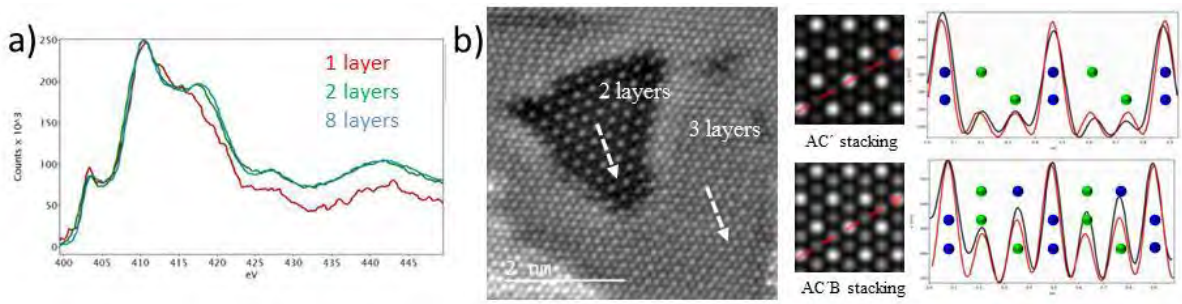

FIG. 1. **a**, N edge of 1, 2 and 8 layers. **b,** HAADF imaging and simulation of AC' and AC'B stacking sequences.

References
[1] K. Watanabe et al., *Nat. Mater.* 3 (2004) 404.
[2] M.H. Khan et al. *Nanoscale.* 8 (2016) 1592

Determination of the internal structure of a new line defect by EELS

Jong Seok Jeong[1], Mehmet Topsakal[1], Peng Xu[1], Bharat Jalan[1], Renata M. Wentzcovitch[1], and K. Andre Mkhoyan[1]

[1] Department of Chemical Engineering and Materials Science, University of Minnesota, Minneapolis, Minnesota 55455, United States

Perovskite oxides form an eclectic class of materials owing to their structural flexibility in accommodating cations of different sizes and valences. They host well known point and planar defects, but so far no line defect has been identified other than dislocations. We report the discovery of a new line defect in $NdTiO_3$ perovskite. STEM-EELS measurements and DFT+U results indicate that it consists of self-organized Ti-O vacancy lines replaced by Nd columns surrounding a central Ti-O octahedral chain containing Ti^{4+} ions, as opposed to Ti^{3+} in the host. The three factors are responsible for this defect formation, that is, presence of a multivalent ion, slightly off stoichiometry, and substrate induced strain, co-existing commonly in epitaxially grown films of perovskites. Considering the wide variety of existing multi-valent perovskite oxides, this new line defect might be created, with the proper control of growth, in others as well. The electronic structure of $NdTiO_3$ with a line defect is strikingly different from that of bulk $NdTiO_3$ and in the presence of a line defect, the band gap narrows by approximately ~0.4 eV. The distinct Ti valence in this line defect introduces the possibility of engineering exotic conducting properties in a single preferred direction and tailoring novel desirable functionalities in this Mott insulator [1,2].

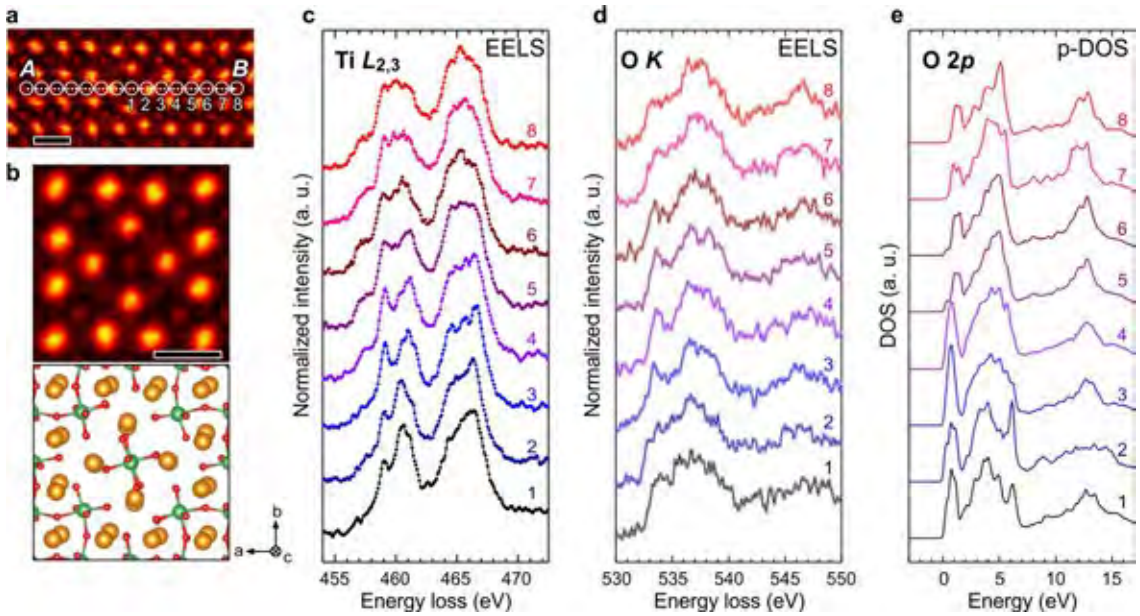

FIG. 1. Atomic structure of the defect core and its detailed STEM imaging, EELS and DFT-U analysis. EELS line profiling was conducted across the defect (from A to B) in (a). The scale bars are 0.5 nm.

References

[1] J.S. Jeong et al., *Nano Lett.* 16 (2016) 6816.

[2] This research was supported in part by NSF DMR-0819885, DMR-1420013, DMR-1410888, EAR-134866, and EAR-1319361.

EMCD : last developments for in situ magnetic transition and rare earth investigation

X. Fu[1], V. Serin[2] and B. Warot-Fonrose[3]

[1] CEMES, CNRS, Univ. Toulouse, BP 94447, 31055 Toulouse, FRANCE

The emerging technique EMCD, Energy-Loss Magnetic Chiral Dichoism, aims to measure the element-specific magnetic moment of solids at a nanometer scale in a transmission electron microscope [1-2]. The moment information is carried in the electron energy-loss spectra obtained from two specific positions, as sketched in Fig. 1(a). Our work explores the application of EMCD by applying it to MnAs/GaAs(001) and $DyFe_2/YFe_2$ superlattice. A breaking of the ferromagnetic order in MnAs is locally investigated *in-situ*, along with crystallographic transition from hexagonal α-MnAs to quasi-hexagonal β-MnAs, as illustrated in Fig. 1(b-e) [3-4]. Moreover, the orbital-to-spin moment ratios of α-MnAs along different magnetic axes are estimated and compared by EMCD [4]. In addition, dichroic signals over Fe-$L_{2,3}$ and Dy-$M_{4,5}$ edges of $DyFe_2/YFe_2$ are simultaneously detected, demonstrating the antiparallel coupling of Fe 3d and Dy 4f moments. EMCD sum rules specified for $M_{4,5}$ edges are also established [5]. Our work presents the last developments of EMCD. It illustrates for the first time the EMCD feasibility for *in-situ* experiments, the potential to explore the magnetic anisotropy, to probe 4f moment and to study moment coupling [6].

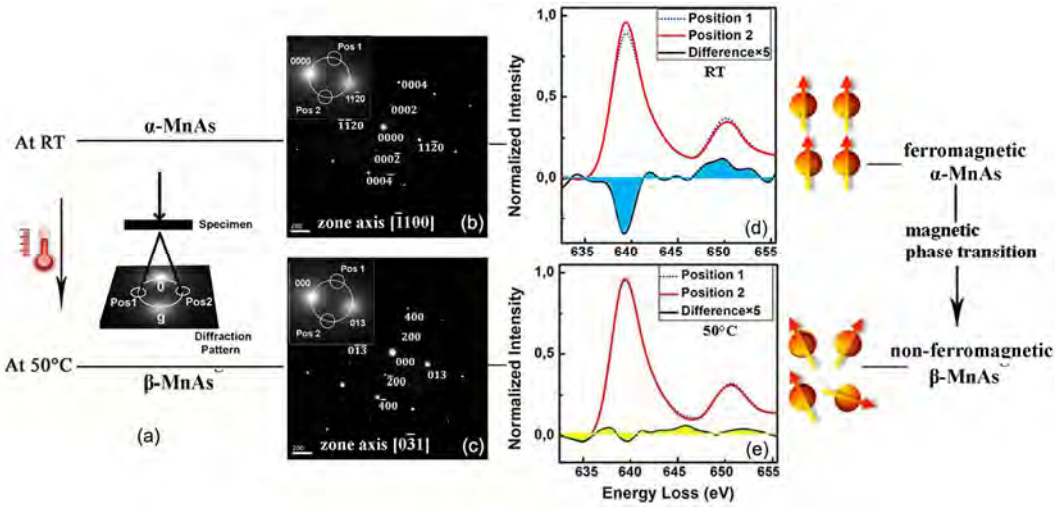

Figure 1. (a) Schematic diagram of *in-situ* EMCD experimental configuration; (b) diffraction pattern (DP) of MnAs obtained along intermediate axis at room temperature (RT) and (c) 50°C, in inserts are energy filtered DPs in two-beam condition; (d) EELS as well as the dichroism spectrum detected at RT and (e) 50°C.

References

[1] Schattschneider, P. *et al. Nature* **441,** 486–488 (2006).
[2] Warot-Fonrose, B. *et al. Ultramicroscopy* **108,** 393–398 (2008).
[3] Fu, X. *et al. Appl. Phys. Lett.* 107, 062402 (2015).
[4] Fu. X, *et al*. *Phys. Rev. B.* 93, 104410 (2016).
[5] Fu. X, et al. *Phys. Rev. B: rapid communication*. 94, 140416 (2016).
[6] This work is supported by the French national project EMMA (ANR12BS1001301) and European Union under the Seventh Framework Program (312483-ESTEEM2).

EELS Probing of lithium based 2-D battery compounds processed by liquid phase exfoliation

A. Pokle[1,2,3], J. Coelho[2,4], E. McGuire[1,2,3], C. Downing[3], P. Casey[2], S. Park[2], V. Nicolosi[2,4]

[1]School of Physics, Trinity College Dublin, Dublin2, Ireland
[2]CRANN, Trinity College Dublin, Dublin2, Ireland
[3]Advance Microscopy Lab, Trinity Enterprise Center, Pearse Street, Dublin2, Ireland
[4]School of Chemistry, Trinity College Dublin, Dublin2, Ireland

Two-dimensional lithiated nanosheets usually show excellent electrochemical performance due to an increase in surface area and shorter diffusion paths. However, processing techniques, such as shear mixing or liquid phase exfoliation could induce phase changes or knock out some of the structural lithium (Li) ions, what in turn might result in poor electrochemical performance. Here different lithiated layered compounds mainly $LiCoO_2$, $LiMn_2O_4$, and $Li_5Ti_4O_{12}$ were chemically exfoliated and investigated using electron energy loss spectroscopy (EELS) for their Li-K edge and looking at the oxygen (O) K edge with their respective transition metal core loss peak (Mn, Co and Ti) which revealed changes in the Energy loss near edge structures (ELNES) when compared to the unlithiated compounds. STEM-EELS analyses confirmed uneven distribution of lithium within the lithiated layered materials (Figure 1). In this work, EELS was used for the first time to detect and to probe the chemical environment of the lithium in liquid phase exfoliated material[1][2].

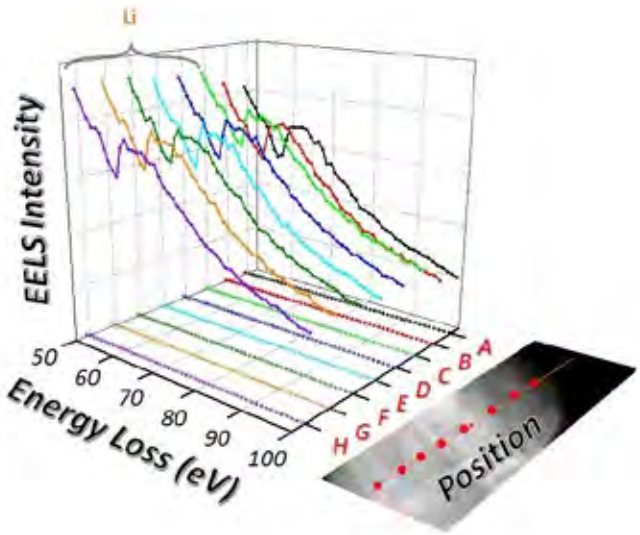

FIG. 1. STEM-EELS of Li K-edge for chemically exfoliated $LiCoO_2$ revealing a small peak at 56 eV, as well as the prominent signal at 62 eV, which indicates the presence of Li-ion.

References

[1] A. Pokle *et al.*, “EELS probing of lithium based 2-D battery compounds processed by liquid phase exfoliation,” *Nano Energy*, vol. 30, pp. 18–26, Dec. 2016.
[2] F. Wang *et al.*, “Chemical distribution and bonding of lithium in intercalated graphite: Identification with optimized electron energy loss spectroscopy,” *ACS Nano*, vol. 5, no. 2, pp. 1190–1197, 2011.

Development of low dose cryo-EELS toward organic molecules structure analysis

A. Maigné[1], M.T. Schreiber[1] , and M. Wolf[1]

[1] Molecular Electron Microscopy Unit, Okinawa Institute of Science and Technology, 1919-1 Tancha, Onna-son, Okinawa, Japan 904-0497

Radiation damage is a major limiting factor in obtaining high resolution images and EEL spectroscopy in cryo-electron microscopy. While it seems commonly admitted that the major part of the damages comes from radiolysis[1], local charging within the ice or the sample has been mentioned several time as a source of damage[2].

During this presentation, we will show how damages can be measured by EELS and how they can be reduced. In order to obtain relevant EELS spectrum at very low dose, we have also studied the advantage of using a direct detection camera as the EELS detector. Figure 1 shows clearly that electron counting increases greatly the overall signal noise ratio at low dose (3 electrons/ $Å^2$ has been) and allows fine structure analysis without damaging the sample.

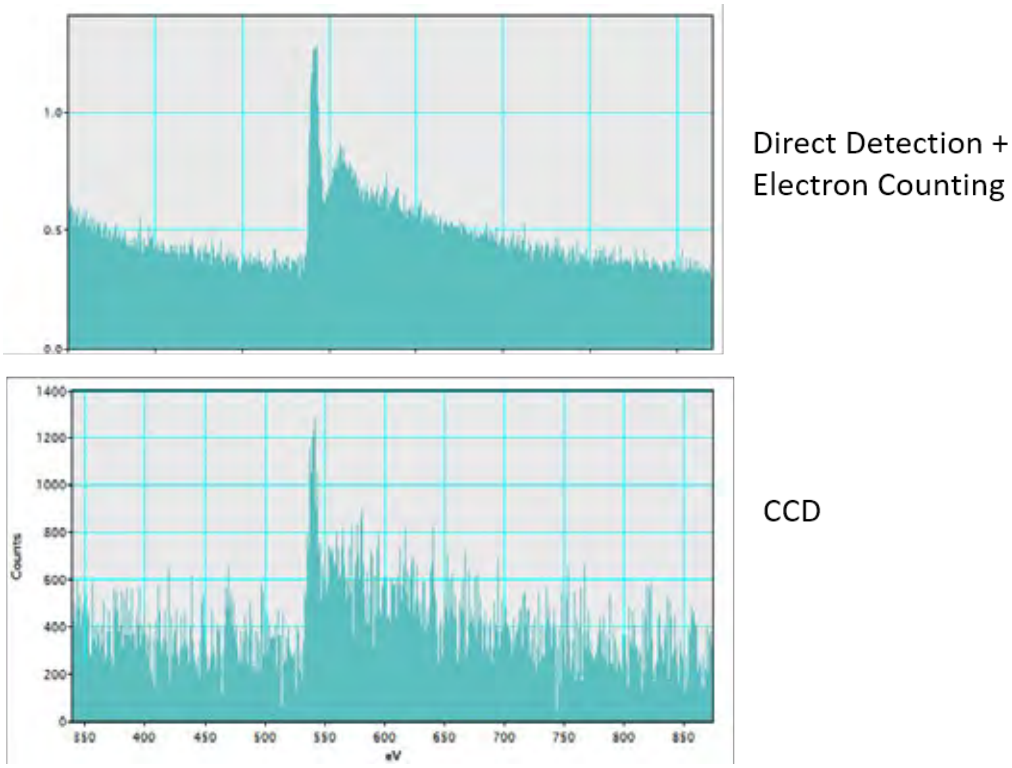

FIG. 1. EELS spectrum showing the oxygen K of ice using a direct detector in electron counting mode compared with the one recorded with a typical CCD. Both spectra were recorded at low dose (3 electrons/ $Å^2$)

References
[1] C. Laffon, S. Lacombe, F. Bournel, P. Parent., 2006. Radiation effects in water ice:a near-edge X-ray absorption fine structure study. Journal of Chemical Physics 125 (20), 204714.
[2] Egerton R.F. 2014. Choice of operating voltage for a transmission electron microscope. Ultramicroscopy 145, 85-93.

Combined EELS/DFT characterization of the surface functionalization of Ti_3C_2 2D-sheets: from local coordination to optical properties.

D. Magné[1], V. Mauchamp[1], M. Bugnet,[2,3] S. Célérier,[4] P. Chartier[1], G. Botton[2] and T. Cabioc'h[1]
[1] Institut Pprime, UPR3346, 86962 Futuroscope-Chasseneuil Cedex France.
[2] Department MSE, McMaster University, Hamilton, ON, Canada.
[3] Laboratoire MATEIS, UMR 5510 CNRS – Université de Lyon – INSA Lyon, France.
[4] IC2MP, UMR 7285, Université de Poitiers, 86073 Poitiers Cedex, France.

In a very similar way to graphene, the surface functionalization of Ti_3C_2 2D-sheets with T=-OH, -F and/or –O groups (see Fig1 –b) has major effects on their properties.[1] Depending on the T-groups' chemical nature and on their location on the Ti_3C_2 surface, the Ti *d* bands that dominate at the Fermi level are drastically affected. In this context, the comparison between monochromated STEM-VEELS data and simulations based on the density functional theory validate the random phase approximation (RPA) as an appropriate theoretical level for the interpretation of low loss spectra [2] (see Fig.1 a and c): an interband transition characteristic of the T-groups' location on the Ti_3C_2 sheets is evidenced[3] and their role on the optical properties (from infrared to visible energy range) is highlighted. In addition, the ELNES at the C-K edge being sensitive to the chemical nature of the T-groups, their analysis based on DFT simulations allows an estimate of the –O content on the Ti_3C_2 surface and shows that –OH and –F groups play a similar role on the site projected electronic structure of the Ti_3C_2 sheets.[4]

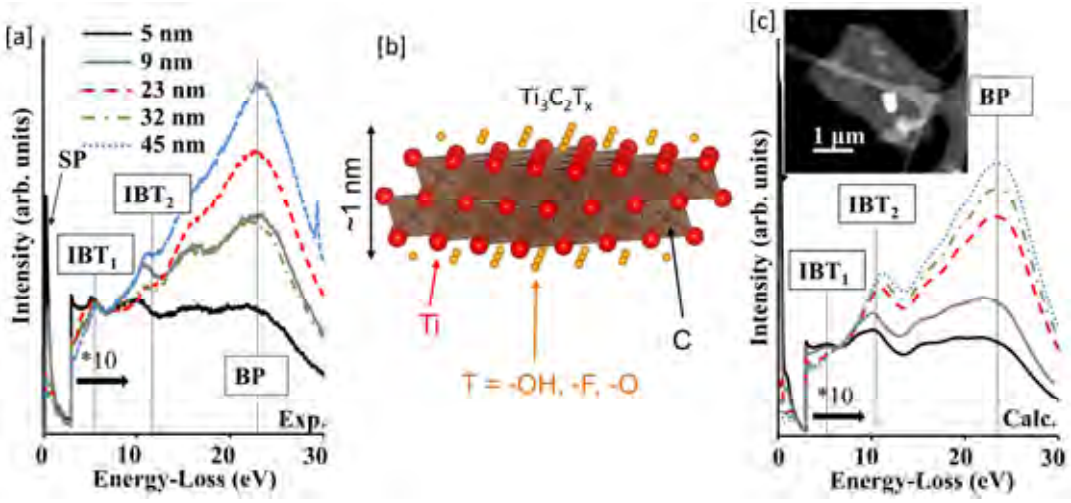

FIG. 1. [a] Experimental and [c] calculated (DFT-RPA) low-loss spectra of Ti_3C_2 stacked sheets of various thicknesses. [b] $Ti_3C_2T_x$ single sheet.

[1] M. Naguib et al., *Adv. Mater.* 26 (2014) 992.
[2] V. Mauchamp et al., *Phys. Rev. B* 89 (2014) 235428.
[3] D. Magné et al., *Phys Rev B* 91 (2015) 201409(R).
[4] D. Magné et al., *Phys. Chem. Chem. Phys.* 18 (2016) 30946.
[5] The "Agence National de la Recherche" is gratefully acknowledged: ANR project n°. 13-BS09-0024-02. This work has been supported by the "Région Poitou-Charentes".

EELS as tool to assess microscopic properties of Bismuth Oxide

P. Torruella[1], C. Coll[1], G. Martín[1], L. López-Conesa[1,2], M. Vila[3, 4], C. Díaz-Guerra[5], M. Varela[5], M.L.Ruiz-González[6], J. Piqueras[5], S. Estradé[1], F. Peiró[1].

[1] LENS, MIND-IN2UB, Departament d'Electrònica, Universitat de Barcelona, 08028 Barcelona, Spain.
[2]TEM-MAT,CCiT, Universitat de Barcelona, 08028 Barcelona, Spain.
[3] Spanish CRG BM25-SpLine beamline at the ESRF, 71 Avenue des Martyrs, 38000 Grenoble, France.
[4] Instituto de Ciencia de Materials de Madrid – ICMM/CSIC, Cantoblanco, 28049 Madrid, Spain.
[5] Departamento de Física de Materiales, Facultad de Ciencias Físicas, Universidad Complutense de Madrid, 28040 Madrid, Spain.
[6] Departamento de Química Inorgánica, Facultad de Químicas, Universidad Complutense de Madrid, 28040 Madrid, Spain.

Bi_2O_3 has sparked interest the fields of optics, electrochemistry and in fuel cells. One of its most celebrated properties is its abnormally high oxygen conductivity[1], which is normally discussed in terms of oxygen vacancy generation and transport. However, most of the literature about this material are studies performed at the macroscopic level and even though local properties such as the electronic environment of the oxygen would be highly interesting, little experimental work has been done in this matter[2]. In order to try to bridge this gap we have performed pioneering core and low-loss EELS studies in three different α- Bi_2O_3 samples which exhibit different oxygen conductivity values. These are the first reported core-loss EELS measurements of this material to our knowledge and as such, how spectral features relate to structural and electronic properties remains unclear. To deal with this we resort to DFT simulations with different oxygen vacancy configurations. In this work we discuss the combined HR-TEM/STEM, EELS and DFT results.

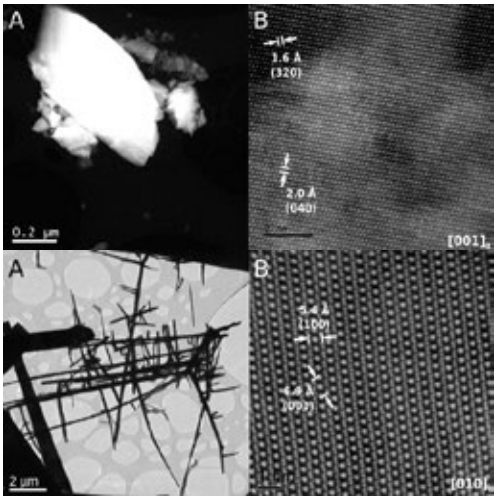

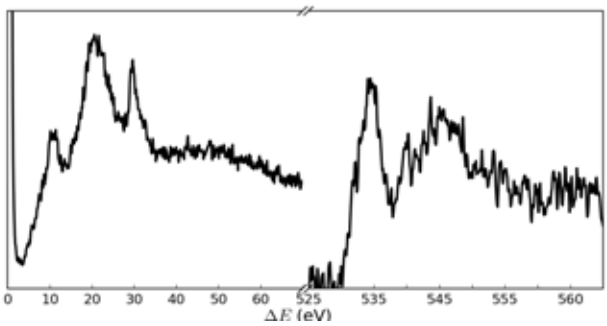

FIG. 1. HAADF images from two of the studied samples: α-Bi_2O_3 commercial powder (top), α-Bi_2O_3 Nanowires (bottom).
FIG. 2. Experimental EELS spectra from the commercial powder.

References
[1] T. Takahashi et al., *J. Appl. Electrochem.* 5 (1975) 187–195.
[2] A. Walsh, J. *Phys. Rev. B* 23 (2006) 1-13.

From Atomic-Scale Ordering to Materials Properties: Aberration-Corrected STEM, Spectroscopy, and Simulation

B. D. Esser[1], T.M. Smith[1], N. Antolin[2], A. Carlsson[3], R.E.A. Williams[1], A. Wessman[4], T. Hanlon[5], H.L. Fraser[1], W. Windl[2], M.J. Mills & D.W. McComb[1]

[1] Center for Electron Microscopy and Analysis, The Ohio State University, USA
[2] Dept. of Materials Science and Engineering,The Ohio State University, USA
[3] FEI Company, Eindhoven 5651, The Netherlands
[4] G.E. Aviation, Cincinnati, Ohio, USA
[5] G.E. Global Research Center, Niskayuna, New York, USA.

Understanding structure-property relationships is at the heart of materials science and engineering. The ability to characterize how atomic-scale structure and composition affect macro-scale properties allows new materials to be engineered more effectively and efficiently. From traditional metallic systems where microstructure dictates mechanical behavior to functional oxide thin films where ordering strongly affects magnetic properties, aberration corrected scanning transmission electron microscopy (STEM), spectroscopy, and simulation can greatly improve our capabilities.

Recently, we have shown that by engineering the composition of a Ni-based superalloy, twin formation is inhibited resulting in a remarkable increase in high-temperature creep strength. [1] For the first time in a metallic system, atomically resolved energy dispersive X-ray spectroscopy (EDX) has been used to study the effects of site-specific segregation of solute atoms along stacking faults in this superalloy. [2] Rigorously quantified EDX results were then used as input to first principles calculations to prove that this segregation energetically prohibits twin formation, effectively halting dislocation motion at higher temperatures, resulting in favorable creep properties.

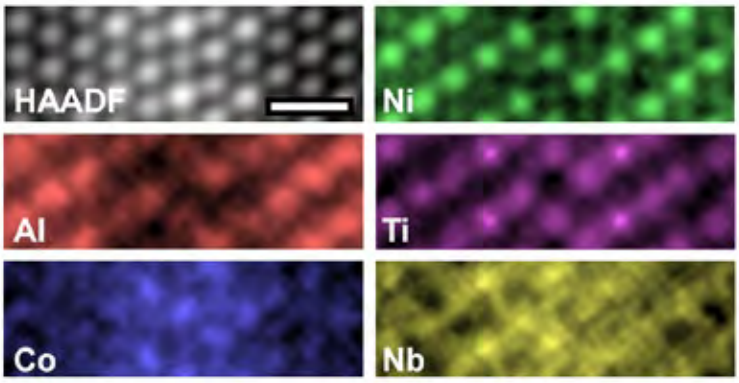

FIG. 1. Atomic-resolution HAADF-STEM image and EDX maps of a stacking fault (center of each map) in a Ni-based superalloy showing site specific segregation of elements. Scale bar is 5 Å.

References
[1] T. M. Smith *et al*, Acta Materialia **100** (2015): 19-31.
[2] T. M. Smith *et al*, Nature Communications **7**, 13434 (2016).
[3] Funding was provided by the Center for Emergent Materials at OSU, an NSF MRSEC (Award Number DMR-1420451), as well as in part by an allocation of computing time from the Ohio Supercomputer Center.

Atomic Configuration of Functionalized Carbon Nanotubes probed via Spatially-Resolved EELS

R. Arenal[1,2]

[1] Laboratorio Microscopias Avanzadas, INA, U. Zaragoza, 50018 Zaragoza - Spain
[2] Fundacion ARAID, 50018 Zaragoza - Spain

Functionalized carbon nanotubes (C-NT) have attracted much attention due to their very promising optoelectronic properties [1]. However, local studies of these hybrid systems are still challenging. Herein, we report a direct investigation at the atomic scale, of covalent and non-covalent functionalized (π-stacked and endohedral) single-walled CNTs, see Figure [2-4]. These studies have been developed via spatially-resolved EELS performed using a liquid-nitrogen holder (−170 °C) and at 80kV. We have examined the different chemical species present in the NTs, determined their average concentration as well as their spatial distribution within the walls and studied their chemical environment and bonding. These studies reveal the supramolecular organization of the organic moieties (in this case, iron-phthalocyanines), opening fascinating perspectives for optoelectronic applications of such nanosystems. All these aspects will be discussed in this contribution.

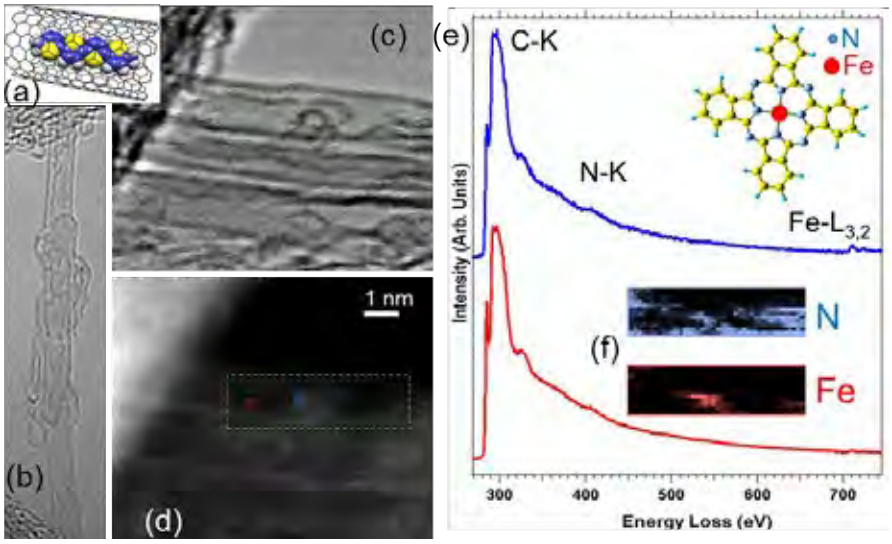

FIG. 1. (a) Atomic-sketch showing the supramolecular order of the iron-phthalocyanine (Fe-Pc) moieties within a single-walled nanotube (SWNT). (b) HRTEM micrograph of a filled SWNT. (c)-(d) BF- and HAADF-STEM images of a bundle of filled SWNT. A 24x12 SPIM-EELS has been recorded in the green marked area on one of these NT. (e) EEL spectra extracted from the squared regions marked in Fig. 1(d). They correspond to 4 EEL spectra each of them. C-K, N-K and Fe-$L_{2,3}$ edges are clearly seen. (f) N and Fe elemental maps. Inset, atomic-sketch of a Fe-Pc (a Fe atom is surrounded by 4 pyrrolic-like subunits).

References

[1] P. Ayala, R. Arenal, A. Loiseau, A. Rubio, T. Pichler, **Rev. Mod. Phys**. 82 (2010).
[2] A. Setaro, M. Adeli, M. Glaeske, D. Przyrembel, T. Bisswanger, G. Gordeev, M. Weinelt, R. Arenal, R. Haag, S. Reich, **Nature Comm**. (2017).
[3] R. Arenal, L. Alvarez, S. Campidelli, R. Le Parc, J.-L. Bantignies, submitted.
[4] We acknowledge funding from the EU under Grant Agreement 696656 Graphene Flagship and the Spanish Ministerio de Economia y Competitividad (MAT2016-79776-P).

Momentum-resolved low-loss EELS of 2D heterostructures – experiments and simulations

Michael J. Mohn, Ralf Hambach, Philipp Wachsmuth, and Ute Kaiser

Central Facility of Electron Microscopy, University of Ulm, D-89081 Ulm, Germany

By means of momentum-resolved EELS, dielectric properties of graphene and other 2D materials can be accessed for different in-plane momentum transfers *q* [1-3]. Here we present momentum-resolved low-loss EELS of a graphene-MoS_2-graphene heterostructure ("sandwich"), which we directly compare to ab initio calculations.
The EELS experiments have been performed at 40 kV in the "SALVE I" prototype TEM [4] equipped with a monochromator and an in-column energy filter. Over an energy range of 50 eV we achieve an energy resolution of 0.1 eV, with a momentum resolution of 0.1 $Å^{-1}$ along the ΓM or ΓK direction in the Brillouin zone [2].
Our simulations are based on time-dependent DFT calculations for graphene and MoS_2 monolayers. For the sandwich structure, we employ additional dielectric model calculations to account for the Coulomb interaction between the layers. This approach allows to gain insights into the interactions between the plasmons in graphene and MoS_2. For the sandwich we find that - like for multilayer graphene [5] – the EEL spectra are correctly described by a layered electron gas (LEG) model (see FIG. 1). However, by using bulk MoS_2 as a test system, we show that for arbitrary multilayer systems it might be necessary to incorporate the finite thickness of each monolayer in the calculations. [6]

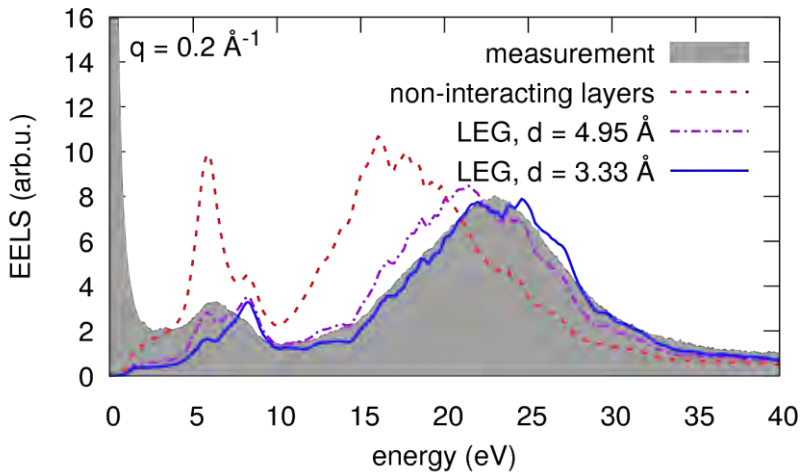

FIG. 1. Momentum resolved EELS of a G-MoS_2-G sandwich for $q = 0.2\ Å^{-1}$ (gray filled curve). LEG model calculations are shown for different layer distances *d* (solid blue line and purple dash-dot line) and in the limit $d \to \infty$ (red dashed line).

[1] M. K. Kinyanjui et al. (2012). EPL 97(5), 57005.
[2] P. Wachsmuth et al. (2013). Phys. Rev. B 88, 075433.
[3] S. C. Liou et al. (2015). Phys. Rev. B 91, 045418.
[4] U. Kaiser et al. (2011). Ultramicroscopy, 111(8), 1239–1246.
[5] V. Jovanović et al. (2011). Phys. Rev. B 84. 155416.
[6] We acknowledge financial support by the German Research Foundation (DFG) and the Ministry of Science, Research and Arts (MWK) of the state Baden-Württemberg within the Sub-Angstrom Low-Voltage Electron Microscopy Project (SALVE).

Probing emerging 2D transition metal dichalcogenides (TMDs) and integrated hetero-structures down to atomic scale

M.J. Kim[1], Q. Wang[1] and J. Oviedo[1]

[1] Department of Materials Science and Engineering, University of Texas at Dallas, Richardson, TX 75080, U.S.A.

Material dimensionality plays a crucial role in determining material physical properties. For example, transition metal dichalcogenides exhibit diverse properties that depend on their composition: semiconductors, semimetals, metals, or superconductors [1-2]. In exploring and developing these emerging materials, aberration-corrected electron microscopy-based techniques such as STEM-HAADF imaging, EELS and EDS, now capable of analyzing these materials with better than 0.1 nm resolution, becomes ever more important. In this talk, I will present our recent studies on the characterization of various 2D layered materials and their integrated hetero-structures for nano-electronics applications. Examples will include: 2H stacked TMDs (MoS_2, $MoSe_2$, WSe_2, and $MoTe_2$), 1T stacked TMDs (SnS_2, $SnSe_2$, $HfSe_2$, and HfS_2), and distorted 1T stacked TMDs (WTe_2). The location and nature of individual atoms, defects, interfaces, and *in-situ* phase transformation and shearing of 2D crystals will be presented and discussed in detail [3].

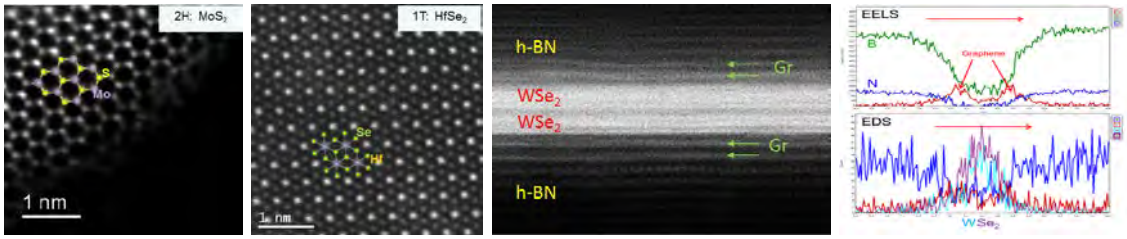

FIG. 1. (Left to Right) STEM HAADF images of 2H-MoS_2, 1T-$HfSe_2$, Double Bi-layer Graphene/WSe_2 Heterostructure, and EELS and EDS profiles confirming the integrated h-BN/bilayer Gr/bilayer WSe_2/bilayer Gr/h-BN hetero-structure.

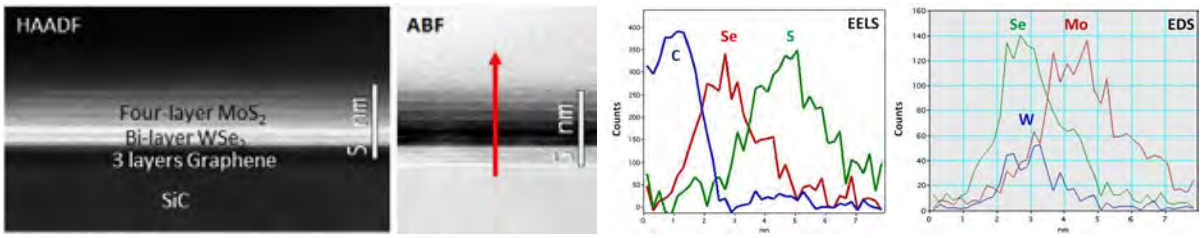

FIG. 2. STEM HAADF and ABF images of 4 layer MoS_2/bi-layer WSe_2/tri-layer epi-graphene grown on SiC. MoS_2 and WSe_2 layers were identified by both EELS and EDS.

References

[1] M. Bockrath et al., *Science* **275** (1997) 1922.
[2] G.R. Bhimanapati et al., *ACS Nano* **9** (2015), 11509.
[3] This work was supported by the Center for Low Energy Systems Technology (LEAST), one of six centers of STARnet, a Semiconductor Research Corporation program sponsored by MARCO and DARPA. Collaborators who contributed to this work are gratefully acknowledged.

The electronic structure of nanostructured bcc-CuCr thin films

C.H. Liebscher[1)], C. Freysoldt[1)], T. Dennenwaldt[2)], T. Harzer[1)], G.Dehm[1)]

[1)] Max-Planck-Institut für Eisenforschung GmbH, 40237 Düsseldorf, Germany
[2)] Interdisciplinary Center for Electron Microscopy, Ecole Polytechnique Fédérale de Lausanne, 1015 Lausanne, Switzerland

Supersaturated Cu-Cr alloys can be synthesized under non equilibrium thin film growth conditions. It was shown that up to a concentration of 67 at.% Cu, the otherwise immiscible elements Cu and Cr are mixed in the body centered cubic (bcc) lattice [1]. High resolution scanning transmission electron microscopy finds that within the nanocrystalline grains, compositional modulations with a wave length on the order of 2 to 5 nm are present, separating regions with up to 85 at.% from those with 42 at.% Cu, but still in the bcc lattice [2]. Forcing Cu to arrange in the bcc instead of the fcc crystal structure certainly affects its electronic structure. Electron energy loss spectroscopy (EELS) reveals a slight change in the near edge fine structure of the Cu-L_{23} edge comparing fcc- with bcc-CuCr alloys. For fcc-Cu, the two peaks in between the L_2 and L_3 edges are stemming from van Hove singularities in the electron density of states at the *L*- and *X*-points in the first Brillouin zone, as seen in the green spectrum of Fig. 1a. In the $Cu_{67}Cr_{33}$ (at.%) thin film only a single peak is observed representing a van Hove singularity at the *N*-point of the first Brillouin zone of the bcc lattice (red and blue spectra). These experimental observations are fully consistent with EEL spectra obtained from density functional theory calculations of pure bcc- and fcc-Cu (Fig. 1b) [2]. However, computed spectra for a bcc-$Cu_{50}Cr_{50}$ (at.%) random solid solution indicate a shift of the van Hove singularity to higher energies that is not observed experimentally. The underlying effects and the influence on the electronic structure of bcc-Cu alloyed with Cr will be discussed in detail.

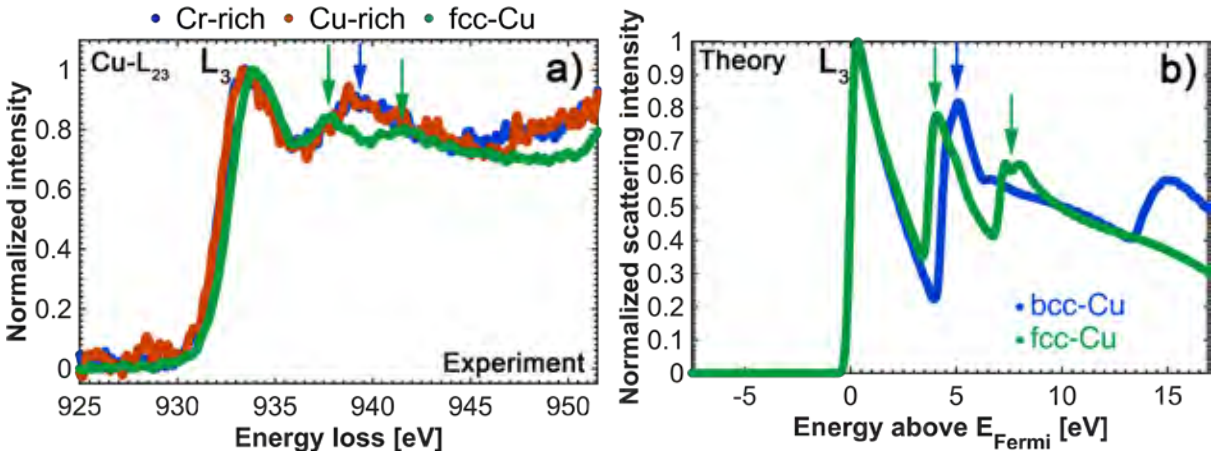

FIG. 1. a) Experimental EEL spectra of the Cu-L_{23} edge obtained in pure fcc-Cu and a $Cu_{67}Cr_{33}$ (at.%) thin film. b) Computed fine structure of the Cu-L_3 edge for fcc- and bcc-Cu.

References

[1] T.P. Harzer et al., *Acta Mater.* 83 (2015) 318.
[2] C.H. Liebscher et al., *Ultramicroscopy* (2016), doi: 10.1016/j.ultramic.2016.07.011.

Electron energy loss spectroscopy study of P-type doped MoS_2 with sub-angstrom beam and ab-initio simulations

G. Nicotra[1], I. Deretzis[1], G. Fisichella[1], A. Piazza[1,2,3], S. Agnello[2], G. Greco[1], C. Bongiorno[1], C. Spinella[1], A. La Magna[1], F. Roccaforte[1] and F. Giannazzo[1]

[1] Consiglio Nazionale delle Ricerche – Istituto per la Microelettronica e Microsistemi, Strada VIII, n. 5 – Zona Industriale, 95121 Catania, Italy
[2] Department of Physics and Chemistry, University of Palermo, Via Archirafi 36, 90143 Palermo, Italy
[3] Department of Physics and Astronomy, University of Catania, Via Santa Sofia, 64, 95123 Catania Italy

Transition metal dichalcogenides (TMDs), such as MoS_2, recently attracted considerable interest for future electronic and optoelectronic applications. In particular, field effect transistors (FETs) with very interesting performances (on/off current ratio $>10^7$ and low subthreshold swing ~ 70 mV/decade) have been demonstrated both using single-layer [1] and multi-layer MoS_2 [2]. Virgin MoS_2 is an unintentionally n-type doped semiconductor and most of the metals exhibit a Fermi level pinning below MoS_2 conduction band [3,4]. P-type doping is required for efficient hole injection, in order to obtain the complementary inversion mode p-channel FETs.
Among the processes allowing the observation of p-type current transport in multilayer MoS_2 transistors, O_2 plasma functionalization of MoS_2 in the source and drain regions seems to be one of the most effective technique. A thorough investigation of the effect of plasma on the material has been performed at atomic scale through energy loss spectroscopy (EELS) coupled with atomic resolution scanning transmission electron microscopy (STEM), and a systematic study of the Mo $M_{3,2}$ excitation edges has been performed starting from pristine MoS_2 going toward the fully oxidized MoO_3 and passing by MoS_xO_y. All the experimental data have been acquired at high energy resolution with our GIF Quantum EELS spectrometer, installed on probe corrected JEOL ARM200F, combined with the simultaneous acquisition, in Dual EELS mode of low energy loss and high energy loss spectra acquired from the same regions in order to have a precise measurement on the edge onset [5]. These data have been then compared with ab-initio simulations, allowing us to clarify the role of O_2 plasma induced modification of the MoS_2 topmost layers on the observed p-type behaviour of the MoS_2 transistors.

References

[1] B. Radisavljevic, et al., Nat. Nanotechnol. 6, 147 (2011).
[2] S. Kim, et al., Nat. Commun. 3, 1011 (2012).
[3] S. Das, et al., Nano Lett. 13, 100 (2013).
[4] F. Giannazzo, et al., Phys. Rev. B 92, 081307(R) (2015).
[5] F. Fabbri, G. Nicotra et al., Nat Commun. 2016; 7: 13044.

EELS analysis of rare earth elements in geological samples

T. Dennenwaldt[1], H. Piet[1,2], J. Badro[2,3], and C. Hébert[1]

[1]Electron Spectrometry and Microscopy Laboratory, Institute of Physics and Interdisciplinary Center for Electron Microscopy, Ecole Polytechnique Fédérale de Lausanne, Lausanne, Switzerland
[2] Earth and Planetary Science Laboratory, Institute of Physics, Ecole Polytechnique Fédérale de Lausanne, Lausanne, Switzerland
[3]Institut de Physique du Globe de Paris, Sorbonne Paris Cité, Paris, France

Determining the Nd/Sm and Lu/Hf ratios in Earth's lower mantle is essential to understand the differentiation processes that took place in the early molten Earth and gave rise to the modern mantle [1]. The lower mantle is composed of the minerals calcium perovskite (CaPv, $CaSiO_3$), bridgmanite (Brg, $(Mg,Fe)SiO_3$) and ferropericlase (Fp, (Mg,Fe)O). Samples consisting of CaPv, Brg and Fp mineral assemblage have been previously synthesized from a rare earth doped glass of pyrolite composition (the average composition of Earth's mantle) in the laser heated diamond anvil cell [2]. EDX and EELS (FIG. 1) in the TEM are used to determine the partitioning of the rare earth elements in the different minerals. Phase identification is done by EDX analysis while the precise ratio studies are performed with EELS. Combining both techniques allows a reliable quantification of Nd, Sm, Lu and Hf in the synthesized minerals. Things to take care of during acquisition are e.g. beam damage of the material. EELS analysis of the CaPv, Brg and Fp phases synthesized at different temperatures and pressures prepared by FIB sectioning will be discussed.

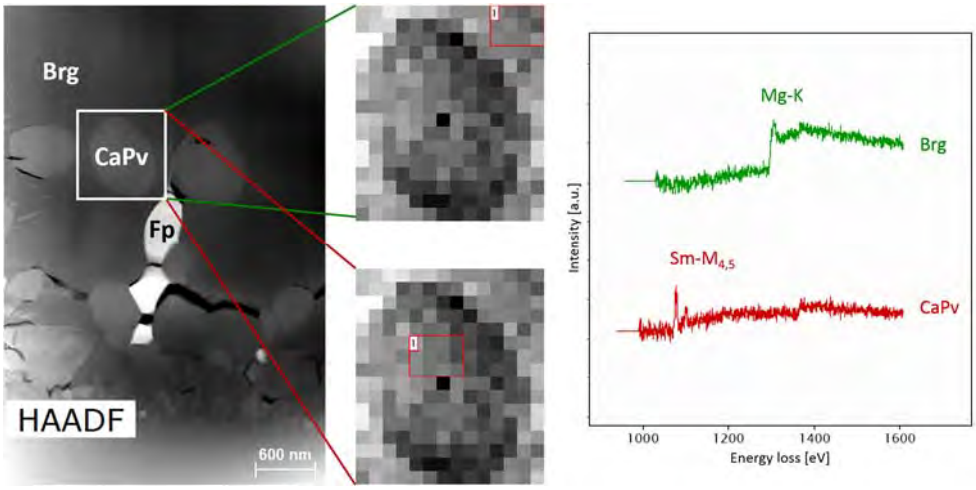

FIG. 1. HAADF image (left) showing the three phases CaPv, Brg and Fp, SI of a CaPv grain surrounded by the Brg matrix (middle) and corresponding EEL spectra (right) showing Sm only in the CaPv grain.

References
[1] M.J. Walter, R.G. Trønnes, *Earth Planet. Sci. Lett.* 225 (2004) 253.
[2] A.E. Ringwood, *J. Geophys. Res.* 67 (1962) 857.

Study on the atomic and electronic structure in CrN/AlN multilayers

Z.L. Zhang [1], X. Gu[1], D. Holec[2], M. Bartosik[3], and P. H. Mayrhofer[3],

[1] Erich Schmid Institute of Materials Science, Austrian Academy of Sciences, Leoben, 8700, Austria

[2]Department of Physical Metallurgy and Materials Testing, Montanuniversität Leoben, 8700, Austria

[3] Institute of Materials Science and Technology, TU Wien, Vienna,1060, Austria

CrN/AlN multilayers have been shown to exhibit a peak in hardness of ～40 GPa and simultanously a low friction coefficient as a function of the bilayer period (Λ). These improvements in mechanical properties have a close relationship with the existence of a metastable face-centered cubic (*fcc*) AlN phase which can be epitaxially stabilized in thin films. Consequently, new physical phenomena and exciting material properties may be introduced by interfaces present in multilayers.
Here, interplanar spacing oscillations in cubic CrN/AlN multilayers were experimentally observed by using spherical aberration-corrected high-resolution transmission electron microscopy (HRTEM), and were corroborated by first principles calculations. These oscillations are closely related to changes in the electronic structure. Electron spectroscopy and microscopy were employed to analyse the strain distribution in the multilayers and obtain generalized relationships between the electronic structure on the one hand, and (non-)stoichiometry or strains in the strained multilayers on the other hand. , These observations were successfully interpreted by means of theoretical calculations. The present study provides atomic-scale insights in the mechanisms of extraordinary strength pertaining to the CrN/AlN multilayers.

Surface probing of oxide catalysts, theory and experiment

V. Tileli[1], E. A. Ahmad[2], G. Mallia[2], R. Webster[2], K. Stoerzinger[3], Y. Shao-Horn[3], & N. M. Harrison[2]

[1]École polytechnique fédérale de Lausanne, 1015 Lausanne,Switzerland
[2]Department of Chemistry, Imperial College, Exhibition Road, SW7 2AZ London UK
[3]Department of Materials Science and Engineering, Massachusetts Institute of Technology, Cambridge, Massachusetts 02139, United States

Oxide particles are catalytic for the oxygen reduction reaction in fuel cells and they are considered a promising candidate for replacing the costly metallic catalysts [1,2]. The performance of such catalysts depends primarily on the structural and chemical character of their surface terminations. Evaluating the structure and chemistry at surfaces on the atomic scale is a challenging task; however, recent advancements of aberration corrected transmission electron microscopy (TEM) instruments have allowed spatial identification of all atomic species in a material with a precision of a few picometers, interpreted with comparison to multislice simulations of the projected atomic structure, while acquiring high energy resolution electron energy-loss spectra (EELS), which can be interpreted with density functional theory (DFT) calculations.

Pristine $LaMnO_3$ particles have been structurally characterized. The results verify the existence of the (100), (001), (010) and (011) Pnma surfaces in powder samples. Theoretical Wulff plots predict the latter two of these are polar surfaces that require reconstruction. Furthermore, optical matrix elements calculations predict a combination of coordination and valence state profile along the surfaces [3,4,5]. To unambiguously determine the surface states, spectra with high-energy resolution and in dual EELS mode were acquire and fitted to the DFT calculations. The results reveal that the oxygen pre-peak is associated with electron exchange between oxygen and manganese and the shift of the Mn L_3 edge can be attributed to two possible scenarios: a reduction of the surface (to Mn^{2+}) and/or a coordination reduction at the surface, which would lead to a reconstructed surface. The discussion focuses on the ability of evaluating active surface sites of catalytic oxide structures using advanced TEM methods combined with DFT calculations.

References

[1] J. Suntivich, H. A. Gasteiger, N. Yabuuchi, H. Nakanishi, J. B. Goodenough, and Y. Shao-Horn, *Nature Chemistry* 3 (2011) 546.
[2] B. Han,K.A. Stoerzinger, V. Tileli, A.D. Gamalski, E.A. Stach & Y. Shao-Horn, *Nature Materials*16 (2017)121
[3] E. A. Ahmad, V. Tileli, D. Kramer, G. Mallia, K. A. Stoerzinger, Y. Shao-Horn, A. R. Kucernak,and N. M. Harrison, *Journal of Physical Chemistry C* 119 (2015) 16804.
[4] H. Tan, S. Turner, E. Yucelen, J. Verbeeck, and G. Van Tendeloo, *Physics Review Letters* 107 (2011) 107602.
[5] E. A. Ahmad, G. Mallia, D. Kramer, V. Tileli, A. R. Kucernak, and N. M. Harrison, *Physics Review Letters* 108 (2012) 259701.

Probing the local electronic configurations in original tubular thermoelectric cobaltates

L. Bocher, D. Pelloquin[2], S. Hébert[2], O. Stéphan[1], and A. Gloter[1]

[1] Laboratoire de Physique des Solides, Univ. Paris-Sud, Université Paris-Saclay, CNRS, 91405 Orsay, France
[2] Laboratoire CRISMAT, ENSICAEN, CNRS, Caen, France

As in all complex oxides, a strong interplay exists in Co-based systems between their lattice, spin, charge, and orbital degrees of freedom; this being a driving force to control their electronic and magnetic interactions. In Co-misfit layers, the CoO_2 hexagonal layers turn out to be at the origin of their metallicity combined with a large thermopower yielding promising thermoelectric (TE) properties. Here, $[Bi_2Sr_2CoO_6]_n[Sr_8Co_6O_{16-\delta}]$ phase reveals an original 2D tubular structure composed of two sub-lattices interconnected through oxygen-deficient CoO_x pillars (Fig. a) and b). This complex network has the ability to accommodate a certain structural and chemical flexibility by tuning locally its oxygen stoichiometry and therefore modulates its charge carriers' concentration. Hence, peculiar TE and magnetic properties were achieved with large oxygen stoichiometry changes. However the key-role played by each Co sites on the local electronic structures remains unresolved to date.

Constant and recent advances in electron spectromicroscopy techniques enable us nowadays to explore precisely the atomic and electronic structures in these low dimensional oxide systems. Here we used a Cs-corrected STEM – NION UltraSTEM 200 – fitted with EELS with a very high sensitivity optic system for tracking the subtle evolution in the Co-$L_{2,3}$ and O-K near-edge fine-structures. We probe the effect of electronic charge transfer on individual Co atomic columns (Fig. e). Using advanced post-treatment analysis on non-monochromated data, we map further their two distinct electronic configurations corresponding to the direct visualisation of the Co charge modulation (Fig c) and d).

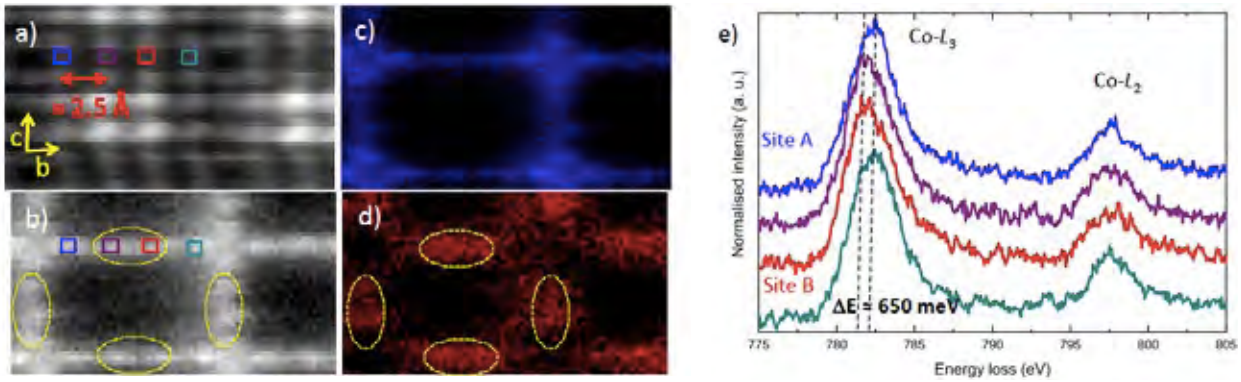

FIG. Local charge modulations in Bi-Sr-Co-O phase a) HAADF intensity and b) Co-L_3 maps, c) higher- and d) lower-energy component maps from vertex component analysis, and e) raw EELS Co-$L_{2,3}$ spectra probed at different atomic sites.

[1] D. Pelloquin et al., *J. Sol. St. Chem.* 148 (1999) 108.
[2] This research was supported by the French microscopy METSA network and the INSIS Energie CNRS department

Linear plasmonic resonators

W. Sigle[1], I. Schubert[2], N. Talebi[1], S. Guo[1], E. Toimil-Molares[2], R. Vogelgesang[3], M. Esmann[3], S. F. Becker[3], C. Lienau[3], P. A. van Aken[1]

[1] Max Planck Institute for Solid State Research, D-70569 Stuttgart, Germany.
[2] Materials Research Department, GSI Helmholtz Center for Heavy Ion Research, D-64281 Darmstadt, Germany
[3] Carl von Ossietzky University, D-26129 Oldenburg, Germany

Linear plasmonic resonators are of potential interest as antennas or waveguides in future optoelectronic circuits. The special case of tapered structures has applications in apertureless near-field optical microscopy and tip-enhanced Raman scattering. Low-loss EELS has become a major tool to study the plasmonic response of such nanostructures. Here we summarize EELS results obtained on nanorods [1], including coupling phenomena [2], and nanotapers [3, 4].
Figure 1 shows the variation of the plasmonic response of a Au nanotaper, showing different modes shifting in energy with distance from the apex.

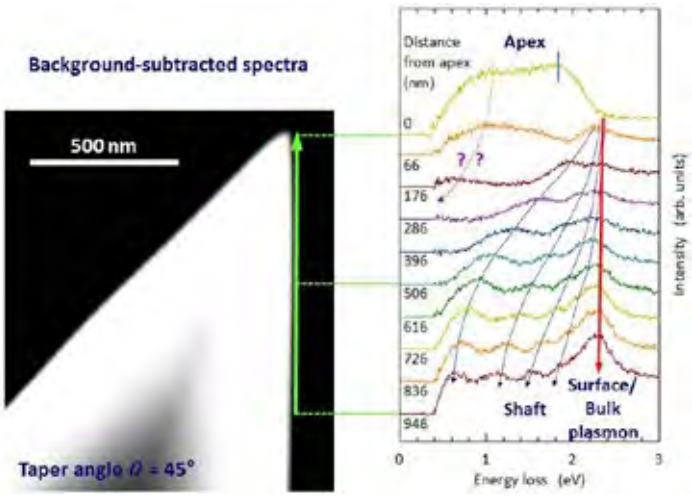

FIG. 1. HAADF image of a gold taper with an opening angle of 45°and the corresponding zero-loss-corrected energy-loss intensity as a function of impact location along the taper shaft.

References
[1] I. Alber et al., *ACS Nano* 5 (2011) 9845.
[2] I. Alber et al., *ACS Nano* 6 (2012) 9711.
[3] N. Talebi et al., *ACS Nano* 9 (2015) 7641.
[4] S. Guo et al., *Nano Letters* 16 (2016) 6137.

Atomic-scale interactions of hydrogen with Aluminum nanoparticles at room temperature

Canhui Wang[1,2], Wei-Chang Yang[1,2], Devika Sil[1,2], Amit Agrawal[1,2], and Renu Sharma[1*]

[1] Center for Nanoscale Science and Technology, National Institute of Standards and Technology, Gaithersburg, MD 20899 (USA)
[2] Maryland NanoCenter, University of Maryland, College Park, MD 20742 (USA)

Recently, optical methods have been used to show that hot electrons generated by surface plasmons can trigger various chemical reactions at room temperature. [1-2] Understanding the reactions promoted by localized surface plasmon resonance (LSPR) is important for designing efficient catalytic systems for a wide range of applications. However, a number of important questions related to this type of reaction processes remain unclear due to the complexity of the reaction kinetics, and lack of spatial resolution available with optical methods. The complexity arises from the dynamic interplay between the nanoparticle and the reactive environment. For instance, gas absorption on the surfaces of the nanoparticles affects the free energy of the exposed surfaces and can lead to morphological change or surface oscillations in nanoparticles. [3, 4] Since the LSPR is known to strongly depend on size, shape and dielectric environment of the particles, any change in either of them will also affect the spatial distribution of intensity and energy of the LSPR. Therefore, one of the fundamental questions that needs to be answered is how the change in the particle morphology (shape) or dielectric environment, during photocatalytic reactions may affect the spatial distribution of LSPR profile on the nanoparticles and if that can be correlated with the locations where each reaction step occurs.
In light of the complexity of the reaction process, we combined an ensemble of techniques to characterize LSPR-promoted chemical reactions at high resolution using an environmental transmission electron microscope with monochromated electron source. In particular, we focus on the LSPR promoted dissociation of hydrogen using Al nanoparticles. Atomic resolution movies and time-resolved electron energy-loss spectra (EELS) are acquired to monitor the crystallographic and chemical change in the particle as well as LSPR locations and shifts during the reaction. Under gaseous environments we observe structure and oscillatory morphological changes in the Al nanoparticle. EELS imaging, with different energy dispersions, is used to acquire both elemental and LSPR maps from the same particle. These combined spectrum images show correlations between the LSPR profile and the morphology of different compounds in the nanoparticle. The comparison between the EELS maps, before and after H_2 is introduced, also show the effect of the gaseous environment on the LSPR generated on the nanoparticle surface locally, reveling selective gas adsorption sites. This combined approach to decipher LSPR-promoted reactions provides time-resolved, atomic-scale information on the reaction kinetics and improves the understanding of the dynamics of LSPR promoted reactions.

References

[1] Sil, Devika, et al. ACS Nano **8(8)**, 7755-7762 (2014).
[2] Zhou, Linan, et al. Nano Lett. **16(2)**, 1478-1484 (2016).
[3] Thomann, Isabell, et al. Nano Lett. **11(8)**:3440-3446 (2011).
[4] Nelayah, Jaysen, et al. Nature Physics, **3(5)**, pp.348-353 (2007).

Room Temperature CO Dissociation on Selective Edges of Gold Nanoparticles

W.D. Yang[1,2], C. Wang[1,2], and R. Sharma[1]

[1] Center for Nanoscale Science and Technology, National Institute of Standards and Technology, Gaithersburg, Maryland 20899 (USA)
[2] Maryland NanoCenter, University of Maryland, College Park, MD 20742 (USA)

Au nanoparticles on oxide supports have drawn great interest as catalyst because of their potential for low-temperature CO oxidation.[1] Both experimental and theoretical results have suggested that adsorption of CO molecules on the Au surface and the resulting catalytic activity are affected by the coordination number of the Au atoms.[1] However, direct evidence for the location of the CO-absorbing sites on the nanoparticle surface, which may be the catalytically active sites, is missing.
In the present work, we take advantage of the plasmonic behavior of Au nanoparticles to measure the energy shifts in localized surface plasmon resonance (LSPR) energy as a function of gas environment, using an environmental scanning transmission electron microscope equipped with a monochromated field-emission gun. We use high energy and spatial resolution electron energy loss spectrum (EELS) imaging to map the LSPR intensities (Fig. 1a) and to identify the location of CO adsorption on a triangular Au nanoparticle, as indicated by the spectral shift of the LSPR peak.[2] The LSPR peak (Fig. 1b) manifested a blue-shift (≈ 0.05 eV) in a CO environment with respect to vacuum at the side of Au triangular nanoparticle. The side consisted of the {311} planes of Au, as identified from the diffraction data collected by tilting the particle. The subsequent core-loss EELS revealed the C K-edge (Fig. 1c) to be associated with amorphous carbon that deposited at the same location (Fig. 1d). We believe that our results can be compared with the recently-reported dissociation of H_2, facilitated by the hot electrons generated from the non-radiative decay of LSPRs.[3] Similarly to H_2, the dissociation energies of CO molecules may be lowered as a result of CO adsorption on selective surfaces/ledges as reported for Fe {100} surfaces.[4] Therefore, the locations that are selective for amorphous carbon deposition may correspond to active sites that display decreased dissociation barriers and enable the hot electron transfer.

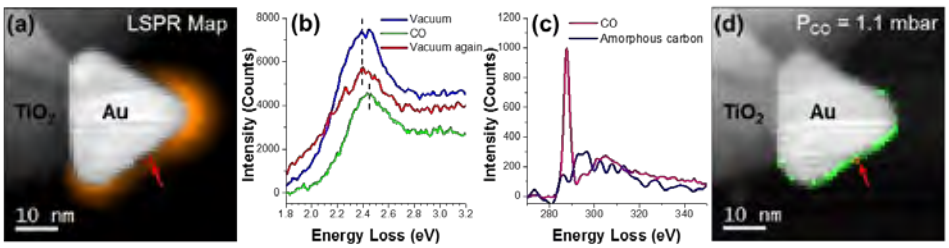

FIG. 1. a) LSPR map (orange) overlaid with the ADF image of Au/TiO2 catalyst in vacuum, b) low-loss spectra of LSPR in vacuum, CO environment and vacuum again, respectively, from the pixel denoted in a), c) core-loss spectra of CO background and deposited amorphous carbon, d) amorphous carbon map (green) overlaid with the ADF image of Au/TiO2 catalyst in CO environment.

References
[1] N. Lopez et al. *J. Catal.* 223 (2004) 232.
[2] G.M. Lari et al. *Phys. Chem. Chem. Phys.* 17 (2015) 23236.
[3] S. Mukherjee et al. *Nano Lett.* 13 (2012) 240.
[4] D.E. Jiang et al. *Surf. Sci.* 570 (2004) 167.

Effect of Ir doping at the $LaAlO_3/SrTiO_3$ interface studied by combined EELS and XPS analyses

M. Lee[1,2], B. Warot-Fonrose[1], R. Arras[1], M. Lippmaa[3], H. Daimon[2] and M.J. Casanove[1]

[1] CEMES, CNRS UPR 8011 and Université de Toulouse, 29 rue Jeanne Marvig 31055 Toulouse, France
[2] NAIST, 8916-5 Takayama, Ikoma 630-0192 Nara, Japan
[3] ISSP, 5-1-5 Kashiwanoha, Kashiwa 277-8581 Chiba, Japan

Oxide electronics has attracted intense attention recently due to the emergence of unexpected physical properties at their interfaces such as a metallic behavior at the $LaAlO_3/SrTiO_3$ (LAO/STO) interface [1]. The properties of this interface are known to be particularly sensitive to the presence of defects as oxygen vacancies or cations disorder. Here, we studied the effect of Ir doping at the n-type $(LaO)^{+1}/(TiO2)^{0}$ interface on the local crystal and electronic structures. Since the less localized nature of 5d orbitals will result in a smaller electron effective mass, potentially leading to a higher mobility, 5d transition metal doping near the interfacial region is indeed expected to tailor the electronic properties of LAO/STO heterostructures [2].
LAO layers, 4 to 5 unit cell thick, were grown by pulsed laser deposition (PLD) on TiO2 terminated STO substrates whose top layers (1 unit cell thick) were doped with 1 to 5% of Ir atoms, and compared to the non-doped LAO/STO interface. Owing to the strong localization of the doped-region and the low percentage of expected defects, both electron energy loss spectroscopy (EELS) and hard X-ray photoelectron spectroscopy (HAXPES) analyses were performed to probe the local variations of the electronic structure at the interface. The results are confronted with atomistic calculations and experimental analyses of a 5%Ir-doped STO layer grown on a STO substrate to help their interpretation.

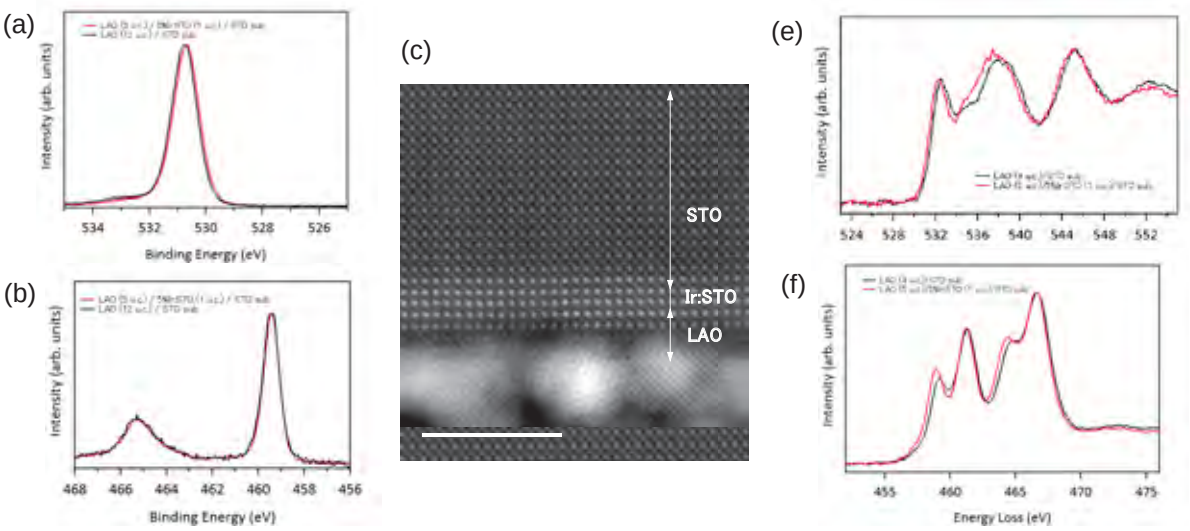

Fig.1 XPS spectra of (a)O 1s and (b) Ti 2p peaks, HAADF-STEM image of (c) Ir doped LAO/STO, EELS spectra of (d) O_K edge and (e) Ti_$L_{2,3}$ edges

References
[1] H. Y. Hwang et al., *Nature Materials.* 11 (2012) 103–113
[2] S. Nazir et al., *Phys.Chem.Chem.Phys*. 18(2016) 2379

Cryo-analytical STEM of dispersed nanoparticles

N. Hondow[1], O. Matar[1], A. Brown[1], and R. Brydson[1]

[1] School of Chemical and Process Engineering, University of Leeds, Leeds LS2 9JT, U.K.

There is the potential for the physicochemical properties of engineered nanoparticles to be exploited in numerous areas including medicine, catalysis, energy and the environment. While many techniques describe nanoparticles in the pristine state, characterisation of the same particles under actual conditions, *i.e.* dispersed at low concentrations in environmental or physiological media, is far more challenging. Conventional TEM, with samples prepared simply by drop casting enabling imaging and analysis of individual nanoparticles but, because of the drying process, does not capture the particle agglomeration in the dispersion or the surface chemistry when hydrated [1]. Alternatively, low dose electron microscopy of nanoparticles suspended in vitreous ice does provide the opportunity for the analysis of the structure and chemistry of the dispersion, both vital characteristics to understand before any successful exploitation of nanoparticles.

We will report on results from the recently installed FEI Titan^3 Themis 300 G2 S/TEM at the University of Leeds which is equipped with FEI SuperX EDX spectrometers, a Gatan Quantum ER imaging filter and Gatan OneView CCD to explore the limits of nanoparticle analysis using STEM-EDX and EELS when the particles are encased in vitreous ice (Fig. 1). Our goal is to identify and analyse the surface coatings on nanoparticles in the frozen hydrated state, thereby extending the capability of near native state imaging and analysis of nanoparticle systems by TEM.

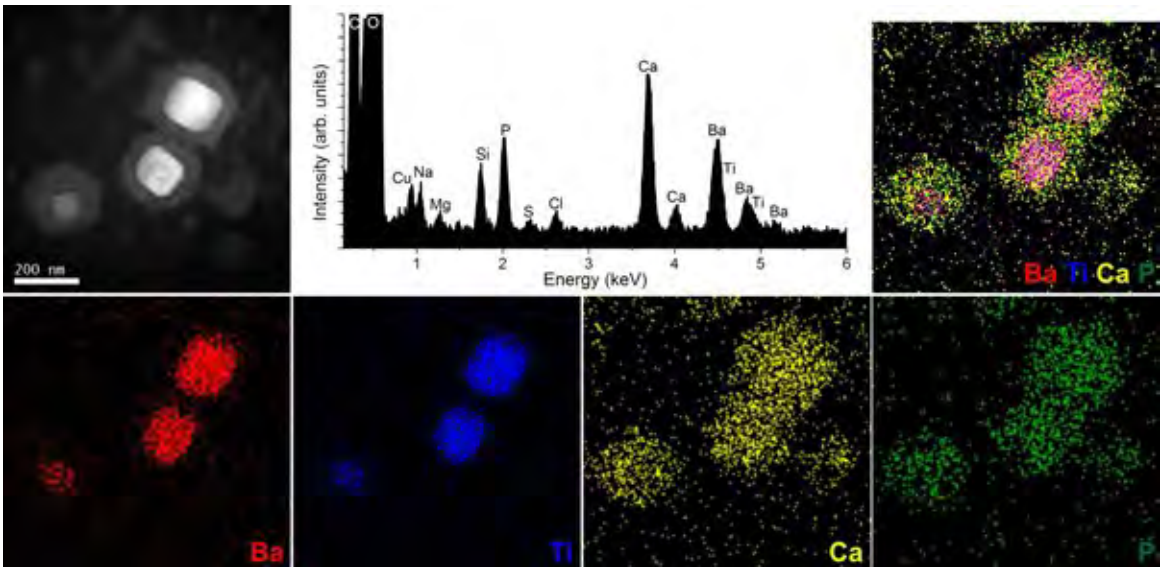

FIG. 1. Cryo-analytical STEM data of polymer coated $BaTiO_3$ nanoparticles dispersed in complete cell culture media, comprising HAADF STEM image, EDX spectrum from the region imaged and EDX maps for Ba *L*, Ti *K*, Ca *K* and P *L*. Note adsorption of Ca and P from the liquid medium onto the nanoparticle and polymer coating.

References

[1] N. Hondow et al., *J. Nanopart. Res.* 14 (2012) 977.

Grain boundary diffusion processed (Nd,HREs)-Fe-B magnets studied by combined STEM and quantitative EELS analysis

S. Šturm[1], K. Žužek-Rožman[1], F. Mehmood[1], A. Ikram[1], M. Soderžnik[1], S. Kobe[1]

[1] Jožef Stefan Institut, Ljubljana, 1000 Slovenia

Small amounts of heavy rare earths, HREs, (Dy,Tb) that partially replace the Nd, typically introduced from the surface of already fully sintered Nd-Fe-B magnet by being exposed to elevated temperatures allowing HRE's to diffuse into the interior of the magnet, have a large, positive influence on the coercivity of the Nd-Fe-B-based magnet. This is mainly attributed to the formation of core-shell grains with a $(Nd_{1-x},(HRE)_x)_2Fe_{14}B$ containing shell and a $Nd_2F_{14}B$ core, where the shell, with its higher anisotropy field resulting from the HRE, hinders magnetisation reversal at the grain edges and leads to an increase in the coercivity of the magnet [1]. In this study the concentration gradient of HREs was indirectly confirmed by measuring the magnetic properties of thin slices, which were cut parallel to one of the magnet surface. It was found that the coercivity measured from the slice cut from the very central region of the magnet is still around 30% higher when compared with the untreated magnet. Although magnetic measurements clearly indicate the presence of HREs, it is not entirely clear what are the underlying phenomena that control the increase of coercivity in relation to the spatial distribution of HREs, typically located at the grain boundaries, within triple pocket phases and the HRE-rich shells. For that purpose, a combined TEM and STEM/EELS study was performed on HRE-rich Nd-Fe-B magnets. The quantitative EELS analyses obtained from the surface regions of the magnet reveals $(Nd_{0.7},Tb_{0.3})_2Fe_{14}B$ crystal grains where Tb is homogeneously distributed within the bulk matrix. Below that region HREs are concentrated at the grain boundaries, triple pockets and within the shell of the $Nd_2Fe_{14}B$ matrix grains, while in the central regions of the magnet the majority of HREs is mainly found at grain boundaries. Figure 1 shows a representative core-shell $Nd_2Fe_{14}B$ matrix grains, combined with the element concentration profiles acquired across the core-shell region. In conclusion, this study allows us to properly correlate the spatial distribution of HRE-rich phases in the microstructure with the resulting coercivity values of individual magnet slices.

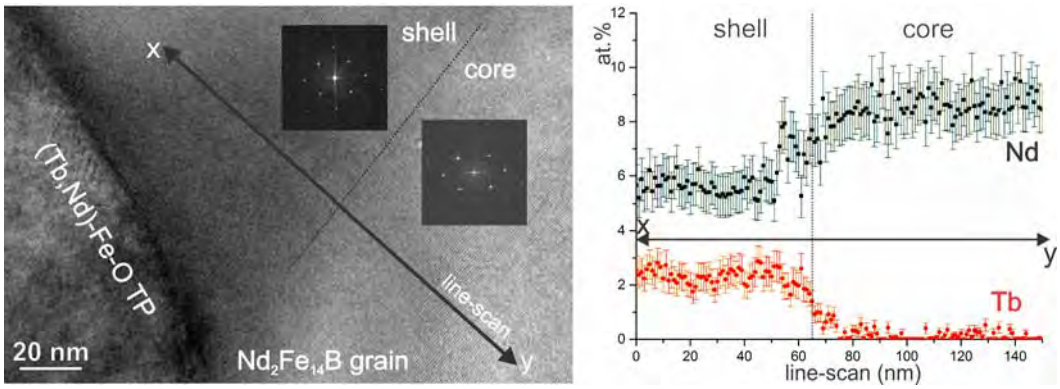

FIG. 1. Core-shell $Nd_2Fe_{14}B$ grain and related element concentration line scans

References
[1] H. Nakamura, et al., *IEEE transactions on magnetics* (2005): 3844-3846.
[2] We acknowledge Horizon 2020 EU project DEMETER (GA No. 674973).

Fundamental insights into the operation of new non-volative memory devices using in-situ and monochromated STEM-EELS

N. Bernier[1,2], V. Delaye[1,2], D. Cooper[1,2], T. Dewolf[1,2], E. McDermott[1,2], R. Berthier[1,2], and G. Audoit[1,2]

[1] University Grenoble Alpes, 38000 Grenoble, France
[2] CEA, LETI, MINATEC Campus, 17 rue des Martyrs, 38054 Grenoble, France

New generations of high-performance and low-cost non-volatile memories are being developed by the semiconductor industry. We show in this presentation how fundamental insights about the operation of these devices has been obtained from EELS analyses on two emerging types of random access memories (RAM): phase-change RAM (PCRAM) and oxide-based resistive RAM (OxRRAM).
The switching processes from low (LRS) to high resistive states (HRS) in OxRRAM remain poorly understood, especially due to the difficulty in revealing small variations of electronic and chemical structure. Moreover, an ex-situ analysis implies changes in specimen preparation and experimental procedure that make the interpretation of analytical data ambiguous. Here, we use in-situ atomic resolution STEM-EELS to characterize the active region in the same device in both resistance states as the device is reversibly switched confirming that the changes are due to electrical switching and not only joule heating (Fig. 1). As a consequence, the fundamental redox processes underlying the resistive switching has been unveiled [1]. In the case of HfO_2 based OxRRAM, we will show how the fine structure analysis of monochromated EEL spectra on in-situ annealed TiN/HfO_2/Ti stacks can bring useful information. The last part of our presentation will be devoted to PCRAM that exhibit fast and reversible phase transformations between crystalline and amorphous states [2]. This work is financially supported by the “Recherche Technologique de Base”, with experiments performed on the Nanocharacterisation platform at MINATEC Campus.

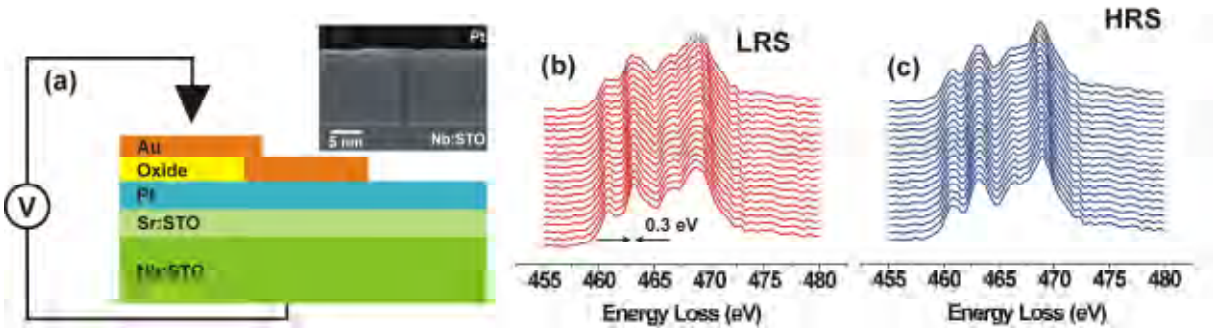

FIG. 1. (a) Schematic of the device with the electrical contact. Inset: High-resolution ADF STEM image of the region of interest in the LRS. Ti L-edge EEL spectra in the (b) LRS and (c) HRS. The spectra were acquired across the Sr:$SrTiO_3$ film in 1.2 nm steps along the purple dotted line shown in the inset of (a). Changes in the Ti spectra caused by the movement of oxygen vacancies can be observed in the LRS at the Pt/STO interface. From this information we were able to directly determine that the switching mechanism was due to area switching and not a localized filament.

References

[1] D. Cooper et al., *submitted to Advanced Materials*.
[2] P. Noe et al., Acta Mater. 110 (2016) 142.

Advanced STEM-EELS for nanotechnology and renewable energy research and development

V. Delaye[1,2] , N. Bernier[1,2]

[1] University Grenoble Alpes, 38000 Grenoble, France
[2] CEA, LETI, MINATEC Campus, 17 rue des Martyrs, 38054 Grenoble, France

In this presentation we will present several examples of how advanced STEM-EELS characterizations is being used to meet the current needs of nanotechnology and renewable energy research and development. Random dopant fluctuations, as an intrinsic source of variability in CMOS transistor performance, remains a serious concern for integrated circuits. Low loss EELS, through the shift of the volume plasmon peak energy, can be used to measure the local dopant concentration [1]. For the first time, we explain here how this technique can be successfully applied to crystalline silicon for detecting active boron atoms. We show how the optimization of energy filter settings and plasmon peak fitting methods on EELS data-cube acquired at 80 kV allows to reach a boron sensitivity level down to $5x10^{19}$ at.cm^{-3}. Furthermore, new applications in microelectronics need the integration of high capacitance devices. HfO_2/Al_2O_3 nanolaminate is a promising high permittivity dielectric, but elemental segregation due to post-deposition annealing may significantly increase the capacitor current leakage. We implemented advanced algorithms, including Vertex Component Analysis (VCA) [2], to decompose the experimental spectrum images (SI), and we will demonstrate that they offer a reliable, user-independent method to address this issue, especially in revealing elemental diffusion at a nanometer scale. Finally, we show how the fabrication of heterojunction (HET) solar cells is supported by STEM-EELS analyses in order to continuously increase the conversion efficiency. In particular, a sample from a "failing" cell was prepared by FIB, but standard analytical STEM analyses failed to reveal any defect. Then a dual EELS profile on a Cs image and probe corrected TEM was acquired, at the interface between amorphous silicon (a-Si) and indium-tin oxide (ITO), in order to measure accurately the oxygen-K edge onset position. The energy shift of this position allowed to identify and measure a silicon oxide layer explaining finally the defectivity of the cell (c.f. FIG. 1.).

This work is financially supported by the “Recherche Technologique de Base”, with experiments performed on the Nanocharacterisation platform at MINATEC Campus.

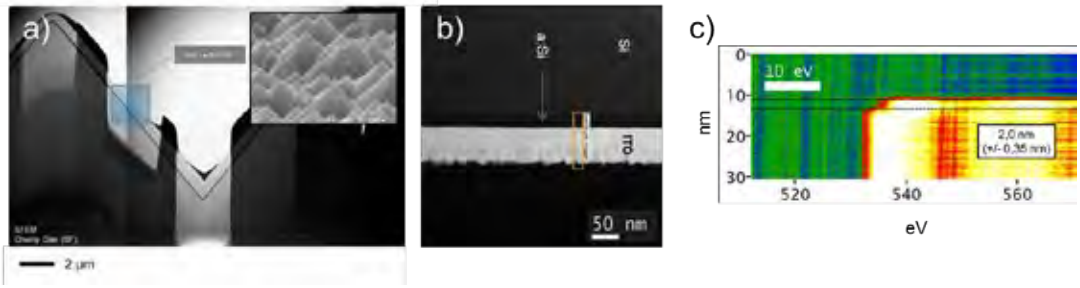

FIG. 1. (a) STEM Bright Field overview of the HET specimen (b) STEM HAADF image, of from top to down : c-Si, a-Si, ITO and capping layer (c) Oxygen K edge profile along the profile at the a-Si ITO interface revealing silicon oxide layer.

References

[1] M. Duchamp et al., J Appl Ph, 113 (2013) 093513.
[2] N. Dobigeon et al., Ultramicroscopy 120 (2012) 25.

STEM investigation of charge and strain distributions at the ferroelectric – doped Mott insulator interfaces

X. Li[1], V. Garcia[2], M. Marinova[1,3], J. Rault[4], A. Barthélémy[2], M. Bibes[2], O. Stéphan[1], C. Colliex[1], A. Gloter[1]

[1] Laboratoire de Physique des Solides, CNRS UMR 8502, Université Paris Sud XI, 91405 Orsay, France.
[2] Thales Research and Technology, Campus de l'Ecole Polytechnique, 1 Avenue A. Fresnel, 91767 Palaiseau, France.
[3] Institut Eugène Chevreul – Université Lille1, 59655 Villeneuve d'Ascq, France.
[4] Synchrotron-SOLEIL, BP 48, Saint-Aubin, F91192 Gif sur Yvette CEDEX, France

The electric field control of functional properties is an important goal in oxide-based electronics. Recently, ferroelectric $BiFeO_3$ (BFO) has been used to obtain a ferroelectric gating in perovskite heterostructures combined with a doped Mott insulator channel ($CaMnO_3$, CMO) [1]. Ferroelectric tunnel junctions based on ultrathin films of BFO sandwiched between CMO and electrodes have also exhibit giant electroresistance [2]. These physical properties strongly depend on the strain and charge distribution in these devices. In this work, we report that charge distribution next to the BFO/CMO interface is highly inhomogeneous by combining grazing-incidence hard x-ray photoemission spectroscopy and STEM-EELS measurements (Fig 1, [3]). Typical sheet carrier densities in the range of 10^{14} cm^{-2} are obtained by EELS that are in line with Hall effect measurements but lower than expected to screen the BFO ferroelectric polarization. Ab-initio modeling concludes of the crucial role of plane termination. The structure of ferroelectric domains in the BFO thin films will also be discussed with respect to the charge in the CMO channel. In particular, BFO structures for different polarization states switched by applying an electric field before the sample preparation for STEM observation will be discussed.

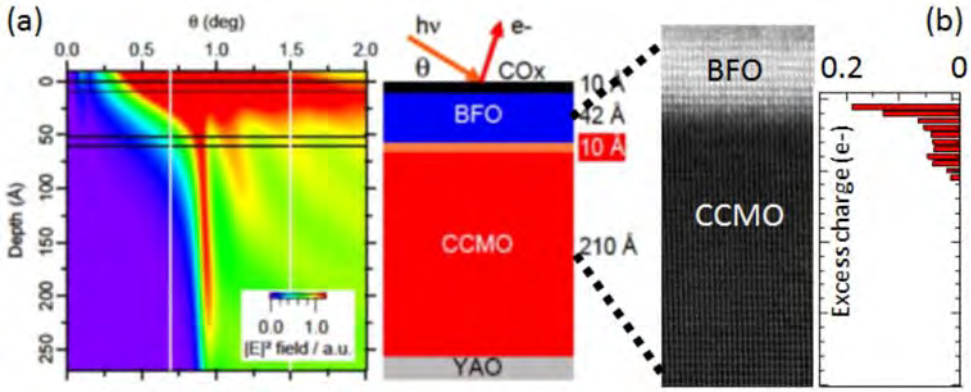

Fig 1. a) Calculation of the depth-resolved electric field strength $|E|^2$ as a function of depth and photon incidence angle. This demonstrates that changing the incidence angle permits selectively probing different depth with photo-emission. b) Excess charge per unit cell at the interface between the CMO and the BFO as measured by STEM-EELS.

[1]Yamada H., Marinova M. et al., *Ferroelectric control of a Mott insulator*, **Scientific Reports** 3, 2834 (2013).
[2] Yamada H., Garcia V. et al., *Giant Electroresistance of Super-tetragonal BiFeO3-Based Ferroelectric Tunnel Junctions*, **ACS Nano** 7, 5385-5390, (2013).
[3] M. Marinova, J. E. Rault, A. Gloter et al., *Depth profiling charge accumulation from a ferroelectric into a doped Mott insulator*, **Nano letters** 15, 2533–2541 (2015).

STEM and EELS investigation of graphene nanoribbon epitaxially grown over SiC

A. Gloter[1], I. Palacio[2], A. Celis[3], M. Nair[2], A. Zobelli[1],M. Sicot[4], D. Malterre[4], C. Berger[5], W. de Heer[5], E. Conrad[5], A. Taleb-Ibrahimi[1], A. Tejeda[1]

[1]Laboratoire de Physique des Solides, CNRS UMR 8502, F-91405 Orsay, France,
[2]UR1 CNRS/Synchrotron SOLEIL, Saint-Aubin, 91192 Gif sur Yvette, France,
[3]Synchrotron SOLEIL, Saint-Aubin, 91192 Gif sur Yvette, France,
[4]Université de Lorraine, UMR CNRS 7198, Institut Jean Lamour, BP 70239, F-54506 Vandoeuvre-lès-Nancy, France,
[5]School of Physics, The Georgia Institute of Technology, Atlanta, Georgia 30332-0430, USA

Graphene nanoribbons grown on the (1-10n) and (-110n) facets of SiC have demonstrated exceptional electronic properties as ballistic transport along their long direction and a band gap in the small direction [1]. In order to understand these electronic properties, we have performed (S)TEM (HAADF, LAADF, ABF, EELS) investigation in combination with STM and ARPES measurements. The (S)TEM have been performed on X-section sample. Using Cs corrected STEM at 60 keV voltage, the structural aspect of the graphene can be maintained for high resolution investigation and EELS spectromicroscopy. In particular we will describe the origin of the metal-semiconductor junction as observed in these graphene [2] and this will be discussed in term of interaction with the substrate and quantum confinement on a complex reconstructed step as presented in figure 1 [3].

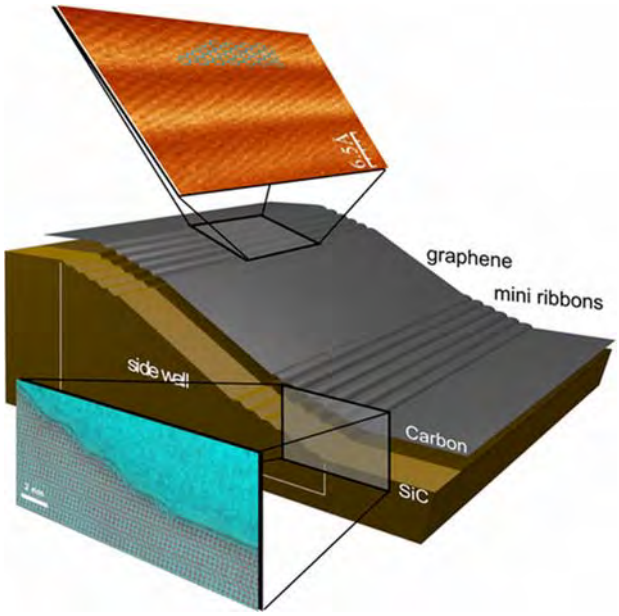

Fig. 1: combination of a STEM-ABF image (cyan) and a STM image (orange) on the graphene nano-ribbon grown over SiC. The obtained overall structure of the graphene has be sketched. STEM-EELS C-K edges have also been obtained at the scale of the carbon monolayer and evidence local changes of the C-K edges due to band gap opening and interaction with the substrate [3].

[1] J. Baringhaus, M. Ruan, F. Edler, A. Tejeda, M. Sicot, A. Taleb-Ibrahimi, A.-P. Li, Z. Jiang, E.H. Conrad, C. Berger, C. Tegenkamp, and W.A. de Heer, **Nature** 506, 349 (2014).
[2] J. Hicks, A. Tejeda, A. Taleb-Ibrahimi, M.S. Nevius, F. Wang, K. Shepperd, J. Palmer, F. Bertran, P. Le Fèvre, J. Kunc, W. de Heer, C. Berger, E. Conrad, **Nature Physics** 9, 49 (2013).
[3] I. Palacio, A. Celis, M. Nair, A. Gloter, A. Zobelli, M. Sicot, D. Malterre, M. Nevius, W. de Heer, C. Berger, E. Conrad, A. Taleb-Ibrahimi and A. Tejeda, **Nano letters** 15, 182-189 (2015).

Mapping of Local Bonding States at Intact Solid-Liquid Interfaces Enabled by Cryo-FIB Lift-Out and Cryo-STEM EELS

M.J. Zachman[1], Z. Tu[2], L.A. Archer[2,3], and L.F. Kourkoutis[1,4]

[1] School of Applied and Engineering Physics, Cornell University, Ithaca, NY, 14853, USA
[2] Department of Materials Science and Engineering, Cornell University, Ithaca, NY, 14853, USA
[3] School of Chemical and Biomolecular Engineering, Cornell University, Ithaca, NY, 14853, USA
[4] Kavli Institute at Cornell for Nanoscale Science, Cornell University, Ithaca, NY, 14853, USA

Solid-liquid interfaces play a critical role in a range of biological, chemical, and physical processes, but often lack high-resolution characterization. One example is lithium metal batteries (LMBs), which offer ten times the anode storage capacity of lithium-ion batteries, but suffer from significant capacity fade and safety hazards due to two processes that occur at the anode-electrolyte interface [1]. These processes, breakdown of electrolyte to form a "solid-electrolyte interphase" (SEI) layer and uneven deposition of lithium metal leading to dendrite growth, are highly interrelated [2]. Understanding the formation and composition of nanoscale SEI layers in their native environment is therefore critical to controlling these processes.

Here, we demonstrate the unique ability of cryo-STEM EELS to provide high-resolution elemental and local bonding state information about intact solid-liquid interfaces. To do this, we prepare electron transparent cross-sections of intact interfaces from cycled LMBs by cryo-focused ion beam (cryo-FIB) lift-out [3]. Using cryo-STEM EELS in combination with multivariate curve resolution (MCR) we then directly track local bonding states at the anode-electrolyte and dendrite-electrolyte interfaces. This provides the first nanoscale compositional information about intact SEI layers in LMBs (Fig. 1), leading to new insights into SEI and dendrite formation.

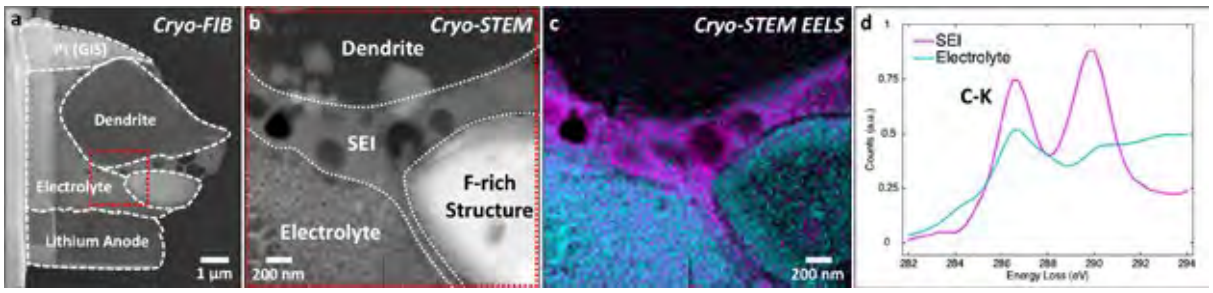

FIG. 1. Mapping of the local carbon bonding state across an intact solid-liquid interface at the surface of a dendrite in a lithium metal battery (LMB). LMB coin cells were opened and snap frozen to preserve the electrolyte, and (a) cryo-focused ion beam (cryo-FIB) lift-out was then used to prepare electron transparent cross-sections of intact anode-electrolyte and dendrite-electrolyte interfaces for cryo-STEM. (b) Nanoscale dark-field STEM imaging revealed a thick SEI layer at the dendrite-electrolyte interface. (c) Carbon EELS mapping and multivariate curve resolution (MCR) analysis clearly resolved two spectral components largely segregated in the electrolyte and SEI, with distinct local bonding environments (d).

[1] J.-M. Tarascon & M. Armand, *Nature* 414 (2001) 359.
[2] X.-B. Cheng *et al.*, *Adv. Sci.* 5 (2015) 1500213.
[3] M.J. Zachman *et al.*, *Microsc. Microanal.* 22 (2016) 1338.

The intermediate phase in Li-ion battery cathode material $Li_{1-x}FePO_4$ investigated by valence electron energy loss spectra

S. Kobayashi [1], C. A. J. Fisher[1], A. Kuwabara[1], Y. Ukyo[2] and Y. Ikuhara[1,3]

[1] Nanostructures Research Laboratory, Japan Fine Ceramics Center, Atsuta, Nagoya 456-8587, Japan
[2] Office of Society-Academia Collaboration for Innovation, Kyoto University, Uji, Kyoto 611-0011, Japan
[3] Institute of Engineering Innovation, The University of Tokyo, Bunkyo, Tokyo 113-8656, Japan

Lithium iron phosphate ($LiFePO_4$) is a commercially important cathode material for lithium ion batteries [1]. Here we report a quantitative study of the spatial distribution of Li ions in a $LiFePO_4$ single crystal after chemical delithiation using valence electron energy loss (EEL) spectroscopy techniques.

Commercially available $LiFePO_4$ single crystals were used for all experiments [2]. EEL spectra were obtained using an EEL spectrometer (Tridiem ERS, Gatan, Inc.) attached to a Wien filter monochromated aberration corrected scanning transmission electron microscope (STEM; JEM-2400FCS, JEOL Ltd.) operated at 200 kV. The exposure time for recording valence EEL spectra per line-spectrum point was less than 0.02 s.

Low-loss (valence) EEL spectra obtained from $FePO_4$ and $LiFePO_4$ are shown in Fig. 1a. A strong peak, labeled ***α*** in Fig. 1a, is observed in the case of $FePO_4$. Line profiles of valence EEL spectra across an interface between the two phases change gradually, as seen in Figs. 1b & 1c. Detailed analysis of the ***α*** peak intensities reveals a linear relationship with the valence state of Fe ions; this means that valence EEL spectra can be used to estimate Li distributions in $Li_{1-x}FePO_4$. The faster recording time for valence EEL spectra than Fe $L_{2,3}$-edge spectra makes measurement of the former a more efficient and reproducible means of estimating Li distributions.

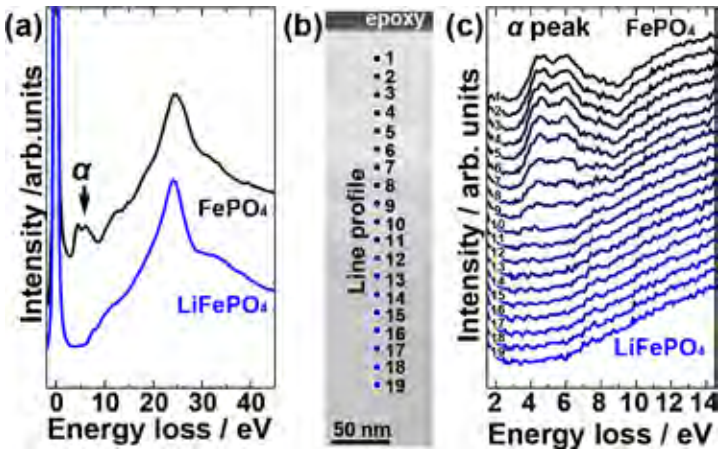

FIG. 1 (a) Low-loss EEL spectra of $FePO_4$ and $LiFePO_4$. (b) ADF STEM image of the region around an interface between $FePO_4$ and $LiFePO_4$. (c) Valence EEL spectra obtained from numbered points in (b).

References

[1] A. K. Padhi et al., *J. Electrochem. Soc.* 144 (1997) 1188−1194.
[2] S. Kobayashi et al., *Nano Lett.* 16 (2016) 5409−5414.
[3] This work was supported by the Research and Development Initiative for Scientific Innovation of New Generation Batteries II (RISING II) project from the New Energy and Industrial Technology Development Organization (NEDO), Japan.

TEM-EELS study on photo luminescent multi-shell nanoparticles

Y. Sato[1], N. Nakahigashi[1], M. Uehara[2], and M. Terauchi[1]

[1] Institute of Multidisciplinary Research for Advanced Materials, Tohoku University, Sendai, 980-8577, Japan.
[2] Advanced Manufacturing Research Institute, AIST, Tosu, Saga, 841-0052, Japan.

Semiconductor nanoparticles, CdSe nanoparticles, with ~10 nm in diameter are applied for light emitting devices. Multi-shell nanoparticles, CdSe/CdS/ZnS nanoparticles (CdSe core particle covered by CdS inner-shell and ZnS outer shell) are synthesized to protect reactive CdSe core from environment and to improve high electron-hole recombination probability. However, the photo luminescent efficiency of multhshell nanoparticle does not always show improvement depending on the synthesizing conditions. To clarify an origin of the luminescent property, it is effective to evaluate dielectric properties of single nanoparticles by using EELS measurement. In this study, high energy-resolution EELS measurements of multishell nanoparticles were conducted by using the monochromator analytical TEM.

Figure shows the comparison between experimental and simulated EELS spectra of a multishell nanoparticle. The simulation was based on the classical dielectric theory [1]. Since the photo luminescent properties should be reflected to the electronic structure around band gap region, spectral structures in energy loss < 5eV are investigated in detail. As a result, spectral structures attributed to interband transitions coming from core and shell could be observed and the intensity profile of the spectra was valid for the dielectric response of the multishell structure. Through the detail investigation of the spectra, dielectric property of single multishell nanoparticle is clarified and relation with the photo luminescent property will be discussed.

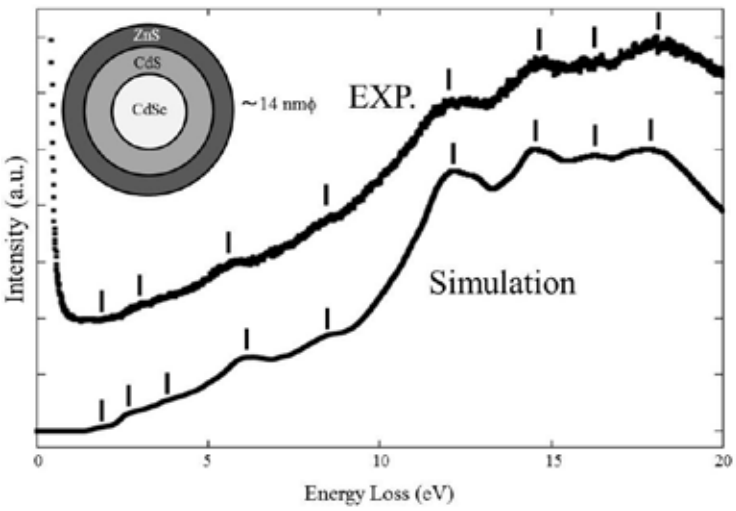

FIG. 1. EELS spectrum obtained from a single multi-shell nanoparticle. Simulated spectrum is also shown for comparison.

References

[1] D. Ugarte et al. Phys. Rev. B, 45 (1992) 4332–4343.

An investigation of interface interaction of Silver-Ceria core-shell nanoparticles via energy electron loss spectroscopy and X-ray absorption spectroscopy.

Eric Tseng[1], Shih Yun Chen[1] and Alexandre Gloter[2]

[1] Department of Materials Science and Engineering, National Taiwan University of Science and Technology, Taipei, Taiwan
[2] Laboratoire de Physique des Solides, Université Paris Sud, CNRS UMR 8502, F-91405 Orsay, France

For a further investigation of interfacial interaction of noble metal and metal oxides in relation to the material magnetism property, silver-ceria core-shell nanoparticles ($Ag@CeO_2$) were prepared firstly via photoreduction and followed chemical reduction methods. The electronic structure of the composite was investigated by atomically resolved energy electron loss spectroscopy (EELS) and bulk sensitive X-ray absorption spectroscopy (XAS). The nature of the charge transfer at the interface between Ag and CeO_2 was revealed by combining measurements of EELS Ag-$M_{4,5}$ and Ce $M_{4,5}$-edge with XAS Ag-L_3, Ag-K, Ce-L_3 and O-K edges (Fig.1). The charge transfer is discussed with respect to the observed enhancement of the ferromagnetism for core-shell particles. A ferromagnetic contribution originating from the polarization of cerium f orbital is then confirmed performing x-ray magnetic circular dichroism (XMCD) at Ce $M_{4,5}$-edge.

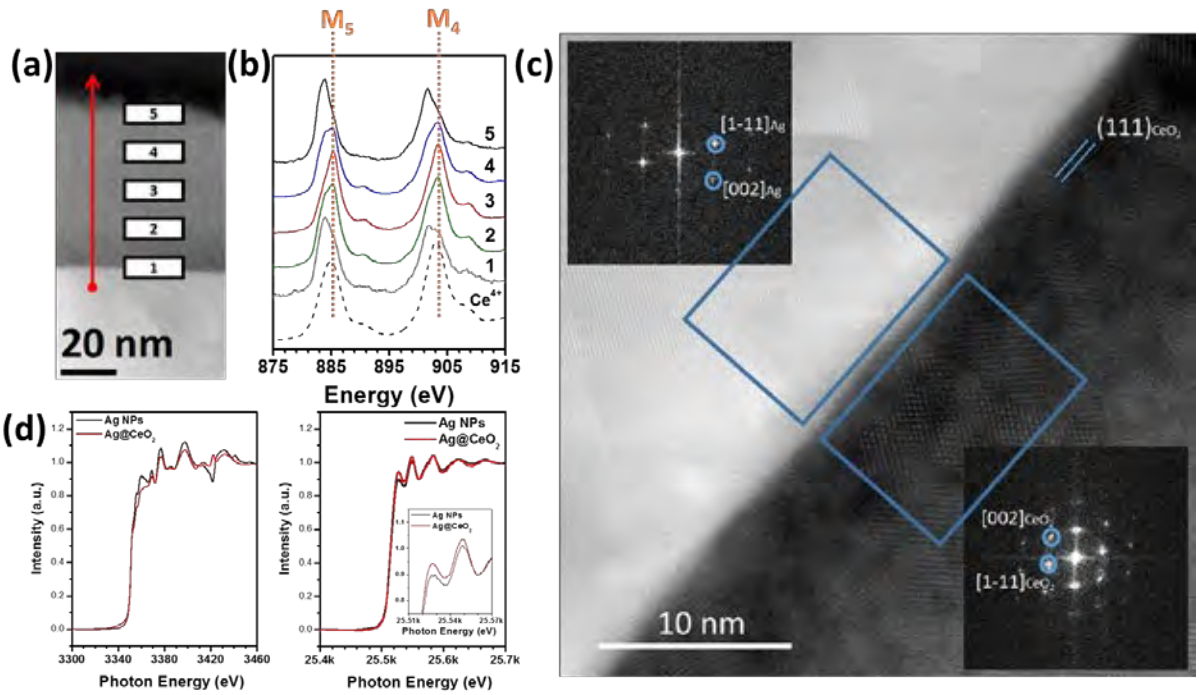

Fig1 : (a) STEM-HAADF image of $Ag@CeO_2$ core-shell nanoparticles and (b) STEM-EELS spectra of Ce $M_{4,5}$-edge positioned in the cross sectional image. (c) STEM-HAADF image of the Ag-CeO_2 interface. (d) XANES of Ag *L*-edge and Ag *K*-edge of Ag nanoparticles in comparison to $Ag@CeO_2$ core-shell nanoparticles

O K-edge fine structures in highly strained $BiFeO_3$ thin films to probe local lattice distortions

F. Pailloux[1] and J. Pacaud[1]

[1] Institut Pprime, UPR 3346 CNRS/Univ Poitiers, 86962 Futuroscope Chasseneuil, France

The homogeneity of $BiFeO_3$ (BFO) thin films, the chemical sharpness and nature of the film/substrate interfaces and the distortions of the unit-cell imposed by the lattice mismatch are among the parameters which strongly impact the tunnel barrier profile and thus the tunnel electro-resistance of ferroelectric tunnel junctions.
It was shown that for BFO thick films grown on $LaAlO_3$ substrate (4.5% compressive misfit), the films are composed of a mixture of a tetragonal-like (T-like) BFO phase and a rhombohedral-like (R-like) phase [1]. For ultrathin films, although the structural analysis showed a single phase BFO layer (Cm s.g.), the presence of a gradually strained T-like phase exhibiting different ELNES fingerprints (fig. 1a and 1b) was demonstrated by ELNES investigations [2].
In order to link fine structures change at the O K-edge to structural distortions of the BFO unit-cell, real space full-multiple scattering (RS-FMS) calculation are carried out with the FEFF9.6 code [3]. Our preliminary results show that the raise of intensity of the A_2 peak is related to the large aspect ratio of the T-like phase compared to the bulk rhombohedral R3c phase. It also suggests that this peak (Fig. 1d) is closely related to the apical O atom of the FeO_5 pyramid, and could be used to probe the distortions of the T-like unit-cell with a possible improved accuracy compared to previous analysis.

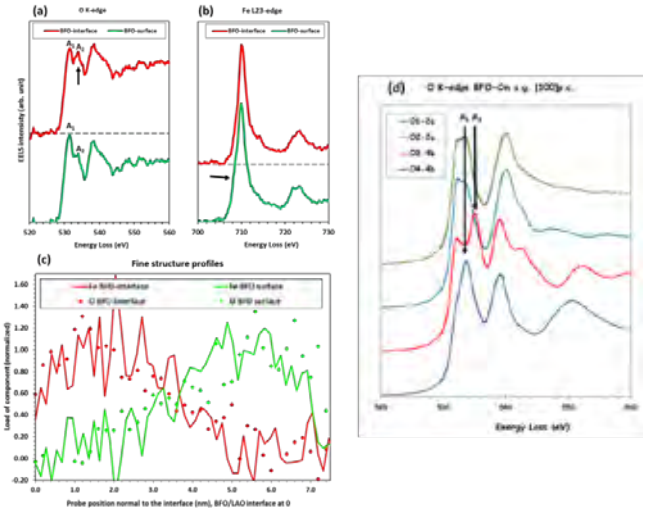

FIG. 1. a) O K-edge showing the strong A_2 peak (red) for the first 4nm of the BFO film close to the film/substrate interface, b) Fe $L_{2,3}$-edge showing the weak shoulder on the L_3-edge (red) associated with the strong A_2 peak, c) profiles of the loads of the fingerprints shown in fig. 1a and 1b, d) RS-FMS calculations of the O-K edge for the four wyckoff sites of the Cm structure; the apical oxygen is in position O3 (red).

References

[1] R.J. Zeches et al., *Science* 326 (2009) 977
[2] F. Pailloux et al. Phys Rev. B 89, 104106 (2014)
[3] K. Jorissen et al., Phys. Rev. B 81 155108 (2010)

Combined STEM-HAADF/ABF and EELS study of the Mn-based spinel and birnessite insertion cathode materials for Mg-ion battery

Elena Tchernychova, Ana Robba, Miran Gaberšček, Robert Dominko

Department for Materials Electrochemistry,
National Institute of Chemistry, Ljubljana 1001, Slovenia

The application of multivalent battery technology where an intercalation cathode is paired with the metal electrode allowing for higher energy density and lower costs is an important line in the field of batteries research. Here, the Mg metal, which besides possessing high volumetric specific capacity of 3833 mAh cm^{-3} and exhibiting no dendrite growth on deposition[1], being safe to handle in ambient atmosphere and largely available, is of special interest[2].
In this study we have investigated the changes in the microstructure at the atomic level and electronic properties of the variants of manganese oxide, a $MgMn_2O_4$ spinel and $(Mg_xNa_y)Mn_2O_4$ birnessite layered phases induced upon delithiation of the initial starting material and their subsequent magnesiation, i.e. Mg insertion performed in magnesium nitrite aqueous electrolyte. The aim of the study was to assess the possible Mg insertion mechanisms into the structurally different manganese oxide based host materials. Firstly, the obtained cyclic voltammetry (CV) results prior assembling a battery were correlated with the structural and compositional changes of these cathode materials by STEM and EELS analysis at the atomic level for different number of cycles. Secondly, the batteries with both de-Li spinel and de-Na birnessite serving as a cathode materials were assembled and galvanostatically magnesiated in aqueous electrolyte. In birnessite, the STEM-ABF and EDX confirmed partial exchange of Na over Mg with the Mg fully occupying the smaller particles and only the outer shells of the larger particles. Same behavior was observed in the spinel material. STEM-ABF images were taken after the third CV cycle, when the initial changes of structure due to the Mg insertion took place. Additionally, the ABF imaging of birnessite confirmed the presence of extra O atoms belonging to the crystal water interlayer that has been reported to play a crucial role in the layered cathode materials by enhancing the ion diffusion as well as suppressing the Mn^{2+} dissolution[3]. Both materials in charged state, i.e. de-Li and de-Na, exhibited etched microstructure, were the initially single-crystalline particle structure had changed into the patchwork of small regions with various crystallites orientation, which was observed by HAADF and ABF imaging. Evaluation of the ELNES data in line profiles of the crystallites aggregates showed changes of the Mn valence towards Mn^{2+} and Mn^{3+}, indicating the presence of Mn_3O_4 spinel phase. Upon galvanostatic magnesiation both spinel and birnessite phases resembled their initial crystalline structures, however, leaving voids and defects behind, with damage being more prominent in the birnessite.

References

[2] H. D. Yoo, I. Shterenberg, Y. Gofer, G. Gershinsky, N. Pour, D. Aurbach, Energy Environ. Sci. 6, 2265, (2013)
[3] J. Muldoon, C. B. Bucur, T. Gregory, Chem. Rev. 114, 11683, (2014)
[5] K. W. Nam, S. Kim, E. Yang, Y. Jung, E. Levi, D. Aurbach and J. W. Choi, Chem. Mater. 27, 3721 (2015)

Direct Imaging of single atoms in ionic liquids and observation of their dynamics

T. Miyata[1] and T. Mizoguchi[1]

[1] Institute of Industrial Science, The University of Tokyo, 4-6-1, Komaba, Meguro, Tokyo, 153-8505, Japan

Ionic Liquids have characteristic properties, such as non-volatility, high ionic density, and hydrophilicity. Owing to such properties, ionic liquids have been studied for wide range of electrical applications. For example, gate media of transistors and electrolytes of rechargeable batteries [1,2]. The relaxation and diffusion dynamics of monatomic ions in ionic liquids are unique due to the strong coulomb interaction between solutes and solvents. Such atomic-scale motion depends on the liquid structure and temperature at each potion and time, i.e., the atoms having low kinetic energy and strongly solvated by the surrounding molecules are trapped and show slow motion, which means that we have to discuss the whole dynamical mechanisms by observing the static and dynamic heterogeneity of ions in ionic liquids. Here, Observation by transmission electron microscopy (TEM) and scanning TEM (STEM) is the only experimental way to know such local atomic dynamics in real space. Therefore, we have firstly applied annular dark-field (ADF) STEM to the atomic imaging in ionic liquids, which forms Z-contrast image. Then, we have performed consecutive observation and discussed the dynamics of monatomic ions in ionic liquids.

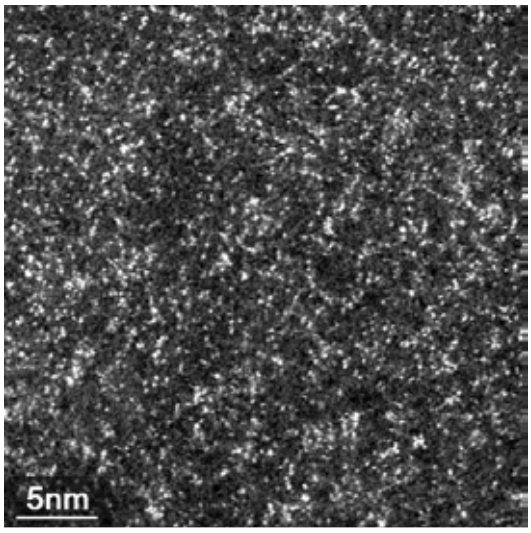

FIG. 1. ADF-STEM image of gold atoms in ionic liquid C_2mimTFSI.

References
[1] Je. Ye et al., *Nat. Mat.* 9 (2010) 125.
[2] M. Lin et al., *Nature* 520 (2015) 324.
[3] This research was supported by Dr. Uesugi at NIMS. The STEM measurements were conducted at the Research Hub for Advanced Nano Characterization, NIMS, under the support of ‘Nanotechnology Platform’ (No. 12024046) of the MEXT, Japan. This study was supported by a Grant-in-Aid from the JSPS Fellows (No. 15J11146).

Observation of insulin amyloid fibrils on graphene supporting films with low-voltage STEM in SEM

T. Ogawa[1], G. Gang[1,2], M. Thieu[1,3], S. Ahn[1,3], T. Ha[1,3], B. Cho[1]

[1] Korea Research Institute of Standards and Science, Daejeon 34113, Rep. of Korea
[2] Chungnam National University, Daejeon 34134, Republic of Korea
[3] Korea University of Science & Technology, Daejeon 34113, Rep. of Korea
[4] Korea Research Institute of Bioscience and Biotechnology, Daejeon 34141, Rep. of Korea

Observation of amyloid fibrils, which are filament shaped proteins, is important in biology and medical science because their aggregation forms are considered as a cause of various diseases such as Alzheimer's diseases and type II diabetes [1]. Recently, we show that utilization of graphene supporting films and low voltage scanning transmission electron microscopy (LV-STEM) in scanning electron microscopy (SEM) is an effective means of observing these fibrils [2]. Insulin amyloid fibrils are formed in vitro, deposited on the graphene films without staining, and observed with an in-lens SEM (S5000, Hitachi), which are equipped with secondary electron (SE) and additional homemade STEM detectors. Fig. 1 (a) shows a STEM image of aggregated fibrils on the graphene at 30 keV. The graphene film reduce background level, and observation on low energy and low detection angle conditions increases signal sensitivity, resulting in enhanced visibility of the fibrils. Fig. 1 also shows a twisted-ribbon structure of the fibrils in (b) STEM and (c) SE images.
We will discuss STEM and SE image formation of the fibrils on the graphene films at the conference. The result offers a simple and easy method for observation of nano-bio materials.

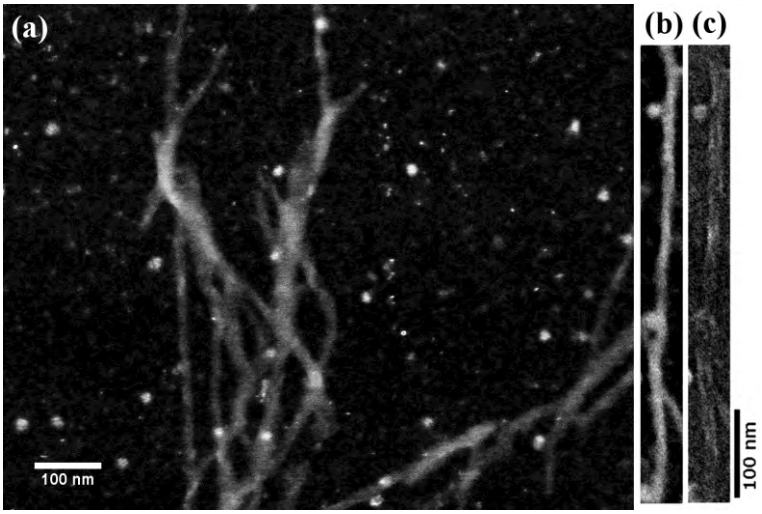

FIG. 1. (a) STEM image of aggregated fibrils on the graphene, (b) STEM and (c) SE images of a twisted-ribbon structure of fibrils.

References

[1] F. Chiti, C.M. Dobson, *Annu. Rev. Biochem*. 75 (2006) 333.
[2] T. Ogawa et al., *Micron,* accepted.
[3] Grant number: 2011-0030233, CAP-14-3-KRISS

The studies of electronic excitations in MoS_2 by EELS

C.T. Wu[1*], J.H. Huang[2], T.H. Hou[2], Y.J. Lee[1], M.W. Chu[3]
[1] National Nano Device Laboratories, National Applied Research Laboratories, Hsinchu City 300, Taiwan
[2] Department of Electronics Engineering and Institute of Electronics, National Chiao Tung University, Hsinchu 300, Taiwan
[3] Center for Condensed Matter Sciences, National Taiwan University, Taipei 106, Taiwan

In this study, we report EELS studies in free-standing layered MoS_2. These STEM-EELS studies show that (in FIG 1) the predominant excitations at ~8.5, ~23 and ~12 eV arise from the respective resonances of bulk and surface plasmons (SP). In addition, the SP peak intensity was found to decay exponentially with the increase in impact parameters, e.g., from 0 to 10 nm away from the planar surface. Moreover, we observed several peaks with the characteristics of surface exciton polaritons [1] occurring near interband transitions in the spectral regime below the SP. Furthermore, discussions corroborating calculations and the momentum-resolved EELS investigations are also elucidated.

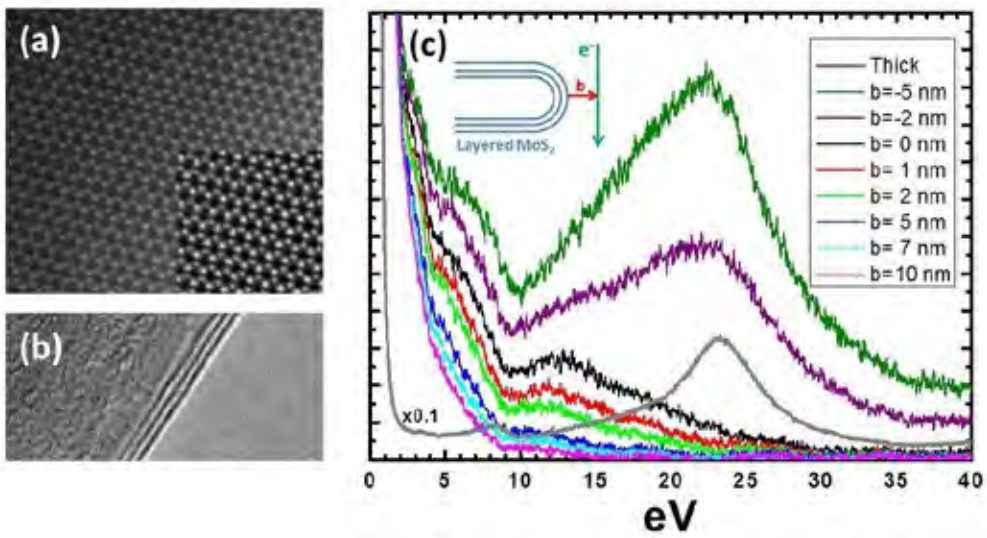

FIG. 1. The impact parameter dependent STEM-EELS spectra of the layered MoS_2.

References
[1] Fuzi Yang, J. R. Sambles, and G. W. Bradberry, PRL, 64, 559–562 (1990).
[2] Acknowledgement: This work was financially supported by the Ministry of Science and Technology, Taiwan.

Understanding Photoluminescence (PL) in porous anodic alumina (PAA) using Electron Energy Loss Spectroscopy

J.H. Jang[1], S. Lee[1], J. Lee[1], H.J.Kim[1], S.Y. Cho[2], J.W. Kim[2], J.H. Kim[2] and S.D. Bu[2]

[1] Center for Electron Microscopy Research, Korea Basic Science Institute, Daejeon, 34133, Republic of Korea
[2] Department of Physics, Chonbuk National University, Jeonju, 561-756, Republic of Korea

Porous anodic alumina (PAA) has ordered pore structures showing characteristic of blue PL. [1] The mechanism of blue PL has been suggested by these, the first is the oxygen vacancy and F + center, and the second is the oxygen vacancy related to the carboxylate. This mechanism has been studied by the interpretation of the bonding molecular orbital of the PAA, such as FTIR, XPS and so on. In particular, such blue PL intensity depends on various conditions such as post-heat treatment temperature and pore size due to the pretreatment condition of PAA, so we have systematically studied the mechanism of blue PL in PAA by using two advantages, a monochromated EELS (energy resolution) and spatial resolution of STEM (Scanning Transmission Electron Microscopy).

Figure 1 shows the ADF (annular dark field) image of PAA and the Al $L_{2,3}$ edge before and after the annealing process. As can easily be seen, the binding of Al $L_{2,3}$ is changed significantly after annealing process. Therefore, to understand the changes of the internal bonding state, we have analyzed in depth additional O *K* edge and C *K* edge analysis. This study will present the mechanism of PL from PAA, based on EELS results.

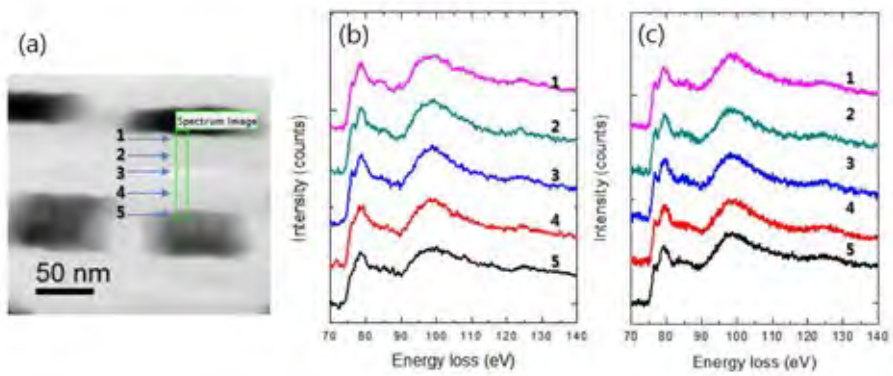

FIG. 1. (a) ADF image of PAA (Al_2O_3), (b) and (c) Al $L_{2,3}$ edge before/after annealing process (EELS spectra is shown after background subtracted and normalized by integrated intensity.)

References
[1] Y. Du et al., *Appl. Phys. Lett.* 74 (1999) 2951.
[2] This research was supported by R&D Convergence Program of NST(National Research Council of Science & Technology) of Republic of Korea.

Electron energy loss spectroscopy of infrared plasmonic antennas

A. Konečná[1,2], P. Sarriugarte[2], T. Neuman[1], J. Damková[2], A. Govyadinov[2], A. Chuvilin[2,3], J. Aizpurua[1,4], and R. Hillenbrand[2,3]

[1] Materials Physics Center, CSIC-UPV/EHU, Donostia-San Sebastián, Spain
[2] CIC NanoGUNE, Donostia-San Sebastián, Spain
[3] IKERBASQUE, Basque Foundation for Science, Bilbao, Spain
[4] Donostia International Physics Center, Donostia-San Sebastián, Spain

Spatially-resolved low-loss electron energy loss spectroscopy (EELS) is a well-established technique for probing optical excitations in nanostructures [1] and with recent instrumental improvements, it can be utilized even in infrared (IR) spectral region [2].
We explore possibilities of IR-EELS for characterizing metallic nanostructures supporting excitations of localized surface plasmons. We present experimental and theoretical results for different antenna geometries (see FIG. 1) and demonstrate that both spectral and spatial information provided by the electron beam is important for an elaborate analysis of such systems.

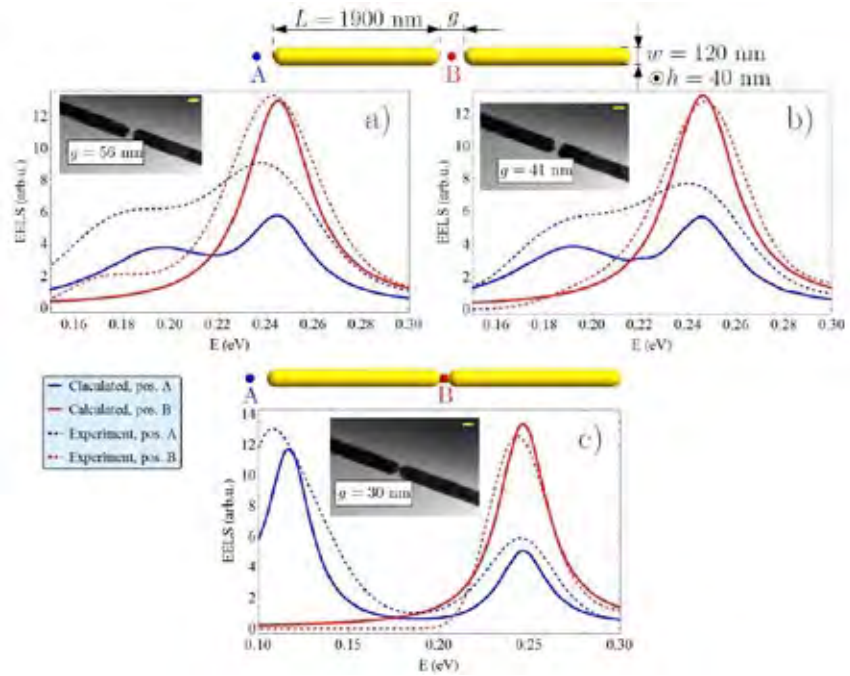

FIG. 1. EEL spectra for 80 keV electron beam probing an antenna with varying gap size in a) and b), respectively, and with a conductive connection in c). The numerically calculated spectra (solid lines) agree with the experimental results (dashed lines) both for the beam position at the side of the antenna (A) and in the gap (B). The observed peaks correspond to excitation of bonding and antibonding modes as reported in Ref. [3]. Scale bars in the inset STEM images are 100 nm.

References

[1] J. García de Abajo, *Rev. Mod. Phys.* 82 (2010), 209.
[2] O. Krivanek et al., *Nature* 514 (2014), 209.
[3] I. Alber et al., *ACS Nano* 6 (2012), 9711.
[4] A. Konečná acknowledges CSMS/FEI scholarship for young researchers.

In-situ observation of binodal type phase coarsening in glass.

K. Nakazawa[1], S. Amma[2], T. Miyata[1], and T. Mizoguchi[1]

[1] The University of Tokyo.
[2] Asahi Glass

Phase separation phenomenon in glass material has been attracted great attentions because it affects the properties of the glass materials, such as transmittance, thermal expansion, and mechanical properties. Thus, the phase separation phenomenon of the glass material has been investigated. In those past investigations, relationship between macroscopic properties and both average size and number density of phases were investigated. However, since a direct observation of the phase separation with high spatial resolution under controlling temperature has been difficult, basic knowledges for the phase separation in the glass materials, such as nucleation and growth behaviors, are still under controversy.

We overcame this difficulty by using new in-situ heating holder, Aduro. Aduro is a MEMS device developed by using microfabrication technology. we prepared CaO-Al_2O_3-SiO_2 glasses of immiscible composition by melt-quenching method. The phase coarsening process are investigated using an aberration corrected scanning electron microscopy (STEM), electron energy loss spectroscopy (EELS), and in-situ heating holder. We successfully visualize the nano-scaled phase separation in the glass, and track its growth behavior at high temperature. The details will be discussed in our presentations.

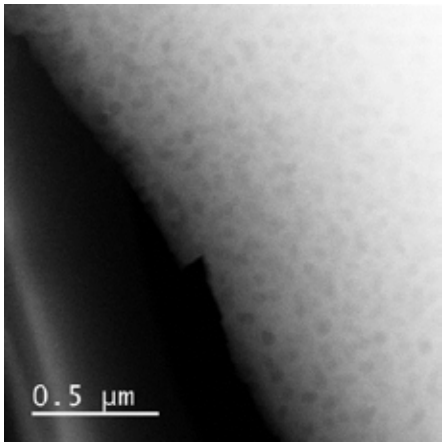

FIG. 1. HAADF image of glass sample heated treatment at 900℃ under 1atm for 15hours.

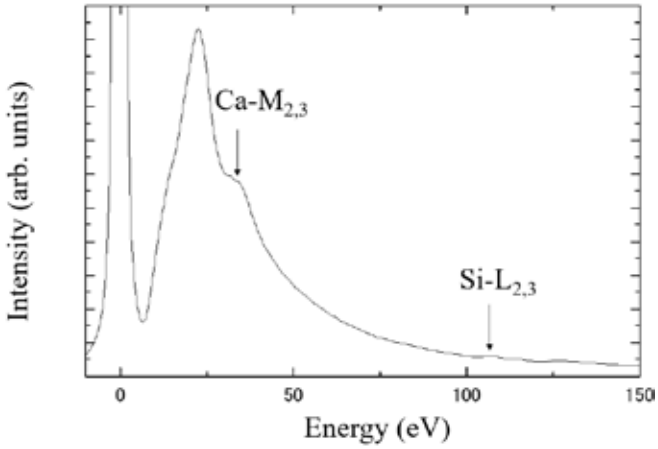

FIG. 2. EEL spectrum of glass sample heated treatment at 900℃ under 1atm for 15hours.

References
[1] I. Lifshitz, V. Slyozov, *J. Phys. Chem.*, **19**, 35 (1961).
[2] Y.Enomoto, M. Tokuyama, K. Kawasaki, *Acta metall.*, **34**, 2119 (1986).
[3] L. Allard et al., *Microsc. Microanal.*, **18**, 656 (2012)

Electron irradiation effects on lithium peroxides

J. Kikkawa[1], T. Shiotsuki[2], S. Koshiya[1], T. Nagai[1], Y. Shimo[2], T. Nito[2] and K. Kimoto[1]

[1] National Institute for Materials Science, 1-1 Namiki, Tsukuba, Ibaraki 305-0044, Japan
[2] Higashifuji Technical Center, Toyota Motor Corporation, 1200 Mishuku, Susono, Shizuoka 410-1193, Japan

Lithium peroxide (Li_2O_2) is an important discharge product for Li–air (or Li–O_2) batteries, which attract much attention because of their potential to provide higher energy density than current Li-ion batteries. Understanding the fundamental properties of Li_2O_2 and their related experimental data remain insufficient, despite their importance for the realization of practical Li–air batteries. Investigations of the Li_2O_2–fast electron interactions are important because of increasing demands for transmission electron microscopy (TEM) investigation of reactions at the electrodes on a nanometer scale.
Using electron energy loss spectroscopy (EELS) and selected-area electron diffraction (SAED), we investigate electron irradiation effects on Li_2O_2. Results of both EELS and SAED show that Li_2O_2-to-Li_2O transformation occurs under high electron dose rates. This reaction in the vacuum is described as $Li_2O_2 \rightarrow Li_2O + 1/2O_2$. It was also found that the total electron dose required to the complete Li_2O_2-to-Li_2O transformation for 80 keV is smaller than that for 300 keV. The main trigger of the transformation is not atomic displacement, sputtering and local heating but structural weakening caused by the inelastic scattering.

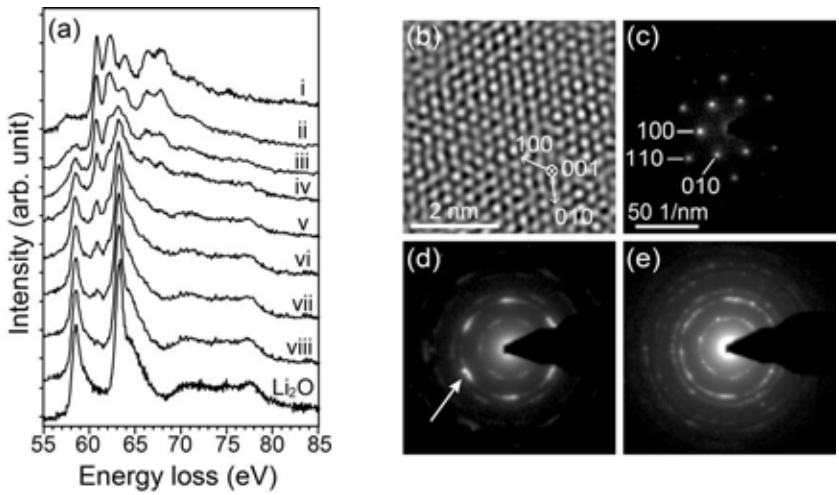

FIG. 1. (a) Variation of EELS Li *K* edge for Li_2O_2 by electron irradiation at −183 °C. Incident electron energy and electron dose increments from Li_2O_2, (i) to (viii) are respectively 80 keV and 1.1×10^{11} electrons/nm^2. Reference spectrum for Li_2O is shown in (a). (b) Fourier-filtered high-resolution TEM image of Li_2O_2 viewed along [001] direction with a low dose of 300 keV electron. [(c)–(e)] Variation of SAED pattern by irradiation with 300 keV electrons. The [001] SAED pattern of Li_2O_2 single particle in (c) changes into SAED pattern of polycrystalline Li_2O in (e). The appearance of arc of diffuse intensity just inside the 110 spot of Li_2O_2, as indicated by the arrow in (d), is attributed to the Li_2O_2-to-Li_2O transformation.

Momentum resolved EELS at high energy resolution: applications and practical considerations

F.S. Hage[1], R.J. Nicholls[2], T.P. Hardcastle[1, 3], A.J. Scott[3], R. Brydson[3], J.R. Yates[2], K. Refson[4], and Q.M. Ramasse[1]

[1] SuperSTEM Laboratory, SciTech Daresbury Campus, Daresbury, UK.
[2] Department of Materials, University of Oxford, Oxford, UK
[3] School of Chemical and Process Engineering, University of Leeds, Leeds, UK.
[4] Department of Physics, Royal Holloway, University of London, Egham, UK.

In the electron microscope, the momentum transfer dependence (*i.e.* dispersion) of electron energy loss (EEL) modes can provide information about a material system that is often obscured in spectra acquired using typical experimental setups optimized for high spatial resolution. Recent advances in electron source monochromation has allowed for the study of vibrational losses [1] as well as valence losses at a level of detail previously inaccessible in the electron microscope [2]. In the present work, valence loss spectra of individual single wall carbon nanotubes (CNTs, Fig. 1a) and vibrational loss spectra of two boron nitride polymorphs (BN, Fig. 1b) were resolved in momentum space at high energy resolution using a Nion UltraSTEM100MC microscope. CNT plasmon dispersions indicate confinement perpendicular to the tube axis (π_1 mode, Fig. 1a) as well as a variable π plasmon confinement parallel to the tube axis (π_2 mode, Fig. 1a) attributed to CNT topological defect concentration. Momentum resolved spectra of cubic and hexagonal BN were compared to theory, identifying contributions from the longitudinal acoustic (LA) and optical (LO) phonon branches along the Γ→X direction (Fig. 1b). Practical considerations for the acquisition of momentum resolved spectra at high energy resolution in the electron microscope, including advantages and disadvantages of serial and parallel spectral collection, will be discussed. [3]

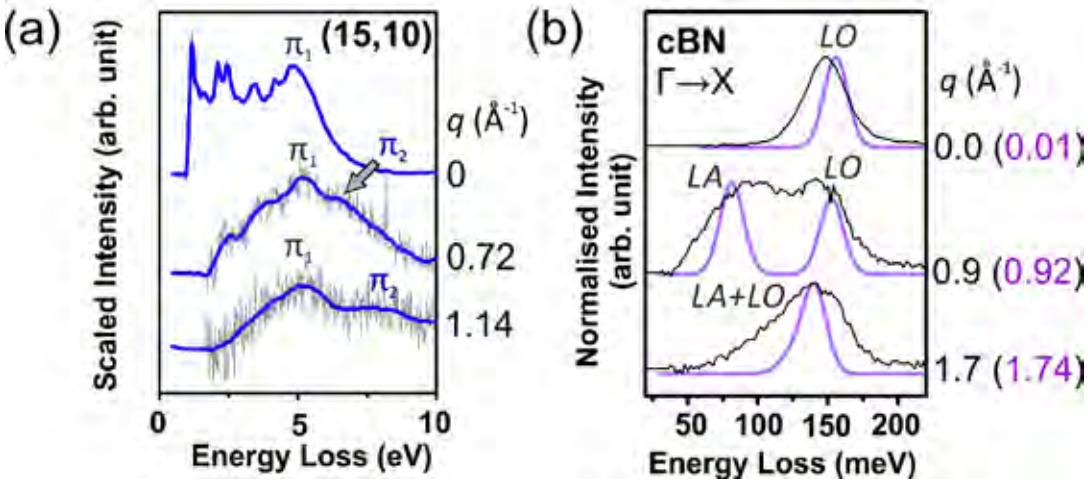

FIG. 1 Background subtracted momentum resolved EEL spectra of (a) an individual single wall (15,10) CNT and (b) cBN (experiment, theory).

References

[1] O.L Krivanek et al., *Nature.* 514 (2014) 209.

[2] D. Keller et al., *APL*, 190 (2016) 153103.

[3] SuperSTEM is the UK EPSRC National Facility for Aberration-Corrected STEM, supported by the UK Engineering and Physical Science Research Council.

Layer-dependent EELS spectra of atomically thin h-BN sheet

N. Kawasaki[1], Y. Otsuka[1], D. Kondo[2], K. Hayashi[2], S. Sato[2]

[1] Toray Research Center Inc., Morphological Research Laboratory, Otsu, Shiga 520-8567, Japan
[2] Fujitsu Limited

Graphene and other 2D materials have attracted a lot of attentions because their electronic and physical properties are unique and controllable. In this study, we evaluated the layer-dependence of electronic structures around band gap energy in h-BN. The numbers of layers were investigated by core-loss EELS shown in FIG.1. Both B-K and N-K intensities of area 2, 3 and 4 were twice, 3 times and 4 times higher than that of area 1. Low-loss EELS spectra from each area were shown in FIG.2. In 6-8 eV energy region, where peaks are usually attributed as π-π^* excitation, double peak structures can be seen, which were also reported in previous studies for h-BN tube [1] and sheet [2]. In the low-loss spectra from area 1, the intensity at 6.4 eV has higher intensity than that at 7.2 eV, which is corresponding to the spectrum from single–wall BN tube [1], so that we can regard area 1 as a monolayer region, and area 2, 3 and 4 as 2, 3 and 4 layers respectively. The peak at 7.2 eV, whose intensity is proportional to the number of layers, should be attributed to π-π^* excitation, because π-orbital is oriented to the stacking direction of h-BN layers. On the other hand, the peak at 6.4 eV should be from surface effect, because this peak is most dominant in monolayer region and become relatively low in thicker h-BN. In sheet samples, the bulk and surface effects could be considered independently of the curvature effect as observed in nanotube sample, so that the layer-dependent electronic structure can also be successfully characterized by experimental spectra.

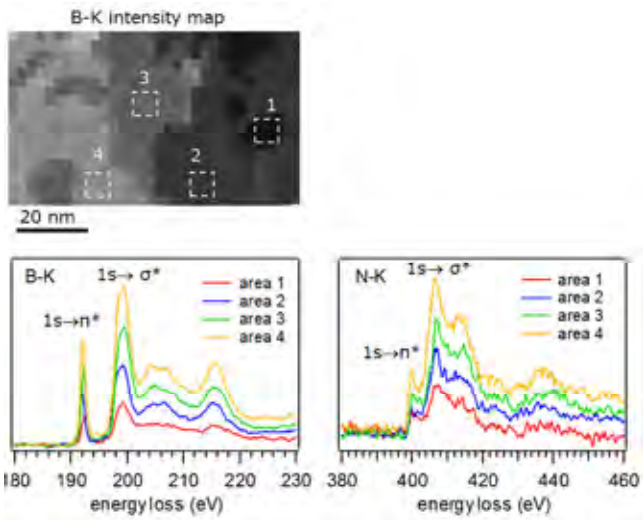

FIG. 1. B-K EELS intensity distribution of atomically thin h-BN sheet. And, B-K, N-K EELS spectra from each area.

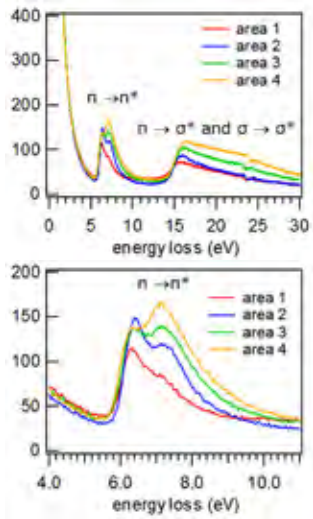

FIG. 2. Low-loss EELS spectra from each area.

References
[1] R. Arenal et al., *Phys. Rev. lett.* 95 (2005) 127601.
[2] C. T. Pan et al., *Phys. Rev. B.* 85 (2012) 045440.
[3] This work was partly supported by JST, CREST.

Study of nanometer-scale gas bubbles in zirconium alloys

S. Dumbill[1], D. Hernandez-Maldonado[2], M.S. Blackmur[3],M. Gass[4] and Q.M Ramasse[2]

[1]National Nuclear Laboratory, Sellafield, CA20 1PG, UK
[2]SuperSTEM Laboratory, STFC Daresbury Campus, Daresbury, WA4 4AD, UK
[3]National Nuclear Laboratory, Culham Science Centre, Oxfordshire, OX14 3DB, UK
[4]Amec Foster Wheeler, 305 Bridgewater Place, Birchwood, WA3 6XF, UK

In the nuclear industry the use of zirconium alloys is commonly used for cladding applications however hydrogen arising from corrosion of the cladding in contact with the cooling water causes the precipitation of hydrides which can lead to the failure of the system. Fuels for future generations of reactors may include the use of metallic uranium-zirconium fuel. During irradiation, the fuel will undergo implantation from fission products including helium causing the formation of a lattice of nanometer-scale bubbles that could act as a barrier to the migration of hydrogen [1]. Accordingly, understanding of the distribution and manifestation of hydrogen in zirconium alloy material is important to the nuclear industry for a number of reasons.

In this work two Zicaloy-4 samples are studied, both present the bubble lattice, one of them having been previously hydrogen charged. The aim of this study is to confirm the presence of helium in the bubbles and determine whether hydrogen becomes associated with the bubbles. The Nion UltraSTEM 100MC 'HERMES' at SuperSTEM has been used to study these samples. Figure 1 shows the analysis of the plasmon peaks of zirconium and helium in the bubble region. For the analysis of the hydrogen, the ultralowloss region of the spectrum has been analyzed finding the presence of a peak at 146eV similar to what has been reported for TiH_2 [2]. To answer the question whether the hydrogen is bound to either zirconium or helium a comparison with the non-charged sample is carried out.

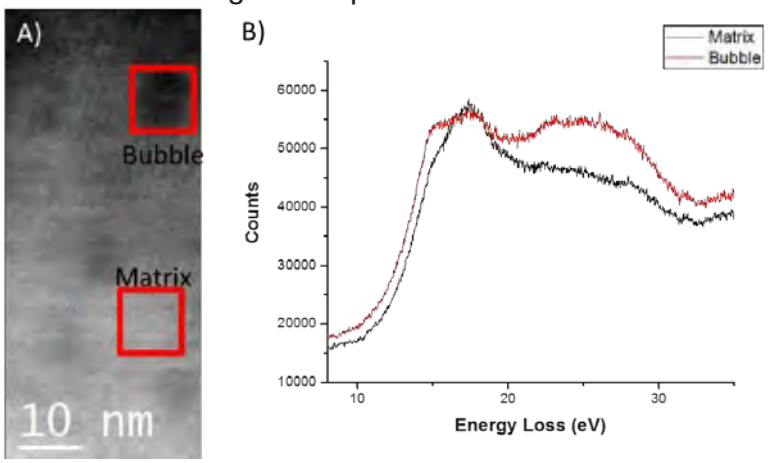

FIG. 1. A) HAADF image of the bubble region. B) Comparison of spectra for the Zr and He plasmon edges at different positions. There is a strong He K-edge signal in the bubble position that is close to being extinct in the matrix.

References

[1] Y. Ueda et al., J. Nucl. Mater. 386-388 (2009) 725.
[2] O.L. Krivanek et al., J. Microsc. 259 (2015) 165.

Atomic structural and chemical investigations of misfit layered nanotubes

L. Lajaunie[1], L.S Panchakarla[2], A. Ramasubramaniam[3], R. Tenne[2] and R. Arenal[1,4]

[1] Laboratorio de Microscopías Avanzadas, Instituto de Nanociencia de Aragón, Universidad de Zaragoza, 50018 Zaragoza,
[2] Department of Materials and Interfaces, Weizmann Institute of Science, Rehovot, 76100 Israel
[3] Department of Mechanical and Industrial Engineering, University of Massachusett,, Amherst, Massachusetts 01003, United States
[4] ARAID Foundation, 50018 Zaragoza, Spain

Misfit layered compounds can be considered as inter-grown materials with a general formula $[(MX)_{1+x}]_m[TX_2]_n$, where M is rare earths, Pb, Sb, etc; T is Ti, V, Cr, Nb, etc. and X is S, Se. They constitute an heterostructure formed by the stacking of TX_2 dichalcogenides layers with MX layers [1]. In 2011, nanotubes based on the SnS-SnS_2 system were synthetized for the first time in large amounts [2]. Later, the syntheses were generalized to many other chalcogenide systems which were extensively studied at the local scale by TEM and associated techniques. However, until now, analogous synthesis of oxide-based MLC NTs has not been demonstrated yet.

Here, we report a chemical strategy for the synthesis of calcium and strontium cobalt oxide-based misfit NTs [3-4]. A combination of high-resolution STEM (HRSTEM)-HAADF imaging (including image simulations), spatially-resolved (SR-EELS), electron diffraction, and density functional theory (DFT) calculations are used to discover the formation of new phases within these nanotubes. This new phases significantly differs from bulk starting material, inducing different electronic properties.

In light of this new structural and chemical information, a growth mechanism for these NTs is proposed. In addition, we will detail the electronic properties of the new MLC phase which we predict as semiconducting in nature in contrast with the bulk phase which is metallic. Comparison with chalcogenide-based misfit NTs of the TbS-CrS_2 system will also be provided [5]. Finally, calculations beyond the DFT level are in progress to derive the band-gaps and dielectric functions of these new phases which will be compared to data extracted from monochromated low-loss EELS [6].

References

[1] J. Rouxel *et al*., J. Alloys Compd. 229, 144 (1995)
[2] G. Radovsky *et al*, Angew. Chem. Int. Ed. 50, 12316 (2011).
[3] LS Panchakarla, L Lajaunie, A Ramasubramaniam, R Arenal and R Tenne, ACS nano 10 (6), 6248–6256 (2016)
[4] LS Panchakarla, L Lajaunie, A Ramasubramaniam, R Arenal and R Tenne, Chem. Mater. 28 (24), pp 9150–9157 (2016)
[5] L.S. Panchakarla, L. Lajaunie, R. Tenne, R. Arenal. J. Phys. Chem. C The Journal of Physical Chemistry C 120 (29), 15600–15607 (2016)
[6] We acknowledge funding from the EU under Grant Agreement 312483-ESTEEM2, Grant Agreement 696656 Graphene Flagship and the Spanish Ministerio de Economia y Competitividad (MAT2016-79776-P).

Revisiting Graphene Oxide Chemistry via Spatially-Resolved Electron Energy Loss Spectroscopy

A. Tararan A.[1], A. Zobelli [1], A. M. Benito [2], W. K. Maser [2] and O. Stéphan [1]

[1] Laboratoire de Physique des Solides, Université Paris-Sud, CNRS UMR 8502, F-91405 Orsay, France
[2] Department of Chemical Processes and Nanotechnology, Instituto de Carboquímica ICB-CSIC, C/Miguel Luesma Castán 4, E-50018 Zaragoza, Spain

Graphene oxide (GO) is obtained by chemical oxidation and exfoliation of natural graphite. In the last decade, GO has attracted a widespread interest for its mechanical strength, tunable optoelectrical properties, simple processability and its potential as precursor for a low-cost and large-scale production of graphene. Indeed, chemical and thermal treatments allow to almost completely remove the oxygen, yielding reduced graphene oxide (RGO). Nevertheless, after about 150 years, the atomic structure of GO and RGO is still greatly debated. At present, the most acknowledged model for GO considers a random functionalization of the carbon basal plane with epoxide and hydroxyl groups, forming graphitic and partially oxidized domains. However, no definitive evidence of this model has been reported due to the lack of chemical analysis at the proper scale. For these reasons, nanometrically spatially-resolved spectroscopy of GO and RGO is highly suitable. In this work we provide the first chemical characterization of GO and RGO thin flakes at the scale of few nanometres, thanks to core Electron Energy Loss Spectroscopy (EELS) in a STEM microscope [1].
A major issue is represented by the extreme sensitivity of these materials to illumination and the use of this technique on GO and RGO has been so far very restricted. A new experimental set up combining a liquid nitrogen cooling system at the sample stage, a low accelerated electron beam (60 keV) and a liquid nitrogen cooled CCD camera with a low read-out noise of three counts r.m.s. and a negligible dark count noise has allowed us to overcome this limitation. Optimal illumination conditions have been defined by monitoring the evolution of the sample under continuous illumination, defining a maximal electron dose before substantial chemical modification of the order of 10^3 $e^-Å^{-2}$ and hence a 3 nm lower limit on the hyperspectral spatial resolution. Chemical maps of the atomic oxygen content of few layers GO and RGO show well separated domains on the scale of tens of nanometres. Overall, the oxygen amount has been observed to vary within 10-50 at.% in GO and 5-20 at.% in RGO. Energy-Loss Near-Edge Structures (ELNES) at the carbon K-edge exhibit well-defined features related to C-O bonding, previously not reported. Moreover different oxidation levels in GO and RGO are characterized by specific ELNES profiles. The highly oxidized regions in GO (~50 oxygen at.%, i.e. 1:1 C/O ratio) correspond to a full functionalization of the carbon network. With the support of complementary DFT numerical calculations, we suggest a model for the highly oxidized regions consisting in a full functionalization with hydroxyls, forming a 2D-sp^3 system.

Reference

A. Tararan, A.Zobelli, A. M. Benito, W. K. Maser, and O. Stéphan, *Chem. Mater.*, 28 (2016) 3741

Investigation of vibrational behavior of gas using ELNES

H. Katsukura[1], T. Miyata[1], M. Shirai[2], H. Matsumoto[2], and T. Mizoguchi[1]
[1]Institute of Industrial Science, Univ. Tokyo, [2]Hitachi High Tech. Co.

The reactions in gaseous phases and at gas-solid interfaces are industrially important, such as solid oxides fuel cell. In order to understand these reactions, identification of the dynamic motions of molecules, such as vibration, in the gases at a local area, such as interface, are crucial. Recently, atomic resolution analysis using transmission electron microscopy under gas environment are available by the grace of the technological developments for in-situ observations. However, the identification of the dynamic behavior of gas using electron microscopy has not been achieved. In this study, we measure electron energy loss spectroscopy (EELS) of gases, and the molecular vibration of the gases were investigated with an aid of the theoretical calculation.

EELS of four type gases, CO, O_2, N_2, and CH_4, were measured at room 298K and 1,273K using environmental TEM (HF-3300). The gaseous structure models were performed with molecular dynamics at 298K and 1,273 K using a force field. Histograms on the bond distance of all the molecules in gaseous models for each temperature were obtained. Then, the populations of the respective molecular structures were obtained from the histogram. The theoretical calculations for respective molecule structures were separately calculated using the first-principles plane-wave basis pseudopotential method, CASTEP code [1]. The theoretical spectra for the gaseous models at the respective temperatures were calculated making the weighted sum.

The experimental and theoretical spectra of oxygen were shown in Fig.1(a). In experimental spectra, small but clear differences were observed between the spectra at 298 K and 1,273 K. In 1,273 K, the intensity of the peak A decreased by approximately 20%, and the peaks B and C becomes broader. The calculated spectrum reproduced the trends in the experimental spectra. Figures 1(b)(c) show the histograms of the O=O bond distance at the 298K and 1,273K, respectively. The model at 1,273K has broader O=O bond length distribution than that at 298K. The broader profile in the spectrum at the 1,273K can be ascribed to the wider variety of the O=O molecular structure, which is made by the stronger motion of molecules. The details and results on other gases will be discussed in the poster.

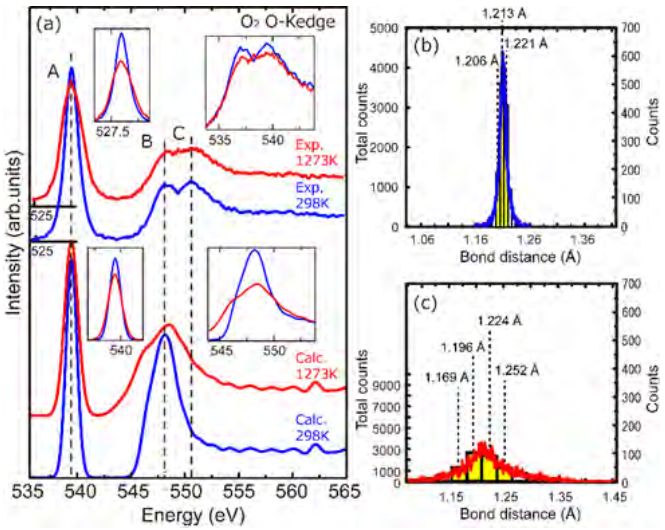

FIG. 1. (a) Experimental and calculated O_2 O-K edge at 298K and 1,273K. (b,c) bond-length histograms at 298K and 1,273K.

References

[1] S. J. Clark et al., Z. Krist. 220 (2005) 567

Collateral beam damage in aromatic small molecules for organic devices

A.E. Goode[1], Q. Ramasse[2], and S. Heutz[1]

[1] Department of Materials, Imperial College London, London, SW7 2AZ, UK.
[2] SuperSTEM Laboratory, Daresbury, Warrington, WA4 4AD, UK.

Aromatic small molecules such as copper phthalocyanine (CuPc) and C_{60} are used as model systems in organic photovoltaic devices. To understand device performance, it is necessary to characterise structure and chemical bonding at the interface. However, realising these measurements at the nanoscale is challenging due to the sensitivity of organic materials to beam damage, a process which is incompletely understood.

Recent studies of amorphous polymer samples containing both aliphatic and aromatic carbon reveal the role of fast secondary electrons in creating collateral damage which extends tens of nanometers beyond the electron probe [1-3]. Here, damage in crystalline aromatic small molecule samples will be investigated in order to determine the highest possible spatial resolution at which organic device interfaces can be mapped by low-loss EELS spectrum imaging.

CuPc thin films have been created using ultramicrotomy of embedded single crystals. Figure 1 shows varying beam damage, measured from the decrease in intensity of the 2 eV peak [4], while a focused electron probe is held at discrete points of varying interpixel distance. This method has been reported previously [3]. The effect of operating voltage and sample cooling on the extent of damage will also be explored.

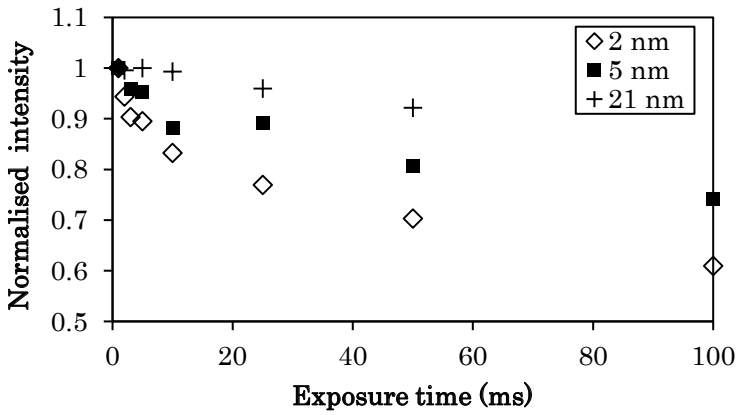

FIG. 1. Variation of the 2 eV signal in CuPc with increasing exposure time to a 50 pA electron probe (at 300kV), using a range of stepping increments. The intensity under the 2eV peak is normalised to intensities acquired using 1 ms exposures.

References

[1] R.F. Egerton et al., *Micron.* 43 (2012) 2-7.
[2] K. Siangchaew et al., *Phil. Mag. A* 80 (2000) 1001-1016.
[3] D. Arayasantiparb et al. The Nature of the Epoxy-Alumina Interphase (2000)
[4] J.A. Alexander et al., *J. Mater. Chem. A.* 4 (2016) 13636-13645.
[5] This research was supported by a Junior Research Fellowship from Imperial College London, sponsored by Dr. Alexandra Porter.

Crystal Structure Analysis of Two-Dimensional Materials using Quantitative Annular Dard-Field Imaging

Shunsuke Yamashita[1], Shogo Koshiya[1], Kazuo Ishizuka[1, 2], and Koji Kimoto[1]

[1] National Institute for Materials Science (NIMS), Tsukuba, Ibaraki 305-0044, Japan
[2] HREM Research Inc., Higashimatsuyama, Saitama 355-0055, Japan

Quantitative annular dark-field (ADF) imaging, in which the ADF intensity at each pixel is normalized by the incident probe current, has attracted much attention because it enables us to compare experimental ADF images with simulated images without any arbitrary scaling parameters [1]. In this study, we acquired ADF images of two-dimensional materials using a Titan^3 (FEI) microscope at 80 kV. Acquired images were converted into quantitative images by a newly developed quantification procedure [2,3]. By combining with multislice simulation, stacking structures of few-layer graphene and polytypes of transition metal dichalcogenide (TMD) were analyzed.

FIG. 1(a) shows a quantitative ADF image of few-layer graphene. Normalized ADF intensities by the incident probe current are called quantitative contrasts in this study. Mean quantitative contrasts measured in 1–4 layer regions were compared with simulated values (FIG. 1(b)). Four types of stacking structures (AAA, ABA, ABC, rotational stacking) were assumed in simulation. The rotational stacking structure, in which the relative rotation angle between each layer is about 30°, shows good agreement with experimental results. Further details and polytype analysis of TMD will be also discussed at the conference.

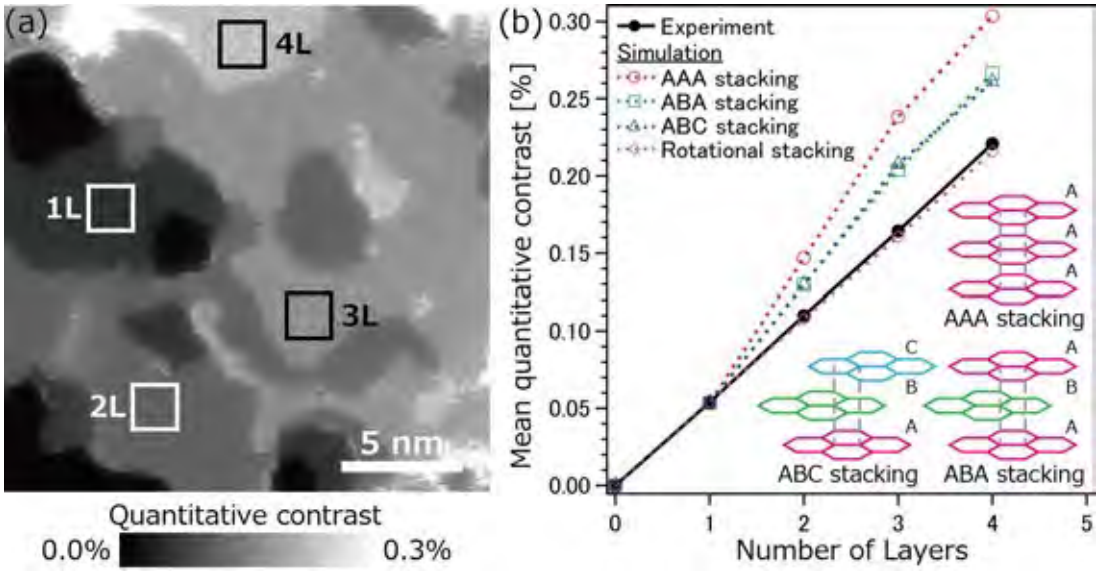

FIG. 1. (a) Quantitative ADF image of few-layer graphene. (b) Mean quantitative contrasts of few-layer graphene as a function of the number of layers.

References
[1] J. M. LeBeau and S. Stemmer, *Ultramicroscopy* 108 (2008) 1653.
[2] S. Yamashita et al., *Microscopy* 64 (2015) 143.
[3] S. Yamashita et al., *Microscopy* 64 (2015) 409.
[4] This study was supported by Grant-in-Aid for Scientific Research on Innovative Areas (Synthesis of Mixed Anion Compounds toward Novel Functionalities).

Improvement of dielectric function measurements on α-Al_2O_3 by 60kV and 200kV TEM-EELS

N. Sakaguchi, L. Tanda, and Y. Kunisada

Faculty of Engineering, Hokkaido University, Kita 13, Nishi 8, Kita-ku, Sapporo, Hokkaido 060-8628, Japan

The dielectric function of α-Al_2O_3 was measured by electron energy-loss spectroscopy (EELS). The influence of Cerenkov radiation was significant in measurements using a 200 kV transmission electron microscope (TEM) and the correct dielectric function could not be obtained using the conventional Kramers-Kronig analysis (KKA). However, we realized that the combination of EELS and the difference method provided an accurate measurement of the dielectric function for α-Al_2O_3 even at an accelerating voltage of 200 kV [1]. The dielectric functions obtained via a 60 kV TEM slightly differed from the optical data in the energy range of 10–20 eV due to the retardation effect, even though Cerenkov loss was thoroughly suppressed. Using the improved KKA routine [2], we obtained the correct dielectric function that agreed with the optical data. The present technique is especially useful in measuring the dielectric function by EELS with a small collection semi-angle.

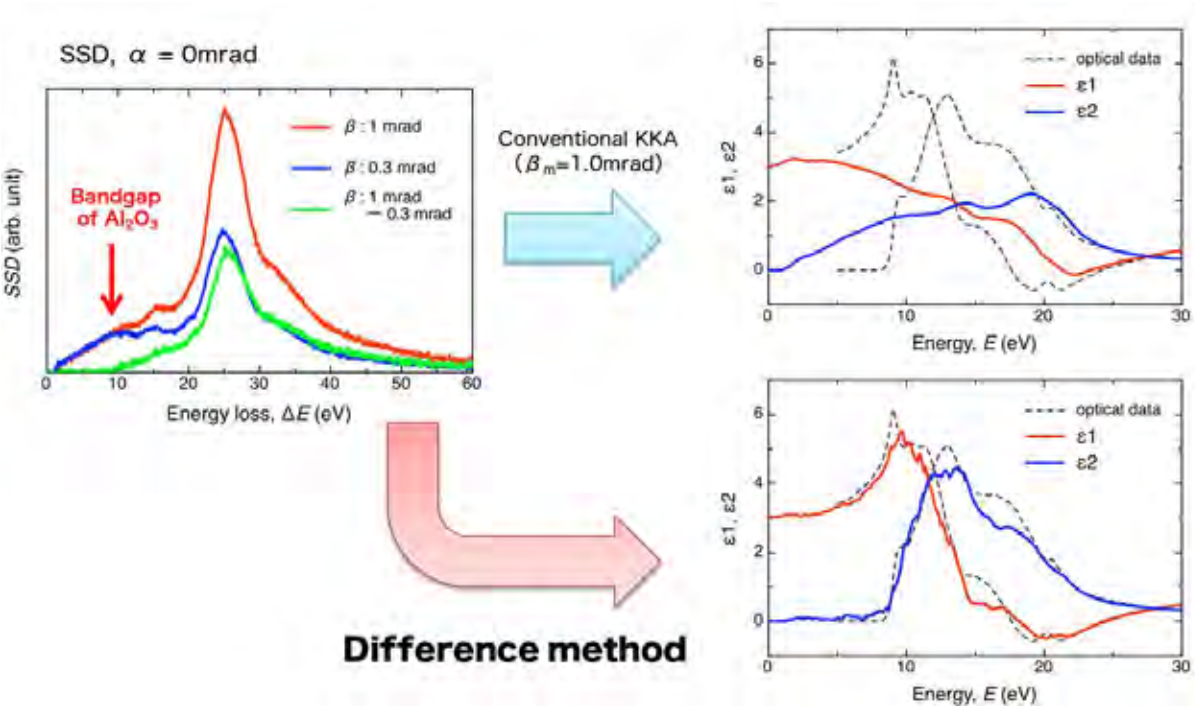

FIG. 1. Dielectric function of α-Al_2O_3 obtained by TEM-EELS. The difference method provides the correct dielectric function even at an accelerating voltage of 200 kV

References

[1] N. Sakaguchi et al., *Ultramicroscopy.* 169 (2016) 37.
[2] N. Sakaguchi et al., *Microscopy.* 65 (2016) 415.

Magnetism and morphology in faceted B2-ordered FeRh nanoparticles

B. Warot-Fonrose[1], M. Liu[1,2] , P. Benzo[1], H. Tang[1], M. Castiella[1], N. Tarrat[1], C. Gatel[1], M. Respaud[3], J. Morillo[1] and M. J. Casanove[1]
[1] CEMES, CNRS UPR 8011 and Université de Toulouse - 29 rue Jeanne Marvig, F-31055 Toulouse, France
[2] Research Center of Laser Fusion, CAEP- Mianyang 621900, China
[3] LPCNO, Université de Toulouse, INSA, UPS, CNRS - 135 avenue de Rangueil, F-31077 Toulouse, France

The FeRh alloy presents a remarkable and unusual magnetic transition from a low temperature antiferromagnetic state (AFM) to a high temperature ferromagnetic state (FM) close to Tc = 370K accompanied by a 1% volume expansion [1]. The transition is obtained for a narrow composition range $0.48<x<0.56$ in the B2-ordered α' crystal phase of $Fe_{1-x}Rh_x$. In recent years, there has been a strong interest for this alloy for applications in microelectronics [2], heat-assisted magnetic recording [3] or magnetic random access memories [4]. While the FM-AFM transition is sharp in the bulk alloy, the persistence of a FM component at low temperature in FeRh thin films raised important questions about the effect of size reduction, interfaces and surface termination on their magnetic properties.
We have predicted by first-principle calculations that the surface configuration can stabilize a low temperature ferromagnetic (FM) state in FeRh nanoparticles in the 6–10 nm range [5]. This has been observed on nanoparticles synthetized by magnetron sputtering. The structure, composition, morphology and Rh-(100) surface termination are confirmed by aberration-corrected (scanning) transmission electron microscopy. The FM magnetic state is verified by vibrating sample magnetometry experiments. The combined theoretical and experimental study emphasizes the strong interplay between surface configuration, morphology and magnetic state in magnetic nanoparticles.

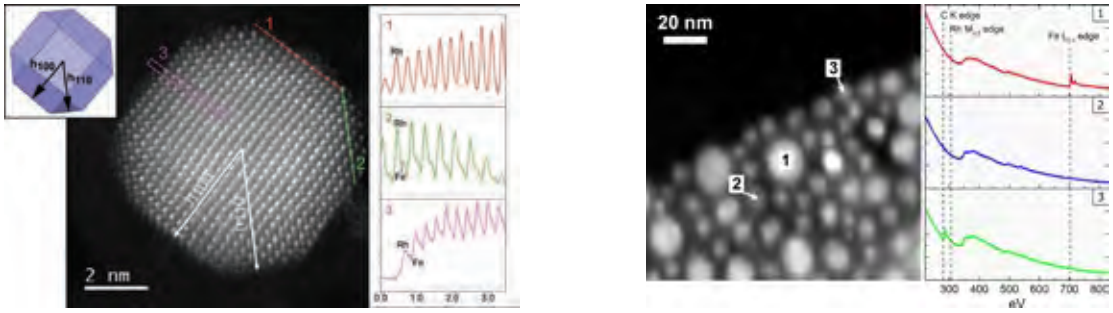

FIG. 1. (left) HAADF-STEM image of a NP observed along the [001] direction of B2-FeRh. (right) EELS analyses of particles deposited by co-sputtering of Fe ad Rh targets

References
[1] Fallot M. and Hocart R., Rev. Sci. 77 (1939) 498
[2] Radu I., et al., Phys. Rev. B 81 (2010) 104415
[3] Cherifi R. O., et al. Nat. Mater. 13 (2014) 345
[4] Marti X., et al. Nat. Mater. 13 (2014) 367
[5] Liu, M., et al. EPL 116 (2016) 27006

Characterization of the electron beam damage of $Li_4Ti_5O_{12}/Li_2TiO_3$ model interface by electron energy loss spectroscopy.

M. Kitta and S. Tanaka

[1]Research Institute of Electrochemical Energy, Department of Energy and Environment, National Institute of Advanced Industrial Science and Technology (AIST), 1-8-31, Midorigaoka, Ikeda, Osaka 563-8577, Japan

Lithium titanium oxides with ternary system (LTO) are widely used for energy and environmental technology. Mostly, $Li_4Ti_5O_{12}$ with spinel structure is widely used for electrode material of Li-ion battery [1], and Li_2TiO_3 with monoclinic structure is also used as a tritium breeder ceramics for international thermonuclear experimental reactor (ITER) [2]. The structural stability is significant for these two type of LTO materials. In former case, it provides stable Li-ion insertion and extraction cycle property. In the latter case, thermodynamically and irradiation stability is needed for effective tritium release. Here we studied structural stability of these two type of LTO materials by electron beam irradiation of transmission electron microscopy, and evaluate their deterioration feature by electron energy loss spectroscopy (EELS).

We prepared $Li_4Ti_5O_{12}/Li_2TiO_3$ model interface specimen for transmission electron microscopy (TEM) study. The interface was irradiated with high dose scanning electron beam, and then investigated by scanning EELS spectrum imaging, continuously.

Fig. (a) shows interface of $Li_4Ti_5O_{12}/Li_2TiO_3$. Square area of black solid line was irradiated by 1.16×10^9 electrons / nm^2 dose amount of electron beam. Ti-*L* ELNES extracted from points 1-4 were shown in Fig. (b). Spectrum 1 and 4 were $Li_4Ti_5O_{12}$ and Li_2TiO_3, respectively. Four peaks show character of Ti^{4+}. Spectrum 2 and 3 shows damaged phase of $Li_4Ti_5O_{12}$ and Li_2TiO_3, where Ti-*L* ELNES was changed from spectrum 1 and 4. Ti^{4+} feature of spectrum 2 is more deterioration than spectrum 3, meaning that $Li_4Ti_5O_{12}$ phase is more affected by the electron beam irradiation.

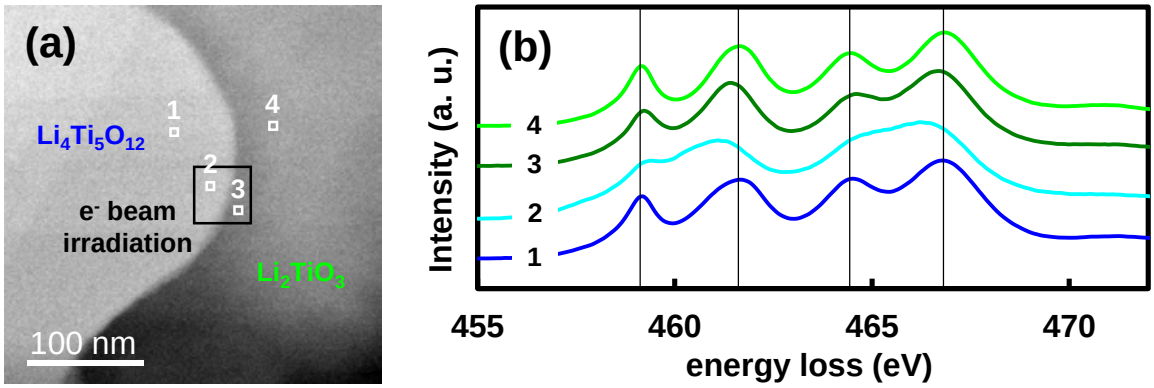

FIG. 1. Characterization of $Li_4Ti_5O_{12}/Li_2TiO_3$ interface by EELS. (a) ADF image of interface. (b) Ti-*L* ELNES extracted from points 1-4 in (a).

References
[1] N. Takami, H. Inagaki, et. al., J. Power Sources 244 (2013) 469-475.
[2] J.G. van der Laan, H. Kawamura, et. al., J. Nuc. Mater. 283 (2000) 99-109.

Noble metal salts on two dimensional materials studied by atomic resolution STEM imaging

H. Okuno[1], D. Kalita[1], C. Alvarez[1], A. Benayad[2], E. Prestat[3], E. Raux[2], H. Le Poche[2], M.T. Dah[1], C. Vergnaud[1], M. Jamet[1], A. Marty[1], P. Pochet[1] and J. Dijon[2]

[1] INAC/CEA-Grenoble, Université Grenoble Alpes, Grenoble 38000 France
[2] LITEN/CEA-Grenoble, Université Grenoble Alpes, Grenoble 38000 France
[3] The University of Manchester, Manchester M13 9PL, UK

Anchoring noble metals such as Au, Pt and Pd onto 2D layered structures such as graphene and transition metal dichalcogenides (TMDs) is of great importance because the coupling of noble metals and 2D layers is expected to generate various new functional materials such as doped graphene transparent electrodes[1] and TMD based catalysts for hydrogen evolution reaction (HER)[2]. The aim of this work is to study how noble metals are dispersed and/or integrated into 2D monolayers, providing a platform to explore future functional materials.

In this work, the noble metals are deposited on poly-crystalline graphene and $MoSe_2$ monolayers via metallic salts. The integration of the nobel metals into the 2D materials was analyzed using *Low Voltage Aberration Corrected (Scanning) Transmission Electron Microscopy (LVAC-(S)TEM)*. Atomic resolution TEM and STEM imaging shows multiple metallic forms of Pt and Au; nanoclusters, nanoparticles, isolated atoms on the surface, and atoms integrated into the 2D monolayers. The positions of the metals are discussed in relation to the atomic structure in monolayers, such as defects and grain boundaries. Furthermore, electron beam irradiation was used to induce crystallization of nanoparticles from metallic salt. The mechanism of metal particle formation from the metallic salt network inside carbon nanotubes was investigated by electron energy loss spectroscopy (EELS).

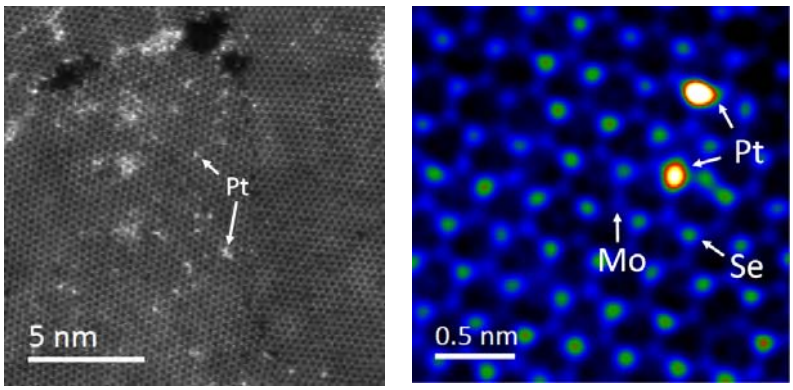

FIG. 1. Pt atoms observed on $MoSe_2$ monolayer surface by STEM HAADF imaging. Some of the Pt atoms are observed at the Se positions

References
[1] X. Huang et al., Nature Communications 4:1444 (2013).
[2] K. C. Kwon et al., J. Mater. Chem. C, 1 (2013) p2463.

Probing core electron orbitals by STEM-EDX mapping

J.S. Jeong[1], M.L. Odlyzko[1], P. Xu[1], B. Jalan[1], and K.A. Mkhoyan[1]

[1] Department of Chemical Engineering and Materials Science, University of Minnesota, Minneapolis, Minnesota 55455, United States

We have shown that by recording EDX maps from crystalline specimens using an aberration-corrected STEM equipped with a high-efficiency X-ray detection system, it is ultimately possible to probe core-level electron orbitals in real-space. In the case of $SrTiO_3$ both the 1*s* and 2*p* orbitals of Sr and Ti atoms are probed; as expected, 1*s* orbitals are always smaller than 2*p* orbitals, and all orbitals are localized on their respective atomic columns (Figure 1). This method should be applicable to any atomic columns in any crystal, and it is limited only by the rate of X-ray collection relative to electron-beam damage of the specimen [1,2].

We also have shown that these experiments allow accurate measurements of the electronic excitation impact parameters due to coulombic beam-orbital interaction, at 300 keV ranging from around 0.1 Å for deeply bound Sr 1*s*, Ti 1*s*, and Sr 2*p* orbitals, to about 0.3 Å for more weakly bound Ti 2*p* core orbitals. Similarly, it will be possible to probe core-level electron orbitals and measure impact parameters using EELS [3].

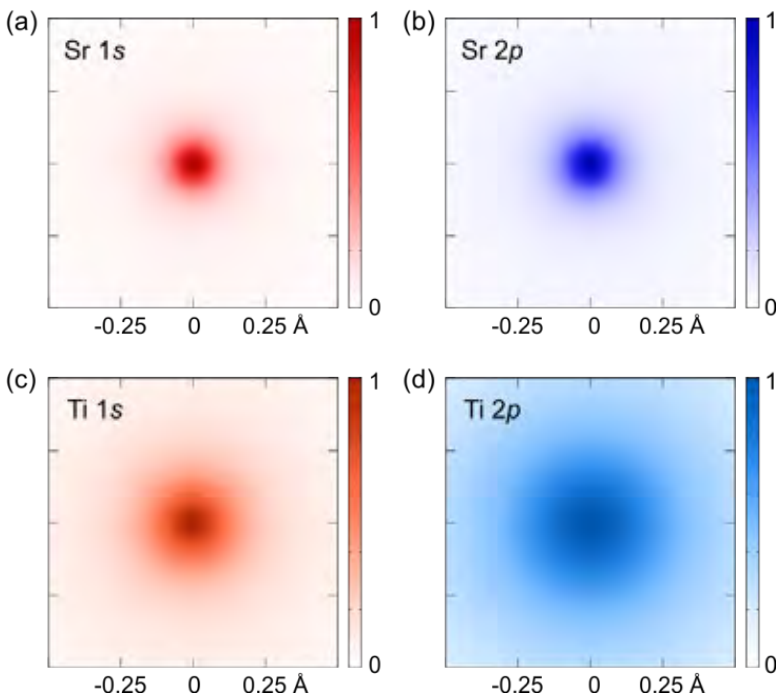

FIG. 1. (a)-(d) Experimentally observed projected excitation potentials for 1*s* and 2*p* orbitals of Sr and Ti, including the effects of atomic thermal vibrations and excitation broadening, obtained from the EDX maps.

References

[1] J.S. Jeong, M.L. Odlyzko, P. Xu, B. Jalan, K.A. Mkhoyan, *PRB* 93 (2016) 165140.
[2] J.S. Jeong and K.A. Mkhoyan, *Microsc. Microanal.* 22 (2016) 536.
[3] This work was supported in part by NSF DMR-1006706 and DMR-1420013.

Convergent-Beam EMCD: Pitfalls and New Approaches

S. Löffler[1,2], T. Schachinger[1,2], W. Hetaba[3,4]

[1] USTEM, TU Wien, Wiedner Hauptstraße 8-10, 1040 Wien, Austria
[2] IFP, TU Wien, Wiedner Hauptstraße 8-10, 1040 Wien, Austria
[3] FHI-Berlin, Faradayweg 4-6, 14195 Berlin, Germany
[4] MPI-CEC, Stiftstraße 34-36, 45470 Mühlheim an der Ruhr, Germany

Energy-loss magnetic chiral dichroism (EMCD) [1] is a widely available tool for studying magnetism on the nanometer and atomic scales. In its classical form, it employs incident and outgoing plane waves. With the high popularity of STEM-EELS and the increasing interest in phase manipulation and electron vortex beams, we investigate the theoretical possibilities and limitations of convergent-beam EMCD.
In particular, we look at two aspects of convergent beam EMCD (see Fig. 1). On the one hand, we investigate the conditions to obtain a large EMCD effect and – more importantly – a good signal-to-noise ratio (SNR). On the other hand, we explore the possibilities of using a post-specimen vorticity filter for directly measuring EMCD [2]. Together, these two approaches promise significant improvements to the versatility, signal strength, and spatial resolution of EMCD [3].

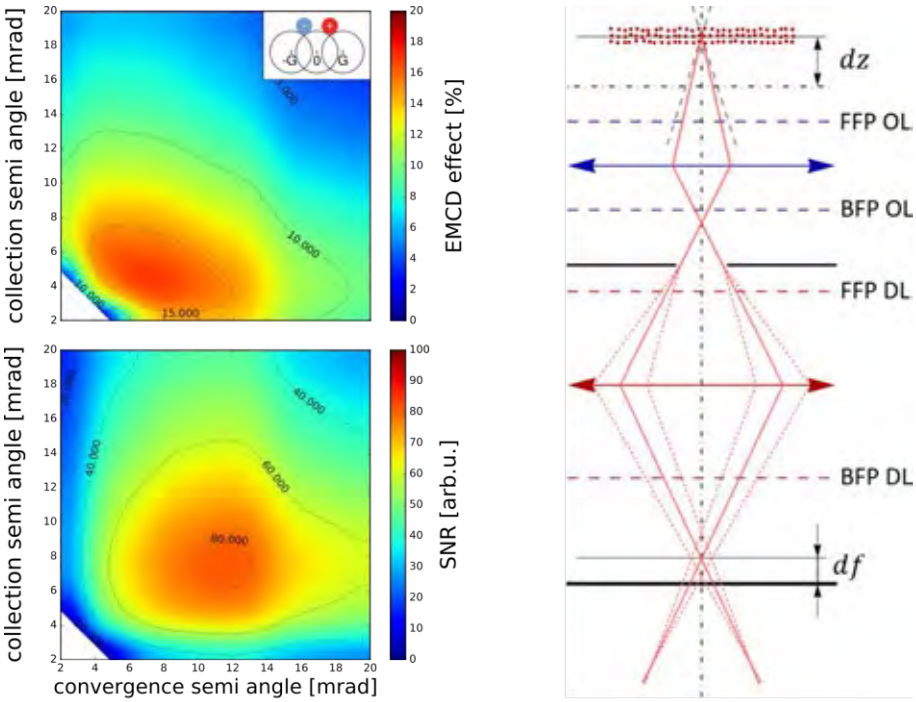

FIG. 1. Left: EMCD effect (top) and SNR (bottom) for convergent beam EMCD with the collection area touching the diffraction disks for 10 nm thick Fe. Right: Measurement setup for using a vortex filter in the selected area aperture (between the objective lens (blue) and the diffraction lens (red)).

References
[1] P. Schattschneider et al., *Nature* 441 (2006) 486.
[2] T. Schachinger et al., *submitted*.
[3] The authors thank Peter Schattschneider for many fruitful discussions. This research was supported by the FWF (grants I543-N20, J3732-N27).

Robust extraction of magnetic signals at sub-nanometer resolution

J. Spiegelberg[1], S. Muto[2], J. Rusz[1], and M. Ohtsuka[3]

[1] Department of Physics and Astronomy, Uppsala University, Box 516, 75120 Uppsala, Sweden
[2] Advanced Measurement Technology Center, Institute of Materials and Systems for Sustainability, Nagoya University, Chikusa-ku, Nagoya 464-8603, Japan
[3] Graduate School of Engineering, Nagoya University, Furo-cho, Chikusa-ku, Nagoya 464-8603, Japan

Electron magnetic chiral dichroism (EMCD) [1] is a technique which allows for investigation of magnetic structures in the electron microscope. Being an inelastic scattering effect, thus accessible with electron energy loss spectroscopy (EELS), the method promises to be able to resolve magnetic momenta of individual atomic columns when measured at highest resolutions. However, while recent advances demonstrate the detection of EMCD signals with sub-nanometer sized electron probes [2], a direct mapping of magnetic structures at such resolutions remained elusive so far, mostly due to the low signal to noise ratio of atomic resolution EEL spectra and the additionally often low variance of the EMCD spectrum.

In this talk we will present the first ever atomic resolution EMCD maps measured using the APR-EMCD scheme [2]. An outlook on qualitative changes of magnetic momenta towards grain boundaries and surfaces will be given. Particular focus is directed to the extraction of the EMCD signal at the given (low) signal to noise ratio.

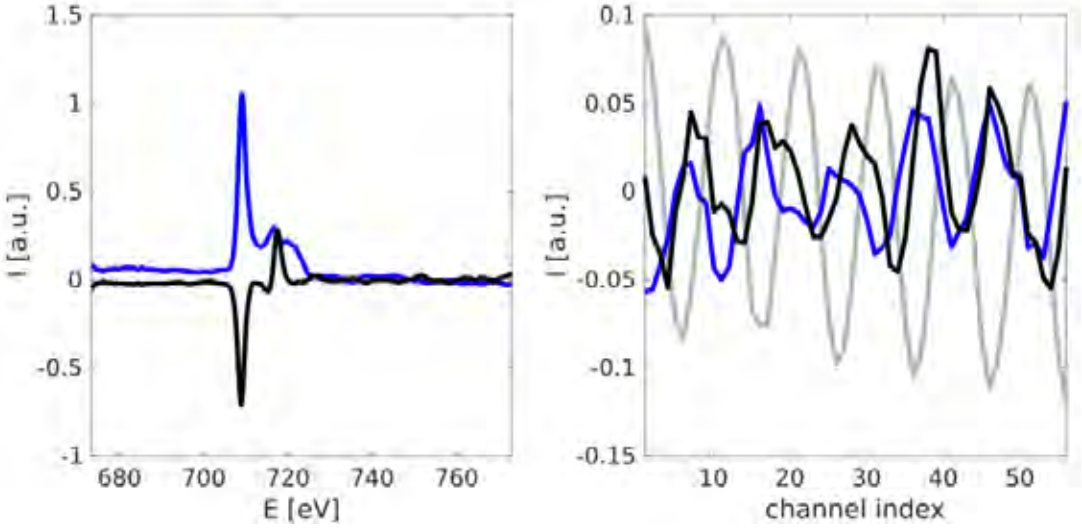

FIG. 1. Extracted non-magnetic (blue) and EMCD (black) signal (*left*) and associated weights of a line scan over several atomic planes, displaying the expected EMCD localization besides the atomic planes [2] (the rescaled mean intensity is shown in gray for comparison).

References

[1] P. Schattschneider et al., *Nature* 441 (2006) 04778.
[2] J. Rusz et al., *Nat. Comm.* 7 (2016) 12672.
[3] This research was supported by JSPS, STINT, CIM, the Swedish Research Council, the Göran Gustafsson's and the K. and A. Wallenberg Foundation.

Surface Plasmon Resonance Modes of Upright Split Ring Resonators Probed by EELS and CL

I.C. Bicket[1], E.P. Bellido[1], S. Meuret[2], A. Polman[2], and G.A. Botton[1]

[1] Dept. of Materials Sci. & Eng., McMaster University, Hamilton, ON, Canada
[2] AMOLF, Science Park 104, 1098 XG Amsterdam, the Netherlands

The split ring resonator (SRR) holds much promise in the field of metamaterials, generating an effective negative permittivity and permeability controlled by the induction of a magnetic dipole moment at resonance frequencies [1]. Using nanoscale SRRs pushes the metamaterial's active properties into the visible or near-infrared (IR) regime, through the excitation of surface plasmon resonance (SPR) modes. The fabrication of an upright SRR opens many possibilities for effective light coupling to induce a magnetic moment parallel to the substrate (Fig. 1a).

We have studied the SPR modes of a single nanoscale upright SRR and an arrangement of multiple SRRs forming a toroidal structure using the complementary techniques of high resolution EELS and cathodoluminescence (CL). EELS provides information on a large energy range, from near-IR to beyond the visible regime (Fig. 1c), but is limited in effectiveness in showing the higher order SPR due to the combination of electron beam scattering and high confinement of short wavelength optical SPR modes. To address this limitation, we used CL to further probe the optical modes, revealing more structure than is accessible through EELS for both the single SRR (Fig. 1b) and toroidal structure.

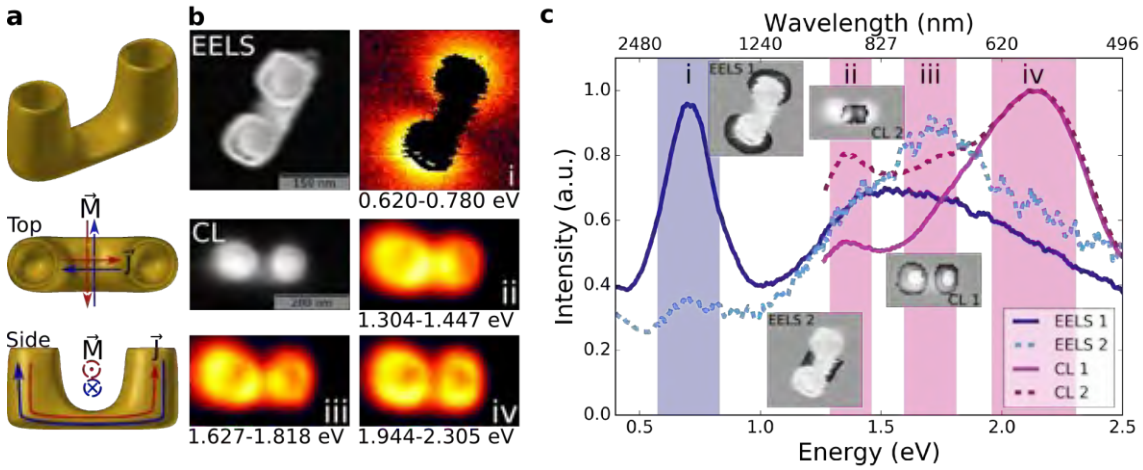

FIG. 1. EELS and CL results from a representative single upright SRR; (a) SRR and induced magnetic dipole configuration; (b) Dark field image (top left) and EELS map of first SPR mode (top right) and SEM image (middle left), CL maps of higher order SPR modes; (c) Spectra from indicated areas.

References

[1] D.R. Smith et al., *Phys. Rev. Lett.* 84 (2000) 4184.

[2] This research was supported by the Natural Sciences and Engineering Research Council. The EELS work was carried out at the Canadian Centre for Electron Microscopy, a facility supported by CFI under the Major Science Initiative program, NSERC and McMaster University.

Implementing electron energy gain spectroscopy in STEM

Pabitra Das[1], Jean-Denis Blazit[1], Marcel Tencé[1], Luiz Tizei[1], Christian Colliex[1], Odile Stéphan, and Mathieu Kociak[1]

[1] Laboratoire de Physique des Solides, Université Paris Sud - ORSAY - FRANCE

The quest for a technique to combine the spectacular spectral resolution of optical probes and spatial resolution of the electron probe has been going on for a long time. However, the possibility of integrating these two probes was first anticipated in 1999 [1], and a few years later, a compact theoretical formalism of the technique named electron energy-gain spectroscopy (EEGS) was proposed [2]. In EEGS, electrons pick up energy from external illumination, normally the coherent output of a finely tuned laser. Although the electrons and photons do not couple linearly in free space due to energy-momentum mismatch, the presence of a nanostructure can break the mismatch by providing the extra momentum through induced light fields, like the evanescent plasmonic field of the nanostructure. Employing synchronized femtosecond pulses of electrons and very intense pulse of photons, electron energy gain has been demonstrated, a technique commonly called as photon-induced near-field electron microscopy (PINEM) [3].
In our lab, we are developing an EEGS setup in one of the existing STEM (VG HB 501). The goal is to do spectroscopy by varying the laser energy and detecting the energy gain of electrons. We use a paraboloid mirror (used in cathodoluminescence) to focus the laser output on the sample surface. In PINEM, pulsed guns are used to detect only those electrons that go through energy gain or loss in interaction with the laser pulse. We propose an alternative to pulsed gun in terms of fast blanking of the electron beam. We will discuss the details of our proposed scheme and the instrumental developments that took place in Orsay so far.

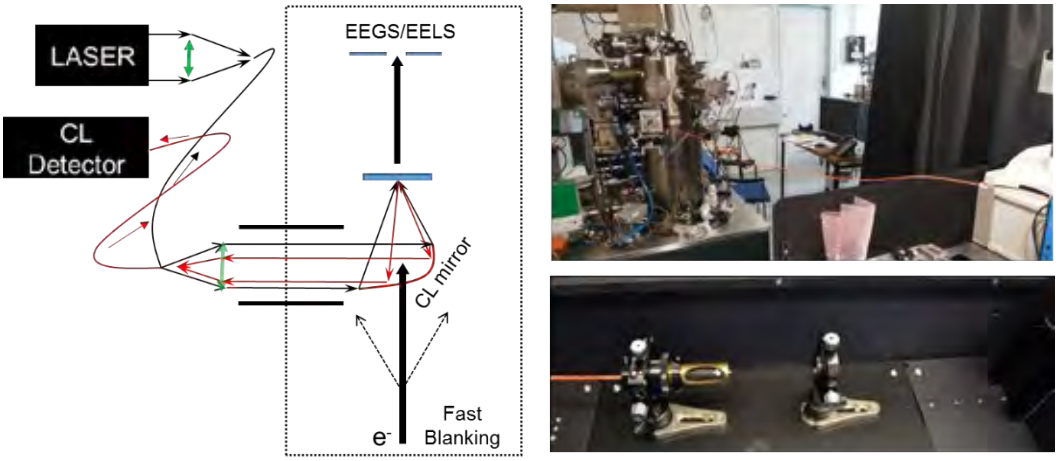

FIG. Schematic of the proposed EEGS set up (left) and the actual set up (right).

References
[1] A. Howie, *Inst. Phys. Conf. Ser.* **1999**, 161, 311.
[2] F. J. García de Abajo, and M. Kociak, *New J. Phys.* **2008**, 10, 073035.
[3] B. Barwick et al. *Nature* **2009**, 462, 902.

Acknowledgement: This project has been supported financially from the ESTEEM 2 project and the French ANR FEMTOTEM project.

Time-Dependent Excited State Response in Nanostructures

P.E. Batson[1], A. Konečná[2], M.J. Lagos[1] and J. Aizpurua[2]

[1] Institute for Advanced Materials, Devices and Nanotechnology, Departments of Physics and Materials Science, Rutgers University, Piscataway, NJ, USA.
[2] Center for Materials Physics (CSIC-UPV/EHU) and Donostia International Physics Center, "DIPC," Donostia-San Sebastian, 20018, Spain

Recently, we calculated the *lateral* forces imposed by a keV electron on a metal nanoparticle, using the time- and spatially-dependent EM fields for the swift electron – nanoparticle system.[1] We can also evaluate, in space and time, the *parallel* forces which drive electron energy loss. The result describes a dielectric response in time and space. In principle, this quantity is accessible by Fourier analysis of the complex frequency dependent specimen response to a driving force having a known amplitude and phase. For a Causal process, we should be able to obtain the complex experimental result from EELS spectra by a Kramers-Kronig (KK) transform, provided we can obtain complete, error-free spectra. Usually, we also restrict this treatment to uniform, thin materials, correcting for surface scattering to remove non-material dependent behavior.

Nanoscale objects are very hard to treat using this approach. Surfaces and interfaces, as mentioned above, shift resonant frequencies, introduce damping mechanisms that do not exist in the bulk material, and create coupling between bulk and aloof behavior in nearby free space. Controlling this behavior would be valuable for the design of better photovoltaics, photocatalysis, and other devices that depend on light matter interaction. We are looking at theoretical details of the microscopic, time dependent behavior of materials, nanoparticles, surfaces and interfaces to better understand the nature of spatially resolved inelastic scattering. We hope to develop tools that allow a more direct spatial probe of behavior on a point by point level in nanostructures. And we think that understanding the time dependence of these processes may be important for better understanding of energy transfer among resonant modes of nanostructures, in the same way that understanding the detailed time dependence of the lateral forces revealed many unforeseen behaviors we describe in [1].

We will review the work on the time dependence of lateral forces, showing how, for instance, expected attractive dielectric forces become repulsive diamagnetic forces during the very close approach of a relativistic electron to a 2nm diameter Au sphere. We will also describe the prediction of a "mini-wake" that occurs within 10-20 attoseconds of the close approach. This remarkable excitation describes a ~ 1nm wavelength fluctuation in charge density that likely packs hundreds of eV energy into the nm sized particle during the close approach of the electron. Later, this fluctuation decays into surface plasmons during femtosecond times. In MgO similar calculations show the decay processes continuing into picosecond times with phonon modes. We will also discuss progress on the project to create a time resolved picture of excited states of a nanoparticle, derived from experimental energy loss data.

PEB and MJL acknowledge support from the Department of Energy, Office of Science, Basic Energy Sciences under Award No. DE-SC0005132. JA and AK acknowledge support from the Spanish Ministry of Economy and Competitiveness MINECO under the Project FIS2013-41184-P.

[1] M.J. Lagos, A. Reyes-Coronado, A. Konečná, P.M. Echenique, J. Aizpurua and P.E. Batson, Attosecond and femtosecond forces exerted on gold nanoparticles induced by swift electrons, Phys. Rev. B, **93** 205440 (2016).

Vibrational EELS probes confined Fuchs-Kliewer modes

H. Lourenço-Martins[1] and M. Kociak[1]

[1] Laboratoire de Physique des Solides, Université Paris-Sud, CNRS UMR 8502, Orsay, France.

Recently, two reports [1,2] have demonstrated the amazing possibility to probe vibrational excitations in nanoparticles with a spatial resolution much smaller than the corresponding free-space phonon wavelength using electron energy loss spectroscopy (EELS). While Lagos et al. [2] evidenced a strong spatial and spectral modulation of the EELS signal over a nanoparticle, Krivanek et al. [2] did not. Here, we show that discrepancies among different EELS experiments as well as their relation to optical near- and far-field optical experiments can be understood by introducing the concept of confined bright and dark Fuchs-Kliewer modes [3] (cFK), whose density of states is probed by EELS. In particular, we show that EELS is directly related to Infra-Red absorption spectroscopy (see Figure) and therefore shares little with Raman spectroscopy. cFK modes are the phononic counterparts of localized surface plasmons; their properties can be deduced by analogy with the later case [4]. We will give simple yet generic formulas for computing their energy, EELS probabilities and optical cross-sections, and show that they allow to rationalize the recent experiments [1,2] in simple terms. These formulas only depend on few parameters (LO and TO energy values essentially). The presented formalism makes it straightforward to predict or interpret phenomena already known for localized surface plasmons such as environment-related energy shifts and surface phonon localization.

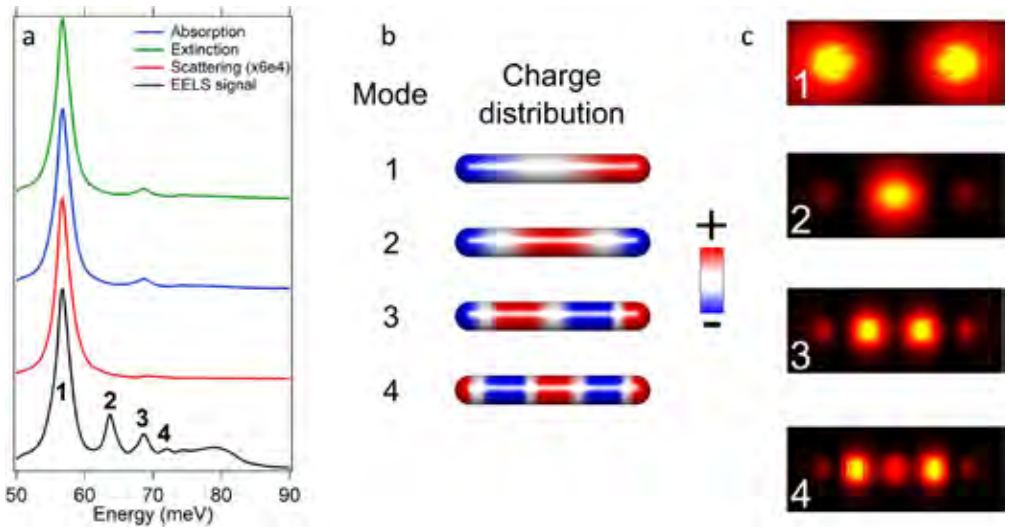

FIG. 1. (a) Simulated EELS spectra and optical cross-sections for an MgO nanorod (200 nmX30 nm) (b) Charge distribution for the four first modes. (c) Corresponding EELS maps. All simulations performed with MNPBEM [5].

References

[1] O. Krivanek et al., Nature 514, 209–212 (2015)

[2] M. Lagos et al., Nature 543, 529–532 (2017).

[3] R. Fuchs & K. L. Kliewer, Phys. Rev. 140, A2076–A2088 (1965)

[4] F. Ouyang et al., Philo. Mag. Part B 60, 481–492 (1989).

[5] U. Hohenester & A. Trügler, Comp. Phys. Com. 183, 370‑381 (2012).

Sponsors

Platinum Plus Sponsors

JEOL Solutions for Innovation

nion

GATAN

FEI™

JEM-F200

JEM-F200 (Nick name : F2) is a multi-functional electron microscope of the next generation to meet diversified needs.
F2 provides a user-oriented integrated-control-environment developed with excellent performance and a variety of functions.

JEOL JEOL Ltd.

3-1-2 Musashino Akishima Tokyo 196-8558 Japan Sales Division Tel. +81-3-6262-3560 Fax. +81-3-6262-3577
www.jeol.com

The business domains of the JEOL Group are classified into “Scientific / Metrology Instruments”, “Industrial Equipment” and “Medical Equipment”.
“Scientific / Metrology Instruments Business” Electron Optics Instruments, Analytical Instruments, Measuring Instruments
“Industrial Equipment Business” Semiconductor Equipment, Industrial Equipment
“Medical Equipment Business” Medical Equipment

GRAND ARM

Atomic Resolution electron Microscope

JEM-ARM300F

The JEM-ARM300F is a highly stable microscope featured with the technology cultivated through the development of the JEM-ARM200F.

The spherical aberration corrector can be mounted to STEM and/or TEM lens systems.

The JEM-ARM300F is the 300kV-ultrahigh resolution electron microscope of the world's highest-performance.

300 kV STEM Imaging (GaN[211])

Dark-field image, Ga-Ga atomic column

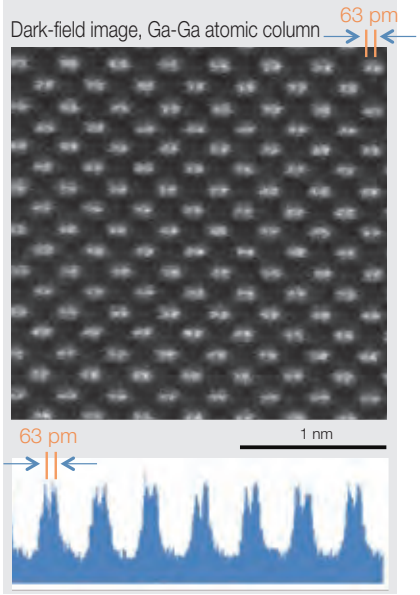

300 kV TEM Imaging (silicon nitride β-Si_3N_4)

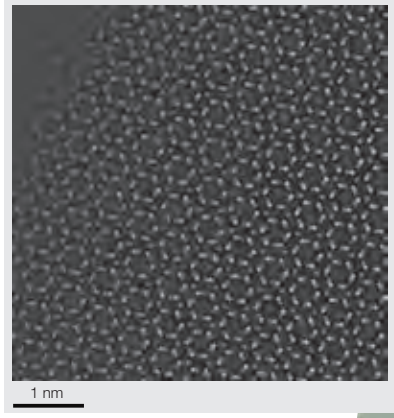

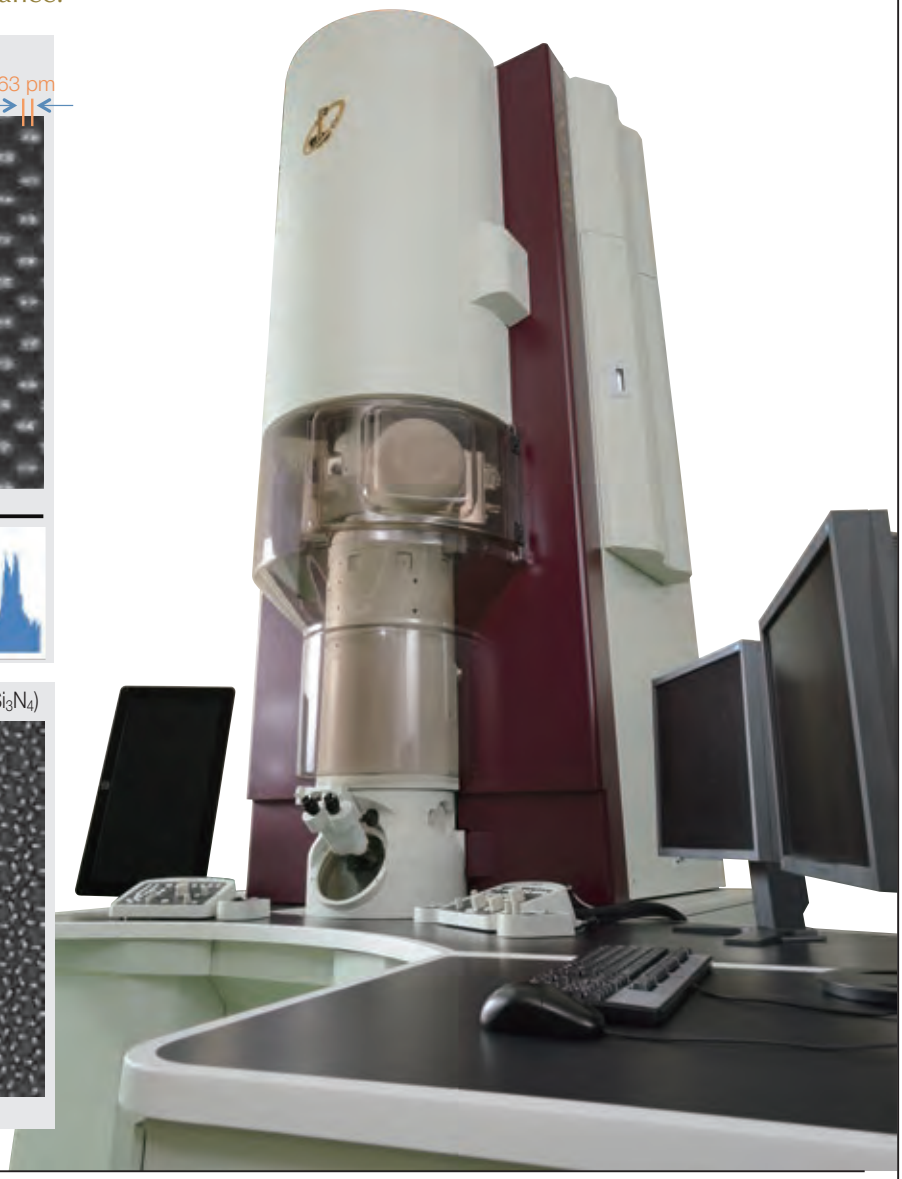

JEOL Ltd. http://www.jeol.com/

1-2 Musashino 3-Chome Akishima Tokyo 196-8558 Japan
Sales Division Telephone:+81-3-6262-3560 Facsimile:+81-3-6262-3577

unique tools for materials science

UltraSTEM MC™

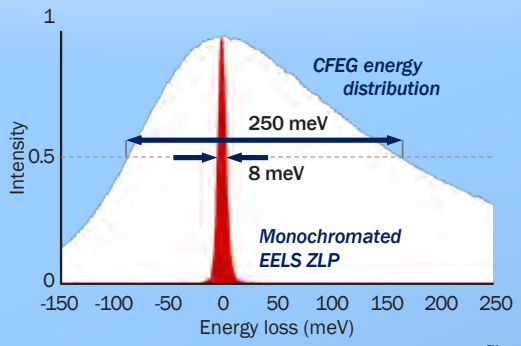

Zero loss peak (ZLP) acquired with Nion UltraSTEM MC™, 8 ms, 60 keV primary voltage, compared to the unmonochromated ZLP. Courtesy Rutgers U.

High Energy Resolution Monochromated EELS-STEM

- 40 – 200 keV
- Dispersing-undispersing
- < 10 meV energy resolution (at 60 keV)

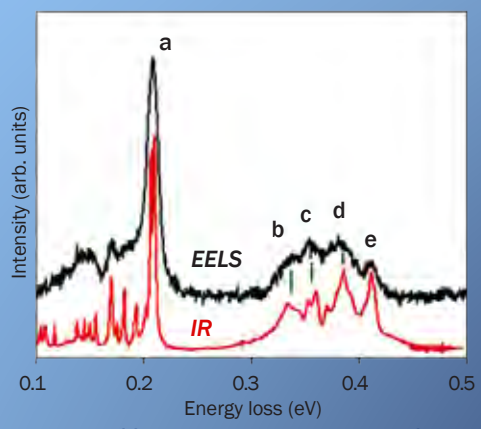

EEL spectrum of Guanine acquired with Nion UltraSTEM MC, aloof mode, 60keV primary voltage, compared with FTIR spectrum. Peaks b-e show vibrations due to different H bonds. Peter Rez et al., Nature Communications 7 (2016) 10945

UltraSTEM 200™

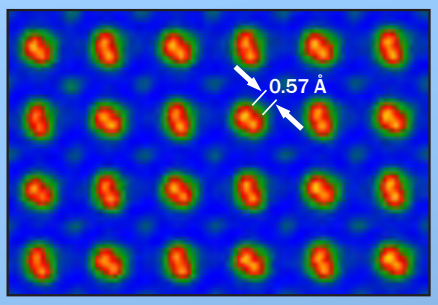

Double Yttrium columns resolved in an HAADF STEM image of a YAP crystal. Alternate double columns have different orientations. Nion UltraSTEM™, 200 keV. Courtesy Dr. M.F. Chisholm, ORNL, and SMRC, U. Tenn.

- 40 – 200 keV
- Ultra-bright CFE electron gun
- Ultra-stable sample stage
- Ultra-high sample vacuum
- 0.6 Å spatial resolution (at 200 keV)
- 0.35 eV resolution EELS
- 0.7 sr solid-angle EDXS

www.nion.com

nion

tools for tomorrow™

world-leading results

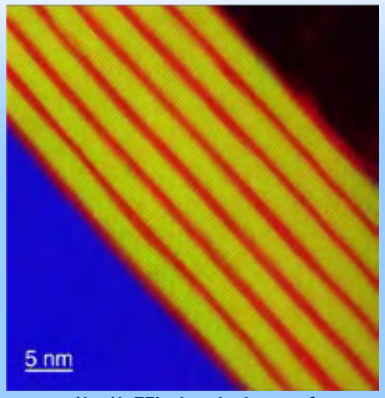

1k×1k EEL chemical map of $LaMnO_3/SrMnO_3$ superlattice.
Monkman et al.,
Nature Mater. 11 (2012) 855-859

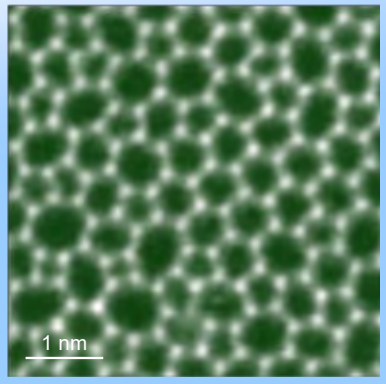

HAADF image of a two-dimensional SiO_2 glass.
Huang et al., Nano Letters 12 (2012) 1081-1086

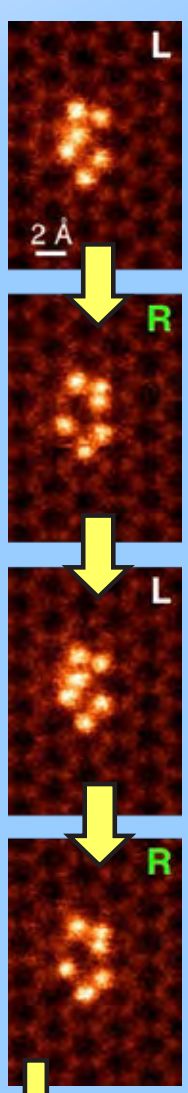

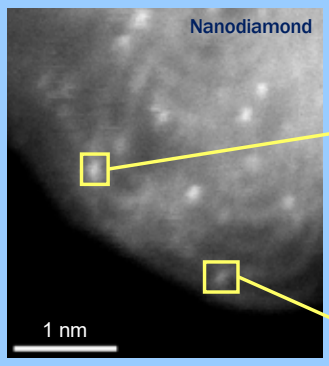

HAADF STEM image of single-atom impurities in meteorite nanodiamond. Stroud et al., Appl. Phys. Lett. 108 (2016) 163101

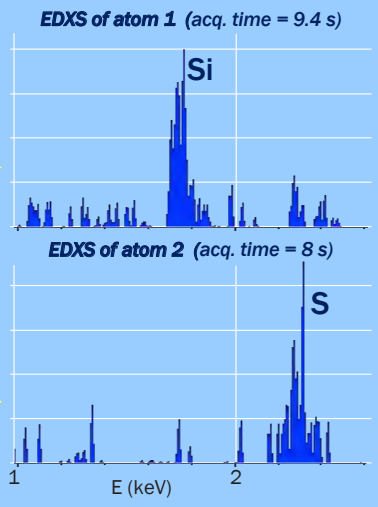

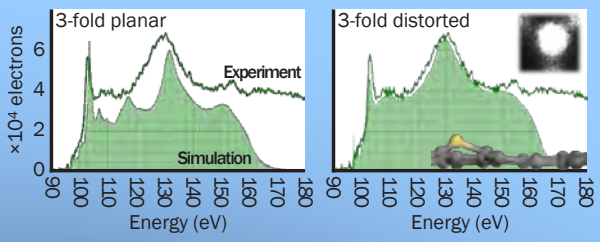

Analyzing the atomic environment of a single Si atom by EELS fine structure studies.
Ramasse et al., Nano Letters 13 (2013) 4989-4995

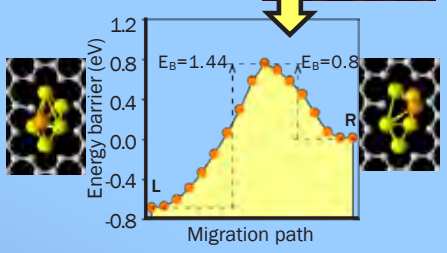

Exploring structural configurations for 6 Si atoms embedded in a 9-atom hole in graphene.
Lee et al., Nature Comms 4 (2013) article 1650

www.nion.com

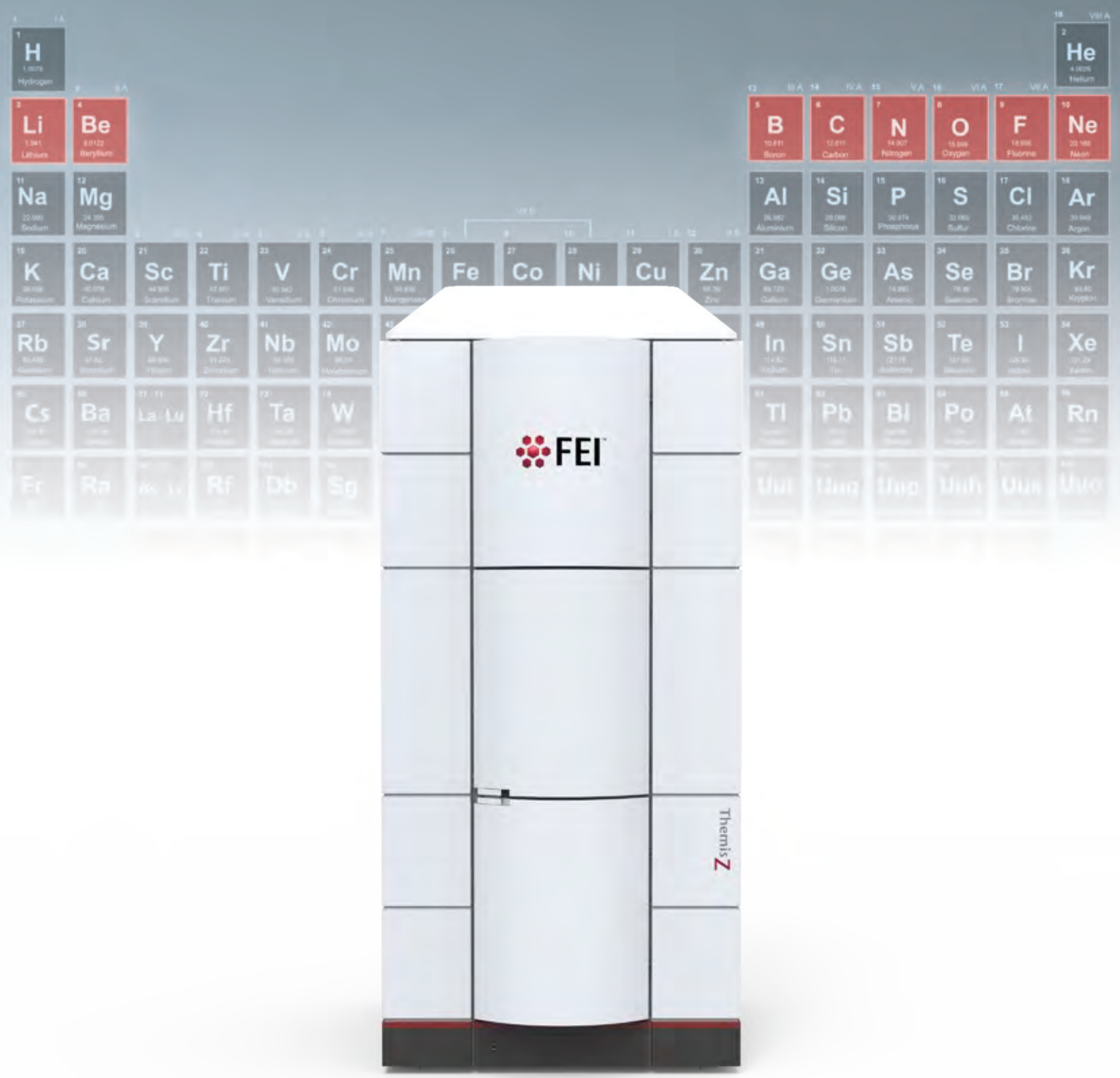

Think you've seen Themis? Meet Z.

We're making it easier to analyze low-Z, beam sensitive materials that are typically difficult to image in STEM mode. Discover how the FEI Themis Z can help you explore the widest range of materials across the periodic table.

Discover more at FEI.com

FEI™

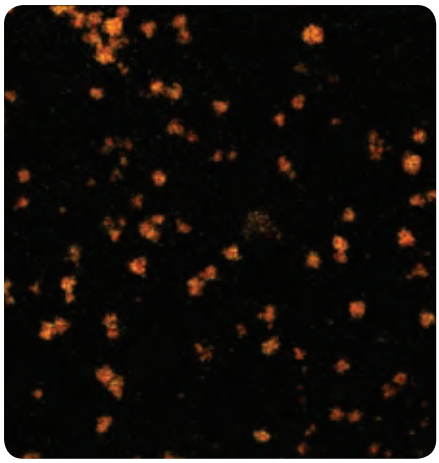

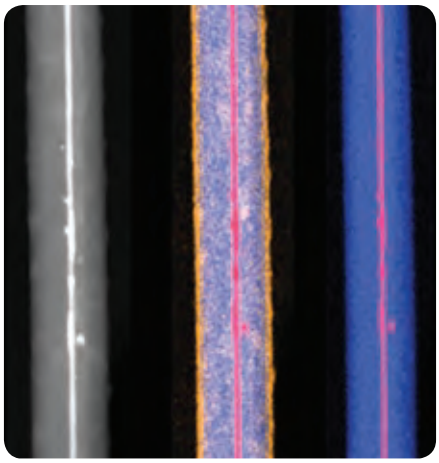

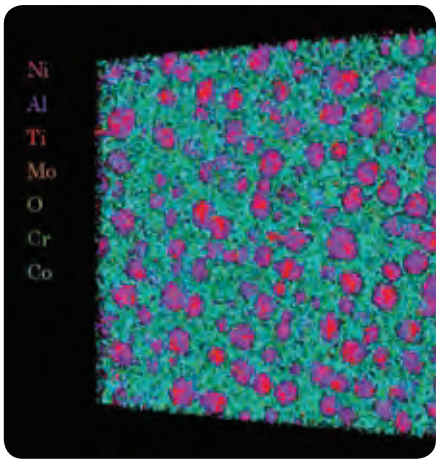

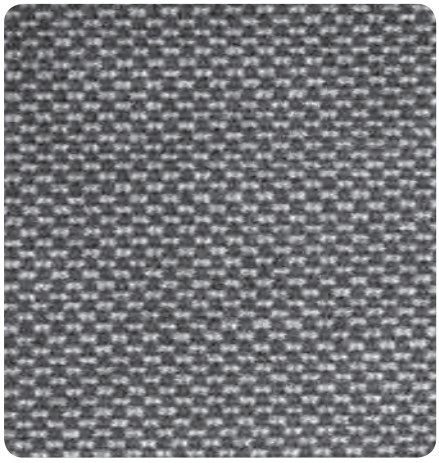

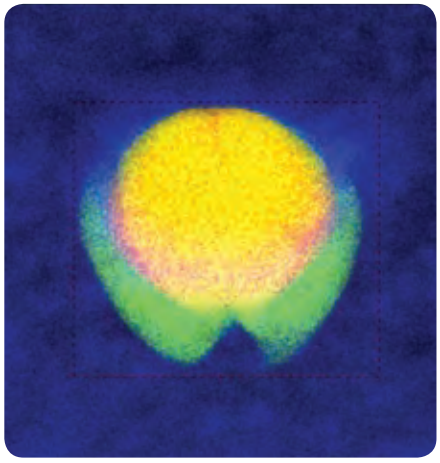

Simply Advanced

Fast imaging and analysis in multiple dimensions

FEI's Talos S/TEM provides the fastest compositional analysis of materials—with superior accuracy and efficiency. Whether you work with metals, light elements or nanoparticles, from macro to atomic scales, Talos gives you the insight to structure and composition for a complete understanding of material properties.

- **Fast EDS Mapping:** Obtain 2D maps in minutes and 3D EDS maps in hours instead of days.
- **Fast navigation and imaging:** Highest throughput, highest resolution uncorrected S/TEM images—even for beam sensitive and challenging materials
- **Space to do more:** FEI TEMs have the space to accommodate additional in situ holders for dynamic imaging, diffraction, and tomography applications

Learn more at **FEI.com/Talos-ms**

FEI™

Elevate Your EELS Experience

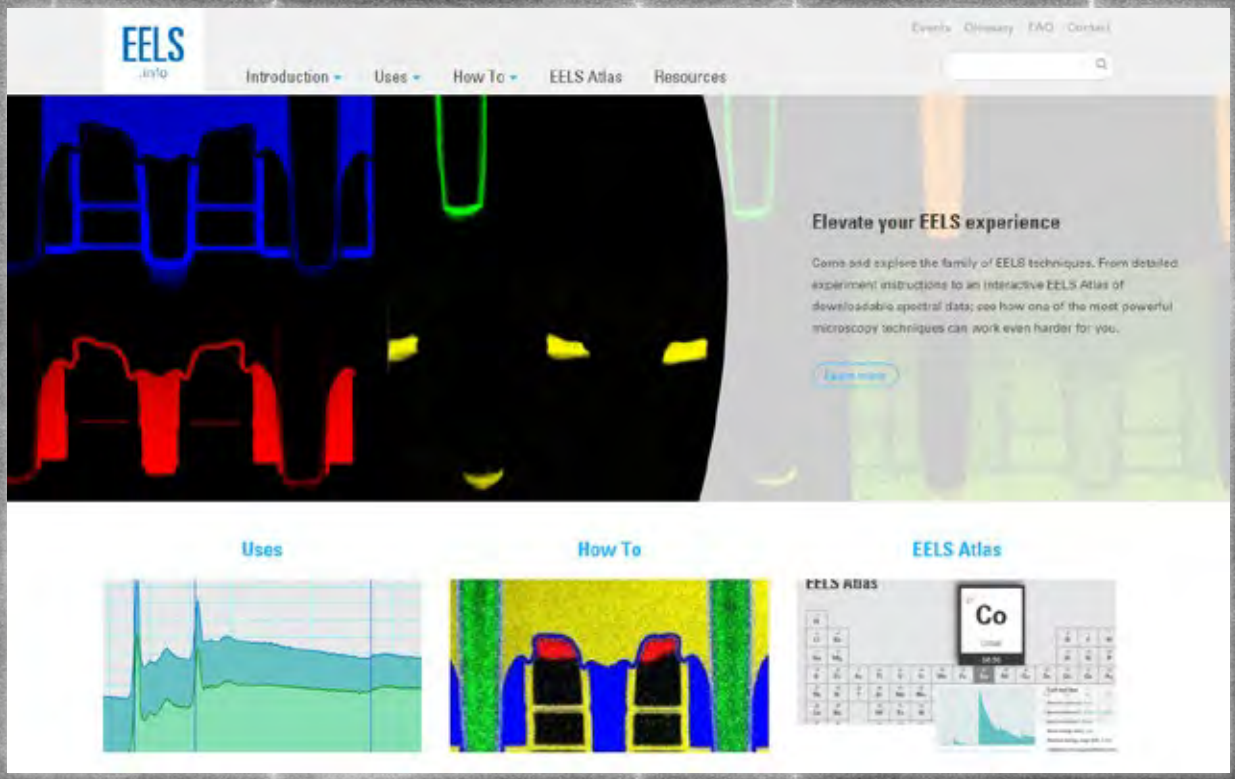

Enhance your EELS knowledge and experience with EELS.info

EELS.info is an educational website aimed at supporting and expanding the EELS community. The website includes:

- Background and theory of EELS based techniques
- Detailed instructions on how to perform and optimize EELS, EFTEM, and SI experiments
- Interactive EELS Atlas of downloadable spectral data and the ability to share your spectra

GATAN

Simplify Your EELS Workflow

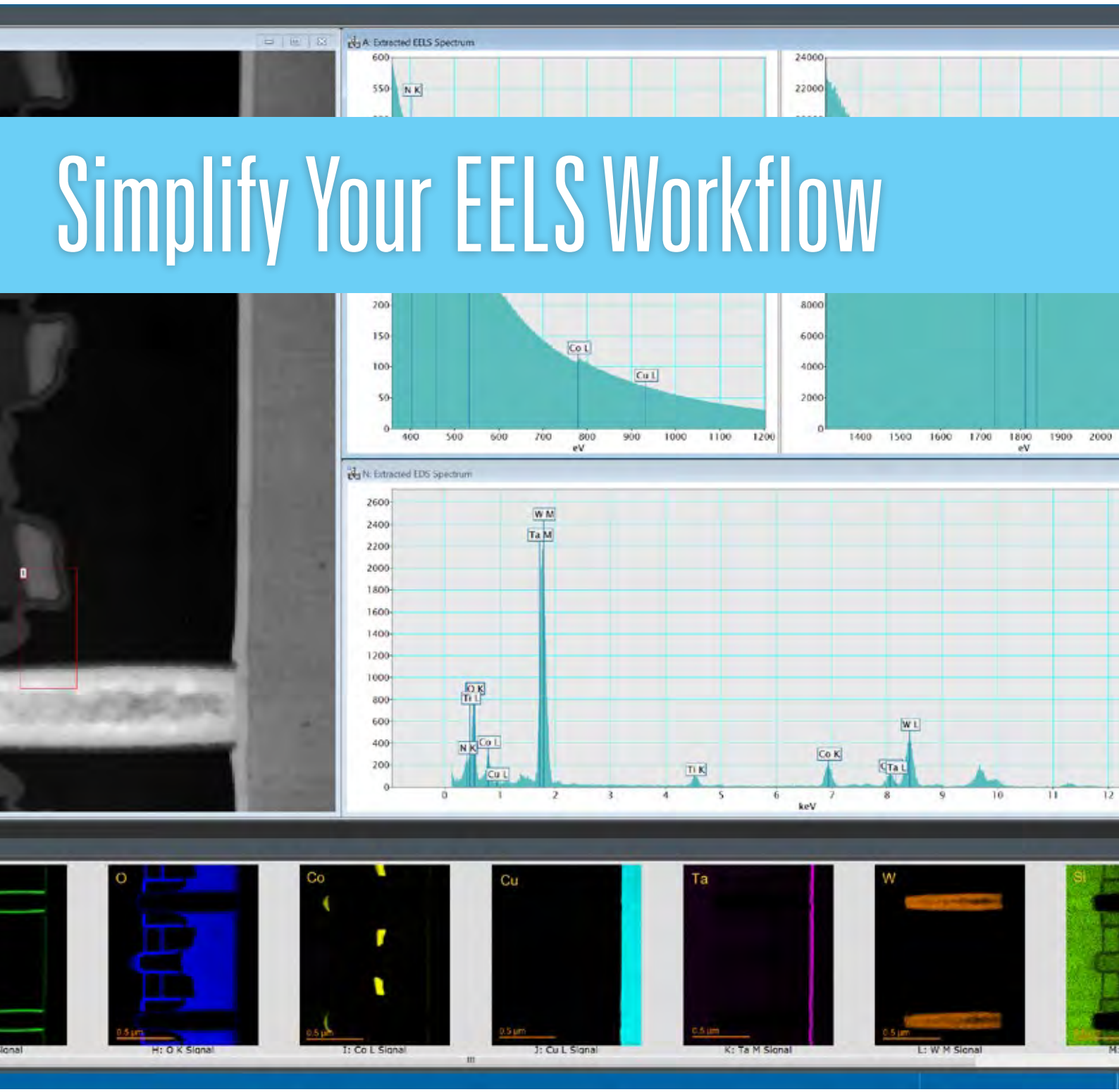

Gatan Microscopy Suite (GMS) 3

Experience a complete re-visioning of electron microscopy's leading software with new, simplified user interface, ease-of-use features, and experiment-oriented workflows.

- Technique-centric workflow that guides you through set up, execution, and analysis
- Tabbed workspaces and data layout manager for a user-friendly experience
- Dedicated view for live data to clearly separate new and old data
- Free offline analysis, processing, and visualization packages

  Now includes support for spectrum image, time series, and 4D STEM-diffraction data

GATAN

Reveal Groundbreaking Results

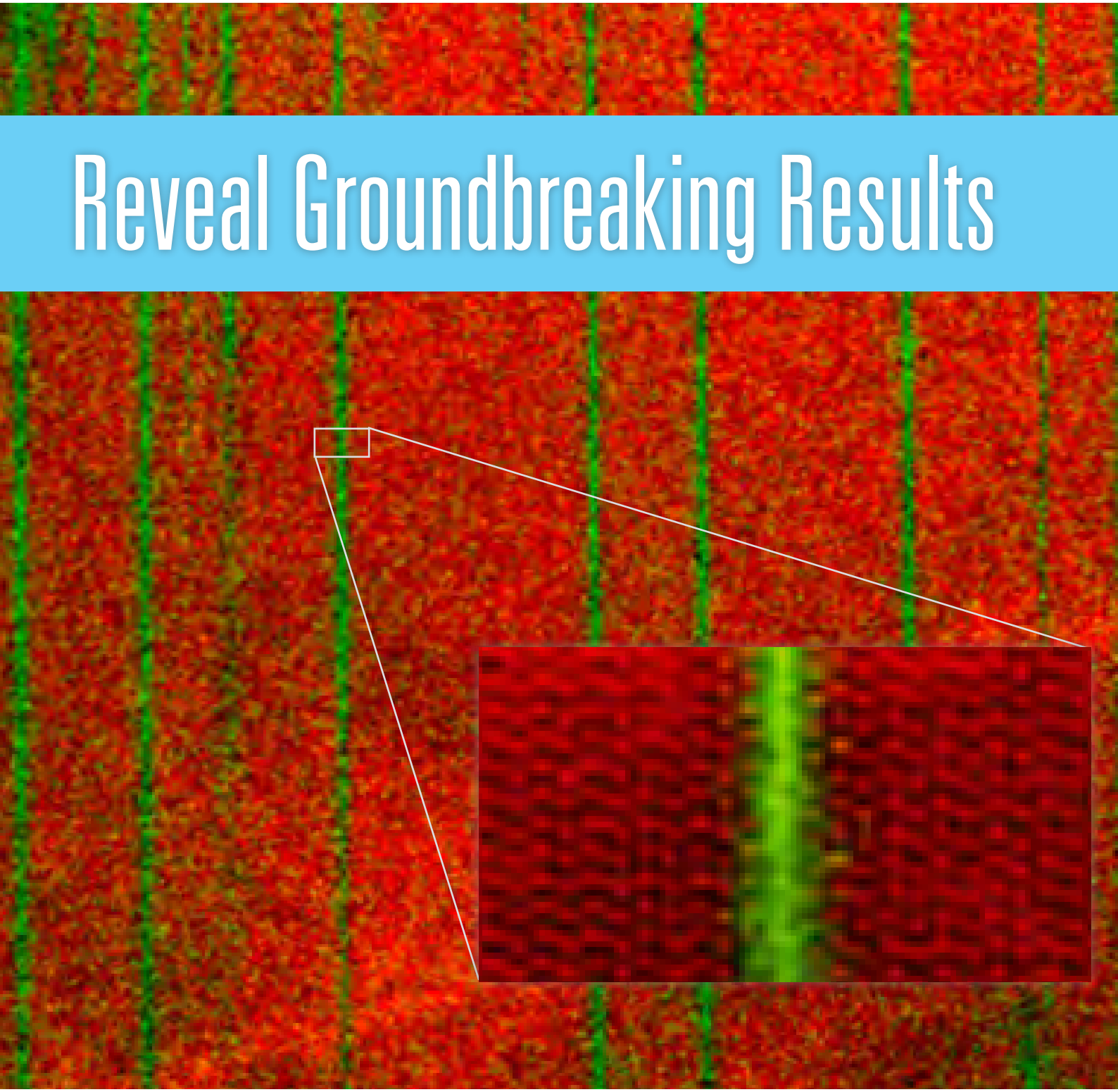

Go beyond what you've seen before

With the right combination of hardware, software, and knowledge, the results are limitless.

- Unified and flexible set up, acquisition, and analysis:
  Simple when you want it. Powerful when you need it.
- Counting mode EELS and EFTEM via the award-winning K2 Summit® detector*
- Provides the broadest energy range support available (from 15 – 300 kV, and beyond)*
- Supports all electron source types and energy resolution requirements*

GATAN

(*) May require custom product configurations. Contact Gatan for details. *Wide band gap semiconductor sample provided by Herbert Schmid. Special thanks to Dr. Giuseppe Nicotra for allowing us the usage of the microscope set up at CNR-IMM in Catania, Italy.*

Platinum Sponsors

HREM Research Inc.

OXFORD INSTRUMENTS

The Business of Science®

Hitachi High-Tech

HITACHI
Inspire the Next

Innovation of the Ultimate LV-STEM

The world's highest-resolution SEM, the Hitachi SU9000, is the pinnacle of low-kV lattice-scale imaging. Diffraction, EDS, EELS, and multiple-signal-filtering technologies are integrated within the Hitachi SU9000 system to provide the next-generation platform for advanced materials research.

SEM / STEM Simultaneous Imaging

Surface & Volume information simultaneously

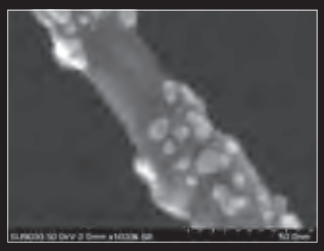

SE image

BF-STEM image

Specimen :
CNT coated by Polybenzimidazole attached with Platinum Nanoparticle

Specimen Courtesy :
A. Prof. Tsuyohiko Fujigaya, Department of Applied Chemistry,
Faulty of Engineering, Kyushu University

Low-Voltage Lattice Imaging

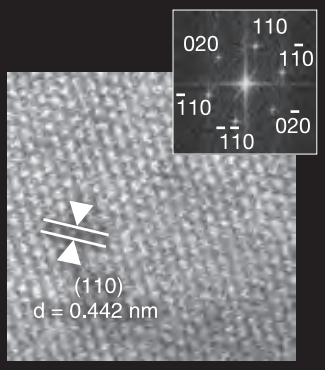

Vacc : 30 kV

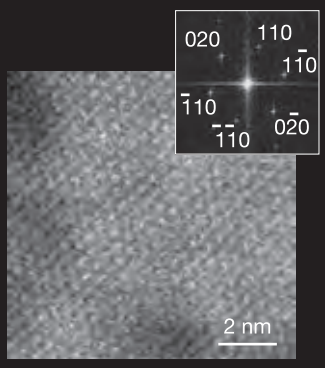

Vacc : 7 kV

Specimen : Pyrophyllite

30 kV STEM / EELS

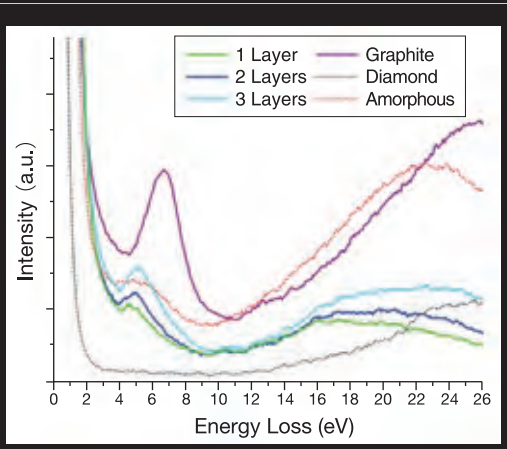

EEL spectra of graphene, amorphous carbon, graphite and diamond

Chemical analysis using STEM/EELS technique is now demonstrated at 30 kV (C, N, O, etc.).

30 kV STEM / EDS

Specimen :
Silver-Copper Nanoparticle

Specimen courtesy :
Dr. Dai Mochizuki,
Department of Applied Chemistry,
Tokyo Institute of Technology

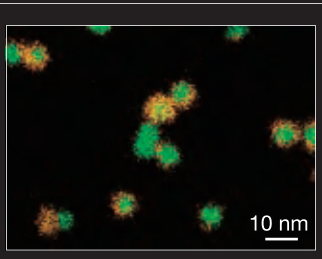

Ag/Cu EDS Layer map
(Orange : Cu-K, Green : Ag-L)

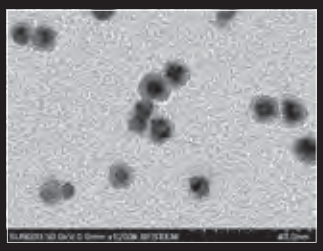

BF-STEM image

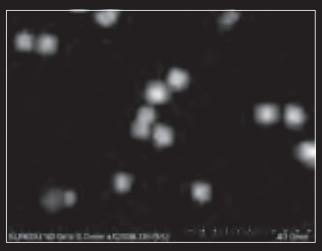

DF-STEM image

Hitachi High-Technologies Corporation

Global/Asia
+81 3 3504 7111 customercenter.ev@hitachi-hightech.com
www.hitachi-hightech.com/global/science/

Europe
+49 2151 643 5310 eminfo@hht-eu.com
www.hitachi-hightech.com/eu/

Americas
+1 800 548 9001 emdwebsite@hitachi-hta.com
www.hitachi-hightech.com/us/

Quantitative Electron Microscopy

HREM Research Inc. Specialized in Electron Microscopy

New Plug-ins

SmartAlign

DigitalMicrograph Plug-in

"SmartAlign" Scan-distortion Compensator

Rigid & Non-rigid Image Registration

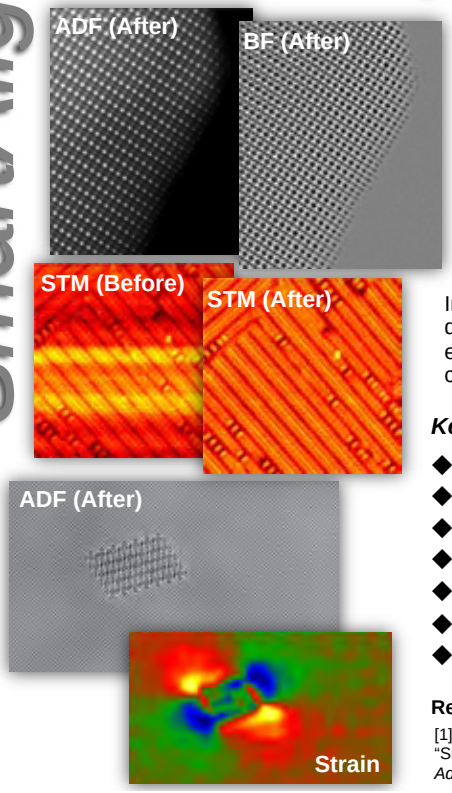

SmartAlign corrects for stage drift and scan distortion using fast multi-frame image acquisition [1], and improves resolution, signal-to-noise ratio, and image-intensity distribution while reducing beam damage effects.

Image-drift causes scans to appear sheared, and non-linear scan-distortions deforms image intensity distribution. The SmartAlign will effectively counter both of these effects, and deliver the images that can be further analyzed quantitatively, say for composition and strain.

Key Features

- Intuitive and interactive workflow for efficient image registration.
- Correction of image offsets, linear drift and non-linear distortion.
- No prior sample knowledge nor symmetry assumption required.
- Correction of distortions across multiple signals, e.g. ADF/ABF.
- Support for multi-frame spectrum-image to increase SNR.
- Support for digital super-resolution mode.
- Custom options included for TEM, STEM, STM/AFM.

References:

[1] L. Jones, H. Yang, T.J. Pennycook, M.S.J. Marshall, S. Van Aert, N.D. Browning, et al., "Smart Align—a new tool for robust non-rigid registration of scanning microscope data", *Advanced Structural & Chemical Imaging* **1**:8 (2015) doi:10.1186/s40679-015-0008-4.

sMoiré

DigitalMicrograph Plug-in

STEM Moiré Analysis

Analysis of STEM digital moiré images for Strain Mapping

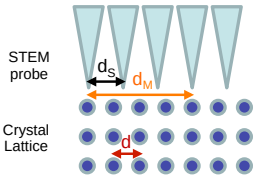

Artificial STEM moirés (d_M) are created in a STEM by deliberately choosing a low magnification where the scan step (d_S) is close to the crystalline periodicity (d) [1, 2].

sMoiré provides strain map from *single* STEM Moiré image using geometric phases [3]

sMoiré generates fully two-dimensional strain maps from *two* STEM Moiré images using the procedure similar to Dark-Field Holography [4] (HoloDark for DM plug-in [5])

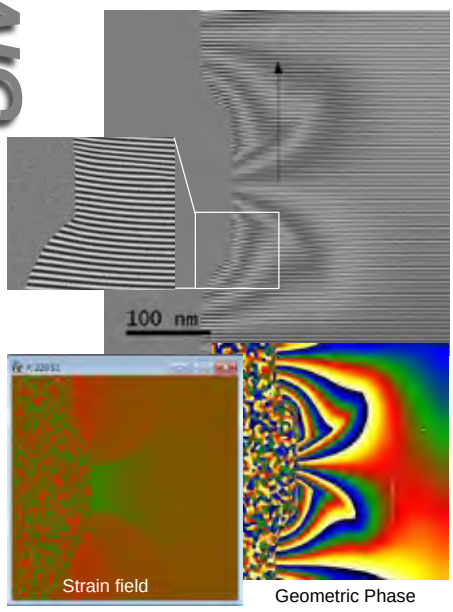

Key Features

- Aligns multiple STEM Moiré images to increase S/N ratio
- Can repeat the single Moiré analysis for a routine work
- Handles a scan-step close to a multiple of lattice spacing
- Aligns two STEM Moiré images by correcting drift, rotation and magnification changes
- Calculate an accurate scan-step from a nominal calibration
- Corrects "fly-back" instability of STEM scan-lines

References:

[1] D. Su and Y. Zhu, *Ultramicroscopy* **110** (2010) 229-233. *Scanning moiré fringe imaging by scanning transmission electron microscopy*.
[2] S. Kim, Y. Kondo, K. Lee, G. Byun, J. J. Kim, S. Lee and K. Lee, *Applied Physics Letters* **102**, 161604 (2013). *Scanning moiré fringe imaging for quantitative strain mapping in semiconductor devices*.
[3] M. J. Hÿtch, E. Snoeck, R. Kilaas, *Ultramicroscopy* **74** (1998) 131–146. *Quantitative measurement of displacement and strain fields from HREM micrographs*.
[4] M.J. Hÿtch, F. Houdellier, F. Hüe, and E. Snoeck, *Nature* **453** (2008) 1086-1089. *Nanoscale holographic interferometry for strain measurements in electronic devices*.
[5] HoloDark – holography for strain, HREM Research Inc.

Quantitative Electron Microscopy

HREM Research Inc.

Specialized in Electron Microscopy

Higashimatsuyama, Saitama, Japan
Tokyo office: Nibanchou, Chiyoda
support@hremresearch.com
www.hremresearch.com

xHREM™ WinHREM™/MacHREM™

FFT-Multislice Simulation Suite

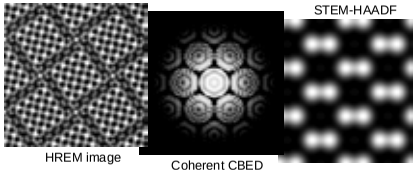

xHREM (Mac/WinHREM) is a versatile simulation suite that generates HREM images, dynamical diffractions, coherent CBED patterns and STEM-HAADF images.

xHREM is based on FFT-multislice dynamical calculation and wave-optics developed by Kazuo Ishizuka (Director of HREM Research).

Jitterbug DigitalMicrograph Plug-in

Scan-noise and Drift Compensator

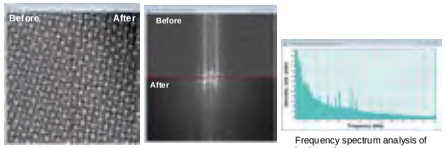

HAADF image of [100] $SrTiO_3$ and its Fourier transform

Frequency spectrum analysis of horizontal scan

Jitterbug will correct STEM image scan-noise, and restore image resolution and SNR. It will rectify image drift and lattice distortion for a crystal sample.

Jitterbug plug-in has originally been developed by Lewys Jones and Peter D. Nellist (University of Oxford).

HoloDark DigitalMicrograph Plug-in

Dark-field holography for strain analysis

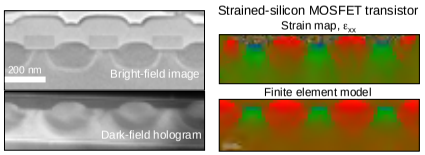

HoloDark generates quantitative deformation and strain maps with high-accuracy (Better than 0.1%) over wide fields of view from a pair of dark-field electron holograms of different diffraction vectors.

HoloDark is based on the patented technique and routines developed by Martin Hÿtch et al. (CNRS).

GPA DigitalMicrograph Plug-in

Geometrical Phase Analysis

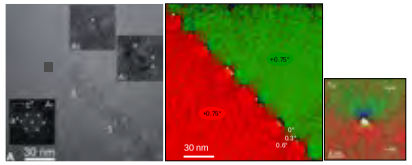

High resolution image

Rotation map

Stress map

GPA generates fully quantitative deformation/rotation and strain maps from a single standard HREM image using geometric phase images.

GPA is based on geometric phase algorithms originally developed by M. Hÿtch (CNRS).

PPA DigitalMicrograph Plug-in

Peak-Pairs Analysis

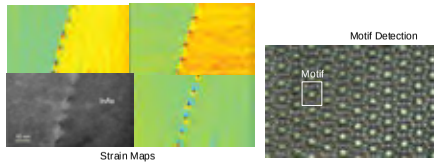

Strain Maps

PPA locates atomic columns at sub-pixel resolution using 2D filtering or a small reference region (Motif), and offers peak intensity analysis and local strain map calculation from high-resolution images.

PPA is based on *Peak-Pairs* algorithm originally developed by Pedro L. Galindo (University of Cadiz).

HREM-Filters DigitalMicrograph Plug-in

Optimal Noise Filters for HREM

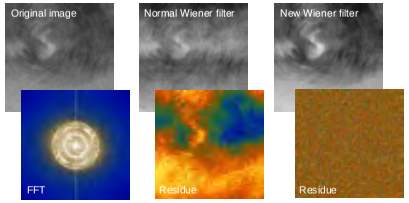

HREM-Filters are sophisticated Wiener and Difference filters that works even for non-ideal crystals, such as a nano-crystal or cylindrical crystal.

New Wiener filter (right) based on local backgrounds extracts all the structure information, while normal Wiener filter (middle) based on radial background does not work for non-ideal crystal.

DeConvHAADF DigitalMicrograph Plug-in

STEM-HAADF Image Deconvolution

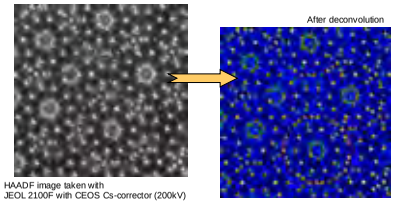

HAADF image taken with JEOL 2100F with CEOS Cs-corrector (200kV)

DeConvHAADF rectifies STEM-HAADF image by eliminating a spread of scan probe due to spherical aberration of the probe forming lens and/or a physical source size. DeConvHAADF works well even on the STEM-HAADF image acquired with a Cs-corrected microscope by correcting a spread due to physical source size.

DeConvEELS DigitalMicrograph Plug-in

Electron Energy Loss Spectrum Deconvolution

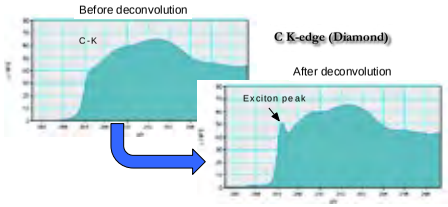

DeConvEELS rectifies an Electron Energy Loss Spectrum (EELS) by deconvoluting with a low-loss or zero-loss spectrum using *Maximum Entropy Method* or *Richardson-Lucy Algorithm*.

FTSR DigitalMicrograph Plug-in

Focal and Tilt Series Reconstruction

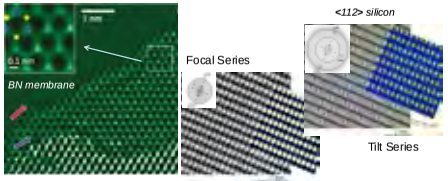

FTSR works with a through focal series (FSR) or tilt series (TSR) of HREM images to reconstruct the complex wave function at the specimen exit surface.

FTSR uses a Wiener filter developed by Angus Kirkland et al. (University of Oxford)

IWFR DigitalMicrograph Plug-in

Iterative Wave Function Reconstruction

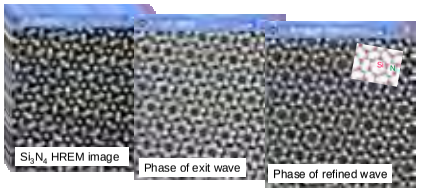

IWFR works with a through focal series of HREM images to reconstruct a complex wave function at the specimen exit surface, and corrects spherical aberration. IWFR uses Gerchberg-Saxton-type iteration using only image intensities developed by Les Allen et al. (University of Melbourne).

MSA DigitalMicrograph Plug-in

Multivariate Statistical Analysis

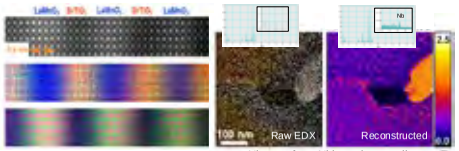

$LaMnO_3/SrTiO_3$ multilayer

Nb map from Ni-based superalloy

MSA finds statistically significant features from spectrum images (XEDS, EELS, EFTEM and cathodoluminescence) using PCA (Principal Component Analysis).

MSA plug-in has originally been developed by Masashi Watanabe (Leigh University).

QED DigitalMicrograph Plug-in

Quantitative Electron Diffraction

LARBED (Large Angle Rocking Beam Electron Diffraction) & PED (Precession Electron Diffraction)

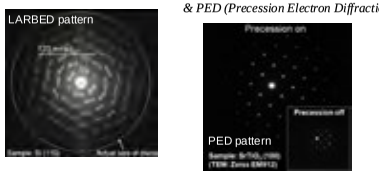

QED acquires LARBED and/or PED patterns from a small area by precisely controlling the nano-sized electron beam in your TEM. The QED calibrates deflector coils, and measures aberrations of illumination system.

QED is based on the patented technique and routines developed by Christoph Koch at Max Planck Institute (now at Ulm University).

QP_t DigitalMicrograph Plug-in

Quantitative Phase Technology

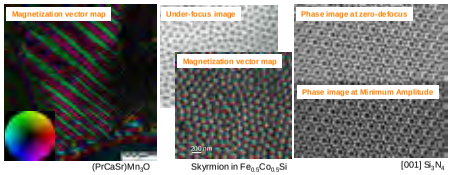

$(PrCaSr)Mn_2O$

Skyrmion in $Fe_{0.5}Co_{0.5}Si$

[001] Si_3N_4

QPt generates a quantitative *in-focus* phase image over a wide range of magnifications only from *three* ordinary bright-field images.

QPt is based on Quantitative Phase Imaging (QPI) technology developed by Keith Nugent et al. (University of Melbourne).

qHAADF DigitalMicrograph Plug-in

Quantitative HAADF Analysis

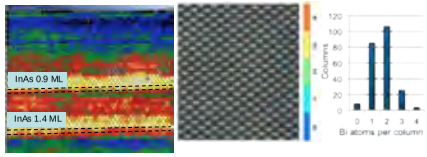

Integrated intensities of InAs-GaAs

Bi content $GaAs_{1-x}Bi_x$

qHAADF performs column-to-column compositional analysis of materials from the integrated intensities of an atomic-column resolved HAADF-STEM image.

qHAADF is based on a method developed by Sergio I. Molina et al. (University of Cadiz).

TEM

X-Max^N 100TLE

High solid angle windowless SDD for TEM

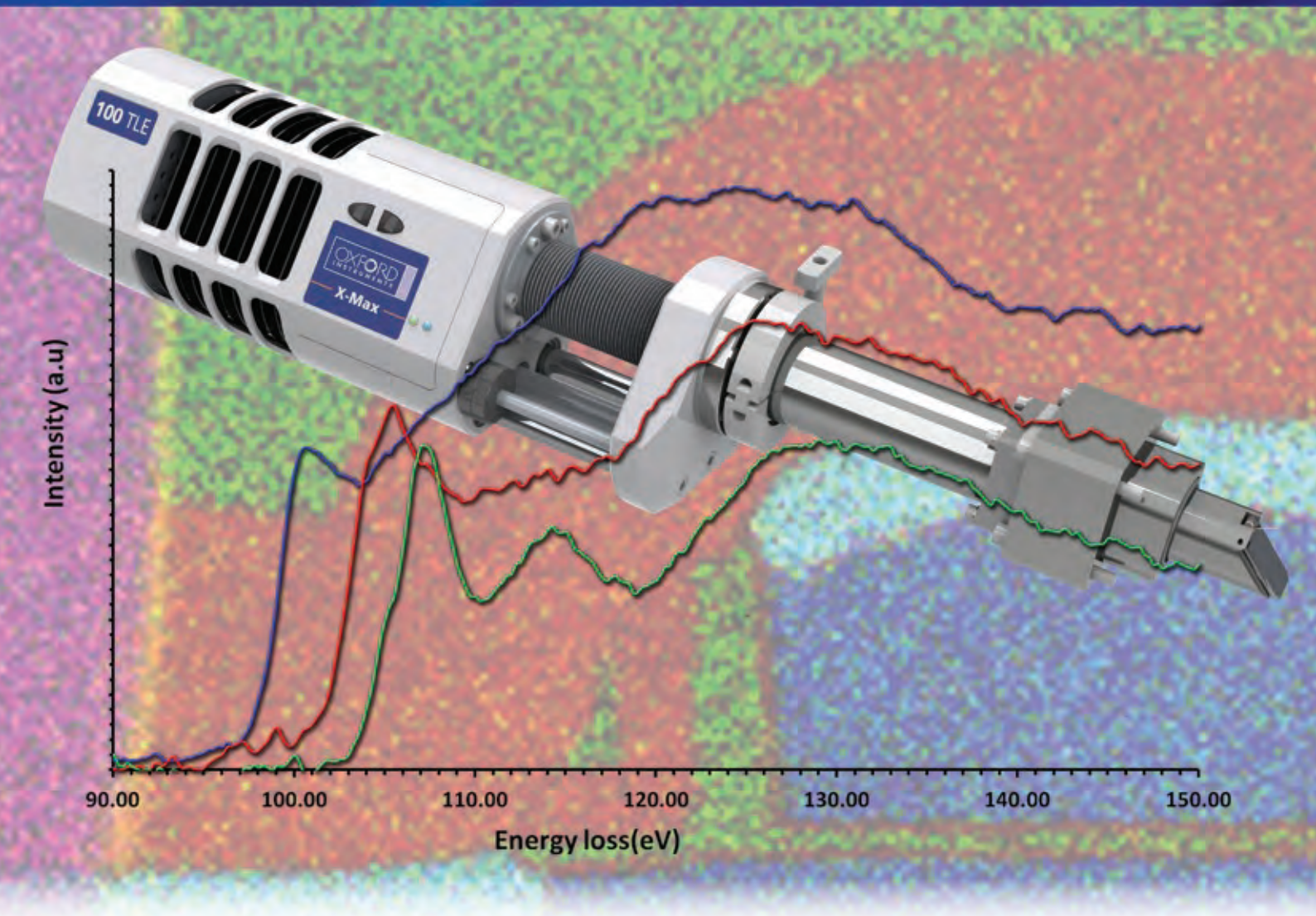

*Power semiconductor device mapped using **X-Max^N** 100TLE for metallic elements, and EELS for Si compounds.*

The **X-Max**^{N} 100TLE exploits an optimised sensor shape, windowless configuration and innovative mechanical design to deliver the highest performance elemental analysis in TEM.

- Solid angle in the range 0.5 to 1.1 sr (configuration dependent)
- Ideal for aberation-corrected TEMs
- Simultaneous EELS capability to deliver elemental and chemical mapping

For application notes visit: www.oxinst.com/TEM

OXFORD INSTRUMENTS

The Business of Science®

EXTREME EDS

X-Max® Extreme

Breakthrough technology for high spatial resolution SEM-EDS

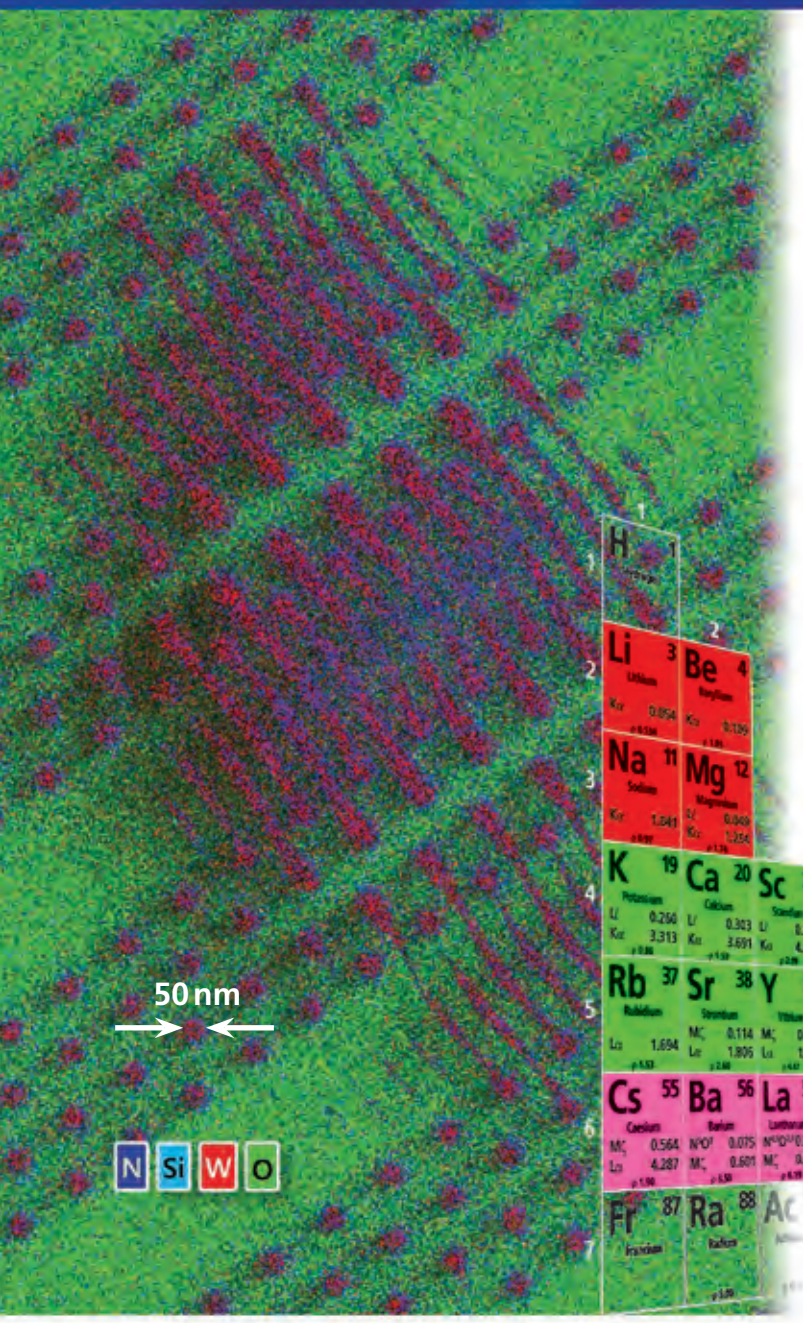

De-layered semiconductor memory structure showing sub 50 nm nodes and partially removed interconnects.

Sample prepared using Fischione Instruments' Model 1063 WaferMill™.

X-Max Extreme Silicon Drift Detector is a breakthrough solution for ultra high resolution FEG-SEM applications that delivers solutions beyond conventional micro- and nano-analysis.

- EDS spatial resolution approaches that of the FEG-SEM
- Surface science sensitivity
- Materials characterisation down to 1 kV
- Extreme light element sensitivity
- Lithium detection
- Nano-characterisation using bulk samples

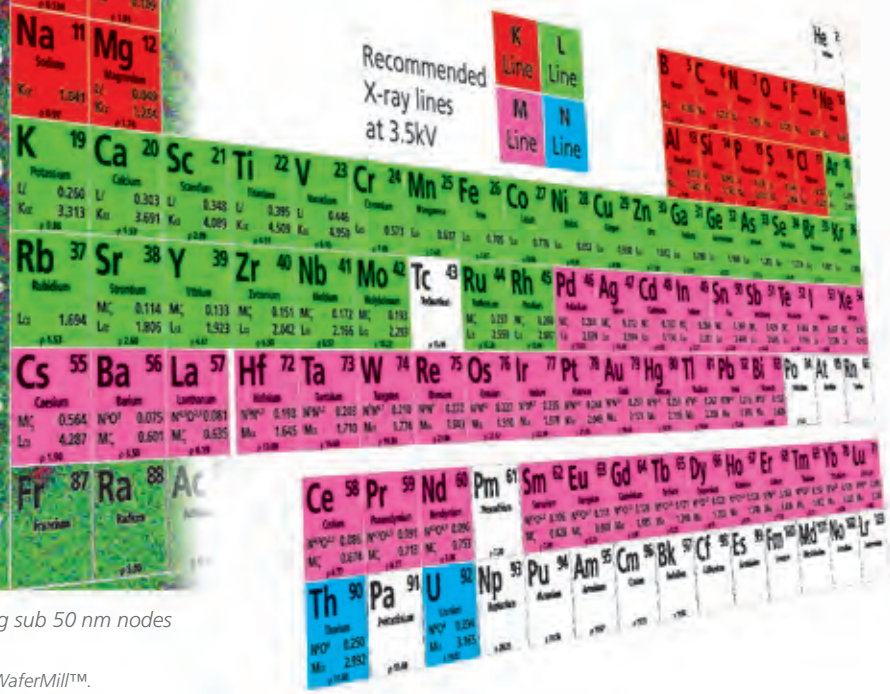

For application notes visit: www.oxinst.com/extreme

OXFORD INSTRUMENTS

The Business of Science®

Gold Sponsors

CEOS
Corrected Electron Optical
Systems GmbH

CEOS wishes you inspiring discussions and new insights at this meeting

To make sure insights continue back home ask your electron microscope vendor if the latest corrector will come with your new EM.

If you wish to learn more about the people who are developing aberration correctors since more than 30 years and other advanced EM components, visit us at: **www.ceos-gmbh.de**

CEOS

Corrected electron optical systems GmbH

Bronze Sponsors

Seamless integration for smart results

EDS

EBSD

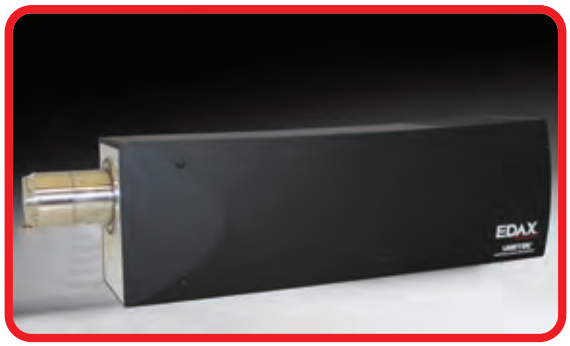

WDS

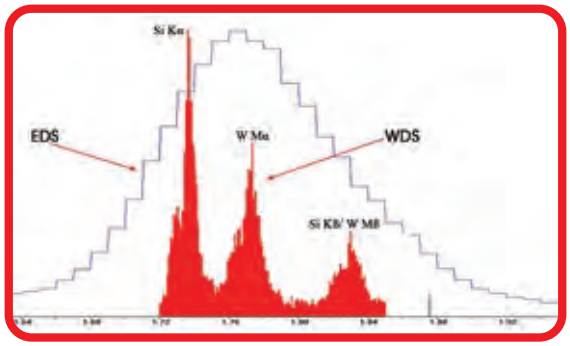

- Market leading EDS systems for fast data collection
- Best EBSD available - OIM Analysis™, NPAR™, PRIAS™
- EDS, EBSD and WDS integrated into a single user interface
- The ultimate solution for every materials challenge

EDAX Smart Insight

AMETEK MATERIALS ANALYSIS DIVISION

電子顕微鏡のための

GENTLE MILL

ファイナル研磨は極低エネルギーで!

300V以下の極低エネルギーから低エネルギー2KVまで安定で制御されたブロードビーム(約φ1.5mm)による研磨は観察や分析に各分野から数多くの評価を得られています。

- ●イオン銃 …… 熱陰極式
- ●加速電圧 …… 100V～2KV
- ●ビーム径(FWHM) …… 750～1,200μm
- ●最大イオンビーム電流密度 …… 10mA/cm²
- ●ビームカレント …… 5～80μA
- ●観察 …… ×50～×400 CCDカメラ
- ●排気 …… ダイヤフラム・ターボ分子ポンプ
- ●装置サイズ(mm) 600(W)×800(D)×650(H)
- ●重量 …… 60kg
- ●オプション …… 非暴露システム

[FIBによるTEM試料の作製例]

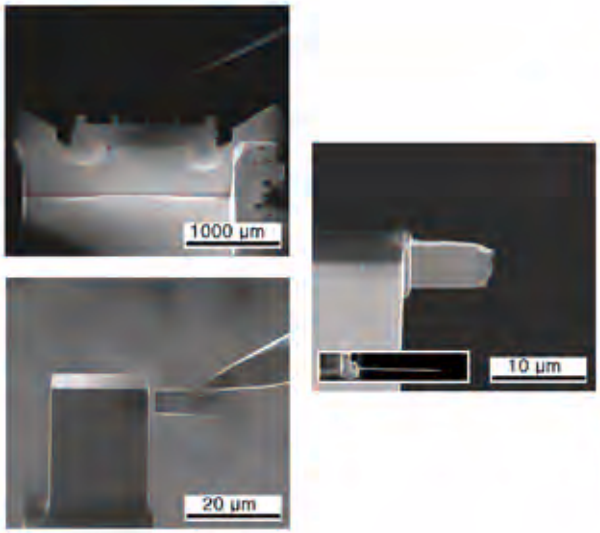

FIBデータは、KAST高度計測センター様のご提供です。

[Gentle Mill加工前後のTEM画像]

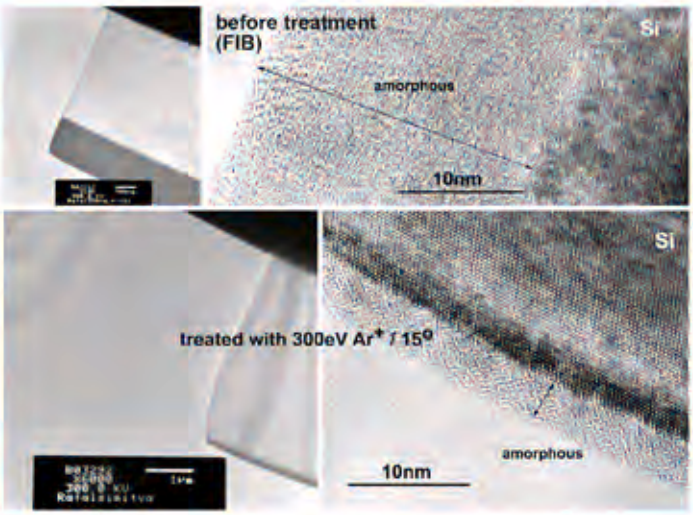

※デモ・TEM観察等は、KAST高度計測センター様内で行っております。

【TECHNOORG·LINDA·HUNGARY】
日本総代理店
JPC 日本フィジテック

〒192-0046 東京都八王子市明神町4-9-1-203
Tel.042-645-9620 Fax.042-645-9621
E-mail:funaya@japan-physitec.jp
http://japan-physitec.jp

透過型電子顕微鏡用試料ホルダー

Transmission Electron Microscopy Sample Holder

北野精機では、透過型電子顕微鏡（Transmission Electron Microscopy：TEM）の実験的な機器・部品を幅広く提供しています。これらの製品は、生物、高分子、セラミックス、半導体、金属など多くの分野における基礎研究をはじめ、新製品の開発やその評価などに幅広く利用されております。
特にTEMホルダーは、研究者の要求に独自のアイデアを注入し、共同で開発され試料内部の形態・結晶構造・組成・電子状態などの高分解能イメージングを可能にすることができます。
また、その他の要求仕様・研究開発目的に応じた特殊機構の試作・共同開発もご気軽にお問い合わせください。

納入実績

- ■試料冷却TEMホルダー
- ■蒸着TEMホルダー
- ■引張り応力計測TEMホルダー
- ■二軸傾斜高温試料TEMホルダー
- ■ガス導入TEMホルダー
- ■真空封止型TEMホルダー
- ■反応ガス2種導入TEMホルダー
- ■その場観察TEMホルダー
- ■クリーニング用TEMホルダー
- ■ガス反応TEMホルダー
- ■ガス・光・導入機構付TEMホルダー
- ■電気特性計測TEMホルダー
- ■真空封止型試料搬送機構

＊その他、御客様の仕様に合わせて試作開発を承っておりますので担当までお問い合わせください。

北野精機株式会社
harashima@kitano-seiki.co.jp

All for Researchers.
KITANO

日本のホルダー屋

Custom built TEM holder and SEM stage from Japan

http://www.melbuild.com

SATO-Holder

- Nano-order stepping
- Insitu Tensile
- Insitu Compression
- X tilt angle: ±60°

EN-Holder

- Piller Sample
- Double tilt
- Y tilt angle: ±7.5°
- Stepping Digit < 0.01°
- Eucentric Mechanism

DTEF-Holder

- Applied field
- Double tilt
- X tilt: ±20° / Y tilt: ±20°
- FIB mesh for applied field

Locus Spy -HM

- Tensile /Compression SEM Stage
- Compact ϕ70mm
- Cost Performance

HATA-Holder
AS-Holder

- For Multi-SDD
- EDS Tomography
- Shuttling to FIB/SEM/SIMS

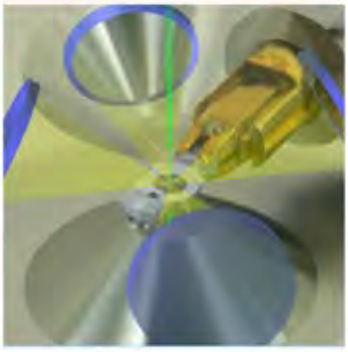

e - Cell
for SEM / FIB

- Gas atomospheric
- Light Irradiation
- Compact ϕ40m

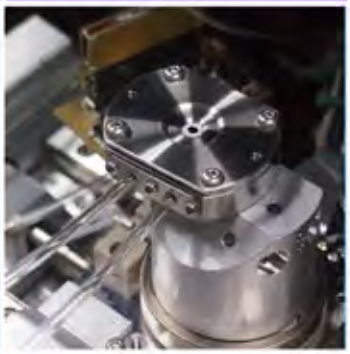

Mel-Build

Mel-Build Corporation 819-0052 3-1-15, Shimoyamato Nishi-Ku, Fukuoka, Japan Tel (+81)92-891-5111 info@melbuild.com

Manufacture and sales of TEM/STEM/FIB Sample Preparation

Micron-pitch grid *(Our original)*

- Grid holes with micrometer pitch spacing.
- Circle and V-shaped mark on the edge gives easy check of front or back, and orientation in the TEM holder.

Grid for FIB sample *(Our original)*

- Λ-shape, U-shape, and L-shape grids are available for each material of Cu, Ti, Mo.
- Several types of specimen fixing port are available; flat or pillar form for U-shape and L-shape, and tip form with 45° or 60° for Λ-shape.

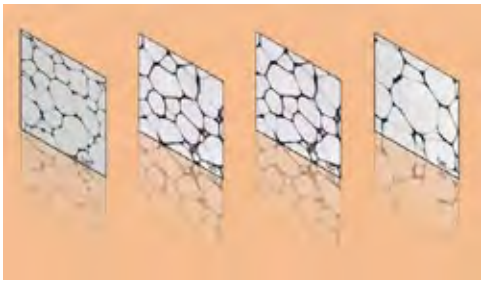

Microgrids

- N series: Different hole size and aperture ratio can be selected.
- R series: Enhanced organic solvent resistance, heat resistance or acidic/alkaline solvent tolerance are avairable.
- M series: Different materials with Al, Au, Ge, Carbon are availrable.

Support Films

- Different support films with various materials, 16 types of series.

SEM Mount and Strage Box

- Mount: Various shapes of specimen stubs are provided.
- Strage box: Variety of strage boxes are provided upon stubs and plates.
- SEM plate: Covenient to store in space-saving case. Newly designed SEM plate with address is available now.

Sample for evaluation of TEM condition

- for Magnification check: Grating replica, Polystyrene latex sphere, etc.
- for Resolution check: Evaporated fine particles of Au, Pt-Pd and Crystal lattice of Carbon graphite, Pyrophyllite, etc.
- for TEM alignment and Adjustment: Various samples are provided.

Sample for evaluation of SEM condition

- for Magnification check: Grating replica, Polystyrene latex sphere, etc.
- for Resolution check: Several specimens are provided for different electron beam sources such as W-, LaB6-, or FE-SEM

(Specimen Techniques for Electron Microscope)

STEM Corporation

6F, Center Bldg., Machida Techno-Park,
2-5-8, Oyamagaoka 2-chome, Machida, Tokyo 194-0215, JAPAN
TEL: +81-42-794-8860 FAX: +81-42-794-8861
E-mail: stem.stem@tbj.t-com.ne.jp URL: http://www2.tbb.t-com.ne.jp/stem.stem/

GOT A MICROSCOPE?

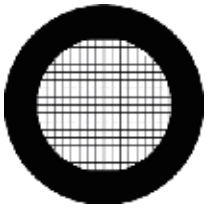
Slim Bar

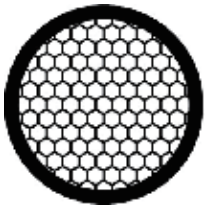
Hexogonal


Parallel


Slot


Index


SEM Finder


SEM Finder


GVHS


Folding


Handle


FIB Half ring


Aperture

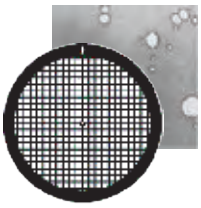
Holey Carbon

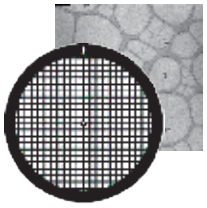
Lacey Carbon

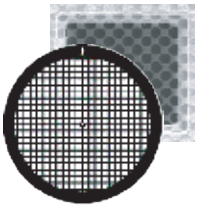
Quantifoil

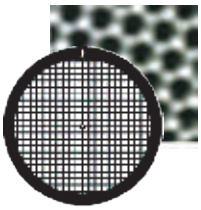
Graphene & GO

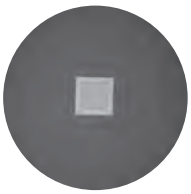
SiN membrane


Si membrane


SiO membrane

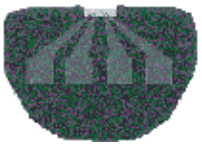
SiN Lift-Out

ALLIANCE Biosystems
Advancing the Science & Accelerating Your Discovery
株式会社アライアンスバイオシステムズ

〒533-0033 大阪市東淀川区東中島1-20-12
Tel 06-6324-8817 / Fax 06-6324-8818

mail: info@alliance-bio.com
www.alliance-bio.com

TEM・SEM用の試料前処理装置の他、特別注文で真空装置・部品も製造・販売。

超精密アモルファス金属コーティング［オスミウムオートコーター］

- φ100mm 大面積試料ステージを採用。
- ホローカソード電極採用で低温・低電圧・低ダメージ設計。
- 四酸化オスミウムの導入量を最適にコントロール。
- 排出口には専用オスミウム・トラップ付属（拡張機能付き）。四酸化オスミウムの大気拡散を完全シャットアウト。排気ダクト接続可能（本体）。
- メンテナンス性の向上（従来品比較）、長いメンテナンス周期を実現。
- オスミウムアンプルを真空室内で容易に割断可能なチャンバー付属。
- サンプル取出しやアンプル交換時の間違え易い操作を完全自動化。

HPC-20

低電圧・低ダメージ　タングステンコーター［マグネトロンイオンスパッター］

- FE-SEM 向けに粒子径 1nm 以下のタングステンをコーティング。
- 空冷式強磁場ターゲット電極を採用。
- プログラム制御により操作ミスを最小限にいたします。
- 特殊金属(Cr、Mo、Ti、Taなど)の成膜が可能。（＊サンプルデモ受付中）
- 回込性、膜強度は高く、オスミウムコーターの代替機としてお勧めです。
- SEM試料用の貴金属コーティング専用機種（低価格）も多数ご用意。

MSP-20-TK

4本の独立した排気ポートを搭載［TEM ホルダー保管装置］

- TEM ホルダーを真空下で保管する装置です。
- 独立した真空室に保管するため、個別に出し入れが可能です。
- プログラム制御による自動排気やインターロック制御を搭載。
- タッチパネル搭載で直感的に操作が行えます。
- TEM ホルダーポートはお客様のご使用になられている TEM ホルダーに合わせて製作する事が可能です。
- 高真空下に保管する事により、コンタミネーションの発生を大幅に軽減。

FEH-02

全自動で含水サンプルを乾燥［t-ブタノール凍結乾燥装置］

- 操作系にタッチパネルを採用し、全ての制御をプログラムで管理。
- デリケートな試料の乾燥を高精細モードで実行するだけです。
- 急ぎの乾燥・変形の少ない試料にはハイスピードモードで素早く乾燥可能。
- 乾燥終了も内部の真空計で自動判断いたします。
- 試料カップはお客様のシャーレをそのまま入れる事も可能となりました。
- 小型デスクトップタイプの高性能機を低価格でご提供いたします。

VFD-30

電子顕微鏡向け前処理機能複合機［マルチ成膜装置］

- 弊社で実績のある VC-100S・MSP-1S・PIB-10 の機能を合体。
- 用途別にチャンバーを2系統持っています。
- カーボン蒸着は TEM 支持膜の補強やX線分析に使用。
- スパッタは SEM 試料を低ダメージで導電処理。50mm φAu-Pd 付属。
- 親水処理は支持膜上に試料を滴下する時やダイヤモンドナイフの親水化に使用します。
- 自動プログラムによるフルオート機能やインターロック制御を搭載。
- オプションでカーボン電極追加、ブレーカー類の追加が可能です。

VES-10

◎親水処理装置・急速凍結器・特別注文真空部品など数多く取り扱っております。

お問合せ先

株式会社 真空デバイス

〒311-4155　茨城県水戸市飯島町 1285-5
Tel：029-212-7600　Fax：029-212-7601
E-mail：device@shinkuu.co.jp
URL：http//www.shinkuu.co.jp

ダイヤモンドナイフ

最高級・最高品質の

DiATOME 社製(スイス)

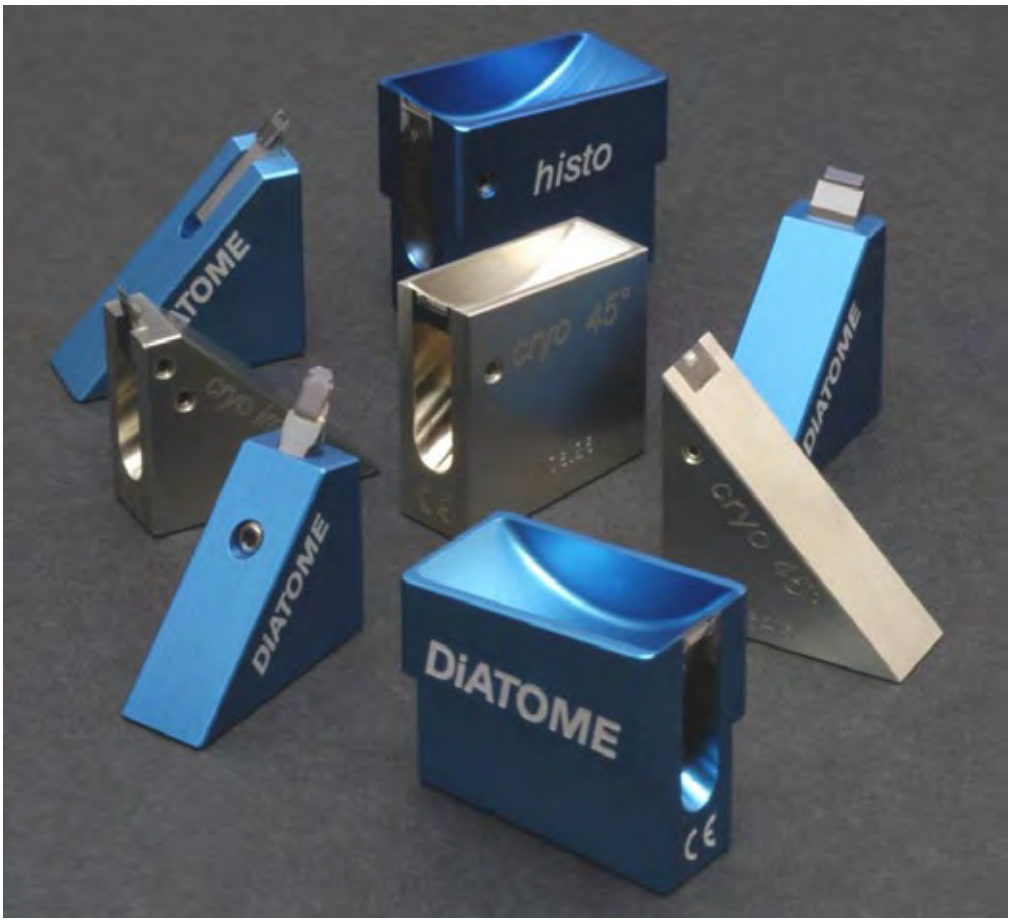

大好評

交換販売も実施中

☆ヒストナイフの交換販売を再開しました☆

お手持ちのダイヤモンドナイフをご提供下さい。
DiATOME社の新品のナイフが再研磨価格に！
＊スミナイフXAC･トリミングナイフは対象外です。

＊詳しくは弊社にお問合せ頂くか、ホームページもしくはカタログをご参照下さい。

日新EM株式会社
〒１６０－０００７　東京都新宿区荒木町２３－９
Tel.03-3355-3001　Fax.03-3353-2888　URL.http://nisshin-em.co.jp/

Author Index

Appendix


大石林山
平成29年 5月17日


Okinawa Okinawa
EDGE2017

	Sun, 14 May	Mon, 15 May		Tue, 16 May		Wed, 17 May		Thu, 18 May		Fri, 19 May
9:00		**Advances in Instrumentation and Data Processing**	Tracy Lovejoy	**Very High Energy Resolution EELS**	Maureen Joel Lagos	**Advances in Theory**	Lorenzo Pardini	**Spectroscopic Imaging**	Gerald Kothleitner	
9:15										
9:30			Huolin Xin		Peter Tiemeijer		Philippe Moreau		Pascale Bayle-Guillemaud	
9:45			Paolo Longo		Quentin Ramasse		Guillaume Radtke		Eric Prestat	
10:00			Renu Sharma		Christian Dwyer		Motofumi Saitoh		Andrew B. Yankovich	
10:15			Xiaoyan Zhong	**Discussion**		**Discussion**			Hikaru Saito	
10:30		Coffee Break		Coffee Break		Coffee Break		Coffee Break		
10:45										
11:00		**Advances in Instrumentation and Data Processing**	Florent Houdellier	**Materials and Biological Applications**	Lena Kourkoutis	**Materials and Biological Applications**	Gianluigi Botton	**Materials and Biological Applications**	Duncan Alexander	Departure
11:15									Franz-Philipp Schmidt	
11:30			Heiko Müller		David W. McComb		Demie Kepaptsoglou		Junhao Lin	
11:45			Damien McGrouther		Catriona M. McGilvery		Nicolas Gauquelin		Michael K. Kinyanjui	
12:00					Vesna Srot		Ming-Wen Chu	**Discussion**		
12:15			David A. Muller		Sean M. Collins		Yohei Sato			
12:30		**Discussion**		**Discussion**		**Group photo**		Lunch		
12:45										
13:00	Arrival	Lunch		Lunch		Lunch				
13:15										
13:30								**Afternoon free for discussion**		
13:45										
14:00		**Afternoon free for discussion**		**Afternoon free for discussion**		**Social event**				
14:15										
14:30										
14:45										
15:00	**Registration**									
15:15										
15:30										
15:45		**Beyond Traditional Spectroscopy and Imaging**	Claus Ropers	**Advances in Theory**	Les Allen			**Materials and Biological Applications**	Matthieu Bugnet	
16:00										
16:15			Masami Terauchi						Robert F Klie	
16:30			Giulio Guzzinati		Jan Rusz				Juan Carlos Idrobo	
16:45			Makoto Kuwahara		Ray Egerton				Rhonda Stroud	
17:00			Luiz H. G. Tizei		Javier Aizpurua			Coffee Break		
17:15										
17:30		Coffee Break		Coffee Break				**Phase Contrast Imaging and Diffraction**	Naoya Shibata	
17:45										
18:00		**Beyond Traditional Spectroscopy and Imaging**	Johannes Jobst	**Posters Oral Summaries P061 – P120**					Eric Van Cappellen	
18:15									Joanne Etheridge	
18:30		**Posters Oral Summaries P001 – P060**						**General discussion / prospectives / Conclusion**		
18:45										
19:00	Dinner					Dinner		**Banquet**		
19:15										
19:30				Dinner						
19:45										
20:00		Dinner								
20:15										
20:30						**Very High Energy Resolution EELS**	Kazu Suenaga			
20:45										
21:00	**Plenary lecture**		Sumio Iijima	**Poster**		**Poster**				
21:15										
21:30										
21:45		**Poster**								
22:00										
22:15										
22:30										
22:45										
23:00										